Primordial black holes as dark matter and Hawking radiation constraints with BlackHawk

Jérémy Auffinger

Université Claude Bernard Lyon 1

N° d'ordre NNT: 2022LYSE1133

THÈSE de DOCTORAT DE L'UNIVERSITÉ DE LYON

Opérée au sein de :

l'Université Claude Bernard Lyon 1

Ecole Doctorale 52

Physique et Astrophysique (PHAST)

Spécialité de doctorat : Physique théorique

Discipline : Cosmologie

Soutenue publiquement le 05/07/2022, par :

Jérémy Auffinger

Primordial black holes as dark matter and Hawking radiation constraints with BlackHawk

Devant le jury composé de :

Dimitrios Tsimpis Professeur, IP2I, Université Lyon 1	**Président**
Marco Cirelli Directeur de recherche CNRS, LPTHE, Sorbonne Université	**Rapporteur**
Jane MacGibbon Associate Professor, Department of physics, University of North Florida	**Rapporteure**
Francesca Calore Chargée de recherche CNRS, LAPTH, Université de Savoie	**Examinatrice**
Etera Livine Directeur de recherche CNRS, Laboratoire de physique, Ecole Normale Supérieure de Lyon	**Examinateur**
Dimitrios Tsimpis Professeur, IP2I, Université Lyon 1	**Examinateur**
Alexandre Arbey Maître de conférence, IP2I, Université Lyon 1	**Directeur de thèse**
Joseph Silk Professeur retraité, IAP, Sorbonne Université	**Invité**

Préambule

Contents

Remerciements

J'aimerais profiter de ce petit espace au début de ce long manuscrit pour remercier tou·tes celleux qui m'ont accompagné durant les 3 ans qu'a duré ma thèse (un peu plus en comptant les années d'étude précédentes). À toutes mes connaissances qui tomberont sur ce manuscrit et qui n'auraient pas le courage d'aller lire le fatras des pages suivantes, vous aurez au moins la satisfaction d'être citées ici.

Sans originalité aucune, il est un peu difficile de lister toutes les personnes qui m'ont permis de mener ce travail à bien. En premier lieu, je tiens à remercier ma famille et mes ami·es qui ont alterné entre soutien et gentille moquerie quant au sujet, à l'avancement, ou à l'utilité de ce long travail.

Je remercie ensuite mon directeur de thèse Alexandre qui m'a encadré pendant 4 ans et demi sans s'offusquer de mes absences, départs en manif, grève générale et balades en forêt. Je remercie également tou·tes les collaborateur·rices avec qui j'ai pu partager, scientifiquement et personnellement, des conversations enrichissantes. Je dois aussi remercier le personnel de l'Université Lyon 1, visible et moins visible, qui a permis que ce travail aboutisse dans de bonnes conditions.

Je tiens à saluer mes élèves, qui ont supporté mes petites blagues et longs monologues pendant des heures, en visio et en présentiel. Vous avez représenté la touche de jeunesse dans cette discipline de vieux.

Je remercie tout particulièrement Isatis, sans qui j'aurais certainement arrêté cette thèse beaucoup plus tôt, et sans qui l'avenir paraîtrait moins beau.

Enfin je vous remercie vous, militant·es ou pas, qui m'avez donné l'espoir d'un monde meilleur et l'envie d'apprendre à vivre autrement.

Résumé

Les trous noirs primordiaux sont au cœur d'un grand nombre de recherches depuis l'époque de la découverte du principe de leur existence. À la fin des années 1960 et au début des années 1970, la théorie dite du « Big Bang chaud » a reçu des confirmations éclatantes d'une part par l'observation du fond diffus cosmologique, et d'autre part par le succès des prédictions des abondances des éléments légers à l'issue de la nucléosynthèse primordiale. L'homogénéité de l'univers à grande échelle a poussé les cosmologistes à postuler l'existence d'une période d'inflation très rapide, qui a duré pendant les premières fractions de seconde de la vie de l'univers. Les petites fluctuations aléatoires de densité ne se sont retrouvées en lien causal qu'à la fin de cette période d'inflation. Si elles ont atteint une amplitude suffisante, ces perturbations ont pu s'effondrer gravitationnellement, ce qui a pu donner naissance à des trous noirs dans l'univers primordial, autrement dit des « trous noirs primordiaux ».

Ces trous noirs ne proviennent pas de la mort d'étoiles, donc leur masse n'est pas assujétie aux limites stellaires habituelles. De fait, en fonction de leur mécanisme de formation, les trous noirs primordiaux pourraient avoir n'importe quelle masse. Une limite inférieure semble inévitable, la masse de Planck, à l'échelle de laquelle des corrections quantiques à la relativité générale devraient s'appliquer. Une limite supérieure provient du fait que pour qu'un trou noir primordial dont la masse est de l'ordre du contenu de la sphère de Hubble se soit formé, il faudrait que tout le contenu de l'univers causalement lié dans cette sphère—notre univers visible—s'y soit effondré dès l'après-Big Bang. Comme de nombreuses structures lointaines peuvent être observées dans le ciel, un tel trou noir maximal n'existe pas. Entre ces deux limites, des trous noirs primordiaux pourraient s'être formés en très grand nombre.

Les trous noirs primordiaux dont la masse est plus petite que celle d'une galaxie se sont formés avant la nucléosynthèse primordiale. Ainsi, ils comptent comme une matière non-baryonique. De plus, leur vitesse est censée être non-relativiste. Ces deux points montrent que les trous noirs primordiaux apparaissent comme un candidat parfait pour la « matière noire », cette matière non-lumineuse qui est supposée être cinq fois plus abondante que la matière ordinaire dans les grandes structures de l'univers. Une première contrainte sur la quantité de trous noirs primordiaux en découle immédiatement : la densité de trous noirs primordiaux ne devrait pas excéder celle de la matière noire. D'autres contraintes sur la densité de trous noirs proviennent de leur impact sur les grandes structures, notamment par friction gravitationnelle avec le gaz environnant ou par rayonnement X dû à l'accrétion de matière à leur surface. D'autre part, des systèmes binaires de trous noirs primordiaux pourraient s'être formés, et leur taux de coalescence devrait être cohérent avec celui observé par les instruments d'interférométrie gravitationnelle pour les trous noirs de masse stellaire. Enfin, de plus petits trous noirs, de la masse d'une lune ou d'une planète, provoqueraient des déviations de la lumière issue des étoiles lointaines lorsqu'ils s'interposent entre l'étoile et la Terre. Ce phénomène de « lentille gravitationnelle », dont la fréquence est étroitement contrainte, réduit l'espace des paramètres libre pour les trous noirs primordiaux. Toutes ces contraintes mises ensemble, les trous noirs primordiaux plus lourds qu'un astéroïde ne peuvent pas contribuer de manière sensible à la densité de matière noire. Qu'en est-il des trous noirs plus petits qu'un astéroïde ?

Le fait que les trous noirs primordiaux peuvent être très légers, et donc très petits—un trou noir

de la masse d'un astéroïde pourrait aisément tenir dans le rayon d'un atome—a poussé Hawking à s'interroger sur leurs propriétés quantiques. Hawking a démontré, dans le régime semi-classique où la métrique de l'espace-temps n'est que la toile de fond de l'évolution des champs quantiques de matière, qu'un trou noir n'est de fait pas tout à fait « noir », mais qu'il émet un rayonnement continu comme s'il était un corps noir d'une température inversement proportionnelle à sa masse. Ce « rayonnement de Hawking » a deux conséquences majeures. La première, c'est qu'un trou noir perd de la masse au court du temps à cause de son « évaporation » par rayonnement de Hawking. Il pourrait finir par disparaître complètement, ou se stabiliser autour de la masse de Planck, selon la théorie valide à ces échelles extrêmes. La seconde, beaucoup plus intéressante, est qu'un trou noir peut être *vu*. En effet, le rayonnement de Hawking concerne tous les champs quantiques existant dans la nature. Un trou noir, si sa température le permet, peut alors émettre un flux de photons, d'électrons, de neutrinos... Cette émission continue est associée à des conséquences sur le milieu environnant les trous noirs primordiaux. Comme ces trous noirs se seraient formés dès les premières fractions de seconde de l'existence de l'univers, leur rayonnement de Hawking aurait pu avoir des effets mesurables sur *toutes* les périodes ultérieures de son développement. Les trous noirs primordiaux modifieraient l'abondance des éléments légers à l'issue de la nucléosynthèse primordiale, ils distordraient le spectre du fond diffus cosmologique, et ils émettraient eux-mêmes un fond de particules de toutes sortes. Enfin, à la fin de leur existence, leur température tendant vers l'énergie de Planck comme leur masse tend vers la masse de Planck, ils apparaîtraient comme des points extrêmement brillants dans les relevés astronomiques.

Ainsi, une gamme entière de nouvelles contraintes se posent sur l'abondance de trous noirs primordiaux pour les masses les plus faibles, en-deçà de la masse d'un astéroïde. Le spectre du rayonnement de Hawking a été calculé dans les années 1970 par Page, et l'évolution des particules fondamentales une fois émises par le trou noir a été déduite par MacGibbon & Webber dans les années 1990. Ces calculs successifs ont permis de placer des contraintes sur les trous noirs par la nucléosynthèse primordiale, le fond diffus cosmologique, l'intensité actuelle des rayons cosmiques et enfin le taux d'explosion de trous noirs dans l'univers local. En conséquence, l'abondance initiale des trous noirs primordiaux est extrêmement limitée pour les masses les plus faibles. En-dessous d'un millier de tonnes, ces trous noirs se seraient de toute façon évaporés avant la nucléosynthèse primordiale, et auraient pu aussi bien n'avoir aucune conséquence sur l'évolution de l'univers. Il reste une étroite fenêtre, autour de la masse d'un astéroïde, pour laquelle les trous noirs primordiaux seraient à la fois suffisamment massifs pour être stables à l'échelle de l'âge de l'univers, et suffisamment petits pour n'avoir aucun effet gravitationel visible autre que leur densité globale. Ces trous noirs primordiaux sont justement les candidats à la matière noire mentionnés plus haut.

Le rayonnement de Hawking de ces trous noirs pourrait être la seule manière de les détecter. Il est donc *primordial* de le calculer le plus précisément possible, afin d'obtenir des prédictions soit sur les signaux à chercher dans les données astronomiques, soit sur les meilleurs instruments à construire pour les observer. Lorsque j'ai commencé ma thèse, il n'existait pas d'outil numérique accessible pour calculer le rayonnement de Hawking des trous noirs primordiaux. Très vite, mon directeur de thèse et moi avons donc décidé que j'écrirais mon propre code, avec l'objectif de le rendre public. Ce travail, dont j'avais sous-estimé la complexité, a occupé une grand partie de ma thèse. C'est ainsi qu'est né `BlackHawk` (dont le nom mélange astucieusement plusieurs allusions). `BlackHawk` est un

code libre et gratuit, que je mets régulièrement à jour pour y intégrer de nouvelles fonctionnalités. Actuellement, `BlackHawk` en est à sa version `v2.1`. `BlackHawk` calcule le rayonnement de Hawking d'une distribution de trous noirs, qui peuvent avoir des masses, des charges électriques ou des vitesses de rotation différentes. Ces trois paramètres définissent entièrement un trou noir dans le cadre du théorème d'unicité habituel. Ensuite, `BlackHawk` utilise différents codes de physique des particules pour prendre en compte les interactions entre particules émises, ainsi que leur potentielle désintégration. Les interactions, et donc les codes, ne sont pas les mêmes à basse, moyenne et haute énergies. Garder `BlackHawk` à jour des évolutions de la physique des particules est un travail de tous les jours (ou plutôt tous les ans). J'ai également écrit plusieurs programmes extérieurs à `BlackHawk` qui permettent d'en tirer tout le potentiel, notamment un code intitulé `Isatis` (l'allusion est ici plus difficile à deviner) qui calcule automatiquement les contraintes sur les trous noirs primordiaux à partir de la sensibilité d'une large gamme d'instruments astronomiques.

Ce manuscrit de thèse rassemble tous les travaux que j'ai menés au cours de ces dernières années, principalement avec `BlackHawk`. Ils sont de deux sortes.

Premièrement, il y a les travaux classiques qui consistent à calculer le rayonnement de Hawking d'une distribution de trous noirs primordiaux et à comparer ce rayonnement à des données astronomiques, dans le but d'en tirer une contrainte sur leur abondance. La publication de `BlackHawk` a grandement stimulé cette recherche, car le code permet de calculer rapidement, précisément et automatiquement le flux de particules. Notamment, la capacité de `BlackHawk` à calculer les taux d'émission de trous noirs en rotation a permis à un grand nombre d'équipes de raffiner leurs propres contraintes pour prendre en compte la vitesse de rotation des trous noirs. J'ai mené deux études de ce type. La possibilité d'intégrer des distributions étendues où tous les trous noirs n'ont pas les mêmes paramètres ouvre sur un calcul plus réaliste et modifie totalement les contraintes. Le fait d'avoir un calcul automatique permet aussi de pouvoir modifier à l'envi les hypothèses sous-jacentes à l'obtention des contraintes. J'ai pu ainsi démontrer que malgré des progrès récents en matière de théorie et d'observations, les contraintes existantes souffrent d'une marge d'erreur considérable.

Deuxièmement, il y a les travaux théoriques sur les propriétés et l'évolution des trous noirs dues à leur évaporation. J'ai étudié notamment la durée de vie et l'évolution du moment angulaire de trous noirs en rotation, utilisé comme critère pour les différencier des trous noirs stellaires. J'ai également obtenu les formules qui permettent de calculer le rayonnement de Hawking d'une classe plus large de trous noirs que les simples trous noirs chargés en rotation. Cette étude était motivée par le fait que la relativité générale telle qu'énoncée par Einstein paraît incomplète au vu des observations les plus récentes, et qu'elle ne peut pas se marier en l'état avec la théorie quantique sans difficultés mathématiques insurmontables. De nombreuses théories alternatives existent, et au sein de ces théories les trous noirs ont souvent une géométrie différente. Le rayonnement de Hawking en est modifié, ainsi que les contraintes. Ces résultats ont été publiés dans deux articles théoriques, et appliqués à un cas particulier issu de la gravitation quantique à boucles. Une autre modification possible de la dynamique des trous noirs primordiaux est leur capacité à produire des champs au-delà du Modèle Standard de la physique des particules. Les trous noirs peuvent ainsi générer de la matière noire si celle-ci est plutôt une nouvelle particule inconnue. La production de matière noire par l'évaporation de trous noirs légers a fait l'objet d'une étude à part entière.

Enfin, j'ai également participé à plusieurs recherches plus spéculatives en lien étroit avec les

trous noirs primordiaux. L'une d'elle traite de la nucléosynthèse primordiale dans un univers dont l'inhomogénéité pourrait être liée à la formation de ces trous noirs, et repose sur l'autre code public `AlterBBN` développé par mon directeur de thèse et mis à jour au début de ma thèse ; tandis que deux autres explorent la possiblité que des trous noirs de masse planétaires soient capturés par des systèmes stellaires. Curieusement, il y a justement de forts soupçons qu'une neuvième planète existe au-delà de Neptune, sans pour l'instant parvenir à mettre la main dessus. Et s'il s'agissait d'un trou noir primordial ?

En conclusion, au cours de ma thèse, j'ai travaillé sur les sujets les plus divers, de la cosmologie primordiale à la théorie mathématique des trous noirs, en passant par la physique des hautes énergies, les rayons cosmiques et l'astronomie planétaire. Le mélange de ces domaines a été extrêment enrichissant et un article de revue est en court d'écriture sur le sujet des contraintes sur les trous noirs primordiaux, liées au rayonnement de Hawking. J'ai également produit le code public et gratuit `BlackHawk` qui est maintenant utilisé par un grand nombre de personnes. D'autres codes publics complémentaires ont commencé à être développés, annonçant une ère de précision numérique dans l'étude des trous noirs primordiaux, appuyée par le lancement de nouveaux instruments d'observation. Pour ma part, il est temps d'aller cultiver des tomates.

Publications

Refereed publications

[1] A. Arbey, J. Auffinger, K. P. Hickerson, E. S. Jenssen, AlterBBN v2: A public code for calculating Big-Bang nucleosynthesis constraints in alternative cosmologies, Comput. Phys. Commun. **248**, 6982 (2020), arXiv:1806.11095 [astro-ph.CO]

[2] A. Arbey, J. Auffinger, BlackHawk: A public code for calculating the Hawking evaporation spectra of any black hole distribution, Eur. Phys. J. C **79**, 693 (2019), arXiv:1905.04268 [gr-qc]

[3] A. Arbey, J. Auffinger, J. Silk, Evolution of primordial black hole spin due to Hawking radiation, Mon. Not. Roy. Astron. Soc. **494**, 1257 (2020), arXiv:1906.04196 [astro-ph.CO]

[4] A. Arbey, J. Auffinger, J. Silk, Constraining primordial black hole masses with the isotropic gamma ray background, Phys. Rev. D **101**, 3010 (2020), arXiv:1906.04750 [astro-ph.CO]

[5] A. Arbey, J. Auffinger, J. Silk, Stellar signatures of inhomogeneous big bang nucleosynthesis, Phys. Rev. D **102**, 3503 (2020), arXiv:2006.02446 [astro-ph.CO]

[6] J. Schneider, A. Arbey, J. Auffinger, Techniques for Constraining the Abundance of Non-planetary Substellar Objects, Res. Notes AAS **4**, 129 (2020)

[7] J. Auffinger, I. Masina, G. Orlando, Bounds on warm dark matter from Schwarzschild primordial black holes, Eur. Phys. J. Plus **136**, 261 (2021), arXiv:2012.09867 [hep-ph]

[8] A. Arbey, J. Auffinger, M. Geiller, E. R. Livine, F. Sartini, Hawking radiation by spherically-symmetric static black holes for all spins. I. Teukolsky equations and potentials, Phys. Rev. D **103**, 4010 (2021), arXiv:2101.02951 [gr-qc]

[9] A. Arbey, J. Auffinger, B. Shams Es Haghi, P. Sandick, K. Sinha, Precision calculation of dark radiation from spinning primordial black holes and early matter-dominated eras, Phys. Rev. D **103**, 3549 (2021), arXiv:2104.04051 [astro-ph.CO]

[10] A. Arbey, J. Auffinger, M. Geiller, E. R. Livine, F. Sartini, Hawking radiation by spherically-symmetric static black holes for all spins. II. Numerical emission rates, analytical limits, and new constraints, Phys. Rev. D **104**, 4016 (2021), arXiv:2107.03293 [gr-qc]

[11] A. Arbey, J. Auffinger, Physics Beyond the Standard Model with BlackHawk v2.0, Eur. Phys. J. C **81**, 910 (2021), arXiv:2108.02737 [gr-qc]

[12] J. Auffinger, Limits on primordial black holes detectability with Isatis: A BlackHawk tool, Eur. Phys. J. C **82**, 384 (2022), arXiv:2201.01265 [astro-ph.HE]

[13] J. Auffinger, Primordial black holes and Hawking radiation constraints – a review, *Submitted to Prog. Part. Nucl. Phys.*, arXiv:2206.02672 [astro-ph.CO]

Conferences & Seminars

[1] Beyond General Relativity, Beyond Cosmological Standard Model; Warsaw, Poland, July 1-5, 2019

[2] Seminar given at HEPHY; Vienna, Austria, October 29th, 2019

[3] Cosmology WG meeting, GdR Gravitational Waves; Paris, France, November 13th, 2019

[4] Seminar given at IAP; Paris, France, January 30th, 2020

[5] Seminar given at IP2I; Lyon, France, September 25th, 2020

[6] TOOLS 2020: Tools for High Energy Physics and Cosmology; Lyon, France, November 2-6, 2020

[7] Seminar given at IAP; Paris, France, January 11th, 2021

[8] PPC 2021: XIV International Workshop on Interconnections between Particle Physics and Cosmology; Oklahoma, USA, May 17-21, 2021

[9] Pheno 2021: Phenomenology 2021 Symposium; Pittsburgh, USA, May 24-26, 2021

[10] PASCOS 2021: 26th International Symposium on Particles, Strings & Cosmology; Daejeon, Korea, June 14-18, 2021

[11] EPS-HEP 2021: European Physical Society conference on High Energy Physics 2021; Hamburg, Germany, July 26-30, 2021

[12] Seminar given at IP2I ("PhD day"); Lyon, France, October 26th, 2021

[13] IRN Terascale meeting; Clermont-Ferrand, France, November 22-24, 2021

[14] TOOLS 2021: Computational Tools for High Energy Physics and Cosmology; Lyon, France, November 22-26, 2021

[15] ILGQS: International Loop Quantum Gravity Seminar; online, February 8th, 2022

Other work

[1] J. Auffinger, G. Laibe, Linear growth of streaming instability in pressure bumps, Mon. Not. Roy. Astron. Soc. **473**, 796 (2018)

[2] A. Arbey, J. Auffinger, Detecting Planet 9 via Hawking radiation, arXiv:2006.02944 [gr-qc]

[3] J. Auffinger, A. Arbey, BlackHawk: A tool for computing Black Hole evaporation, *PoS* TOOLS2020, 024 (2021), arXiv:2012.12902 [gr-qc]

[4] A. Arbey, J. Auffinger, AlterBBN, *PoS* TOOLS2020, 032 (2021)

[5] A. Arbey, J. Auffinger, J. Silk, Primordial Kerr Black Holes, *PoS* ICHEP2020, 585 (2021), arXiv:2012.14767 [astro-ph.CO]

[6] A. Arbey, J. Auffinger, M. Geiller, E. R. Livine, F. Sartini, Hawking radiation of non-standard black holes, *PoS* EPS-HEP2021, 066 (2022)

[7] J. Auffinger, A. Arbey, P. Sandick, B. Shams Es Haghi, K. Sinha, Dark radiation constraints on light primordial black holes, *PoS* EPS-HEP2021, 147 (2022), arxiv:2201.04946 [astro-ph.CO]

[8] J. Auffinger, A. Arbey, Beyond the Standard Model with BlackHawk v2.0, *PoS* CompTools2021, 017 (2021), arXiv:2207.03266 [gr-qc]

Contents

Introduction

Primordial black holes (PBHs) have attracted considerable attention from the time of their theoretical proposal in the late 1960's and early 1970's to the recent period of BH observations by gravitational wave (GW) events. PBHs form in the early universe, at the end of the inflation era, and not from the usual collapse of stars. Thus, they can span a very wide range of masses, from the Planck scale to the mass enclosed in the Hubble horizon of the present universe, depending on their formation mechanism.

Constraints on the PBH abundance then provide invaluable access to the conditions of the early universe, such as its homogeneity and equation of state. The non-definitive observation of PBHs so far places strong limits on the cosmological history of the universe.

PBHs are most interesting because their mass density can contribute to the missing "dark matter" (DM) density of the universe. Indeed, PBHs are non-baryonic if they formed before Big Bang Nucleosynthesis (BBN), and they behave as cold DM (CDM). The very simple nature of PBHs makes them a perfect CDM candidate.

The possible very small mass of PBHs has led Hawking to explore their quantum properties. The proposal of "Hawking radiation" (HR), namely the phenomenon by which "black holes" emit a quasi-thermal flux of particles, has revolutionized the thermodynamics approach to BHs in the 1970's. HR is based on semi-classical general relativity, where fields are treated quantum mechanically on a classical metric background. It has also a trivial consequence: all BHs lose mass continuously and may finally disappear in an evanescence mechanism whose complete description requires a full quantum gravity theory.

Since it has been shown that BHs emit quasi-thermally all particles in the "spectrum of Nature", people have tried to extract a PBH signal from the observational data, without success so far. This absence of signal has been interpreted as a constraint on the PBH abundance over a wide span of masses, in the lower mass range. Indeed, the power emitted by a BH evaporation is inversely proportional to its mass squared. Thus, PBHs with planetary (upward) mass have so faint a radiation spectrum that the background HR can be neglected altogether. However, PBHs with an initial mass of that of an asteroid would be ending their evaporation in the present epoch, filling the universe with energetic radiation. Even lighter PBHs would have already disappeared.

Thus, PBHs can be divided into three categories. Those with small masses that already evaporated, those with asteroid mass that produce high energy radiation at the present epoch, and those with high masses that have negligible HR. Only the two first categories can be constrained by HR, which is the focus of this thesis work, while only the two last can contribute to the DM density, if one puts aside putative Planck mass stable remnants at the end of evaporation.

The PBH HR impact on cosmology is diverse and depends on the period of evanescence, on the type and energy of fields emitted and on the interactions between these fields and the ambient material. Thus, precise calculation of the PBH constraints with HR requires that all ingredients are assessed correctly. The HR rate was computed numerically in the 1970's, and the behaviour of the emitted material was convolved with Standard Model (SM) particle physics in the 1990's. When this thesis work started, modern numerical tools to obtain the HR rates were nowhere to be found. That is why, from the beginning, this thesis relied on the development of a public code named `BlackHawk`, that would compute the HR of PBHs to improve upon previous studies. This code has met its community and is now used by a wide range of teams around the globe, for both theoretical

and experimental prospects of PBHs. With my thesis director A. Arbey, and many collaborators, we have used it thoroughly to derive new interesting results and constraints on PBHs. The code is continuously updated and enhanced with new features, which represents a major part of my work.

`BlackHawk` allows to compute precisely the HR rates for non-standard PBHs, beyond SM (BSM) particles, and extended mass and angular momentum distributions. The pre-existing constraints on PBHs generally did not take these subtleties into account, so this thesis work represents a great step forward to a precision era in PBH studies.

Outline. In this manuscript, I present the results I obtained with `BlackHawk` in various contexts. All the results presented below have already been published, see the list in the Preamble. In Chapter 1, I review the history of the PBH paradigm, placed in a standard cosmological model. The PBH formation is briefly described, with particular focus on the extended mass and angular momentum distributions. In Chapter 2, I review the history of HR, in the context of the SM of particle physics. I give all the fundamental equations and present example plots of particle spectra from BHs with different (non-standard) geometries. I also discuss in detail the BH evolution and the case of extended distributions. In Chapter 3, I present the code `BlackHawk` and list some of its major features and options. The output is described, as well as the numerical methods used to compute the HR rates. Chapter 4 is the main part, as I give there all the new constraints on PBHs I obtained using `BlackHawk`. I first review the state-of-the-art constraints. Second, I present the `BlackHawk` tool `Isatis` designed to compute automatically precise PBH constraints from HR, applied to the standard Schwarzschild BH case. Third, I give new constraints in the rotating Kerr case for both PBHs evaporating now and in the early universe, contributing to the γ-ray background and the dark radiation (DR). Fourth, I explore the consequences of direct DM emission by PBHs before BBN. Last, I give an application of `BlackHawk` to the case of non-standard HR constraints based on loop quantum gravity. I finally conclude with some general prospects on PBHs, HR and my personal thoughts about modern science. Supplemental material is given in the Appendices: Appendix A provides the basic commands to compile and launch the code and a complete list of the publications using `BlackHawk`; in Appendix B I give PBH-related works performed during this thesis, namely a study on inhomogeneous BBN, and more speculative results on the hypothesis that Planet 9 is a PBH and that PBHs may be captured by stellar systems.

Note to the reader. The bibliography of this thesis work is very extensive due to two reasons. First, I have performed very diverse studies, with the common thread of PBH constraints and HR. I have worked on (P)BHs from both the theoretical and experimental point of view; I have studied PBH evaporation in the early and present universe; I have focused on extended mass and angular momentum distributions; and I have broadened the existing constraints to non-standard particle physics and BH geometries. With the addition of BBN and planetary physics discussed in the Appendices, a great part of cosmology and astrophysics is encountered in this manuscript. Second, I have written a review article precisely on the subject of PBH HR constraints. This led me to perform a complete historical overview of the related papers, and I included some of these discussions in the present manuscript.

Throughout this manuscript, I use a natural system of units defined by $G = \hbar = c = k_{\rm B} =$

$4\pi\epsilon_0 = 1$, and the metric signature $(-+++)$, unless stated otherwise. This manuscript has been typesetted using a modified `Rev-Tex 4.2` bibliography style with modified macros from ADS/NASA (norm ISO 4). Throughout this manuscript, I use several acronyms which are listed in the Table below, by alphabetical order.

acronym	meaning	acronym	meaning
BBN	big bang nucleosynthesis	PHL	Page–Hawking limit
BH	black hole	PMR	Planck-mass remnant
BHD	black hole domination	PSD	phase-space distribution
BSM	beyond the Standard Model	QCD	quantum chromodynamics
CDM	cold dark matter	QED	quantum electrodynamics
CMB	cosmic microwave background	QNM	quasi-normal mode
CL	confidence level	RD	radiation domination
CR	cosmic ray	RN(BH)	Reissner–Nordström (black hole)
CSSO	compact sub-stellar object	S(BH)	Schwarzschild (black hole)
DM	dark matter	SM	Standard Model (of particle physics)
d.o.f.	degree(s) of freedom	SMBH	supermassive black hole
DR	dark radiation	SNR	signal-to-noise ratio
EGXB	extragalactic γ/X-ray background	TNO	trans-Neptunian object
EM	electromagnetic	TOV	Tolman–Oppenheimer–Volkov
EMDE	early matter domination era	TPC	trans-Planckian conjecture
EW	electroweak	UCMH	ultra-compact mini halo
FLRW	Friedmann–Lemaître–Robertson	WDM	warm dark matter
	–Walker	WIMP	weakly interacting massive particle
f.o.v.	field of view		
GC	Galactic center		
GF	greybody factor		
GO	geometrical optics		
GRB	γ-ray burst		
GUT	grand unified theory		
GW	gravitational wave		
HD(BH)	higher-dimension (black hole)		
HR	Hawking radiation		
ISM	interstellar medium		
K(BH)	Kerr (black hole)		
LOS	line of sight		
LQG(BH)	loop quantum gravity (black hole)		
MD	matter domination		
MG&W	MacGibbon & Webber		
NFW	Navarro–Frenck–White		
PDM	particle dark matter		

Chapter 1

Primordial black holes

Contents

In this Chapter, I briefly go through the standard cosmological model in Section 1.1 and I draw a historical review of primordial black hole ideas in Section 1.2. Then, I present the basic features of primordial black hole formation in Section 1.3. The primordial black hole constraints will be treated in the last Chapter 4.1.

1.1 Standard cosmological model

The standard cosmological model is a theory of the history of the universe developed since the late 1920's.[1] For a historical account of what is shortly addressed below, see Ref. [1] (and references therein). For the more involved technical aspects, see Ref. [2] (and references therein). It was first discovered that the nebula in which we are is not the only one in the universe, but there are also remote objects that are not part of it. Hence, the universe can be described as a collection of galaxies with a great variety of shapes, separated by huge voids. The luminosity of these nebulae were measured and it was discovered that they move away from the Earth with a Doppler shift that increases with their distance. This law, denoted as the Hubble law, can be written

$$v = H_0 D \,, \tag{1.1}$$

where v is the remote galaxy speed, D is its absolute distance and H_0 is the Hubble parameter today. Hence, all galaxies seem to move away from all others. This was interpreted as a direct clue that the universe is in expansion [3] (see also [4]). It seemed a more reasonable deduction than to assume that our galaxy occupies a preferred spot in the universe and that we should lie in the exact center of a past explosion dispersing the galaxies. The expansion of the universe is described by a quantity called the redshift z, which is a measure of the Doppler dilution of the radiation wavelength with the expansion. Let $D(t)$ be some measure of distance at cosmological time t, then at time t'

$$\frac{D(t')}{D(t)} = \frac{1+z(t)}{1+z(t')} \,. \tag{1.2}$$

The tensorial Einstein equations of general relativity, which must be used to describe the link between the universe density content and its gravitational dynamics (expressed in terms of curvature), are

$$G_{\mu\nu} + \Lambda g_{\mu\nu} = 8\pi T_{\mu\nu} \,, \tag{1.3}$$

where the Einstein tensor $G_{\mu\nu} \equiv R_{\mu\nu} - \frac{1}{2} R g_{\mu\nu}$ is a combination of the Ricci tensor $R_{\mu\nu}$ and of the Ricci scalar R (thus a curvature-related quantity), $T_{\mu\nu}$ is the stress-energy tensor (thus a density-related quantity) and $g_{\mu\nu}$ is the space-time metric. The content of the universe in terms of energy density hence causes the curvature of the space-time metric; inversely the features of the space-time metric cause a displacement of the energy density. The quantity Λ is a "cosmological constant" that must be added in full generality. These field equations admit a lot of interesting solutions. Any such solution can be expressed with the infinitesimal space-time element $\mathrm{d}s^2$ as

$$\mathrm{d}s^2 \equiv g_{\mu\nu}\mathrm{d}x^\mu = g_{tt}\mathrm{d}t^2 + g_{rr}\mathrm{d}r^2 + g_{\theta\theta}\mathrm{d}\theta^2 + g_{\varphi\varphi}\mathrm{d}\varphi^2 \,, \tag{1.4}$$

in 3D Boyer-Lindquist coordinates (this set of spherical coordinates will prove convenient).

Considering that the universe is an isotropic and homogeneous collection of galaxies, that can be approximated on sufficiently large scales by a homogeneous density distribution, the metric coefficients g_{ii} should only be functions of r and t (isotropy condition) satisfying further the homogeneity

[1] This introductory Section is based in part on the recent book by Peebles "Cosmology's Century: An Inside History of our Modern Understanding of the Universe" [1] and that of P. Peter & J. P. Uzan "Cosmologie primordiale" [2].

fluid	equation of state
matter	$w = 0$
radiation	$w = 1/3$
cosmological constant	$w = -1$
curvature	$w = -1/3$

Table 1.1: Equation of state $P = w\rho$ for different cosmological fluids.

condition. Friedmann, Lemaître, Robertson & Walker (FLRW) independently found the general solution to the Einstein equations. The FLRW metric solution is

$$\mathrm{d}s^2 = -\mathrm{d}t^2 + a(t)\left(\frac{1}{1-kr^2}\mathrm{d}r^2 + r^2\mathrm{d}\Omega^2\right), \tag{1.5}$$

where $\mathrm{d}\Omega^2 \equiv \mathrm{d}\theta^2 + \sin^2\theta\mathrm{d}\varphi^2$ is the solid angle element. There are 2 free parameters in this equation:

- k is a general curvature term (independent of the local density content of the universe), which can be reduced without loss of generality to 3 values $k \in \{-1, 0, 1\}$, corresponding respectively to an open hyperbolic universe, an open flat universe, and a closed universe.
- $a(t)$ is the scale factor of the universe, describing its general size evolution; it is related to the redshift by
$$\frac{a(t)}{a(t')} = \frac{1+z(t')}{1+z(t)}, \tag{1.6}$$
and to the Hubble parameter by
$$H(t) \equiv \frac{\dot{a}}{a}. \tag{1.7}$$

Injecting this solution back into the Einstein equations, and using the energy conservation law, one obtains 2 independent equations referred to as the Friedmann equations

$$\begin{cases} \left(\dfrac{\dot{a}}{a}\right)^2 = H^2 = \dfrac{8\pi}{3}(\rho + \rho_k + \Lambda), \\ \dfrac{\ddot{a}}{a} = -\dfrac{4\pi}{3}(\rho - 2\Lambda + 3P), \end{cases} \tag{1.8}$$

In these equations, ρ and P are the energy density and pressure of the universe (for matter and radiation), and $\rho_k \equiv -3k/8\pi a^2$ is an equivalent curvature density. The equations of state $P = w\rho$ for some particular fluids are given in Table 1.1.

Under the assumption that the universe is globally flat, $k = 0$, the Friedmann equations depend only on the density of the universe, that is the matter and radiation content (plus an eventual cosmological constant). Hence, with the observation that the universe is in expansion, rewinding the film backwards makes it collapse to a singular size. The Friedmann equations then predict that the early universe would be denser and hotter than the contemporary one: radiation behaves as

$\rho_{\rm R} \propto a^{-4}$ and baryonic matter as $\rho_{\rm B} \propto a^{-3}$; so that $\rho \underset{a,t\to 0}{\longrightarrow} +\infty$. This behaviour gave rise to a model called the "hot Big Bang" model, with a density-temperature singularity at $t \to 0$. Let's define at this point the cosmological fraction of some fluid f of density $\rho_f(t)$

$$\Omega_f(t) \equiv \frac{\rho_f(t)}{\rho_{\rm c}(t)}\,, \tag{1.9}$$

where $\rho_{\rm c}(t) \equiv 3H(t)^2/8\pi$ is the critical density. This fraction evolves with time, thus hereafter when no time dependency is mentioned it is assumed that $t = t_0$, the age of the universe.

I now assume that the universe began some long time ago in a very hot and dense state and then expanded until reaching its current state. One cannot expect to describe what happened at times before the Planck time $t \lesssim t_{\rm Pl}$ as that would necessitate quantum corrections to general relativity that are beyond the scope of this thesis. As the universe expands, it cools down and it should be expected that its temperature passes progressively from the Planck temperature down to the observed very cool universe temperature today. This cooling down would be accompanied by transitions in the composition of the universe. When $T \sim \Lambda_{\rm EW} \sim 45\,{\rm GeV}$, an electroweak (EW) phase transition should occur where the Higgs symmetry should be broken and the particles acquire their mass. At lower temperatures $T \sim \Lambda_{\rm QCD} \sim 100 - 300\,{\rm MeV}$, the quantum chromodynamics (QCD) of quarks and gluons should coalesce into hadrons (baryons and mesons), that is hadronization. Then, EW interactions should freeze out and neutrinos should decouple from the rest of the plasma. The nucleons remain the only long-lived hadrons. The relation $\mathrm{p} \longleftrightarrow \mathrm{n}$ freezes out just before nuclear fusion reactions become effective: nucleons fuse into light nuclei with a complex set of nuclear reactions, continuously making and breaking new elements, until these reactions freeze out too. Only stable nuclei escape the nuclear era called "Big Bang nucleosynthesis" (in opposition with stellar nucleosynthesis which builds up heavier elements inside stars). The universe is still very hot, but cools down enough that the matter density, diluting only as $\rho \propto a^{-3}$, end up dominating the initially far more denser radiation bath. After this matter-radiation equality that separates radiation domination (RD) from matter domination (MD), matter only drives the expansion of the universe in the Friedmann equations. The universe is composed of nuclei and free electrons, totally ionized because of the hot radiation temperature. Later, the photons decouple from the nuclei and electrons which bind to form neutral atoms. This first light from photon emission by free electron capture by protons (emitted at 13.6 eV) is called the "cosmic microwave background" (CMB) and is a distinct signature of this model. "Microwave" because as the universe cools down, this background light is redshifted from 13.6 eV down to radio wavelengths, following the Friedmann equations. This is when structures should start to form (galaxies, clusters of galaxies). Inside these first lightless structures (this is the "Dark Ages"), clouds of gas should gravitationally collapse and the first Population III (Pop III) stars should light up. Their light should then strongly reionize their environment. These stars are very massive and do not last for a long time, but explode in supernovae, giving rise to a second generation of Pop II stars, and then Pop I stars (the Sun is one of them) characterized by a high fraction of "metals", *i.e.* elements heavier than hydrogen built in previous generations of stars. In the clouds of dust and gas around these stars, instabilities should make the disk of material collapse into numerous planets and moons.

Here we are today, on the thin crust of a small rocky planet orbiting a Sun among billions of stars in a spiral galaxy among billions of others, in an ever expanding and cooling universe, wondering about the growth of trees and the randomness of the weather and pointing our ever more advanced instruments towards the depths of the sky. This story is roughly the "standard cosmological model".[2]

In the 1960's, some striking evidence were found that distinguished this rather complicated model from competing ones (constant generation of matter, static universe, *etc.*). Let me cite 3 of them:

- the microwave background was observed by Penzias & Wilson at a temperature of $\sim 3\,\mathrm{K}$ (the modern value is $\sim 2.7\,\mathrm{K}$);
- the power-law spectrum of the initial perturbations of the FLRW universe was predicted by Zel'dovich and Harrison;
- spectacular advance in nuclear reaction theories permitted to predict the yield of light elements from BBN, which corresponded remarkably well with observations.

This picture however suffers from some uncertainties. Nothing above explains why there should be only matter, in the form of baryons (and extremely few antibaryons) around us. This $\mathrm{B}/\overline{\mathrm{B}}$ asymmetry means that most of the initially equally produced baryons and antibaryons annihilated, producing a tremendous amount of radiation, but that some asymmetry caused the baryons to "win" with a baryon-to-photon number ratio of $\sim 10^{-9}$. This value accords very well with both the BBN and CMB observations. However, local variations could be possible if the universe was somehow inhomogeneous on small scales due to random fluctuations, resulting in small patches of different elemental composition. What caused this asymmetry is generally referred to as the "baryogenesis", namely the mechanism that produced the slight overdensity of baryons compared to antibaryons.

Then, it was observed that the CMB was surprisingly isotropic, even on scales that were not in causal contact in the far past. This pointed towards the possibility that the universe went through a period of rapid (exponential) inflation just after the Big Bang, maybe driven by a scalar inflaton field, ending with a reheating of the universe (the generation of all the initial radiation density) maybe caused by the decay of this very inflaton. Inflation would have broken the causal link between inhomogeneities, preventing them to distort the frame of the universe.

Most interestingly, the measure of the universe average density showed that the universe is globally flat, that is, its curvature is very close to $k = 0$ and thus its density is precisely the critical density ρ_c. However, galaxy counts, and the relation between galaxy luminosity and their stellar content, showed that there is approximately one order of magnitude difference between the average luminous density and the critical density. Furthermore, clusters of galaxy exhibit a gravitational dynamics that is once more in strong disagreement with the amount of luminous galaxies inside them [5, 6]. Finally, the measure of the rotation curves of galaxies showed that stars at the luminous fringes of spiral galaxies rotate with a velocity that would be expected if the galaxy contained much more mass than what is accounted for by inner gas clouds and stars. The same "missing/hidden

[2]For an even more approximate version, I refer the reader to the video "History of the world" by Bill Wurtz (available on YouTube).

mass"—understand non-luminous—ratio at these very different locations and scales of the universe was interpreted as an unknown general component of the universe called "dark matter" (DM).[3]

1.2 Historical overview

[4]Using only Newtonian mechanics, Laplace predicted a long time ago that if there were an object sufficiently dense that the escape velocity at its surface was faster than the speed of light, it would be totally black and absorb anything that would come gravitationally bound to it. That is precisely what a "black hole" would do. Schwarzschild was the first one to derive the solution of the spherically symmetric and static Einstein equations around a pointlike mass M in 1916 [9] (hereafter SBH, for Schwarzschild BH), right after Einstein published the general relativity framework

$$\mathrm{d}s^2 = -G(r)\mathrm{d}t^2 + \frac{1}{F(r)}\mathrm{d}r^2 + H(r)\mathrm{d}\Omega\,, \tag{1.10}$$

with

$$\begin{cases} F(r) = G(r) = 1 - \dfrac{r_\mathrm{S}}{r}\,, \\ H(r) = r^2\,, \end{cases} \tag{1.11}$$

and $r_\mathrm{S} \equiv 2M$ is the Schwarzschild radius, illustrated in Fig. 1.1. At space infinity, that is $r \gg r_\mathrm{S}$, the metric becomes asymptotically flat, and reduces to the Minkowsky metric

$$\mathrm{d}s^2 = -\mathrm{d}t^2 + \mathrm{d}r^2 + r^2\mathrm{d}\Omega^2\,, \tag{1.12}$$

which is the empty and flat solution to the Einstein equations. There is a singularity of the metric at $r = 0$, corresponding to a real curvature singularity as the Ricci scalar R goes to infinity, and a fake singularity (R is finite) at $r = r_\mathrm{S}$, which can be resolved by a change of coordinates. The singularity is an intricate problem, but the general relativity calculations show that the worldlines of free-falling objects toward the singularity exchange time and space characteristics precisely at $r = r_\mathrm{S}$, denoted as the BH horizon of events. Hence, any signal emitted from a probe that would have crossed the horizon would never reach an observer at infinity but remain enclosed in the BH. The interior of the BH horizon is causally separated from the exterior by the event horizon, which effectively hides away the metric singularity and satisfies the "cosmic censorship conjecture" [10] (CCC).[5] Interestingly, "invisible collapsed objects", (*i.e.* BHs), were proposed very early as a potential candidate for DM [11, 12], while other candidates are reviewed in Section 2.1.

The Maxwell equations were included in that framework to obtain the metric around a pointlike mass M with electric charge Q by Reissner and Nordström [13, 14] (hereafter RNBH, for Reissner–Nordström BH) with the metric coefficients

$$\begin{cases} F(r) = G(r) = 1 - \dfrac{r_\mathrm{S}}{r} + \dfrac{r_\mathrm{Q}^2}{r^2}\,, \\ H(r) = r^2\,, \end{cases} \tag{1.13}$$

[3]For a complete history of DM, I refer the reader to the book by Peebles [1] or to the more succinct review [7].

[4]This Section is partially inspired from the review article "Primordial black hole constraints with Hawking radiation – a review" [8] under writing.

[5]Resolution of the singularity problem in the context of BHs will be discussed further in Section 4.6.

where $r_Q \equiv Q^2$. This metric exhibits one real singularity at $r = 0$ and two fake coordinate singularities at

$$r_\pm \equiv r_\mathrm{S} \frac{1 \pm \sqrt{1 - Q^{*2}}}{2}\,, \tag{1.14}$$

where r_- is a Cauchy horizon and r_+ is the BH event horizon. $Q^* \equiv Q/M$ is the reduced (dimensionless) BH charge.

The case of a rotating BH with angular momentum $a \equiv J/M$, which is only axisymmetric, is more mathematically involved and was solved by Kerr in 1963 [15] (hereafter KBH, for "Kerr BH"). The metric is here

$$\mathrm{d}s^2 = \left(\mathrm{d}t - a\sin^2\theta \mathrm{d}\phi\right)^2 \frac{\Delta}{\Sigma} - \left(\frac{\mathrm{d}r^2}{\Delta} + \mathrm{d}\theta^2\right)\Sigma - \left((r^2+a^2)\mathrm{d}\phi - a\mathrm{d}t\right)^2 \frac{\sin^2\theta}{\Sigma}\,, \tag{1.15}$$

where $\Sigma(r) \equiv r^2 + a^2\cos^2\theta$ and $\Delta(r) \equiv r^2 - 2Mr + a^2$. The Cauchy and event horizons are located at

$$r_\pm \equiv r_\mathrm{S} \frac{1 \pm \sqrt{1 - a^{*2}}}{2}\,, \tag{1.16}$$

where $a^* \equiv a/M$ is the reduced (dimensionless) angular momentum or "BH spin".

The combination of these two solutions gives the Kerr–Newman metric around a charged, rotating mass [16, 17]. The horizons are located at $r_\pm = r_\mathrm{S}(1 \pm \sqrt{1 - Q^{*2} - a^{*2}})/2$. A comparison of the radii of a SBH with those of a KBH or RNBH for different values of a^* and Q^* is given in Fig. 1.2.

One immediately remarks that when $a^*, Q^* \to 0$, the SBH is recovered, while in the opposite limit $a^*, Q^* \to 1$, the Cauchy and event horizons radii collapse to the value $r_\mathrm{S}/2$. In this case, denoted as "extremal", the BH is ill-defined as the coordinate singularity at the BH center $r = 0$ is not hidden behind a horizon—the CCC is violated; this limit is shown as a black vertical line in Fig. 1.2.

BHs result in general from the collapse of some energy density inside its own Schwarzschild radius. At the end of its Main Sequence evolution, a large star's central nuclear engine shuts down after producing iron and the gravitation forces win against the failing nuclear reactions' radiation pressure. For a certain parameter space of stellar conditions, the star can collapse into a "stellar" BH (sometimes denoted as "astrophysical" BH). Tolman, and Oppenheimer & Volkoff [18, 19] (TOV) derived a limiting inferior mass for these BHs that is $M_\mathrm{TOV} \sim M_\odot$ (modern studies give $M_\mathrm{TOV} \sim 2\,M_\odot$ [20]). Upper limits on their mass are more dubious but it is generally not expected that genuine stellar mass BHs of more than $\sim 100\,M_\odot$ can form. Nowhere else in the present universe is there standard matter denser than the interior of stars.

However, as explained in Section 1.1, the universe was order of magnitudes denser in the past. Then, it is not unimaginable that in the early universe, patches of the universe which were overdense relatively to the average density due to some statistical fluctuation collapsed into early non-stellar BHs. These are generally denoted as "primordial black holes". The very first mention of PBHs dates back to 1966: Zel'dovich & Novikov, in a paper entitled "The hypothesis of cores retarded during expansion and the hot cosmological model" [21], spoke about "retarded cores" [22] whose evolution,

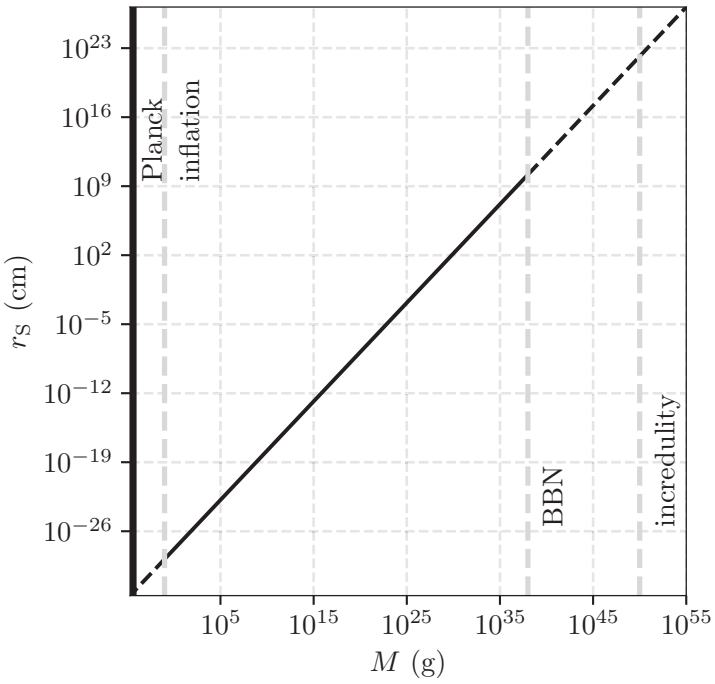

Figure 1.1: Radius of a SBH as a function of its mass for the SBH. The vertical solid line at $M = M_{\rm Pl}$ represents the TPC, the vertical dashed line at $M \sim 0.1\,$g represents the inflation limit, the vertical dashed line at $M \sim 10^{38}\,$g represents the BBN limit and the vertical dotted line at $M \sim 10^{50}\,$g represents the "incredulity limit".

because of gravitational collapse, would escape the overall expansion of the universe, and describe these cores to have radius $R < 2M$ which is precisely the radius of a SBH.

This original idea seems to have gone quite unnoticed[6] until Hawking published the paper "Gravitationally collapsed objects of very low mass" [23]. The idea was fundamentally the same as Zel'dovich & Novikov, *i.e.* large perturbations collapsing after inflation inside their Schwarzschild radius to give BHs (explicitly named here). The collapse was described as a classical process, hence a lower limit was imposed on the mass of the BH formed $M > M_{\rm Pl} \sim 2 \times 10^{-5}\,$g for general relativity to be valid. Hawking further proposed a bound on the number of these collapsed objects by considering the "deceleration" of the expansion of the universe measured at that time, that gave an estimation of the average mass density of the universe to be $\rho \sim 10^{-28}\,$g, whereas the observed abundance of "visible" matter was $\rho_{\rm vis} \sim 10^{-31}\,$g. Hawking concluded this argument by stating that:

[6]The Zel'dovich & Novikov paper, while translated in English, was originally published in a Russian journal. A lot of cosmology/BH related ideas from the Cold War period encountered while redacting the review [8] were published independently both by Russian and American cosmologists, and it appears by simple citation check that the Russian papers were mostly cited by Russian researchers and *vice versa*.

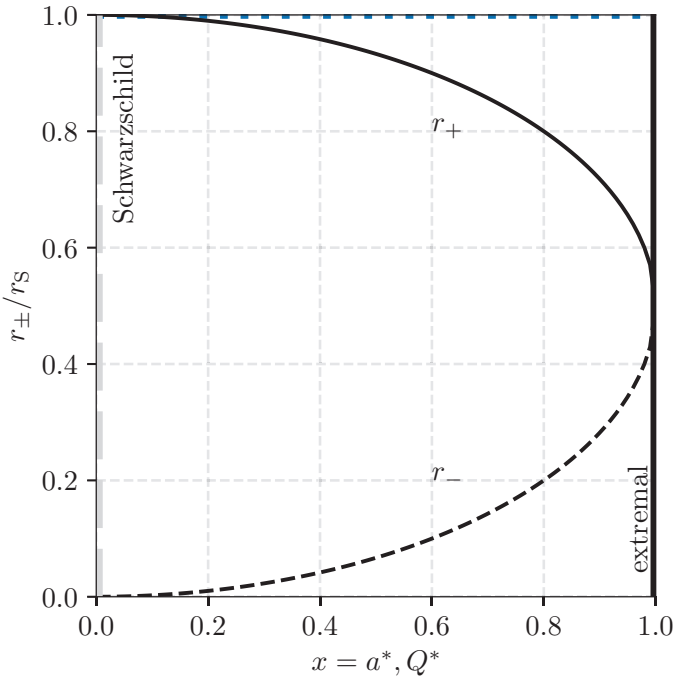

Figure 1.2: Event (solid) and Cauchy (dashed) horizons radii $r_\pm$ normalized to the Schwarzschild radius (dotted) r_S for a KBH ($x = a^*$) and RNBH ($x = Q^*$). The vertical line at $x = 0$ represents the Schwarzschild limit and the vertical solid line at $x = 1$ represents the extremal limit.

> *[. . .] it is tempting to suppose that the major part of the mass of the Universe is in the form of collapsed objects. This extra density could stabilize clusters of galaxies which, otherwise, appear mostly not to be gravitationally bound.* [23]

The smallest of these BHs, with Schwarzschild radius smaller than a nucleus, could be constantly traversing compact objects like the Earth without leaving any trace.

Some years later, Carr & Hawking returned to the examination of the accretion argument from Zel'dovich & Novikov to see if the early BH production was a viable scenario [24]. It was shown in this paper that catastrophic accretion should not occur but take place at a rate far slower than the expansion of the universe, however:

> *The obvious place to look for such giant black holes* [that would have accreted rapidly] *would be in clusters of galaxies where they might provide the missing mass necessary to bind clusters gravitationally.* [24]

These claims, together with that of [11, 12], constituted the prelude of the "DM = PBHs" scenario.

1.3 Primordial black hole formation

[7]Carr & Hawking [24] first quantitatively described the process of PBH formation, which was numerically computed in [26] (for a recent review, see [27]). A region of locally enhanced density can collapse if its radius is smaller than the associated Jeans length. The collapse must supplant the pressure forces (which depend on the equation of state of the cosmological fluid) and the universe expansion.

At time t, the collapsing region must be of order of the particle horizon size $\propto H(t)^{-1}$ for causal reasons. This is the *standard scenario*, which relies on the assumption that there was a spectrum of primordial inhomogeneities. Modern calculations show that in this scenario a PBH formed during radiation domination (RD) has an initial mass M_i linked to its formation time t_f by [25]

$$M_\mathrm{i}(t_\mathrm{f}) = \frac{\gamma}{2H(t_\mathrm{f})} \sim 10^{15}\,\mathrm{g}\left(\frac{t_\mathrm{f}}{10^{-23}\,\mathrm{s}}\right), \tag{1.17}$$

where γ is a parameter linked to the collapse mechanism. For spherical collapse during RD, $\gamma \sim 0.2$ [28]. In the usual model of PBH formation, PBHs form after the inflation period, hence there is an inferior limit on the size of the particle horizon derived from CMB observations $H(t_\mathrm{f})^{-1}$ [29] translating into an inferior limit on the mass of PBHs

$$M_\mathrm{min} \sim 0.1\,\mathrm{g}\,. \tag{1.18}$$

However, this constraint applies only to conventional inflationary scenarios, *i.e.* the standard slow-roll models of inflation with Einstein gravity (see *e.g.* the review [30] and references therein). In more sophisticated scenarios, like *e.g.* the recent model [31], the scale of inflation can not be determined by CMB observations. An absolute lower limit on the PBH mass is the Planck mass M_Pl at which quantum gravity effects should be sizeable and our understanding of general relativity collapses. PBHs forming with size smaller than the Planck length $\ell_\mathrm{Pl} \sim 10^{-35}\,\mathrm{m}$ would have formed at times before the Planck time $t_\mathrm{Pl} \sim 10^{-43}\,\mathrm{s}$ which is forbidden by the recently proposed trans-planckian conjecture [32] (TPC).

An upper limit on the mass of PBHs at formation can be derived from the fact that they should form before the onset of BBN for them not to spoil the baryon-to-photon ratio

$$M_\mathrm{BBN} \sim M(t_\mathrm{f} \approx 1\,\mathrm{s}) \sim 10^5\,M_\odot\,. \tag{1.19}$$

There are also trivial coherence reasons to believe that there is no giant PBH of $M \gtrsim M_\mathrm{incr} \sim 10^{50}\,\mathrm{g}$ occupying most of the Hubble sphere today, first because there are other complex structures in the sky, second because if there were a giant PBH, we would be falling onto it due to its gravitational attraction and would see a strong Doppler dipole feature in the CMB [33, 34]. The limits M_Pl, M_min, M_BBN and M_incr are represented by vertical lines on Fig. 1.1.

The list of PBH formation scenarios is extensive, and I refer the reader to the recent reviews [28, 35] for a complete description. They include:

[7]This Section is partially inspired by the paper "Bounds on warm dark matter from Schwarzschild primordial black holes" [25] I wrote with I. Masina and G. Orlando.

- collapse of primordial overdensities (the *standard scenario*) (see *e.g.* [27] for a modern assessment);[8]
- collapse of inflaton fields;
- collapse of topological defects;
- collapse from bubble collision due to an early first order phase transition.

In particular, some formation mechanisms (*e.g.* grand unified theory—GUT—phase transition) explain both PBH formation and later cosmological events (*e.g.* PBH baryogenesis mediated by GUT bosons [36]); and "failed" PBH collapse can be at the origin of inhomogeneous BBN (see Appendix B.1). In general, an alternative cosmological model results in very different PBH constraints [37]. Of interest for me here is the fact that some of these formation mechanisms imply an EMDE (Section 1.3.1), or result in extended PBH mass (Section 1.3.2) or spin distributions (Section 1.3.3).

1.3.1 Formation of PBHs during an EMDE

Formation of PBHs during an EMDE (denoted as "dust phase") driven by metastable particles was reviewed in detail in [38]. It was shown that PBH formation is easier in this case due to reduced pressure forces, and that the relationship between a PBH mass and its formation time, as well as the link between the fraction of PBHs at formation and at evaporation are deeply connected to the "dust phase" parameters:

> *The PBH spectrum is a link between all the astrophysical data that have the nature of restrictions on the PBH spectrum and the unified gauge theory parameters that determine the spectrum of the initial perturbations and the parameters of the dust stages.* [38]

These constraints depend on the EMDE parameters and are in general weaker than the corresponding RD constraints [39]. More recent studies of PBHs formed during an EMDE have been performed by [40–46], with a focus on long-lived PBHs existing in the current universe, and their interplay with DM physics.

1.3.2 Mass distributions

One prominent feature of the seminal review of PBH constraints by Carr [47] is the use of the Press–Schechter formalism [48] designed for scale-invariant perturbations in the early universe and the formation of structures. Carr predicted that the mass spectrum of PBHs should be in general a power-law with exponent $\mathrm{d}n \propto M^{-f(w)}\mathrm{d}M$ where $f(w)$ is some function of the equation of state parameter $P = w\rho$ and where the collapse into a PBH happens once the density perturbation exceeds

[8] This scenario seems deprecated due to the tremendous increase of the fluctuation spectrum needed at small scales compared to the CMB (see the very explicit Fig. 1 of [35]). This has motivated more exotic formation scenarios, and refutes the usual claim that PBH DM is compelling because it does not require new physics.

some threshold $\Delta\rho/\rho > \delta$. In the RD era of the hot Big Bang model, one obtains $f(w) = 5/2$. This exponent should be modified for PBH formation during an EMDE.

Hence, the mass spectrum of PBHs was originally believed to be *extended* and to span a rather large range of masses (from $M_{\rm Pl}$ upward). This link between primordial scale-invariant fluctuations of density and the PBH abundance shows that:

> *PBHs are unique since they alone could be expected to survive the dissipative effects which erase all other imprints of conditions in the first second of the universe.* [47]

The monochromatic distribution of PBHs often used to derive abundance constraints is then only a convenient approximation to a more realistic extended mass distribution. This poses the *mathematical* question of how to convert the constraints obtained for monochromatic mass distributions to extended ones?

Yokoyama [49] was the first, to my knowledge, to try and use an analytical procedure of conversion. This followed the discovery of the critical behaviour of the PBH collapse process by Niemeyer & Jedamzik [50, 51]. The critical collapse mechanism can lead to the formation of PBHs with mass $M < M_{\rm hor}$; hence at each cosmological epoch, a distribution of PBHs masses would arise. The total distribution would then be the sum of these instantaneous formations. Yokoyama observed that there is not much change in the constraints, except in the $M \gtrsim 10^{15}\,$g mass range, because of the steep fall-off of the critical collapse spectrum. This computation showed however that using an extended mass function can *broaden* the excluded PBH parameter space.

At about the same time [52], calculations showed that a monochromatic peak in the primordial fluctuation power spectrum results in fact in a log-normal PBH mass distribution, centered around the characteristic horizon scale at formation. This distribution was further refined using peak theory [53, 54]. In fact, a Gaussian log-normal function can mimic any peak in the PBH distribution resulting from a particular mechanism of formation [55]. The most common PBH mass distributions are described *e.g.* in [56].

Concerning conversion methods, pioneering analytical and numerical work was done in [56–60], which confirmed that the constraints on an extended distribution should be more stringent than the expected constraint resulting from the addition of monochromatic ones. This contradicted the claims of [61, 62] arguing that extended mass functions could simply be "fitted inside the holes" of the constraint plot given below in Fig. 4.1.[9] For HR constraints, I advocate the use of `BlackHawk` which can directly compute the full HR spectrum for any PBH distribution *before* applying the constraints. Constraints for an extended mass distribution are discussed below in Section 4.3, while the `BlackHawk` literature is listed in Appendix A.2.

1.3.3 Spin distributions

PBHs formed during RD are believed to have negligible spin [63], which has also been proven for the critical collapse mechanism [64]. On the other hand, PBHs formed during an EMDE could have sizeable to near-extremal spin [41, 65–67]. In any case, *some* of the PBHs should form with a

[9] The "fitting" method was still defended during the 2018 CERN TH Institute "Primordial vs. Astrophysical origin of black holes".

significant spin [68], and PBHs can also be spun up either through early accretion processes [69] or through hierarchical mergers [70].

The problem is then the same as for extended mass distributions. The constraints on SBHs could be converted to KBHs using some analytical procedure; or realistic extended spin distributions could be reduced to their peak/average value [71]. I instead advocate the use of the `BlackHawk` capacity to simulate extended distributions of *both* mass and spin to compute accurate constraints. Constraints for spinning PBHs are discussed below in Sections 4.3 and 4.4, while the `BlackHawk` literature is listed in Appendix A.2.

Chapter 2

Hawking radiation

Contents

In this Chapter, I briefly go through the Standard Model of particle physics in Section 2.1 and I draw a historical review of the Hawking radiation paradigm in Section 2.2. Then, I present the basic equations of Hawking radiation in Section 2.3 and obtain the primary and secondary emission spectra in Sections 2.4 and 2.5. I mention the results for extended mass distributions in Section 2.6. I deduce the primordial black hole evolution due to the Hawking process in Section 2.7.

2.1 Standard Model of particle physics

[1]The Standard Model of particle physics (SM) is the theory that describes the fundamental particles and their interactions. The idea that the material world can be divided into fundamental indivisible species dates back to Antiquity. However, it is only at the end of the XIX$^{\text{th}}$ century that this theory acquired a predictive power with the discovery of the charged electron. The photon as a carrier of light energy was known for a long time, but its behaviour as a quanta was exposed only with the photoelectric effect. Afterwards, chemistry and nuclear physics experiments have put in evidence the structure of the atom, with a nucleus composed of protons (charged, stable) and neutrons (unstable). The structure of matter revealed itself as the experiments increased in energy, with a collision at energy E probing a fundamental scale of size $L \sim E^{-1}$. Neutrinos were predicted in the 1930's to explain the characteristics of the β decays, at the same epoch when the muons (a second family of charged lepton with the electron) were observed in cosmic rays (CRs) and the graviton was predicted to mediate the gravitational interaction. The theory of Maxwell describing the electromagnetic (EM) interactions was quantized in the 1950's in a model called quantum electrodynamics (QED). In the 1960's, the theory of the weak interaction describing the same β-decay of nuclei gave rise to the Glashow–Weinberg–Salam model of the EW interactions, in the first unification of two fundamental interactions (QED and weak interaction). The development of particle accelerators in the late 1950's–1970's resulted in the production of numerous particles in detectors with a mass spectrum very dense above an energy scale of some hundreds of MeV. To explain this matter of fact, two models were in competition at that time:

- the "Hagedorn model" that predicted an exponential explosion of the number of degrees of freedom (d.o.f.) above that energy scale [73–75];
- the "Gell-Mann model" that systematically described the observed particle states as a combination of a finite number of 3 flavors of quarks and 8 mediating gluons [76], in a theory called quantum chromodynamics (QCD).[2]

In the 1960's, the Higgs field was finally proposed to explain the rest masses of particles due to a symmetry spontaneously broken at low energy [78–80]. This was the state of the art in the early 1970's, when HR was discovered.

The modern view of the SM of particle physics embeds fundamental particles and gauge bosons to mediate interactions between them:

- the charged massive leptons are divided into 3 families: electron, muon, tau and their antiparticles;
- the neutrinos of extremely low mass are divided into 3 corresponding families: electron neutrino, muon neutrino and tau neutrino which are Majorana particles;

[1]This Section is partially inspired from the book by Samueli "Le modèle standard de la physique des particules : de l'électron au boson de Higgs" [72].

[2]See also the reports by Zweig [77].

particle	symbol	mass (GeV)	spin	internal d.o.f.
Higgs boson	h^0	1.2503×10^2	0	1
photon	γ	0	1	2
gluons	g	0	1	16
W bosons	$W^\pm$	8.0403×10^1	1	6
Z boson	Z^0	9.11876×10^1	1	3
neutrinos	$\nu_{e,\mu,\tau}, \overline{\nu}_{e,\mu,\tau}$	0	1/2	6
electron	$e^\pm$	$5.109989461 \times 10^{-4}$	1/2	4
muon	$\mu^\pm$	$1.056583745 \times 10^{-1}$	1/2	4
tau	$\tau^\pm$	1.77686	1/2	4
up quark	$u, \overline{u}$	2.2×10^{-3}	1/2	12
down quark	$d, \overline{d}$	4.7×10^{-3}	1/2	12
charm quark	$c, \overline{c}$	1.27	1/2	12
strange quark	$s, \overline{s}$	9.6×10^{-2}	1/2	12
top quark	$t, \overline{t}$	1.7321×10^2	1/2	12
bottom quark	$b, \overline{b}$	4.18	1/2	12
graviton	G	0	2	2

Table 2.1: Properties of the elementary particles of the Standard Model, in addition to the graviton [81]. The number of quantum d.o.f. is the product of the family, antiparticle, colour and helicity multiplicities. Neutrinos are here considered massless.

- the massive quarks of the QCD model are divided into 3 families or "flavors" with 2 members each: up and down, charm and strange, top and bottom, with their antiparticles;
- the 3 interactions are mediated by gauge bosons: the massless photon mediates the EM interaction, the 8 massless gluons mediate the strong interaction, and the massive bosons $W^\pm$ and Z^0 mediate the weak interaction;
- the massive Higgs boson, which is related to the rest masses of particles by their interaction with the Higgs field;
- it is often presumed that there exists a bosonic massless graviton to mediate a quantized version of the gravitational interaction, even if such a theory has not yet been made fully coherent.

A summary of the particle properties is given in Table 2.1.

The SM is assuredly not the final theory of particle physics, and that for several reasons (this is not a complete list): there is no DM component in this model; the dark energy causing the acceleration of the expansion of the universe is also absent; the neutrinos are proven to be massive by observation of their flavor oscillations; some measurements of particle physics experiments have shown discrepancies with the SM predictions (a famous recent one is the $g-2$ muon magnetic moment) and a renormalizable theory of quantum gravity is still to be found.

Hence, plentiful of models have been proposed to explain the new observational data while safeguarding all the extremely precise SM predictions already confronted to experiments. The most famous is the "supersymmetric" model where each particle has a "superpartner". These models could embed a quantum theory of gravity (like the "loop quantum gravity" or LQG model), and some of them require additional dimensions like string theory. For a discussion of these in the context of HR see Sections 4.5 and 4.6. Other DM candidates include axions and right-handed neutrinos. For complete review and history of those ideas see [7, 82].

2.2 Historical overview

2.2.1 Thermodynamics aspects

[3]In the 1970's, some work was done in order to conciliate BH mechanics with known theories of thermodynamics. Indeed, BHs seemed to violate the 2$^{\text{nd}}$ law of thermodynamics as they can swallow a great amount of information with only modification of mass M, charge Q and angular momentum J. As BHs are described only by these three quantities, as stated by the "no-hair" theorem set out by Israel [84–86], there is a loss of entropy known as the "information paradox" [87]. Thus, Bekenstein [88] proposed a generalized second law for BHs:

> *The black hole entropy plus the common entropy in the black hole exterior never decreases.* [88]

In BH physics, one quantity that never decreases whatever be the material swallowed is the surface area A. Thus, Bekenstein intuited that the entropy of a BH is proportional to A, and based on information theory the relationship

$$S = \frac{\ln(2)}{8\pi} A \,, \tag{2.1}$$

was proposed.

This claim was further supported by some analog version of the first law of thermodynamics

$$\mathrm{d}M = \Theta \mathrm{d}A + \vec{\Omega} \cdot \mathrm{d}\vec{J} + \Phi \mathrm{d}Q \,, \tag{2.2}$$

where $\mathrm{d}\vec{J}$ (resp. $\mathrm{d}Q$) is the change in angular momentum (resp. charge) of the BH while $\vec{\Omega}$ (resp. Φ) plays a role analog to angular frequency (resp. electric potential). Thus, the term Θ in front of the entropy change would be identified as an effective temperature whose expression depends on the surface gravity κ of the BH.

The same year, Bardeen, Carter & Hawking [89] went one step further by giving explicitly the 4 laws of BH mechanics. In this paper, the entropy was found to be $S = A/4$ in the first law, which seemed a better choice than Bekenstein's, so that the effective temperature was identified as

$$T = \frac{\kappa}{2\pi} \,. \tag{2.3}$$

[3]This Section is partially inspired by the review article "Primordial black hole constraints with Hawking radiation – a review" [8] under writing. For an *inside* history, I refer the reader to the account by Page [83].

The second law was refined by adding a discussion about BH mergers (the area of the final BH must be superior to the area of the two original BHs). A third law was postulated:

> *It is impossible [. . .] to reduce* [T] *to 0 by a finite sequence of operations.* [89]

because this would leave a naked singularity forbidden by the CCC. Finally, a zeroth law about the constant value of T across the BH area was enunciated. Then followed an erroneous statement in sync with the view at that time that a BH can only accrete matter and radiation:

> *In fact the temperature of a black hole is absolute zero* [because it] *cannot be in equilibrium with blackbody radiation at any non-zero temperature.* [89]

precisely because a BH can only *accrete* matter and radiation. For a complete modern review of the thermodynamics of BHs, I refer the reader to [90, 91]. The 4 laws of BH thermodynamics are:

0$^{\text{th}}$ law: the temperature of a BH $T = \kappa/2\pi$ is constant over its event horizon;

1$^{\text{st}}$ law: the infinitesimal evolution of the BH mass is given by $\mathrm{d}M = T\mathrm{d}A/4 + \vec{\Omega}\cdot\mathrm{d}\vec{J} + \Phi\mathrm{d}Q$;

2$^{\text{nd}}$ law: the total entropy composed of that of a black hole $S = A/4$ plus that of the rest of the universe can only increase;

3$^{\text{rd}}$ law: the temperature of a BH cannot be decreased to absolute 0 by a finite number of operations.

2.2.2 Quantum mechanics aspects

2.2.2.1 BH stability

At about the same epoch, theoretical work was pursued in order to check whether BHs were stable objects regarding quantum mechanics, that is, can BHs develop diverging perturbations that would challenge their survival. This was particularly interesting for KBHs as these can experience stimulated emission of bosonic fields through "superradiance" effects [92], which would efficiently extract mass and angular momentum from the black hole and could lead to "black hole bombs" [93].[4] Teukolsky & Press published a series of 3 papers [95–97] in which they study the stability of the Kerr metric against a spin s equal to 1, 1/2 and 2 wave scattering. The separated equations for the scalar case were derived earlier by Carter [98].[5] They obtained the fundamental separated radial and angular equations for the propagation of a wave of spin s and energy E outside a BH of mass M, in semi-classical general relativity (*i.e.* classical metric and quantum fields)

$$\Delta^{-s}\frac{\mathrm{d}}{\mathrm{d}r}\left(\Delta^{s+1}\frac{\mathrm{d}R}{\mathrm{d}r}\right) + \left(A_{Eslm}(r) - \lambda_{Eslm}\right)R = 0\,, \tag{2.4}$$

[4] For a complete review of the "superradiance" effect I refer the interested reader to [94].

[5] This problem was also explored by Starobinskii & Churilov for bosonic fields in [99, 100] and Unruh for the fermionic field in [101].

$$\frac{1}{\sin\theta}\frac{\mathrm{d}}{\mathrm{d}\theta}\left(\sin\theta\frac{\mathrm{d}S}{\mathrm{d}\theta}\right)+\left(B_{Eslm}(r)+\lambda_{Eslm}\right)S=0\,, \tag{2.5}$$

valid for each angular mode (l,m) of the wave, with some eigenvalue λ_{Eslm} and functions $A_{Eslm}(r)$ and $B_{Eslm}(r)$. The radial equation was later called the "Teukolsky equation" (for a general derivation of this equation, see Section 2.3 below). Resolution of this equation with the correct boundary conditions yields the transmission (absorption) and reflection coefficients of a wave over a BH horizon and thus the "superradiant" amplification of incident bosonic waves, while fermions are not superradiant.

2.2.2.2 Hawking papers

Confronted with the possible existence of PBHs with size and mass way beyond the classical stellar processes—in fact in the quantum mechanics regime—Hawking wondered how quantum mechanics effects would come into play. This led to the famous discovery that BHs are not "black" but radiate a steady flux of particles like thermal bodies. This was first proposed in a paper published in Nature in 1974 entitled "Black hole explosions?" [102]. In this paper, Hawking claimed that:

> *It seems that any black hole will create and emit particles such as neutrinos or photons at just the rate as one would expect if the black hole was a body with a temperature of* $[T=\kappa/2\pi]$. [102]

which is precisely the temperature encountered when reconciling BH mechanics with thermodynamics. Hawking immediately suspected a deep fundamental link between this temperature (blackbody emission) and the effective temperature in BH thermodynamics (entropy).[6] Follows:

> *As a black hole emits this thermal radiation one would expect it to lose mass. This in turn would increase the surface gravity* $[\kappa\propto 1/M$ for SBHs$]$ *and so increase the rate of emission.* [102]

Hence, any BH would have a finite lifetime that can be estimated if its luminosity follows the blackbody law $L\sim AT^4$. Rapid integration shows that a PBH with the critical mass $M_*\sim 10^{15}\,\mathrm{g}$ would have evaporated by today if formed just after inflation.[7] Due to the inverse power-law dependency of the emissivity with the mass, a very powerful "explosion" is to be expected at the end of the BH evolution.

[6] Bekenstein reexamined their 2nd law of BH thermodynamics [103] taking HR into account. From the microcanonical ensemble point of view, their study showed that the entropy "lost" in the BH at initial collapse is totally recovered in the form of thermal radiation. There is an infinite number of configurations that can collapse into a BH, and the one that contains most entropy is the pure thermal bath. As the emission process is random and proceeds with a tremendous number of single emitted quanta, microcanonical statistics predicts that the most probable total state of emission is distributed following the thermal distribution [104] (see also [90, 91]). On the same grounds, it is more probable that two BHs coalesce to form a bigger BH with greater area (and thus entropy) than for a big BH to spontaneously bifurcate into two smaller ones with less total area (and thus entropy).

[7] Given the roughness of this estimation and the uncertainty concerning the age of the universe at that time, it is remarkable that the estimation by Hawking falls within 50% of the modern value $M_*=5\times10^{14}\,\mathrm{g}$.

The details of HR were given in a subsequent longer paper from 1975 entitled "Particle creation by black holes" [105].[8] The calculations were based on quantum mechanics in curved spacetime. I will not give them here but refer the reader to Ref. [106] which follows step by step the original Hawking derivation in a comprehensive way. Basically, the flux of particle originates in the fact that an observer close to the BH is freely falling with an acceleration given by the surface gravity κ, while an observer far away from the BH horizon is at rest in the BH frame. Thus, they define different local bases and vacuum quantum states and the conversion between these bases results in a net thermal flux of particles at infinity with rate

$$\frac{\mathrm{d}^2 N}{\mathrm{d}t\mathrm{d}E} = \frac{1}{2\pi} \frac{\Gamma_{Eslm}}{e^{E/T} - (-1)^{2s}} , \tag{2.6}$$

where Γ_{Eslm} is precisely the absorption coefficient encountered by Teukolsky & Press, here interpreted as a spontaneous emission coefficient. It will later on be called "greybody" (or "graybody") factor (GF) as it encodes the departure of the BH from a pure blackbody: not all radiation is absorbed but some part is reflected (or, equivalently, spontaneously emitted).

The rate of emission was given in [105] for massless scalar fields from a SBH but extension to higher spin s fields for a Kerr-Newmann BH was straightforwardly obtained by adding the corresponding angular velocity and electric potential into the Boltzmann factor

$$\frac{\mathrm{d}^2 N}{\mathrm{d}t\mathrm{d}E} = \frac{1}{2\pi} \frac{\Gamma_{Eslm}(\Omega, \Phi)}{e^{(E - m\Omega - q\Phi)/T(M, a^*, Q)} - (-1)^{2s}} , \tag{2.7}$$

where $\Omega = 4\pi a/A$ and $\Phi = 4\pi Q r_+/A$ [107]. The tendency of BHs to emit aligned momentum and same-charge particles is apparent from the form of the effective chemical potential in Eq. (2.7).

For the emission of a particle of non-zero rest mass μ to be kinematically allowed, the energy of emission must be $E > \mu$. However, the rate of emission is exponentially suppressed at high energies, hence:

> *As the temperature rose, it would exceed the rest mass of particles such as the electron and the muon and the black hole would begin to emit them also.* [105]

Therefore, if the number of kinematically allowed d.o.f. of emission increases monotonically with energy, such as in the "Hagedorn model", then the last emission would indeed be explosive.

The evolution of the BH was considered as quasi-static so that backreaction can be ignored. The successive particles are emitted independently. Furthermore, to avoid problems with Planck scale naked singularities, Hawking assumed that when reaching this scale the system shall "disappear altogether" in a final flash of energy. Many interpretations were subsequently given as for this spontaneous emission. Hawking proposed that it could be grasped considering the spontaneous creation of pairs of particles and antiparticles just outside the horizon with a Boltzmann distribution given by the temperature of the BH, with one half escaping to infinity with positive energy and the second half falling inside the BH with negative energy, therefore decreasing its mass. Another analogy proposed is the spontaneous decay of the BH because of particles tunneling out of the horizon [108]. For later HR derivation and interpretations, I refer the interested reader to [90].

[8] As clearly appears when considering the dates of publication, the physics community was already discussing and using the Hawking results before this second paper was published.

2.2.3 Later calculations

2.2.3.1 Greybody factors

The Hawking process was then firmly established on statistical mechanics, quantum mechanics and general relativity grounds. That new process and the finite lifetime of BHs has immediate consequences on PBH constraints. PBHs with initial mass $M < M_*$ cannot participate in the DM density today, and their evaporation may leave observational signatures, as discussed in the first ever PBH review by Carr [47].[9] In fact, the evaporation of small PBHs may be the only reasonable way to detect them.

Very early arguments by Gibbons [110] and Carter *et al.* [111] showed that even if formed with non-zero charge and angular momentum, a BH would lose them more rapidly than its mass and end up as a simple SBH for most of its lifetime. The relevant timescales for the mass M, angular momentum J and electric charge Q are

$$\tau_M \propto M^3, \qquad \tau_J \propto M^3, \qquad \tau_Q \ll \tau_M, \tau_J \,. \tag{2.8}$$

For rotating PBHs, even if the temperature $T \to 0$ as the angular momentum approaches the extremal limit $a^* \to 1$, Carter argued that the superradiant scattering will compensate so that the lifetime $\tau(a^* \lesssim 1) \sim \tau(a^* = 0)$. Hence, if formed initially rotating, a PBH should keep its angular momentum for most of its lifetime; this in fact contradicts the above statement. The situation is very different for charged BHs since a rapid discharge process called the Schwinger effect [112] neutralizes the BH independently of its HR rate in a timescale much shorter than the mass loss, due to spontaneous pair-production of charged particles in the intense electric field of the BH (see also [113]). In fact, it is estimated that only supermassive BHs (SMBHs) formed with appreciable charge would still be charged today—they are protected from the Schwinger effect by the non-zero mass of the electron. Hence, for quite a long time, HR by PBHs was considered only for SBHs.

The GFs represented the complicated part of the Hawking process analysis. Apart from some high- and low-energy limits, the calculation of GFs requires numerical tools. Page was the first to compute them numerically in 1976-1977. In the first paper of a series of three [107], Page considered the massless particles that where known at the time (*i.e.* photons, neutrinos, gravitons) and thus ignored the scalar case. The emission of such particles would lead to a progressive decrease in the mass (and angular momentum) of BHs grasped by the Page coefficients for KBHs

$$\begin{pmatrix} -f(M,a^*)/M^2 \\ -g(M,a^*)a^*/M \end{pmatrix} \equiv \frac{\mathrm{d}}{\mathrm{d}t}\begin{pmatrix} M \\ J \end{pmatrix} = \sum_i g_i \sum_{lm} \int_0^{+\infty} \frac{1}{2\pi} \frac{\Gamma_{Eslm}(a^*)}{e^{(E-m\Omega)/T(a^*)} - (-1)^{2s_i}} \begin{pmatrix} E \\ m \end{pmatrix} \mathrm{d}E \,, \tag{2.9}$$

where i spans the spectrum of particles and g_i is their number of internal d.o.f. (polarization, color). With these coefficients, the equations of evolution of BH mass and spin are simply

$$\begin{aligned} \frac{\mathrm{d}M}{\mathrm{d}t} &= -\frac{f(M,a^*)}{M^2} \,, \\ \frac{\mathrm{d}a^*}{\mathrm{d}t} &= \frac{a^*(2f(M,a^*) - g(M,a^*))}{M^3} = \frac{-a^* f(M,a^*) h(M,a^*)}{M^3} \,, \end{aligned} \tag{2.10}$$

[9] A review was also published on the Soviet side [109] but it went almost unnoticed.

where $h(M,a^*) \equiv g(M,a^*)/f(M,a^*)-2$. The GFs Γ_{Eslm} were obtained from the computer programs of Teukolsky & Press for the cross-section σ of a field on a BH metric [95–97]. Page checked that the correct analytical behaviours were obtained at low energies for all spin fields

$$\sigma_s(E) \equiv \frac{\pi}{E^2}\sum_{lm}\Gamma_{Eslm} \underset{ME\to 0}{\sim} \begin{cases} A \\ 2\pi M^2 \\ \frac{4}{9}AM^2(3-a^{*2}) \\ \frac{16}{225}AM^4\left(5+\frac{5a^{*2}}{4}+a^{*4}\right)E^2 \end{cases} \underset{a^*\to 0}{\sim} \begin{cases} 16\pi M^2 & \text{scalar} \\ 2\pi M^2 & \text{fermion} \\ \frac{64}{3}\pi M^4E^2 & \text{vector} \\ \frac{256}{45}\pi M^6E^4 & \text{tensor} \end{cases} \tag{2.11}$$

to first order terms in a^*. The dominant mode of emission is always the lower angular momentum one $l = s$ for SBHs, and the cross-section is cut-off at low energy with harder cut-off for higher spins. The spin 0 case was treated separately by Sanchez to obtain the scalar cross-section [114, 115] (see also the later work [116–118]). In the high energy limit the cross section is the same for all spins

$$\sigma_s(E) \underset{EM\to+\infty}{\longrightarrow} 27\pi M^2\,, \tag{2.12}$$

which corresponds to geometrical optics (GO) limit.

With these numerical results, Page was able to determine the fraction of BH mass ending up in neutrinos, photons and gravitons and found 81% ν's, 17% γ's and 2% G's. In a second paper [119], Page wanted to check:

> *[...] the validity of the assumption that most black holes which emit significantly today are not rotating.* [119]

The Page factors f and g were thus computed to great accuracy and fitted with cubic spline functions up to the extremal value $a^* = 1$ for field spins 1, 1/2 and 2, and it was observed that the contribution of a massless spin s field to $h(M,a^*)$ could be fitted linearly as $h_s(M,a^*=0) = as - b$ (a, b are positive constants). This is remarkable since the relationship between a^* and M is obtained from Eqs. (2.10) to be

$$\frac{\mathrm{d}\ln(a^*)}{\mathrm{d}\ln(M)} = h(M,a^*)\,. \tag{2.13}$$

Hence, as the linear relation for each spin component implies that $h_{s=0}(M,a^*=0)$ is negative, and $h_{s=0}(M,a^*\to 1)$ is certainly positive, then the function $h_{s=0}(M,a^*)$ must admit a zero at some non-zero value of a^*. This implies in turn that

> *[...] if there were a large enough number of massless scalar fields (unknown at present) to dominate the emission, a^* might indeed hung up at some non-zero value.* [119]

which would invalidate the hypothesis that all PBHs are SBHs today.

Remarkably, accurate computation shows that for near extremal $a^* \to 1$ BHs, the importance of emission of particles follows the opposite spin order as for the Schwarzschild case, *with the higher spins associated with the higher rate of emission.* Overall, ν's rate is multiplied by ~ 13, γ's rate by ~ 107 and G's rate by more than 26 000. The lifetime of a BH is further reduced by a $\mathcal{O}(1)$ factor.

The case of charged RNBHs was treated in the third paper [120]. Random emission of charged particles must produce fluctuations of the BH charge. Thus, the preferred emission of particles of the same charge as the BH causes the rates of emission of charged particles to fluctuate. Page examined emission of massive charged leptons (*i.e.* the known $e^{\pm}$ and $\mu^{\pm}$ at that time) by initially neutral BHs. For a fermion with charge $\pm e$, the rate of emission is modified by $(2-5)\%$ only as the rms value of the BH charge Q^* is $\sim (2-6)e$ (depending on the lepton rest mass μ). More dramatic is the change in the emitted power due to the kinematic cut-off $E > \mu$: numerical calculation showed that $\sim 50\%$ of the power is lost at $E \gtrsim \mu$ for a BH of temperature $T \sim \mu$.

2.2.3.2 Effective potentials

There is a fundamental difficulty in computing the GFs numerically: the Teukolsky equation (2.4) is a differential equation of second order with rather peculiar oscillatory behaviour and a $1/r$ decrease at infinity. Hence, extraction of the GFs requires very high accuracy. MacGibbon & Webber noted in 1990:

> *[. . .] rough estimates of the contributions from other species can be obtained by plotting the logarithms of the contributions per helicity or polarization as a function of s and then interpolating. This gives reasonable accuracy without recourse to the extraordinary computational time required for the full determination of* [the GFs]. [121]

Hence, the (tabulated) Page results have been readily used until public tools like `BlackHawk` provided automatic computation of the GFs.

In studying the Schwarzschild [122, 123] and Kerr metric stability [124], a technique was developed to transform the radial Teukolsky equation into a Schrödinger wave equation with an effective potential, denoted as the "Regge-Wheeler" potential for the SBH. This technique was extended to the KBH in a series of papers by Chandrasekhar & Detweiler [125–128].[10] A full description of the technique is given below in Section 2.3.[11]

2.2.3.3 High energy and interactions

Contemporary to Page's calculation of the GFs, Carter *et al.* [130] performed a long discussion of the BH evaporation at high energy (that is, above the QCD scale $\Lambda_{\rm QCD}$), in an attempt to examine the behaviour of the emitted particles with respect to interactions. With the knowledge of particle physics available at that time:

> *Even if Hawking* [evaporation] *remains valid* [above] *the hadronic threshold, it cannot be used to give an automatically reliable estimate of what happens in the high energy limit because of our ignorance of the number of kinds of particle state [. . .] that should be taken into account.* [130]

[10] These developments were done in the context of GW and quasi-normal mode (QNM) calculations and seem to have gone rather unnoticed by the HR community.

[11] Kodama and Ishibashi (*e.g.* [129]) developed a formalism that goes straight from the metric to the short range potentials, by means of the stress-energy tensor and without computing the intermediate Teukolsky equations.

This could only be assessed with high-energy observation of a PBH evaporation with good energy resolution. They distinguished two extreme models:

- "Hawking picture": the emission is independent, no interactions occur and the flux is described by the Fermi-Dirac (for fermions) or Bose-Einstein (for bosons) distribution;
- "Landau picture": strong interactions between emitted particles cause the flux to achieve local thermal equilibrium so that it is described by a perfect fluid equation.

These two models result in very different observational signatures. About the first model, valid in the standard quark model:

> *[. . .] one would be seeing the direct result of creation at the ultra high* [PBH] *temperature. If such a phenomenon could be actually observed it would provide uniquely valuable information about what actually takes place at such high energies.* [130]

On the other hand, in the second model, presumably valid if the "Hagedorn model" equation of state is the correct description:

> *The simplest and most obvious hypothesis to make is that the energy is released in the form of an homogeneous cloud of matter very much analogous to the expanding fireball of the Big Bang universe.* [130]

The calculations showed additionally that:

> *[. . .] the final output will be observed exclusively in the form of only medium energy gamma rays* [of $m_e < E < m_\pi$] *in an explosive burst [. . .] soon after the hole enters the hadronic* [regime]. [130]

The timescale of this "fireball" was estimated to be $\tau \sim 10^{-8}\,\mathrm{s}$, very short compared to the usual $\tau \propto M^3 \sim 10^{13} - 10^{15}$s lifetime of a $T \sim \Lambda_{\mathrm{QCD}}$ BH in the "Hawking picture". The debate about the correct model has persisted until the SM equation of state was firmly based on accelerator data.

In a second review about PBHs using Page's numerically computed GFs, Carr [131] discussed how the theoretical uncertainties of HR can affect the cosmological constraints. They identified: *i*) the spectrum of particles emitted at high energy; *ii*) the interactions between the emitted particles. Different predictions arise from the "elementary" and "composite" particle models:

- "elementary particle model", in which BHs emit a finite set of elementary ingredients (3 families of quarks) and the number of d.o.f. saturates at high energy, corresponding to the "Gell-Mann model";
- "composite particle model", in which BHs emit an exponentially increasing number of hadronic d.o.f. with increasing energy, corresponding to the "Hagedorn model".

Furthermore, the "composite particle" model predicts that when the temperature is high enough, as in the first seconds of the universe, then the Hagedorn d.o.f. interact so much that the outgoing flux behaves as an optically thick medium. Thus, a BH appears as some kind of "fireball" decaying into

$\Lambda \sim 250\,\mathrm{MeV}$ radiation. The existence of a "fireball" around exploding PBHs has been the subject of many subsequent debates.

In 1984, Oliensis & Hill [132] analysed what should be the form of the HR at high energies, say $E \gg$ GeV. They argued that, contrarily to the "Hagedorn model", the new physics d.o.f. should appear only "logarithmically" at high energies, in coherence with the renormalization group results: up to the Planck scale, they did not expect more than a factor $\times 10$ in this number. Based on the "elementary" particle model, they showed that:

> *[...] Hawking radiation is very simple—the emission rate is just the right magnitude for particles to be emitted and decay approximately independently.* [132]

They continued by stating that:

> *The situation resembles the $e^{\pm}$ annihilation. For this process, we know that the long distance interactions have no effect on the short time propagation of the particles, but simply dress them into independent jets over a long time.* [132]

However, the situation is inverted at energies low compared to the thresholds of d.o.f. increase:

> *At very low energy $T \ll \Lambda_{\mathrm{QCD}}$ the long range force is not relevant. The black hole is not hot enough to radiate isolated constituents. [...] Instead low mass bound states and other light particles will be radiated.* [132]

meaning that pions are radiated for energies $E \lesssim 200\,\mathrm{MeV}$. They numerically estimated that 99.9% of the emitted particles do not experience interactions with one another (they only consider $2 \to 2$ number conserving interactions). They finally suggested that QCD fragmentation functions be used to compute the final outcome of the jets.

The next major development came in 1990-1; in a series of two papers entitled "Quark- and gluon-jet emission from primordial black holes", MacGibbon & Webber [121, 133] revolutionized the computation of the HR of PBHs by "convolving the Hawking emission formulas with a Monte Carlo QCD jet code" to compute the evolution, hadronization and decay of the primary particles into stable secondary particles. This of course relied on the "elementary particle" model, which had in the mean time been tested against prolific accelerator data. This was the first time that QCD jet interactions were taken into account in PBH studies and constituted a first answer to the questions asked by Carter *et al.*. Hereafter, most people used this "MacGibbon & Webber" (hereafter MG&W) model to compute the HR yields. In particular, the code `BlackHawk` that I developed with A. Arbey is a direct modern adaptation of these ideas, see Chapter 3.

In the first paper [121] dedicated to the instantaneous emission, MG&W showed that:

> *[...] the total emission differs dramatically from previous calculations and is dominated by the* [quark] *jet fragmentation products. The spectra have a significant component at energies well below the black hole temperature, arising from the decays.* [121]

which was explained by the fact that above Λ_{QCD}, there are numerous quark and gluon d.o.f. available to PBH primary evaporation. These particles, once emitted, behave the same way as in

accelerator experiments and, because of the QCD confinement properties, form jets. These jets are characterized by a plentiful multiplicity and require computational Monte Carlo treatment. As a corollary, they used:

> *[...] the more conventional particle-physics view that a black hole emits only those particles which appear elementary on the scale of the radiated energy.* [121]

This had dramatic consequences on *e.g.* the rate of emission of nucleons, which were believed to be emitted directly once $T \gtrsim m_{\mathrm{p,n}}$. In particular, there is always massive particle creation, but it is exponentially suppressed if $T \ll \mu$ where μ is the particle rest mass. Here, nucleons are only one of the (subdominant) constituents of the QCD jets, because it is the quarks and gluons that are fundamental at $E \sim 1\,\mathrm{GeV}$. This rule admits an exception:

> *Since the pion rest masses are smaller than the effective quark masses, however, pions should be directly emitted at the energies below* $[\Lambda_{\mathrm{QCD}}]$. [121]

The precise behaviour of the HR at $T \sim \Lambda_{\mathrm{QCD}}$ remains a source of uncertainty, as well as the effective masses used for gluons (600 MeV) and quarks (340 MeV for u and d).

MG&W used the cross-sections numerically computed by Page [107] for the primary spectrum as well as their low- and high-energy limits. The emission theory for coloured gauge bosons was based on old arguments by Perry [134]; however the EW massive gauge bosons were not included in the analysis. Perry showed that:

> *[...] the black hole will act as a source of* [the gauge fields] *and conserve* [their quantum numbers]. *[...] The black hole will remain neutral with respect to colour, and so a colourless final state for the emission products is guaranteed.* [134]

The massive quarks are associated with the same cross-section as the fermions, and the (effectively) massive gluons to that of the photons.

On a practical point of view, MG&W used a modified version of the public code `BIGWIG` [135, 136] and its successor `HERWIG` [137] to force $\mathrm{e}^{\pm}$ collisions to generate pairs of particles and antiparticles of primary type i (to ensure color/charge conservation into the codes) and examined the spectrum of secondary particles of types j produced by the jets. This allowed to obtain branching ratios $\mathrm{d}N_{i\to j}\mathrm{d}E$ that can afterwards be plugged into the Hawking formula to obtain the secondary spectra

$$\frac{\mathrm{d}^2 N_j}{\mathrm{d}t\mathrm{d}E} = \sum_i \int \frac{\mathrm{d}N_{i\to j}}{\mathrm{d}E} \frac{\mathrm{d}^2 N_i}{\mathrm{d}t\mathrm{d}E} \mathrm{d}E\,. \tag{2.14}$$

MG&W were limited by the capabilities of the codes to primary energies $E = 0.02 - 100\,\mathrm{GeV}$—below, there were too scarce data to compare the fragmentation functions against; above, the behaviour of particle physics was unknown.

In their study, they restricted themselves to "experimentally verified" species relevant for their energy range, in particular the third family of leptons and quarks. They rejected the Higgs boson and most notably the graviton, at odds with all previous studies. They argued that any new

species would have negligible effect on the instantaneous and integrated spectra, except if they were characterized by a high number of d.o.f. (as in supersymmetric theories).

In the second paper [133], MacGibbon alone studied the lifetime emission of a BH. The calculation of the Page coefficient $f(M)$ was updated with a new determination of the relevant d.o.f. as a function of the temperature. Each massless d.o.f. contributes to $f(M)$ amounting to

$$f_s \equiv \int_0^{+\infty} \frac{\mathrm{d}^2 N_s}{\mathrm{d}t \mathrm{d}E} \mathrm{d}E \simeq \begin{cases} 0.267 & \text{scalar} \\ 0.147(2) & \text{(charged) fermion} \\ 0.060 & \text{vector} \\ 0.020 & \text{Rarita-Schwinger} \\ 0.007 & \text{tensor} \end{cases} \tag{2.15}$$

One can note that the value of $f_{3/2}$ is provided even if at that time, no numerical computation of the spin $^3/_2$ GFs existed yet. The explanation is to be found in a footnote, given above: this value was obtained by interpolation from the other spins. Then, they showed that a good fit to the contribution $f_i(M)$ of a massive field i to the total $f(M)$ can be obtained by considering an exponential rise of its contribution from 0 to f_s with a turning point at $T \simeq \mu_i$, where the precise value depends on the spin of the particle.[12] The MG&W model was challenged by several authors in the 1990's:

- Cline & Hong [139] argued that the correct model of HR must lie between the two extreme "Hagedorn" and "Gell-Mann" models (or equivalently between the "elementary" and "composite" particle models);

- Heckler [140, 141] claimed that taking into account number non-conserving interactions of the $2 \to 3$ kind, the density of an expanding plasma around an exploding PBH can grow very fast (somewhat different results are obtained by Kapusta in [142, 143]);

- Belyanin *et al.* [144] finally predicted that a full magneto-hydrodynamic plasma should develop around evaporating PBHs, based or earlier ideas from Rees & Blandford [145, 146].

All of these competing models relied on the formation of some kind of "photosphere" or "fireball" around PBHs, due to non-negligible interactions between emitted particles [147]. They predicted very different HR signatures in the astronomical observations, in particular concerning the PBH final bursts. The party was definitely settled by MacGibbon *et al.* [148] in 2008 in a very detailed study of all the relevant interactions. The MG&W model is now commonly used by all HR papers, including this manuscript.

[12] for an up-to-date derivation of the Page factor with this method, see [138].

2.3 Fundamental equations

[13]In this Section, I present all the modern equations necessary to compute the HR of spherically symmetric and static BHs as well as KBHs. I remain agnostic about the origin of the BHs under consideration. As pointed by Hawking [102, 105], the HR process from the horizon is completely symmetric to an absorption process from spatial infinity. The master equation giving the rate of emission of some d.o.f., labelled i, is

$$\frac{\mathrm{d}^2 N_i}{\mathrm{d}t\mathrm{d}E} = \frac{1}{2\pi}\frac{\Gamma_{Es_ilm}(x_j)}{e^{E'/T(x_j)} - (-1)^{2s_i}}\,, \tag{2.16}$$

It exhibits three main quantities: *i*) the temperature $T(x_j) \equiv \kappa/2\pi$, which is related to the geometry of the BH encoded by the set of parameters $\{x_j\}$; *ii*) the total energy E' which is the energy of the emitted field possibly corrected by an effective chemical potential; and *iii*) the GF $\Gamma_{Eslm}(x_j)$ which is related to both the BH geometry and the field internal d.o.f. Quantities *i*) and *ii*) are trivial but the GF *iii*) requires involved algebraic and numerical tools. To obtain the emission probability, one needs to solve the equations of motion for spin 0, 1, 2, 1/2 and 3/2 massless fields with the correct boundary conditions, which I do explicitly below.

2.3.1 Spherically symmetric black holes

I consider first spherically-symmetric static metrics, which constitute a subset of Petrov type D metrics [154].[14] In four-dimensional Boyer–Lindquist coordinates, the general form of such metrics is

$$\mathrm{d}s^2 = -G(r)\mathrm{d}t^2 + \frac{1}{F(r)}\mathrm{d}r^2 + H(r)\mathrm{d}\Omega^2\,, \tag{2.17}$$

where $\mathrm{d}\Omega^2 = \mathrm{d}\theta^2 + \sin\theta\,\mathrm{d}\varphi^2$ is the solid angle in spherical coordinates. Within this family of metrics, I further focus on solutions to the Einstein equations (1.3) which are asymptotically flat. This means that at spatial infinity the functions F, G, and H must satisfy the asymptotic conditions

$$F(r) \underset{r\to+\infty}{\longrightarrow} 1\,, \qquad G(r) \underset{r\to+\infty}{\longrightarrow} 1\,, \qquad H(r) \underset{r\to+\infty}{\sim} r^2\,. \tag{2.18}$$

Many usual metrics fall into this category, like that of the SBH and RNBH. One particular case that will be especially relevant is

$$G(r) = F(r) \equiv h(r)\,, \quad \text{and} \quad H(r) = r^2\,, \tag{2.19}$$

to which I refer as "*tr*-symmetric" (for time-radius symmetric). The SBH is an example of a *tr*-symmetric metric.

[13]This Section is inspired by the two papers I wrote with A. Arbey, M. Geiller, E. R. Livine & F. Sartini entitled "Hawking radiation by spherically-symmetric static black holes for all spins" [149, 150] as well as by the manual of the code `BlackHawk` I developed with A. Arbey [151, 152]. The interested reader will find additional mathematical details in the book by Chandrasekhar "The Mathematical Theory of Black Holes" [153].

[14]The same procedure was followed for the Kerr–Newman BH (*e.g.* [155, 156]) and the Kerr–Newmann-(anti)de Sitter BH [157].

2.3.1.1 Equations of motion

I may now describe the dynamics of matter fields in these types of spacetime, that is, I will derive the general Teukolsky equation for all spin massless fields. This can be done either by studying the equations of motion written in terms of the metric, or by using the Newman–Penrose formalism. In the following, I will use the most direct method to obtain the results.

Massless spin 0. I first consider a massless scalar field ϕ. In this case, it is easier to write the Proca equation in curved spacetime

$$\Box\phi = \frac{1}{\sqrt{-g}}\partial_a\big(g^{ab}\sqrt{-g}\,\partial_b\phi\big) = 0\,, \quad \text{where} \quad \sqrt{-g} = \sqrt{\frac{G}{F}}H\sin\theta\,. \tag{2.20}$$

For the other types of fields, the multiplicity of the vector, spinor or tensor components makes it difficult to obtain a single equation of motion when working directly with the metric. A simple and efficient way to bypass this difficulty is to exploit the Newman–Penrose formalism [153, 158], which relies on a reformulation of the equations of motion using a null tetrad field. A choice of null tetrad such that $g^{ab} = -l^a n^b - n^a l^b + m^a\bar{m}^b + \bar{m}^a m^b$ is given by

$$\begin{aligned} l^a &= \left(\frac{1}{G}, \sqrt{\frac{F}{G}}, 0, 0\right), \qquad m^a = \left(0, 0, \frac{1}{\sqrt{2H}}, \frac{i}{\sqrt{2H}\sin\theta}\right), \\ n^a &= \left(\frac{1}{2}, -\frac{\sqrt{FG}}{2}, 0, 0\right), \quad \bar{m}^a = \left(0, 0, \frac{1}{\sqrt{2H}}, \frac{-i}{\sqrt{2H}\sin\theta}\right), \end{aligned} \tag{2.21}$$

where m and $\bar{m}$ are complex conjugate. This tetrad satisfies $l\cdot n = -1$ and $m\cdot\bar{m} = 1$, while all other scalar products vanish. Introducing $e^a_i = (e^a_1, e^a_2, e^a_3, e^a_4) \equiv (l^a, n^a, m^a, \bar{m}^a)$, the λ-coefficients are defined as

$$\lambda_{ijk} \equiv \big(e^a_i e^b_k - e^a_k e^b_i\big)\partial_a e_{jb}\,. \tag{2.22}$$

These coefficients enter the definition of the so-called Ricci spin (or rotation) coefficients

$$\gamma_{ijk} \equiv \frac{1}{2}(\lambda_{ijk} + \lambda_{kij} - \lambda_{jki}), \tag{2.23}$$

and some specific linear combinations of these Ricci coefficients are then denoted by

$$\begin{array}{lll} \kappa \equiv \gamma_{311}\,, & \rho \equiv \gamma_{314}\,, & \epsilon \equiv (\gamma_{211} + \gamma_{341})/2\,, \\ \sigma \equiv \gamma_{313}\,, & \mu \equiv \gamma_{243}\,, & \gamma \equiv (\gamma_{212} + \gamma_{342})/2\,, \\ \lambda \equiv \gamma_{244}\,, & \tau \equiv \gamma_{312}\,, & \alpha \equiv (\gamma_{214} + \gamma_{344})/2\,, \\ \nu \equiv \gamma_{242}\,, & \pi \equiv \gamma_{241}\,, & \beta \equiv (\gamma_{213} + \gamma_{343})/2\,. \end{array} \tag{2.24}$$

For the family of metrics (2.17), the only non-vanishing components are real and given by

$$\rho = -\frac{H'}{2H}\sqrt{\frac{F}{G}}\,, \quad \mu = -\frac{H'}{4H}\sqrt{FG}\,, \quad \gamma = \frac{G'}{4}\sqrt{\frac{F}{G}}\,, \quad \beta = -\alpha = \frac{\cot\theta}{2\sqrt{2H}}\,, \tag{2.25}$$

where $X' \equiv \partial_r X$ denotes the derivative in the radial direction. In the tr-symmetric case, these spin coefficients are the same as in [159]. One defines the covariant derivatives along the four directions of the tetrad (2.21) as

$$D \equiv l^a \nabla_a \,, \quad \Delta \equiv n^a \nabla_a \,, \quad \delta \equiv m^a \nabla_a \,, \quad \bar{\delta} \equiv \bar{m}^a \nabla_a \,. \tag{2.26}$$

These derivatives satisfy the general commutation relation

$$\big(D - (p+1)\epsilon + q\rho + \bar{\epsilon} - \bar{\rho}\big)(\delta - p\beta + q\tau) = \big(\delta - (p+1)\beta + q\tau + \bar{\pi} - \bar{\alpha}\big)(D - p\epsilon + q\rho) \,, \tag{2.27}$$

where p and q are arbitrary constants. This identity, which is valid for type D metrics (see Eq. (2.11) of [95]), is pivotal in what follows. In particular, for the family of spherically-symmetric static metrics (2.17) that I focus on, it reduces to

$$(D + q\rho - \rho)(\delta + p\alpha) = (\delta + p\alpha)(D + q\rho) \,. \tag{2.28}$$

I am now equipped with the necessary material to write down the Newman–Penrose equations of motion for fields of various spins.

Massless spin 1. For a massless gauge boson, satisfying the Einstein-Maxwell field equations $\mathrm{d}F = 0$ and $\mathrm{d} * F = 0$, the general form of the Newman–Penrose equations is [95, 153, 159]

$$D\phi_1 - \bar{\delta}\phi_0 + (2\alpha - \pi)\phi_0 + \kappa\phi_2 - 2\rho\phi_1 = 0 \,, \tag{2.29a}$$
$$D\phi_2 - \bar{\delta}\phi_1 + (2\epsilon - \rho)\phi_2 + \lambda\phi_0 - 2\pi\phi_1 = 0 \,, \tag{2.29b}$$
$$\Delta\phi_0 - \delta\phi_1 - (2\gamma - \mu)\phi_0 - \sigma\phi_2 + 2\tau\phi_1 = 0 \,, \tag{2.29c}$$
$$\Delta\phi_1 - \delta\phi_2 - (2\beta - \tau)\phi_2 - \nu\phi_0 + 2\mu\phi_1 = 0 \,, \tag{2.29d}$$

where the three Maxwell scalars are

$$\phi_0 \equiv F_{ab} l^a m^b \,, \quad \phi_1 \equiv \frac{1}{2} F_{ab}(l^a n^b + \bar{m}^a m^b) \,, \quad \phi_2 \equiv F_{ab} \bar{m}^a n^b \,. \tag{2.30}$$

The cancellation of many of the Ricci coefficients for the family of metrics (2.17) allows to write the first and third equations as a coupled system involving ϕ_0 and ϕ_1 only, *i.e.*

$$(2\alpha - \bar{\delta})\phi_0 + (D - 2\rho)\phi_1 = 0 \,, \tag{2.31a}$$
$$(\Delta - 2\gamma + \mu)\phi_0 - \delta\phi_1 = 0 \,. \tag{2.31b}$$

These coupled first order equations can then be turned into a pair of decoupled second order differential equations. One applies δ to the first equation, and applies $D - 3\rho$ to the second one. Adding the two resulting equations, and using the identity (2.28) with $p = 0$ and $q = -2$, gives a differential equation involving ϕ_0 only

$$\Big((D - 3\rho)(\Delta - 2\gamma + \mu) - \delta(\bar{\delta} - 2\alpha)\Big)\phi_0 = 0 \,. \tag{2.32}$$

This is the equation of motion for a massless spin 1 field.

Massless spin 2. For purely gravitational perturbations, which are equivalent to a massless spin 2 graviton field, the general form of the Newman–Penrose equations is [95, 153]

$$(D-4\rho-2\epsilon)\psi_1-(\bar{\delta}-4\alpha+\pi)\psi_0+3\tilde{\kappa}\psi_2^\circ=0\,, \tag{2.33a}$$
$$(\Delta-4\gamma+\mu)\psi_0-(\delta-4\tau-2\beta)\psi_1-3\tilde{\sigma}\psi_2^\circ=0\,, \tag{2.33b}$$
$$(D-4\rho-\bar{\rho}-3\epsilon+\bar{\epsilon})\tilde{\sigma}\psi_2^\circ-(\delta-4\tau+\bar{\pi}-\bar{\alpha}-3\beta)\tilde{\kappa}\psi_2^\circ-\psi_0\psi_2^\circ=0\,, \tag{2.33c}$$

where the ψ_i are the perturbed components of the Weyl tensor (*e.g.* $\psi_0\equiv -C_{abcd}l^am^bl^cm^d$), ψ_2° is the only non-vanishing background component, and the tilde on a spin coefficient indicates a perturbed quantity. I specialize to the family of metrics (2.17), remove the vanishing unperturbed spin coefficients, apply the operator $\delta-2\beta$ to the first equation, and the operator $D-5\rho$ to the second one, add the two and make use of identity (2.28) with $p=2$ and $q=-4$. I obtain an equation involving solely ψ_0, with the $\tilde{\sigma}\psi_2^\circ$ and $\tilde{\kappa}\psi_2^\circ$ contributions replaced by $\psi_0\psi_2^\circ$ thanks to the third equation. The resulting equation reads

$$\Big((D-5\rho)(\Delta-4\gamma+\mu)-(\delta+2\alpha)(\bar{\delta}-4\alpha)-3\psi_2^\circ\Big)\psi_0=0\,, \tag{2.34}$$

where the background ψ_2° is given by the Ricci identity as [153]

$$\psi_2^\circ=D\mu-\delta\pi-\bar{\rho}\mu-\sigma\lambda-\pi\bar{\pi}+(\epsilon+\bar{\epsilon})\mu+(\bar{\alpha}-\beta)\pi+\nu\kappa \quad\longrightarrow\quad \psi_2^\circ=D\mu-\rho\mu\,. \tag{2.35}$$

Equation (2.34) is the equation of motion for a massless spin 2 field.

Massless spin 1/2. The Newman–Penrose equations for the massless Dirac spin 1/2 field are [95, 159]

$$(\bar{\delta}-\alpha+\pi)\chi_0-(D-\rho+\epsilon)\chi_1=0\,, \tag{2.36a}$$
$$(\Delta-\gamma+\mu)\chi_0-(\delta+\beta-\tau)\chi_1=0\,, \tag{2.36b}$$

where χ_i are the two components of the spinor. I now specialize to the metrics (2.17). I remove the vanishing spin coefficients, apply the operator $\delta-\alpha$ to the first equation, apply the operator $D-2\rho$ to the second one, subtract the two and make use of identity (2.28) with $p=-1$ and $q=-1$. This produces a decoupled differential equation for χ_0 only

$$\Big((D-2\rho)(\Delta-\gamma+\mu)-(\delta-\alpha)(\bar{\delta}-\alpha)\Big)\chi_0=0\,. \tag{2.37}$$

This is the equation of motion for a massless spin 1/2 field.

Massless spin 3/2. Finally, the general form of the Newman–Penrose equations for a Rarita–Schwinger massless spin 3/2 field is [160]

$$(D-\epsilon-3\rho)H_{001}-(\bar{\delta}-3\alpha+\pi)H_{000}-\psi_2^\circ\psi_{000}=0\,, \tag{2.38a}$$
$$(\delta-\beta-3\tau)H_{001}-(\Delta-3\gamma+\mu)H_{000}-\psi_2^\circ\psi_{001}=0\,, \tag{2.38b}$$

where $H_{000} = (\delta - 2\beta - \bar{\alpha} + \bar{\pi})\psi_{000} - (D - 2\epsilon + \bar{\epsilon} - \bar{\rho})\psi_{001}$ is a combination of the spinor components, and ψ_2° is the same background component as in Eq. (2.35). Specializing to the metric ansatz (2.17), I remove the vanishing spin coefficients, apply the operator $\delta + \alpha$ to the first equation, apply the operator $D - 4\rho$ to the second one, subtract the two and use identity (2.28) with $p = 1$ and $q = -3$. This leads to an equation on $H_0 \equiv H_{000}$ only, which reads

$$\Big((D - 4\rho)(\Delta - 3\gamma + \mu) - (\delta + \alpha)(\bar{\delta} - 3\alpha) - \psi_2^\circ\Big) H_0 = 0\,, \tag{2.39}$$

where I have also used $(D - 3\rho)\psi_2^\circ = 0$ and $(\delta - 3\tau)\psi_2^\circ = 0$, which follow from the Bianchi identities [95]. Eq. (2.39) is the equation of motion for a massless spin $^3/_2$ field.

Master equation. Following [161, 162], one notes that Eqs. (2.32), (2.34), (2.37) and (2.39) for $s > 0$ fields can be recast under the remarkably compact form

$$\begin{aligned} &\big\{ \left[D - (2s-1)\epsilon + \bar{\epsilon} - 2s\rho - \overline{\rho}\right](\Delta - 2s\gamma + \mu) \\ &- \left[\delta + \overline{\pi} - \overline{\alpha} - (2s-1)\beta - 2s\tau\right]\left(\overline{\delta} + \pi - 2s\alpha\right) \\ &- (2s-1)(s-1)\Psi_2\big\}\tilde{\Phi}_s = 0\,, \end{aligned} \tag{2.40}$$

with $\tilde{\Phi}_s = (\phi_0, \psi_0, \chi_0, H_0)$ depending on the field spin.

I will now show how the various Eqs. (2.20), (2.32), (2.34), (2.37), (2.39) for all spins, or equivalently Eqs. (2.20) and (2.40), can be transformed into radial Teukolsky equations.

2.3.1.2 Teukolsky equations

In this section I derive an equivalent of the radial Teukolsky equation for all spins in the general spherically-symmetric and static metric (2.17). The first step of this calculation consists in developing explicitly all the terms in Eqs. (2.20), (2.32), (2.34), (2.37) and (2.39). Then, based on the spherical and time symmetries of the metric (2.17), I choose

$$\big(\phi, \phi_0, \psi_0, \chi_0, H_0\big) = \Phi_s(r) S^s_{lm}(\theta, \varphi) e^{-iEt}\,, \tag{2.41}$$

as an ansatz for the wavefunctions. Here S^s_{lm} are the spin-s weighted spherical harmonics for angular modes (l, m), satisfying the equation

$$\left(\frac{1}{\sin\theta}\partial_\theta(\sin\theta\,\partial_\theta) + \frac{1}{\sin^2\theta}\partial_\varphi^2 + \frac{2is\cot\theta}{\sin\theta}\partial_\varphi + s - s^2\cot^2\theta + \lambda^s_l\right) S^s_{lm} = 0\,, \tag{2.42}$$

where the separation constant is $\lambda^s_l \equiv l(l+1) - s(s+1)$. In the spin 0 case, $S^0_{lm} = Y_{lm}$ are just the spherical harmonics. As I consider metrics with spherical and not axial symmetry, the dependency on the angular momentum projection m factorizes as $S^s_{lm}(\theta, \varphi) = S^s_l(\theta) e^{im\varphi}$. Expanding with (2.41) the equations of motion obtained above for all spins decouple the angular and radial equations, just like in the Schwarzschild and Kerr cases [95, 97]. Furthermore, the time symmetry replaces time

derivatives by the energy E of the field. The final result takes a remarkably simple form, and I obtain the one-dimensional radial Teukolsky equation written in the general form[15]

$$A_s\big(B_s\Phi_s'\big)' + \left(\omega^2 + i\omega s\sqrt{\frac{F}{G}}\left(\frac{GH'}{H} - G'\right) + C_s\right)\Phi_s = 0\,, \tag{2.43}$$

The consistency of this equation can be checked by choosing a tr-symmetric metric with (2.19). Inserting this in (2.43) reproduces the Teukolsky master equation for all spins derived in [159], which is

$$\frac{1}{\Delta^s}\big(\Delta^{s+1}\Phi_s'\big)' + \left(\frac{\omega^2 r^2}{h} + 2i\omega sr - \frac{is\omega r^2 h'}{h} + s(\Delta'' - 2) - \lambda_l^s\right)\Phi_s = 0\,, \tag{2.44}$$

where in [159] the notation is $\Delta(r) \equiv r^2 h(r)$.

2.3.1.3 Short-ranged potentials

The next step towards an applicable formulation of the equations of motion for the computation of the GFs is to write the Teukolsky equations (2.43) in the form of a Schrödinger wave equation with short-ranged potentials. Even if the equations can in principle be solved in the form (2.43), precise and stable numerical computations require to work with potentials which fall off at least as $1/r^2$ at infinity. Furthermore, working with real-valued potentials also constitutes an appreciable bonus. One therefore needs to get rid of the first order radial derivatives and of the complex isE terms in Eq. (2.43), which have a $1/r$ behaviour at infinity.

For all of this section, it is convenient to define a generalized Eddington–Finkelstein "tortoise" coordinate r^* as [163, 164]

$$\frac{\mathrm{d}r^*}{\mathrm{d}r} = \frac{1}{\sqrt{FG}}\,. \tag{2.45}$$

In what follows I will give the expressions of the potentials with both the r^* and r coordinates, because the first one is more concise and the second one is better suited for numerical calculations. Furthermore, I will also consider the general redefinition of the wave function as

$$\Psi_s \equiv \Phi_s\sqrt{\frac{B_s}{\sqrt{FG}}}\,, \tag{2.46}$$

where all quantities are functions of r and I keep track of the spin s. Finally, for each spin my goal will be to find a wave function Z_s satisfying the general Schrödinger-like equation

$$\partial_*^2 Z_s + \Big(\omega^2 - V_s\big(r(r^*)\big)\Big)Z_s = 0\,, \tag{2.47}$$

with spin-dependent potentials V_s, and where ∂_* denotes the derivative with respect to the "tortoise" coordinate r^*. Spins 0 and 2 are already treated in the literature, while spins $1/2$ and 1 require more work, and in particular the use of the Chandrasekhar transformation. I now study in some detail these aspects.

[15] The details of the calculations and the explicit form of the radial functions $A_s(r)$, $B_s(r)$, and $C_s(r)$ are given in Appendix A of [149].

Massless spin 0. For the massless spin 0 field, there is no complex term in Eq. (2.43), and all the terms are already decreasing faster than $1/r^2$ at infinity because of the fall-offs (2.18). Applying the transformations (2.45) and (2.46), one obtains simply a Schrödinger wave equation for $Z_0 \equiv \Psi_0$, with a potential given by [163]

$$\begin{aligned} V_0\big(r(r^*)\big) &= \frac{G\lambda_l^0}{H} + \frac{1}{2}\sqrt{\frac{FG}{H}}\left(\sqrt{\frac{FG}{H}}H'\right)' \\ &= \frac{G\lambda_\ell^0}{H} + \frac{\partial_*^2\sqrt{H}}{\sqrt{H}}\,. \end{aligned} \tag{2.48}$$

This is the short-ranged potential for the massive spin 0 field in the metric (2.17).

Massless spin 2. For the massless spin 2 field, Ref. [164] follows Ref. [153]. They consider clever combinations of the metric components and the vanishing of the Ricci tensor components at first order in the perturbation to obtain directly a decoupled radial equation of the Schrödinger-like form, with the potential

$$\begin{aligned} V_2\big(r(r^*)\big) &= \frac{G(\lambda_l^2+4)}{H} + \frac{FGH'^2}{2H^2} - \frac{1}{2}\sqrt{\frac{FG}{H}}\left(\sqrt{\frac{FG}{H}}H'\right)' \\ &= \frac{G(\lambda_l^2+4)}{H} + \frac{(\partial_* H)^2}{2H^2} - \frac{\partial_*^2\sqrt{H}}{\sqrt{H}}\,. \end{aligned} \tag{2.49}$$

This is the short-ranged potential for the massless spin 2 field in the metric (2.17).

Massless spins 1 and 1/2. The above results, which are already present in the literature, are now completed by deriving the short-ranged potentials for spins 1 and 1/2. I follow here the method which was used by Chandrasekhar & Detweiler to find the short-ranged potentials for the Kerr metric [125–128]. Applying the transformations (2.45) and (2.46) to (2.43) for $s = 1$ and 1/2 gives an equation of the form

$$\left(E^2 + iEs\sqrt{\frac{F}{G}}\left(\frac{GH'}{H} - G'\right) + D_s\right)\Psi_s + \partial_*^2\Psi_s = 0\,. \tag{2.50}$$

The only way to suppress the complex term without re-introducing first order derivatives is to change the unknown function Ψ_s by a linear combination of itself and its first order derivative. In this context, this is called the "Chandrasekhar transformation". I first define the intermediate function Y_s by

$$\Psi_s = \alpha_s Y_s\,. \tag{2.51}$$

This function is such that Eq. (2.50) can be written in the form

$$\Lambda^2 Y_s + P_s\Lambda_- Y_s - Q_s Y_s = \partial_*^2 Y_s + \omega^2 Y_s + P_s(\partial_* Y_s + i\omega Y_s) - Q_s Y_s = 0\,, \tag{2.52}$$

with two functions P_s and Q_s, and the operators

$$\Lambda_\pm \equiv \partial_* \pm i\sigma\,, \quad \text{and} \quad \Lambda^2 \equiv \Lambda_\pm\Lambda_\mp = \partial_*^2 + \sigma^2\,, \tag{2.53}$$

with $\sigma \equiv -E$. When written using Eq. (2.51), Eq. (2.50) becomes

$$\partial_*^2 Y_s + \omega^2 Y_s + i\omega s\sqrt{\frac{F}{G}}\left(\frac{GH'}{H} - G'\right)Y_s + D_s Y_s + \frac{1}{\alpha_s}\big(2\partial_*\alpha_s\partial_* Y_s + Y_s\partial_*^2\alpha_s\big) = 0\,. \tag{2.54}$$

Comparing this result with Eq. (2.52) then reveals that the two new functions are defined by the requirements

$$Q_s = -D_s - \frac{\partial_*^2\alpha_s}{\alpha_s}\,, \quad \text{and} \quad P_s = \frac{2\partial_*\alpha_s}{\alpha_s} = s\sqrt{\frac{F}{G}}\left(\frac{GH'}{H} - G'\right) = s\,\partial_*\ln\left(\frac{H}{G}\right). \tag{2.55}$$

One can then show that this gives

$$Q_1 = \frac{G(\lambda_\ell^1 + 2)}{H}\,, \quad Q_{1/2} = \frac{G(\lambda_\ell^{1/2} + 1)}{H}\,, \quad \text{and} \quad \alpha_s = \left(\frac{H}{G}\right)^{s/2}. \tag{2.56}$$

Note that Q_s takes a remarkably simple form, as displayed here, in the case of spins $1/2$ and 1. Unfortunately, this is not true for spins 2 and $3/2$, in which case the explicit expression is actually much more complicated. The solution for α_s, however, is valid for all spins.

In order to continue with a lighter notation, from now on I get rid of the explicit spin label s from all the various functions involved. I further decompose Y as a linear combination of the function Z, satisfying the Schrödinger wave equation (2.47), and its derivative by writing

$$Y \equiv f\Lambda_+\Lambda_+ Z + W\Lambda_+ Z\,, \tag{2.57}$$

where on the right-hand side f and W are two unknown functions. The Schrödinger equation (2.47) takes the form $\Lambda^2 Z = VZ$, where V is the searched for short-ranged potential. Acting on Eq. (2.57) with Λ_- and using $\Lambda_+ = \Lambda_- + 2i\sigma$ then leads to

$$\Lambda_- Y = \big(\partial_*(fV) + WV\big)Z + \big(fV + \partial_*(W + 2i\sigma f)\big)\Lambda_+ Z \equiv -\frac{\beta}{\alpha^2}Z + R\Lambda_+ Z\,, \tag{2.58}$$

where on the right-hand side I have introduced two unknown functions β and R. Acting once again with Λ_- on both sides gives

$$\Lambda_-\Lambda_- Y = \left(2i\sigma\frac{\beta}{\alpha^2} - \partial_*\left(\frac{\beta}{\alpha^2}\right) + RV\right)Z + \left(\partial_* R - \frac{\beta}{\alpha^2}\right)\Lambda_+ Z\,. \tag{2.59}$$

Next, I use $\Lambda_+ = \Lambda_- + 2i\sigma$ once again to rewrite equation (2.52) in the form

$$\Lambda_-\Lambda_- Y = -(P+2i\sigma)\Lambda_- Y + QY = \left(\frac{\beta}{\alpha^2}(P + 2i\sigma) + QfV\right)Z + \big(Q(W+2i\sigma f) - (P+2i\sigma)R\big)\Lambda_+ Z\,, \tag{2.60}$$

where P is given in equation (2.55). Matching the Z and $\Lambda_+ Z$ terms of these two different expansions for $\Lambda_-\Lambda_- Y$ now implies

$$RV - QfV = \frac{\partial_* \beta}{\alpha^2}\,, \quad \text{and} \quad \partial_*(\alpha^2 R) = \beta + \alpha^2\big(Q(W + 2i\sigma f) - 2i\sigma R\big)\,, \tag{2.61}$$

in addition to which one should remember that, because of Eq. (2.58), there are also the definitions

$$-\frac{\beta}{\alpha^2} = \partial_*(fV) + WV\,, \quad \text{and} \quad R = fV + \partial_*(W + 2i\sigma f). \tag{2.62}$$

Now, one can check by a direct substitution that the four previous equations lead to the conservation equation

$$\partial_*\big(\alpha^2 R f V + \beta(W + 2i\sigma f)\big) = 0\,, \tag{2.63}$$

which is a generalization of Chandrasekhar's result. Let's call this constant K, which will later on simplify the calculations neatly. Let's also define the quantity $T \equiv W + 2i\sigma$. Using the identity (2.63) to remove an unwanted derivative of the potential V (which would have caused further difficulties), Eqs. (2.61) and (2.62) finally reduce to the system of four equations

$$RV - QfV = \frac{\partial_* \beta}{\alpha^2}\,, \tag{2.64a}$$

$$\partial_*(\alpha^2 R) = \beta + \alpha^2(QT - 2i\sigma R)\,, \tag{2.64b}$$

$$R(R - \partial_* T) + \frac{\beta T}{\alpha^2} = \frac{K}{\alpha^2}\,, \tag{2.64c}$$

$$R = fV + \partial_* T\,, \tag{2.64d}$$

where Eq. (2.64c) has been obtained by combining Eqs. (2.62) and (2.63). This is the system to solve in order to prove that a solution Z satisfying the Schrödinger wave equation with a potential V does indeed exist. This system follows from the form of the "Chandrasekhar transformation", and is valid for all spins. Chandrasekhar & Detweiler solved it for the Kerr metric and for massless spins 0, 1, 2 and $1/2$. Below, the solution for the general case of the metric (2.17) for spin 1 following [125], and for spin $1/2$ following [128] are obtained.

Spin 1. In the case of spin 1 one can look for a simple solution, *i.e.* suppose that the unknown quantities are linear in σ and of the form $A = A_1 + 2i\sigma A_2$, and that the desired potential V is of course independent of σ (together with Q which is the initial potential without the iE part). Looking at the system (2.64) shows that the only σ^2 term comes from R_2, requiring $R_2 = 0$. Then, one can further assume that $\partial_* T_2 = 0$. The only remaining terms in $i\sigma$ come from f_2 and $\partial_*\beta_2$, which are removed by imposing $f_2 = 0$ and β_2 to be constant. Both R and f are thus also independent of σ with these hypotheses. I decompose

$$T \equiv T_1 + 2i\sigma T_2\,, \quad K \equiv K_1 + 2i\sigma K_2\,, \quad \text{and} \quad \beta \equiv \beta_1 + 2i\sigma\beta_2\,. \tag{2.65}$$

With all these assumptions, the system (2.64) simply becomes

$$RV - QfV = \frac{\partial_* \beta_1}{\alpha^2}\,, \tag{2.66a}$$

$$\partial_*(\alpha^2 R) = \beta_1 + 2i\sigma\beta_2 + \alpha^2\big(Q(T_1 + 2i\sigma T_2) - 2i\sigma R\big)\,, \tag{2.66b}$$

$$R(R - \partial_* T_1) + \frac{1}{\alpha^2}\big(\beta_1 T_1 + 2i\sigma(\beta_1 T_2 + \beta_2 T_1) - 4\sigma^2\beta_2 T_2\big) = \frac{1}{\alpha^2}(K_1 + 2i\sigma K_2)\,, \tag{2.66c}$$

$$R = fV + \partial_* T_1\,. \tag{2.66d}$$

Identifying the no-σ and σ terms in Eq. (2.66b) gives the two equations

$$\partial_*(\alpha^2 R) = \beta_1 + \alpha^2 Q T_1\,, \quad \text{and} \quad R = \frac{\beta_2}{\alpha^2} + Q T_2\,, \tag{2.67}$$

while doing the same in (2.66c) leads to

$$R(R - \partial_* T_1) + \frac{1}{\alpha^2}\big(\beta_1 T_1 - 4\sigma^2\beta_2 T_2\big) = \frac{K_1}{\alpha^2}\,, \quad \text{and} \quad \beta_2 T_1 + \beta_1 T_2 = K_2\,. \tag{2.68}$$

From the last equation, the numerical value of the constant T_2 can be absorbed in the other unknown quantities, thus I set $T_2 = 1$ and define $\kappa \equiv K_1 + 4\sigma^2\beta_2$. In order to rewrite the system in an elegant way, let's define the function

$$\mathcal{F} \equiv \alpha^2 Q = l(l+1)\,. \tag{2.69}$$

With this, the second equation in (2.67) gives

$$\alpha^2 R = \beta_2 + \mathcal{F}\,, \tag{2.70}$$

which can then be injected in the first equation of (2.67) to find

$$\partial_* \mathcal{F} = \beta_1 + T_1 \mathcal{F}\,. \tag{2.71}$$

I use Eq. (2.68) to eliminate β_1 from all other equations, and Eq. (2.70) to eliminate R. The previous equation can be written as

$$T_1 = \frac{1}{\mathcal{F} - \beta_2}(\partial_* \mathcal{F} - K_2)\,, \tag{2.72}$$

and (2.66c) can be rewritten in the form

$$\frac{1}{\alpha^2}(\mathcal{F} + \beta_2)^2 - (\mathcal{F} + \beta_2)\partial_* T_1 + T_1(K_2 - \beta_2 T_1) = \kappa\,. \tag{2.73}$$

Substituting the expression (2.72) for T_1, I finally obtain an identity on $\mathcal{F}$ which reads [125]

$$\mathcal{F}(\partial_*\mathcal{F})^2 + (\beta_2^2 - \mathcal{F}^2)\partial_*^2\mathcal{F} + \frac{\mathcal{F}^4}{\alpha^2} - \left(\frac{2\beta_2^2}{\alpha^2} + \kappa\right)\mathcal{F}^2 + (2\kappa\beta_2 - K_2^2)\mathcal{F} + \left(\frac{\beta_2^4}{\alpha^2} - \kappa\beta_2^2\right) = 0\,. \tag{2.74}$$

The goal is now to find a set of constants β_2, κ, and K_2 compatible with this identity. Since $\mathcal{F}$ is a constant given simply by $\mathcal{F} = l(l+1)$, this is actually straightforward. I deduce that $\beta_2 = \pm l(l+1)$

and $K_2 = 0$, while κ is unconstrained. I choose $K_1 = 0$ and obtain $\kappa = 4\sigma^2\beta_2$. Finally, since Eq. (2.72) does not constrain T_1, I choose $T_1 = 0$, which implies $\beta_1 = 0$ thanks to Eq. (2.68). I have therefore found a consistent set of constants satisfying the assumptions, and all the remaining functions can be analytically computed. At the end, Eqs. (2.66a) and (2.66d) lead to the very simple result

$$V_1\big(r(r^*)\big) = Q_1 = l(l+1)\frac{G}{H}\,. \tag{2.75}$$

This is the short-ranged potential for a massless spin 1 field in the metric (2.17), which is moreover coherent with the potential obtained in [165] based on conformal invariance.

Spin 1/2. In order to study the case of spin 1/2, I first note that the definition of $\mathcal{F}$ gives the simple result

$$\mathcal{F} = \alpha^2 Q = \left(\lambda_\ell^{1/2} + 1\right)\sqrt{\frac{F}{G}}\,. \tag{2.76}$$

In spite of this simple form, using the same hypotheses as for spin 1, I find that identity (2.74) has no solution. I therefore need to make fewer assumptions than above. I will in fact follow [128], and go back to the system of equations (2.64). In this system, integrations can be avoided by assuming

$$\partial_* T = 0\,, \quad \text{and} \quad \partial_*(\alpha^2 R) = 0\,, \tag{2.77}$$

which in turn implies that $\tilde{R} \equiv \alpha^2 R$ is a constant. Thus one has the system

$$V = \frac{\partial_*\beta}{\tilde{R}} + \frac{(\lambda_\ell^{1/2}+1)}{\alpha^4}\,, \tag{2.78a}$$

$$0 = \beta + \frac{(\lambda_\ell^{1/2}+1)T}{\alpha^2} - 2i\sigma\tilde{R}\,, \tag{2.78b}$$

$$\frac{\tilde{R}^2}{\alpha^4} + \frac{\beta T}{\alpha^2} = \frac{K}{\alpha^2}\,, \tag{2.78c}$$

$$\frac{\tilde{R}}{\alpha^2} = fV\,, \tag{2.78d}$$

where, in order to obtain Eq. (2.78a), I have used Eq. (2.78d). One sees that Eq. (2.78a) already gives the potential as a function of β and $\tilde{R}$. The goal is therefore to determine these functions. For this, let's set $T = 2i\sigma$ by analogy with the final result of [128] and the result of the spin 1 calculation. Eq. (2.78b) becomes

$$\beta = 2i\sigma\left(\tilde{R} - \frac{(\lambda_\ell^{1/2}+1)}{\alpha^2}\right)\,, \tag{2.79}$$

and Eq. (2.78c) gives

$$\tilde{R}^2 + 4\sigma^2(\lambda_\ell^{1/2}+1) = \alpha^2(4\sigma^2\tilde{R} + K)\,. \tag{2.80}$$

In this equation, everything is a constant except α, so I identify separately

$$K = -4\sigma^2\tilde{R}\,, \quad \text{and} \quad \tilde{R} = \pm 2i\sigma\sqrt{(\lambda_l^{1/2}+1)}\,. \tag{2.81}$$

I finally use Eq. (2.78a) to write the potential as

$$\begin{aligned} V_{1/2}\big(r(r^*)\big) &= \big(l(l+1)+1/4\big)\frac{G}{H} \pm \sqrt{l(l+1)+1/4}\,\partial_*\left(\sqrt{\frac{G}{H}}\right) \\ &= \big(l(l+1)+1/4\big)\frac{G}{H} \pm \sqrt{l(l+1)+1/4}\,\sqrt{FG}\left(\sqrt{\frac{G}{H}}\right)'. \end{aligned} \tag{2.82}$$

This is the short-ranged potential for the massless spin 1/2 field in the metric (2.17).

Summary. I have obtained the short-ranged massless potentials for all spins in elegant forms summarized as

$$V_0 = \nu_0\frac{G}{H} + \frac{\partial_*^2\sqrt{H}}{\sqrt{H}}\,, \tag{2.83a}$$

$$V_1 = \nu_1\frac{G}{H}\,, \tag{2.83b}$$

$$V_2 = \nu_2\frac{G}{H} + \frac{(\partial_* H)^2}{2H^2} - \frac{\partial_*^2\sqrt{H}}{\sqrt{H}}\,, \tag{2.83c}$$

$$V_{1/2} = \nu_{1/2}\frac{G}{H} \pm \sqrt{\nu_{1/2}}\,\partial_*\left(\sqrt{\frac{G}{H}}\right)\,, \tag{2.83d}$$

where I have defined for conciseness $\nu_s \equiv \lambda_l^s + 2s$. These results are surprisingly compact, and extend the existing literature to the case of spin 1 and 1/2 massless fields in the metric (2.17).

2.3.1.4 The *tr*-symmetric case

There are numerous physically-motivated spherically-symmetric and static metrics of the form (2.17). These examples come from both classical general relativity and modified theories of gravity with *e.g.* quantum gravity corrections. I restrict the discussion to solutions that have an interesting PBH application, that is the SBH, the RNBH and the higher-dimensional BH (HDBH). All three solutions are reviewed below. Using a *tr*-symmetric ansatz, which depends only on a single function

$h(r)$, the massless potentials (2.83) become

$$V_0 = h\left(\frac{l(l+1)}{r^2} + \frac{1}{r}h'\right), \tag{2.84a}$$

$$V_1 = h\frac{l(l+1)}{r^2}, \tag{2.84b}$$

$$V_2 = h\left(\frac{l(l+1)}{r^2} - \frac{1}{r}h' + \frac{2(h-1)}{r^2}\right), \tag{2.84c}$$

$$V_{1/2} = h\frac{l(l+1)+1/4}{r^2} \pm h^{1/2}\frac{\sqrt{l(l+1)+1/4}}{r}h' \mp h^{3/2}\frac{\sqrt{l(l+1)+1/4}}{r^2}. \tag{2.84d}$$

The first three potentials, which are bosonic, can be written as a single master potential[16]

$$V_s = h\left(\frac{\ell(\ell+1)}{r^2} + \frac{1-s}{r}h' + \frac{s(s-1)(h-1)}{r^2}\right). \tag{2.85}$$

SBH potentials. For the Schwarzschild metric, recall that

$$F = G \equiv h = 1 - \frac{r_{\rm S}}{r}, \quad \text{and} \quad H = r^2, \tag{2.86}$$

where $r_{\rm H} = r_{\rm S} = 2M$ is the Schwarzschild radius of the event horizon. The short-ranged potentials, which coincide in this simple case with the well-known Regge–Wheeler potentials [122], are represented by dashed lines on Figs. 2.1, 2.2 and 2.3. The SBH potential for the Raritta–Schwinger field of spin $^3/_2$ can be found *e.g.* in [167].

RNBH potentials. After the SBH solution, the simplest PBH relevant tr-symmetric solution is the charged RNBH with

$$F = G = h = 1 - \frac{r_{\rm S}}{r} + \frac{r_{\rm Q}^2}{r^2}, \quad \text{and} \quad H = r^2. \tag{2.87}$$

where $r_{\rm Q} = Q$ and $r_{\rm H} = r_+ = r_{\rm S}(1+\sqrt{1-Q^{*2}})/2$. For neutral particles (*i.e.* with no additional coupling between the charge of the BH and that of the particle), the potentials take the form

$$V_0 = \frac{\nu_0}{r^2} + \frac{(1-\nu_0)r_{\rm S}}{r^3} + \frac{r_{\rm Q}^2(\nu_0-2) - r_{\rm S}^2}{r^4} + \frac{r_{\rm Q}^2 r_{\rm S}}{r^5} - \frac{2r_{\rm Q}^4}{r^6}, \tag{2.88a}$$

$$V_1 = \frac{\nu_1}{r^2} - \frac{\nu_1 r_{\rm S}}{r^3} + \frac{\nu_1 r_{\rm Q}^2}{r^4}, \tag{2.88b}$$

$$V_2 = \frac{\nu_2+2}{r^2} - \frac{(\nu_2+3)r_{\rm S}}{r^3} + \frac{(\nu_2+4)r_{\rm Q}^2 + r_{\rm S}^2}{r^4} - \frac{r_{\rm Q}^2 r_{\rm S}}{r^5} + \frac{2r_{\rm Q}^4}{r^6}, \tag{2.88c}$$

$$V_{1/2} = \frac{\nu_{1/2}}{r^2} - \frac{\nu_{1/2}r_{\rm S}}{r^3} + \frac{\nu_{1/2}r_{\rm Q}^2}{r^4} \mp \frac{\sqrt{\nu_{1/2}}}{2}r\sqrt{1 - \frac{r_{\rm S}}{r} + \frac{r_{\rm Q}^2}{r^2}}\left(\frac{2}{r^3} - \frac{3r_{\rm S}}{r^4} + \frac{4r_{\rm Q}^2}{r^5}\right). \tag{2.88d}$$

[16] Note that the last term in this master potential is absent from Eq. (6) of [166], but is coherent with the above results and with that of [164]. I therefore conclude that the master equation of [166] is not valid for spin 2.

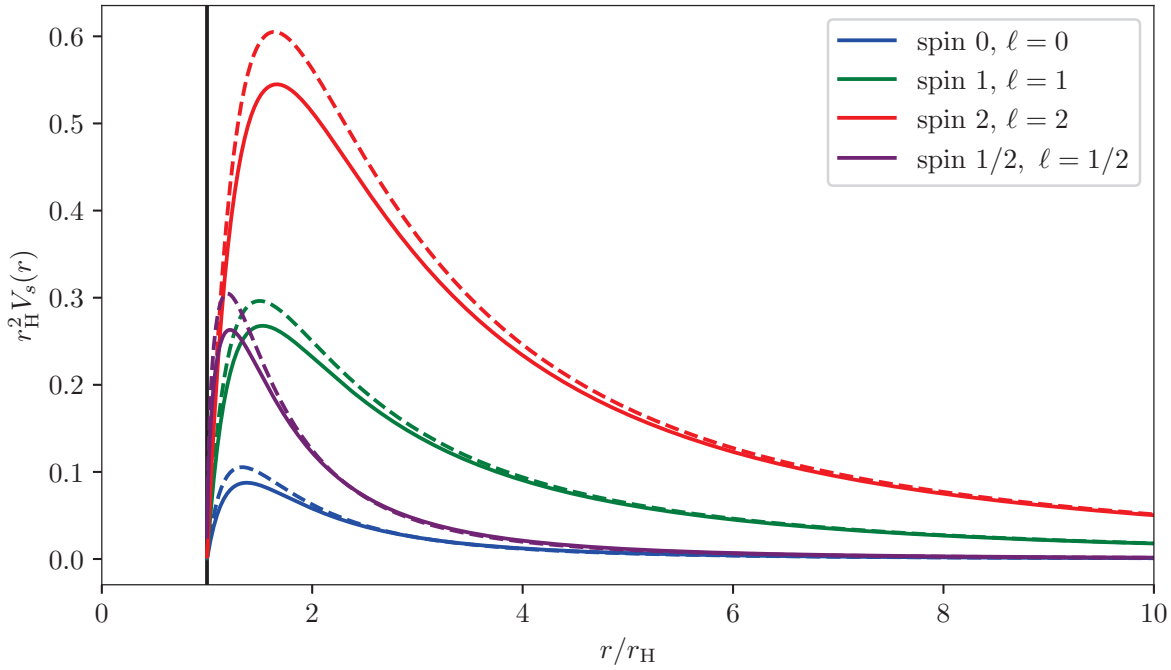

Figure 2.1: Comparison of the potentials for a charged BH with $r_{\rm Q} = r_{\rm S}/3$ (solid lines) and for the Schwarzschild metric (dashed lines). The vertical black line represents the BH event horizon. [taken from [149]]

These potentials are shown on Fig. 2.1 for the minimum possible angular momenta $l = s$ and for $r_{\rm Q} = r_{\rm S}/3$ (*i.e.* $Q = 2M/3$).[17]

HDBH potentials. Another simple case of *tr*-symmetric metrics describes a BH in $(4 + n)$ dimensions [169–171]. The HDBH solution has a peculiar history. Extensions to general relativity were proposed concomitantly by Randall & Sundrum [172, 173] (RS model) and also by Arkani-Hamed, Dimopoulos & Dvali [174–176] (ADD model) invoking the existence of additional spatial dimensions to explain the hierarchy problem between the magnitude of the gravitational interaction and that of the other forces. There is one in the RS model and several in the ADD model. These dimensions can have large sizes R and are in fact only constrained by experiments to $R \lesssim 10^{-6}$ m [177]. The extra spatial dimensions are compact, and the usual SM particles have a dynamics confined to the $(3 + 1)$ brane, which is why these models are denoted as "braneworld" cosmologies. Only the graviton can propagate inside the supplementary "bulk" dimensions because of its numerous

[17] The potential for the spin $^3/_2$ field was derived in [168].

Kaluza-Klein modes.[18] The most interesting aspect of those theories is that they predict a reduction of the Planck mass to an effective value $M_{\rm eff}$ linked to the number of extra dimensions n and their size R

$$M_{\rm Pl}^2 \sim M_{\rm eff}^{n+2} R^n \,. \tag{2.89}$$

Thus, with sufficiently large extra dimensions, the Planck scale can be reduced to $M_{\rm eff} \gtrsim 10\,\text{TeV}$, which is consistent with current accelerator data provided that SM particles are confined to the brane. The Large Hadron Collider, under construction at that time, planned collisions at TeV energies and beyond, raising the fear that mini-HDBHs could form [180, 181] and then swallow the entire Earth. This was evidently an absurd prediction as if it were the case, then mini-HDBHs should form constantly in the upper atmosphere due to CR spalliation [182] with no catastrophic consequences until now. Furthermore, this neglects the fact that mini-BHs of that size should evaporate by HR well before they accrete much surrounding matter—in fact, they should decay quasi-instantaneously [183, 184]. A more reasonable but depressing conclusion was that the collider experiments had reached a intrinsic limit as increasing further the energy would only result in BH formation, which was interpreted as "The end of short distance physics" [185]. Nevertheless, this little story triggered prolific searches on HDBHs and their HR as a probe to higher-dimensional physics in accelerators and CR studies.[19] As reviewed *e.g.* in [179], the geometry of a HDBH with radius $\ell_{\rm Pl} \ll r_{\rm H} \ll R$ is specified by

$$F = G = h \equiv 1 - \left(\frac{r_{\rm H}}{r}\right)^{n+1}, \quad \text{and} \quad H = r^2 \,, \tag{2.90}$$

where the horizon radius is

$$r_{\rm H} = \frac{1}{\sqrt{\pi} M_{\rm eff}} \left(\frac{M}{M_{\rm eff}}\right)^{1/(n+1)} \left(\frac{8\Gamma\big((n+3)/2\big)}{n+2}\right)^{1/(n+1)} , \tag{2.91}$$

and Γ is here the Euler gamma function. In this geometry, the massless potentials become

$$V_0 = \frac{\nu_0}{r^2} + \frac{r_{\rm H}^{n+1}(n+1-\nu_0)}{r^{n+3}} - \frac{(n+1) r_{\rm H}^{2n+2}}{r^{2n+4}} \,, \tag{2.92a}$$

$$V_1 = \frac{\nu_1}{r^2} - \frac{\nu_1 r_{\rm H}^{n+1}}{r^{n+3}} \,, \tag{2.92b}$$

$$V_2 = \frac{\nu_2 + 2}{r^2} - \frac{\big(\nu_2 + 2 + (n+1)\big) r_{\rm H}^{n+1}}{r^{n+3}} + \frac{(n+1) r_{\rm H}^{2n+2}}{r^{2n+4}} \,, \tag{2.92c}$$

$$V_{1/2} = \frac{\nu_{1/2}}{r^2} - \frac{\nu_{1/2} r_{\rm H}^{n+1}}{r^{n+3}} \mp \frac{\sqrt{\nu_{1/2}}}{2} \sqrt{1 - \left(\frac{r_{\rm H}}{r}\right)^{n+1}} \left(\frac{2}{r^2} - \frac{(n+3) r_{\rm H}^{n+1}}{r^{n+3}}\right) . \tag{2.92d}$$

[18] A very complete review of HR by HDBHs can be found by the interested reader in [178] which updates very good material from [179].

[19] In the context of the LHC and CRs, at least four event generators were made public that computed the spectrum of particles from HDBHs decay, namely `Charybdis` [186, 187], `Catfish` [188], `BlackMax` [189–191] and `QBH` [192]. These are very specific but complementary to our own code `BlackHawk`.

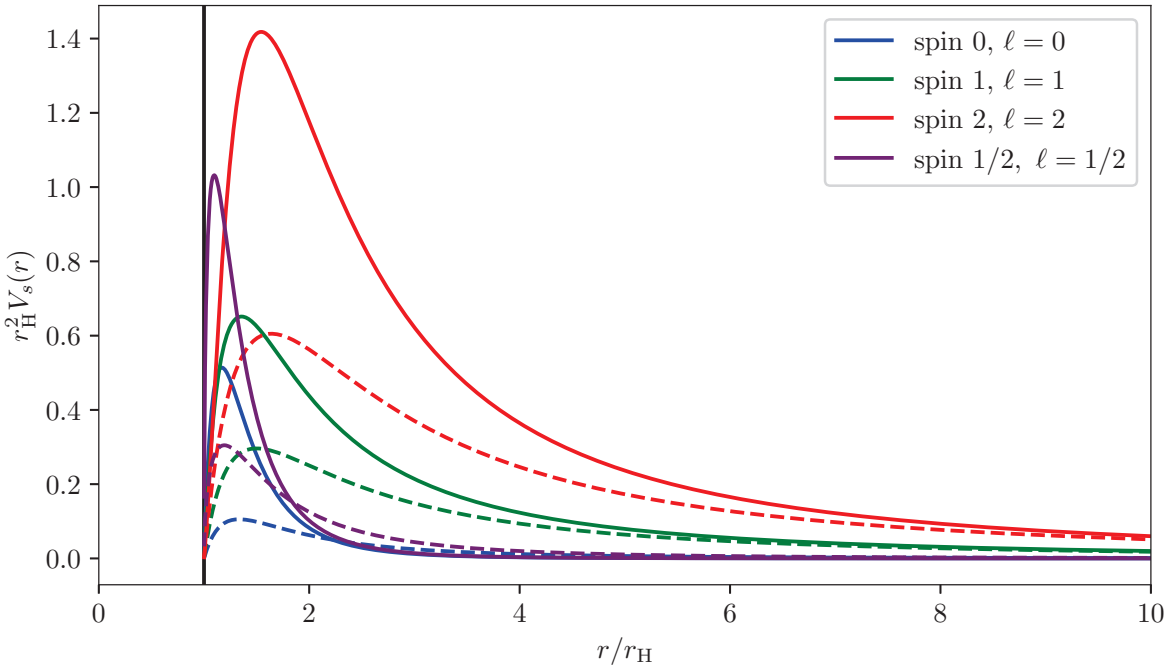

Figure 2.2: Comparison of the potentials for a HDBH with $n = 2$, $M = 10^{10}\,M_{\rm Pl}$ and $M_{\rm eff} = 10\,\text{TeV}$ (solid lines) and for the Schwarzschild metric (dashed lines). The vertical black line denotes the BH horizon. [taken from [149]]

Note that these potentials describe the radiation truncated to the four-dimensional (t, r, θ, φ) subspace adapted for SM particles, and in particular does not describe the radiation within the extra dimensions. The graviton emission rate is amplified by a numerical factor depending on the number of extra spatial dimensions (Kaluza-Klein modes), as pointed out by [171]. In Fig. 2.2 I plot the HDBH potentials and compare them to the Schwarzschild ones for $n = 2$, $M = 10^{10}\,M_{\rm Pl}$ and $M_{\rm eff} = 10\,\text{TeV}$.

2.3.1.5 A regular example: polymerized black hole

There are spherically symmetric and static metrics that are not of the tr-symmetric family. It is notably the case of most of the "regular" metrics, that is to say metrics which do not exhibit a curvature singularity at their center. These metrics were introduced to regularize the infinities arising naturally in cosmology and in BH physics: in cosmology, the Big Bang is replaced by a "bounce" that avoids infinite compression at $t = 0$ [193]; in BH physics the central singularity is replaced by a region of finite size. There are many examples of such solutions to the Eintein (and Friedmann) equations (see the discussion in Section 4.6). Here, for the sake of the example, I focus on the BH metrics which arise in loop quantum gravity [194] (LQG), where effective semi-

classical corrections due to effects of quantum gravity give rise to so-called "polymerized" BHs. There are many proposals for deriving such metrics, which are solution of the Einstein (or Friedmann) equations. Results for the potentials and HR can be compared to [163, 164]. The metric coefficients are

$$F = \frac{(r-r_+)(r-r_-)r^4}{(r+r_*)^2(r^4+a_0^2)}\,, \quad G = \frac{(r-r_+)(r-r_-)(r+r_*)^2}{r^4+a_0^2}\,, \quad \text{and} \quad H = r^2 + \frac{a_0^2}{r^2}\,. \tag{2.93}$$

Here a_0 is the "area gap" of LQG, and the radii are given by

$$r_+ = 2\mathfrak{m} \equiv r_{\rm H}\,, \quad r_- = 2\mathfrak{m}P^2\,, \quad \text{and} \quad r_* = \sqrt{r_+ r_-}\,, \tag{2.94}$$

where $P \equiv (\sqrt{1+\epsilon^2}-1)/(\sqrt{1+\epsilon^2}+1)$ is the so-called polymeric function, and the parameter $\mathfrak{m}$ is related to the Arnowitt–Deser–Misner mass M [195] (ADM) by $M = \mathfrak{m}(1+P)^2$. These polymerized BH solutions therefore have two free parameters, which are a_0 and ϵ. With these ingredients, the massless potentials become

$$\begin{aligned} V_0 = \frac{(r-r_+)(r-r_-)}{(r^4+a_0^2)^4}\Big(&\nu_0 r^{12} + (2\nu_0 r_* + r_+ + r_-)r^{11} + (\nu_0-2)r_*^2 r^{10} + 2a_0^2(\nu_0+5)r^8 \\ &+ 2a_0^2\big(2\nu_0 r_* - 5(r_+ + r_-)\big)r^7 + 2a_0^2 r_*^2(\nu_0+5)r^6 \\ &+ a_0^4(\nu_0-2)r^4 + a_0^4(2\nu_0 r_* + r_+ + r_-)r^3 + a_0^4\nu_0 r_*^2 r^2\Big), \end{aligned} \tag{2.95a}$$

$$V_1 = \nu_1 \frac{r^2(r-r_+)(r-r_-)(r+r_*)^2}{(r^4+a_0^2)^2}\,, \tag{2.95b}$$

$$\begin{aligned} V_2 = \frac{(r-r_+)(r-r_-)}{(r^4+a_0^2)^4}\Big(&(\nu_2+1)r^{12} + (2\nu_2 r_* + r_+ + r_-)r^{11} + (\nu_2+2)r_*^2 r^{10} + a_0^2(2\nu_2-11)r^8 \\ &+ 2a_0^2\big(\nu_2 r_* + 5(r_+ + r_-)\big)r^7 + a_0^2 r_*^2(\nu_2-10)r^6 \\ &+ a_0^4(\nu_2+1)r^4 + a_0^4(2\nu_2 r_* - r_+ - r_-)r^3 + \nu_2 a_0^4 r_*^2 r^2 + a_0^6\Big), \end{aligned} \tag{2.95c}$$

$$\begin{aligned} V_{1/2} = {}& \nu_{1/2}\frac{r^2(r-r_+)(r-r_-)(r+r_*)^2}{(r^4+a_0^2)^2} \\ &\pm \frac{\sqrt{\nu_{1/2}}}{2}\frac{r\sqrt{(r-r_+)(r-r_-)}}{(r^4+a_0^2)^3}\Big((r^4+a_0^2)\Big[r^2(r+r_*)(2r-r_+-r_-) \\ &+ 2r^2(r-r_+)(r-r_-) + 2r(r-r_+)(r-r_-)(r+r_*)\Big] - 8r^5(r-r_+)(r-r_-)(r+r_*)\Big). \end{aligned} \tag{2.95d}$$

In Fig. 2.3 I show these potentials compared to the Schwarzschild ones for $\epsilon = 0.8$ and $a_0 = 10^{-10} r_{\rm S}^2$. For this particular example, the spin 0 potentials almost coincide because of the cancellation of most of the corrections due to the choice of the fundamental angular mode $l = 0$.

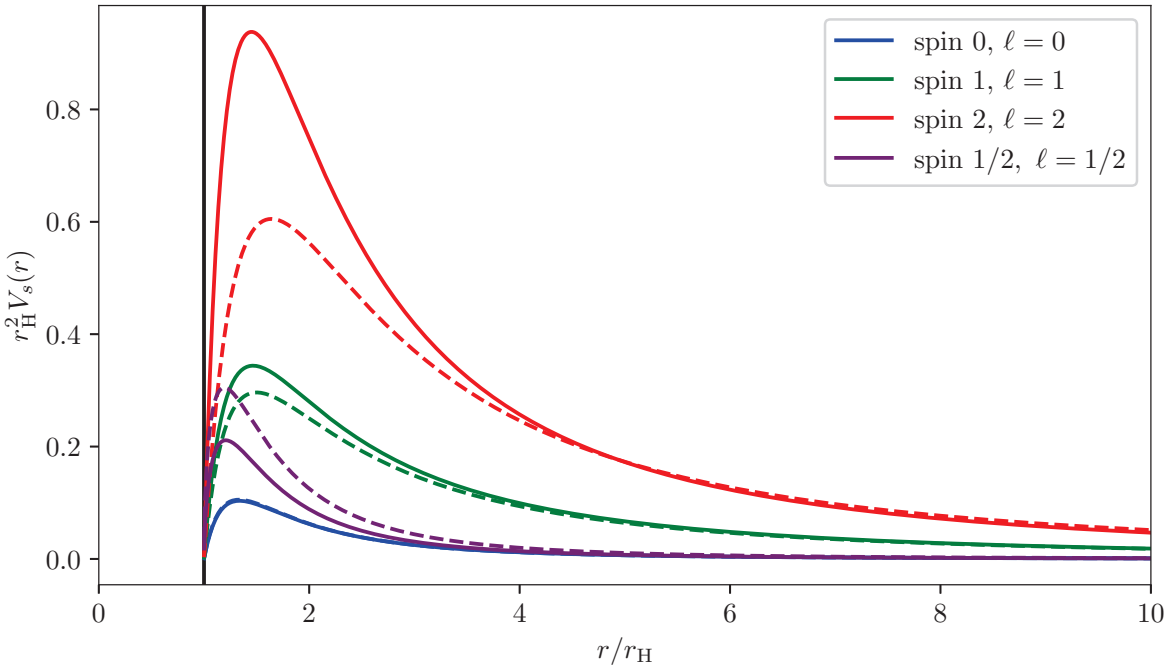

Figure 2.3: Comparison of the potentials for a polymerized BH with $\epsilon = 0.8$ and $a_0 = 10^{-10} r_{\rm S}^2$ (solid lines) and for the Schwarzschild metric (dashed lines). The vertical black line denotes the BH horizon. [taken from [149]]

2.3.2 Kerr black holes

The last example I will display is the KBH, as this solution is presumably of foremost importance in the PBH context. The Kerr algebra is much more complicated than the spherically-symmetric one due to the less restrictive axisymmetry. The concrete consequence is that some Ricci coefficients (2.24) do not cancel so that the Newman–Penrose formalism becomes quite inextricable. However, most of the steps followed in Section 2.3.1 are still valid, but the calculations are lengthier. This was all sorted out in the Chandresekhar & Detweiler papers for spins 0, 1, 2 and 1/2 [125–128] and later by Torres del Castillo for spin 3/2 [160]. Recall that the metric is

$$\mathrm{d}s^2 = \left(\mathrm{d}t - a\sin^2\theta \mathrm{d}\phi\right)^2 \frac{\Delta}{\Sigma} - \left(\frac{\mathrm{d}r^2}{\Delta} + \mathrm{d}\theta^2\right)\Sigma - \left((r^2+a^2)\mathrm{d}\phi - a\mathrm{d}t\right)^2 \frac{\sin^2\theta}{\Sigma}\,, \tag{2.96}$$

where $\Sigma(r) \equiv r^2 + a^2\cos^2\theta$ and $\Delta(r) \equiv r^2 - 2Mr + a^2$, and the horizons are located at

$$r_\pm \equiv r_{\rm S}\frac{1 \pm \sqrt{1-a^{*2}}}{2}\,. \tag{2.97}$$

The "tortoise" coordinate is now defined as

$$\frac{\mathrm{d}r^*}{\mathrm{d}r} = \frac{\rho^2}{\Delta}\,, \tag{2.98}$$

where $\rho(r)^2 \equiv r^2 + \alpha^2$ and $\alpha^2 \equiv a^2 + am/E$. The Teukolsky equation (2.43) is modified and the potentials are [151, 196, 197][20]

$$V_0(r) = \frac{\Delta}{\rho^4}\left(\nu_0 + \frac{\Delta + 2r(r-M)}{\rho^2} - \frac{3r^2\Delta}{\rho^4}\right), \tag{2.99}$$

$$V_{1/2,\pm}(r) = \nu_{1/2}\frac{\Delta}{\rho^4} \mp \frac{\sqrt{\nu_{1/2}\Delta}}{\rho^4}\left((r-M) - \frac{2r\Delta}{\rho^2}\right), \tag{2.100}$$

$$V_{1,\pm}(r) = \frac{\Delta}{\rho^4}\left(\nu_1 - \alpha^2\frac{\Delta}{\rho^4} \mp i\alpha\rho^2\frac{\mathrm{d}}{\mathrm{d}r}\left(\frac{\Delta}{\rho^4}\right)\right), \tag{2.101}$$

$$\begin{aligned} V_2(r) = \frac{\Delta}{\rho^8}\Bigg(q - \frac{\rho^2}{(q-\beta\Delta)^2}\Big((q-\beta\Delta)\left(\rho^2\Delta q'' - 2\rho^2 q - 2r(q'\Delta - q\Delta')\right) \\ + \rho^2(\kappa\rho^2 - q' + \beta\Delta')(q'\Delta - q\Delta')\Big)\Bigg). \end{aligned} \tag{2.102}$$

The λ^s_{lm} functions now depend on the combination $a \times E$ and on the angular momentum projection m due to axisymmetry, and are eigenvalues of the spin-s weighted spheroidal harmonics $\tilde{S}^s_{lm}(\theta,\varphi)$. In the potential for spin 2 particles, the following quantities appear:

$$q(r) = \nu_2\rho^4 + 3\rho^2(r^2 - a^2) - 3r^2\Delta\,, \tag{2.103}$$

$$\beta_\pm = \pm 3\alpha^2\,, \tag{2.104}$$

$$\kappa_\pm = \pm\sqrt{36M^2 - 2\nu_2(\alpha^2(5\nu_2+6) - 12a^2) + 2\beta\nu_2(\nu_2+2)}\,, \tag{2.105}$$

and still $\nu_s \equiv \lambda^s_{lm} + 2s$.[21] The potential for the spin 3/2 has been derived later for the Kerr(–Newman) geometry [196, 197]

$$\begin{aligned} V_{3/2}(r) = \frac{\Delta}{\rho^6}\Bigg(q - \frac{1}{(q-\beta_2\Delta^{1/2})}\Big((q\Delta^{1/2} - \beta_2\Delta)\{\rho^2\Delta^{1/2}q'' - \rho^2 q(\Delta^{1/2})'' - 2r[q'\Delta^{1/2} - (\Delta^{1/2})'q]\} \\ + \rho^2[\kappa_2\rho^2 - \Delta^{1/2}q' + q(\Delta^{1/2})'](q'\Delta^{1/2} - (\Delta^{1/2})'q)\Big)\Bigg), \end{aligned} \tag{2.106}$$

where the intermediate quantities are

$$q = \nu_{3/2}\rho^2 + \nu_{3/2}\alpha^2 + 2Mr - 2a^2\,, \tag{2.107}$$

$$\beta_{2,\pm} = \pm 2\sqrt{a^2 - \nu_{3/2}\alpha^2}\,, \tag{2.108}$$

$$\kappa_{2,\pm} = \pm\sqrt{\nu^3_{3/2} + \nu^2_{3/2}}\,. \tag{2.109}$$

and $\nu_s \equiv \lambda^s_{lm} + 2s$.

[20] I find that the spin 0 potential had a missing "r" in [127].

[21] A complete derivation of these equations can be found in the book by Chandrasekhar [153] and the potentials are drawn in the Chandrasekhar & Detweiler papers.

2.3.3 Calculation of the greybody factors

2.3.3.1 General procedure

I have now reduced the equations of motion of massless fields to Schrödinger-like wave equations of the form

$$\frac{\mathrm{d}^2 Z_s}{\mathrm{d}r^{*2}} + \big(E^2 - V_s(r^*)\big) Z = 0\,, \tag{2.110}$$

with short-ranged potentials $V_s(r^*)$ expressed as functions of the adequate "tortoise" coordinate r^*. The next step is to compute the GFs, that is to say the absorption coefficients of these effective potentials. This task may be performed analytically by using a path-integral formalism (*e.g.* [198]). I solved it numerically inside `BlackHawk` as explained in Section 3.1. The boundary conditions for $Z(r^*)$ are naturally [123]

$$\begin{cases} Z(r^*) \underset{r^*\to-\infty}{\sim} A^{\mathrm{in}}_{\mathrm{hor}} e^{-iEr^*}\,, \\ Z(r^*) \underset{r^*\to+\infty}{\sim} A^{\mathrm{in}}_{\infty} e^{-iEr^*} + A^{\mathrm{out}}_{\infty} e^{+iEr^*}\,, \end{cases} \tag{2.111}$$

which describe a purely ingoing wave at the horizon. Indeed, the HR emission coefficient is strictly equivalent to the absorption coefficient. It is obtained as

$$\Gamma_{Eslm}(x_j) = \left|\frac{A^{\mathrm{in}}_{\mathrm{hor}}}{A^{\mathrm{in}}_{\infty}}\right|^2, \quad \text{and} \quad \sigma_{Eslm}(x_j) \equiv \frac{\pi}{E^2}\Gamma_{Eslm}(x_j)\,. \tag{2.112}$$

Finally, the total cross-section σ_{Es} for an internal d.o.f. (color, helicity) of a massless field of spin s is obtained by summing over the independent partial waves (l,m). In the case of a spherically-symmetric BH, this sum is simplified by the fact that each angular momentum projection m provides the same contribution to σ_{Es}, resulting in a $(2l+1)$ factor. Hence,

$$\frac{\pi}{E^2}\Gamma_i(E) = \sigma_{Es} = \sum_{l,m} \sigma_{Eslm} \underset{\text{sph. sym.}}{\longrightarrow} \sum_{l} (2l+1)\sigma_{Eslm}\,. \tag{2.113}$$

The contribution of each partial wave (l,m) to σ_{Es} is not trivial. In the Schwarzschild case, it was shown by [107] that only the lowest mode contributes, that is $l = s$, at low energy. This is not true at high energy where higher modes are important [115]. Furthermore, for rotating BHs, the increase in the scattering cross-section due to the coupling between the angular mode and the BH spin (which is different from the "superradiant" instability) makes higher modes more and more important when a^* increases [153, 199]. Finally, as the energy corrected for rotation $E' = E - m\Omega$ depends on m, it is not possible to express the total cross-section in a simple formula. I note at this level that the derivation of the equations of motion and the short-ranged potentials above are completely valid for QNM calculations, with only different boundary conditions (see *e.g.* [164, 200]).

2.3.3.2 Low- and high-energy limits

Analytical formulas can be derived for the low- and high-energy limits of the GFs, as I will develop below in the case of the spherically symmetric and static metric (2.17). These formulas are necessary to check whether the numerical calculations are accurate.

High-energy limit. [22]The high energy limit is usually called the "geometrical optics" (GO) approximation, because fields of all spins scatter on the BH as an optical obstacle whose extension is given by the effective area $A_{\rm eff}(x_j)$ enclosed by the last unstable circular orbit. This area depends on the set of parameters $\{x_j\}$ of the BH metric. Let $b_{\rm c}$ be the critical impact parameter for which the incoming massless fields would reach an unstable circular orbit of radius $r_{\rm c}$. For a general BH metric of the form (2.17), this is called the "photon sphere", defined as the innermost unstable circular orbit for a massless test particle in rotation around the BH. Photons follow null geodesics, meaning that for an affine parameter λ one has

$$0 = g_{\mu\nu}\frac{\mathrm{d}x^\mu}{\mathrm{d}\lambda}\frac{\mathrm{d}x^\nu}{\mathrm{d}\lambda}\,. \tag{2.114}$$

Along every geodesic there are two conserved quantities, the energy E and the angular momentum L of the field, associated respectively to the Killing vector fields ∂_t and ∂_φ. Using the metric ansatz (2.17) they are given by

$$E \equiv G\frac{\mathrm{d}t}{\mathrm{d}\lambda}\,, \quad \text{and} \quad L \equiv H\frac{\mathrm{d}\varphi}{\mathrm{d}\lambda}\,. \tag{2.115}$$

Inserting these expressions into Eq. (2.114) and choosing a planar orbit at $\theta = \pi/2$, one gets

$$\left(\frac{\mathrm{d}r}{\mathrm{d}\lambda}\right)^2 = \frac{1}{F}\left(\frac{E^2}{G} - \frac{L^2}{H}\right) \equiv -V_{\rm eff}\,. \tag{2.116}$$

The radial acceleration is then given by $\mathrm{d}^2r/\mathrm{d}\lambda^2 = -V'_{\rm eff}$. Remark that one could obtain the same result by directly calculating the radial geodesic equation. In order to have an unstable circular orbit there must be a critical radius $r_{\rm c}$ such that $V'_{\rm eff}(r_{\rm c}) = 0$ and $V''_{\rm eff}(r_{\rm c}) < 0$. Since on this orbit the radial velocity must be vanishing, one can also use Eq. (2.116) to constrain the energy and the angular momentum to satisfy

$$V_{\rm eff}(r_{\rm c}) = 0 \quad \Longrightarrow \quad \frac{L^2}{H(r_{\rm c})} = \frac{E^2}{G(r_{\rm c})}\,. \tag{2.117}$$

It is then straightforward to verify that the condition for the unstable orbit reduces to

$$V'_{\rm eff}(r_{\rm c}) = 0 \quad \Longrightarrow \quad \frac{G'(r_{\rm c})}{H'(r_{\rm c})} - \frac{G(r_{\rm c})}{H(r_{\rm c})} = 0\,, \tag{2.118a}$$

$$V''_{\rm eff}(r_{\rm c}) < 0 \quad \Longrightarrow \quad H(r_{\rm c})G''(r_{\rm c}) - H''(r_{\rm c})G(r_{\rm c}) < 0\,. \tag{2.118b}$$

The critical impact parameter for a massless particle is then defined with respect to the energy and the angular momentum of the field as

$$b_{\rm c}^2 \equiv \frac{L^2}{E^2} = \frac{H(r_{\rm c})}{G(r_{\rm c})}\,. \tag{2.119}$$

[22]I am grateful to F. Sartini for the derivation of this high-energy limit.

Finally, the effective area (classical scattering) of the BH is given in $4+n$ dimensions as

$$\sigma_\infty = A_{\rm eff}(x_j) = \frac{\pi^{(n+2)/2} b_{\rm c}^{n+2}}{\Gamma\big((n+4)/2\big)}\,, \tag{2.120}$$

where Γ is the Euler gamma function.

In the tr-symmetric case, for which one has $F(r) = G(r) \equiv h(r)$ and $H(r) = r^2$ in Eq. (2.17), the conditions (2.118) reduce to [201, 202]

$$h'(r_{\rm c}) - \frac{2}{r_{\rm c}} h(r_{\rm c}) = 0\,, \quad \text{and} \quad h''(r_{\rm c}) - \frac{2}{r_{\rm c}^2} h(r_{\rm c}) < 0\,. \tag{2.121}$$

Then, the impact parameter is given by

$$b_{\rm c} = \frac{r_{\rm c}}{\sqrt{h(r_{\rm c})}}\,. \tag{2.122}$$

In the Schwarzschild case, one obtains for all particle spins (see *e.g.* [121] and references therein)

$$\sigma_\infty = 27\pi M^2 \equiv \sigma_{\rm GO}\,, \tag{2.123}$$

which is the usual GO approximation cross-section.[23] To compare these results to the limit at high energies, let's define the quantity

$$\beta_\infty \equiv \frac{\sigma_\infty}{\sigma_{\rm GO}} = \frac{A_{\rm eff}(x_j)}{(27/4)\pi r_{\rm S}^2}\,. \tag{2.124}$$

Low-energy limit. At low energy, massless fields of each spin behave differently, as shown by the results obtained by Page in Eqs. (2.11). Several methods have been used to obtain the low energy limits for the cross-section. Classical scattering arguments apply to the low energy limit of the spin 0 field, as can be found *e.g.* in [203] which uses the partial wave decomposition and the small angle approximation for the LQGBH.

More generally, authors use a "matching" method which consists in reducing the radial spin-dependent Teukolsky equation (2.43) to a simplified version in the "far field" region ($r \to +\infty$) and in the "horizon" region ($r \to r_{\rm H}$). Depending on the number of poles (number of horizons) of the metric components F and G, the differential equation obtained is some form of a Heun equation (*e.g.* [204]). This dependency on the number and quality of poles makes it difficult to provide a general procedure to obtain the desired equation, especially in the general non-tr-symmetric case $F \neq G$. Then, solving in each region independently, while applying the correct boundary conditions, and matching the two solutions in the intermediate region gives an analytical expression for the GF.[24] This expression can be expanded in the limit $Er_{\rm H} \to 0$ to obtain the analytical low energy limit for the cross-section. One further simplification is that at low energy, only the lowest

[23] Note that some authors use for simplicity the "pure blackbody" approximation that is often incorrectly written as $\sigma = A = \pi r_{\rm S}^2$, which differs from the GO approximation (2.123) by a numerical factor.

[24] Arguments that justify the matching procedure are given *e.g.* in [205].

momentum partial wave $l = s$ participates significantly to the result [107]. This is the method used *e.g.* in [107, 159, 205–208]. In the Schwarzschild case, the low energy limits are given in Eqs. (2.11). In the low energy limit, the spin dependency makes me define the quantities

$$\beta_s \equiv \frac{\sigma_{s,\text{low}}}{\sigma_{s,\text{S}}}\,, \tag{2.125}$$

where the low energy limits in the Schwarzschild case are given in Eqs. (2.11).

Numerical check. I fit the numerical cross-sections computed for various energies E at low and high energies to obtain the coefficients β_∞ and β_s. I also check that the exponent of the energy dependency corresponds to the expected one up to 0.01% precision (0 for spins 0 and $1/2$, 2 for spin 1 and 4 for spin 2). The fitting of the high energy constant limit is complicated by the oscillatory behaviour of the cross-section at high energies (see the spectra below in Section 2.4). The asymptotic value is reached from below for spin 2, thus the fitting procedure always slightly underestimates the value of β_∞, but the coherence with other spins results is clear. In all 3 examples presented here, I checked that when the extra-Schwarzschild parameters go to 0 (charge, number of extra dimensions, polymerization parameter), the Schwarzschild results are recovered, that is $\beta_\infty = 1$ and $\beta_s = 1$.

RNBH cross-sections. The numerical cross-sections I computed inside `BlackHawk` are consistent with [119]. At high energy and for a RNBH with charge Q^*, it was shown in *e.g.* [209] that the GO limit for the cross-section for all spins is

$$\beta_\infty^Q = \frac{(3+\sqrt{9-8Q^{*2}})^4}{216(3-2Q^{*2}+\sqrt{9-8Q^{*2}})}\,, \tag{2.126}$$

which can also be obtained from Eq. (2.120). At low energies, the general study of [205] applies and the low frequency limits are for all spins

$$\begin{cases} \beta_0^Q = r_+^2/r_\text{S}^2\,, & \beta_1^Q = r_+^2(r_+-r_-)^2/r_\text{S}^4\,, \\ \beta_2^Q = r_+^3(r_+-r_-)^3/r_\text{S}^6\,, & \beta_{1/2}^Q = (r_+-r_-)^2/r_\text{S}^2\,. \end{cases} \tag{2.127}$$

The comparison to the numerical results is shown in Fig. 2.4, with very good agreement.

HDBH cross-sections. The numerical cross-sections I computed inside `BlackHawk` are consistent with [159, 170, 171]. In [159] (and references therein) it was shown that for a number of extra dimensions n, the limiting value of the effective area of the horizon is $A_\text{eff}(n) = 4\pi r_\text{c}^2$ where

$$r_\text{c} \equiv \left(\frac{n+3}{2}\right)^{1/(n+1)} \sqrt{\frac{n+3}{n+1}}\, r_\text{H}\,, \tag{2.128}$$

and r_H is given by Eq. (2.91) which implies that the high energy cross-section satisfies

$$\beta_\infty^n = \left(\frac{r_\text{H}}{r_\text{S}}\right)^2 \left(\frac{n+3}{2}\right)^{2/(n+1)} \left(\frac{n+3}{n+1}\right), \tag{2.129}$$

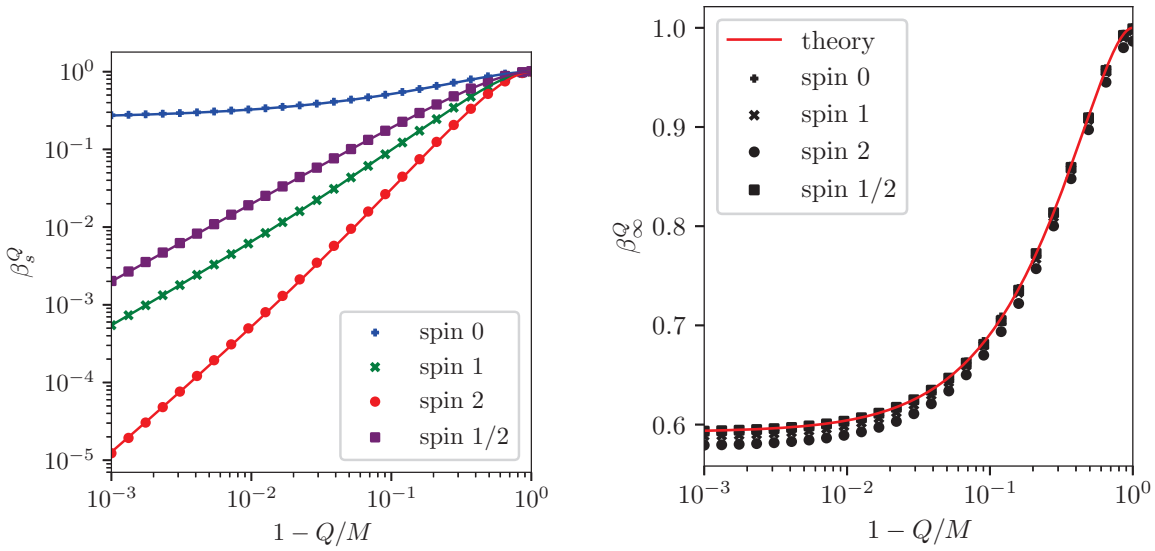

Figure 2.4: Comparison of the numerical RNBH cross-sections with the low-energy limits of Eqs. (2.127) (**left**) and with the high-energy limit of Eq. (2.126) (**right**). Data points are shown as markers and theoretical formulas as solid lines. [taken from [150]]

which could also have been obtained thanks to Eq. (2.120). On the other hand, at low energy I obtain cross-sections compatible with [159, 206, 207]

$$\begin{cases} \beta_0^n = r_{\rm H}^2/r_{\rm S}^2\,, & \beta_1^n = \dfrac{4r_{\rm H}^4}{r_{\rm S}^4}\left[\dfrac{\Gamma(1/(n+1))\Gamma(2/(n+1))}{(n+1)\Gamma(3/(n+1))}\right]^2, \\ \beta_2^n = \dfrac{16r_{\rm H}^6}{r_{\rm S}^6}\left[\dfrac{\Gamma(1/(n+1))\Gamma(4/(n+1))}{(n+1)\Gamma(5/(n+1))}\right]^2, & \beta_{1/2}^n = 2^{4-4/(n+1)}r_{\rm H}^2/r_{\rm S}^2\,. \end{cases} \tag{2.130}$$

Note that the low-energy asymptotic limit for spin 2 is not given explicitly in [207]. However, their Eqs. (37) and (38) are valid for spin 2, as shows a careful follow-up of all the steps from the Teukolsky master equation. Note also that in [210] only the analytical results for spin 2 emission *in the bulk* are given, while I focus here on *brane* emission.[25] The results are shown in Fig. 2.5 (right panel). The comparison to the numerical results is given in Fig. 2.5, with still very good agreement.

LQGBH cross-sections. In the literature, the spin 0 case was historically treated first, theoretically in [163, 211, 212] and numerically in [203]. Then, spins 0 and 1/2 were studied in [213], where in the spin 1/2 case the Teukolsky equation was solved numerically without the intermediate

[25] The two differ only by a numerical factor counting the Kaluza-Klein modes of the graviton, see *e.g.* the discussion in [171].

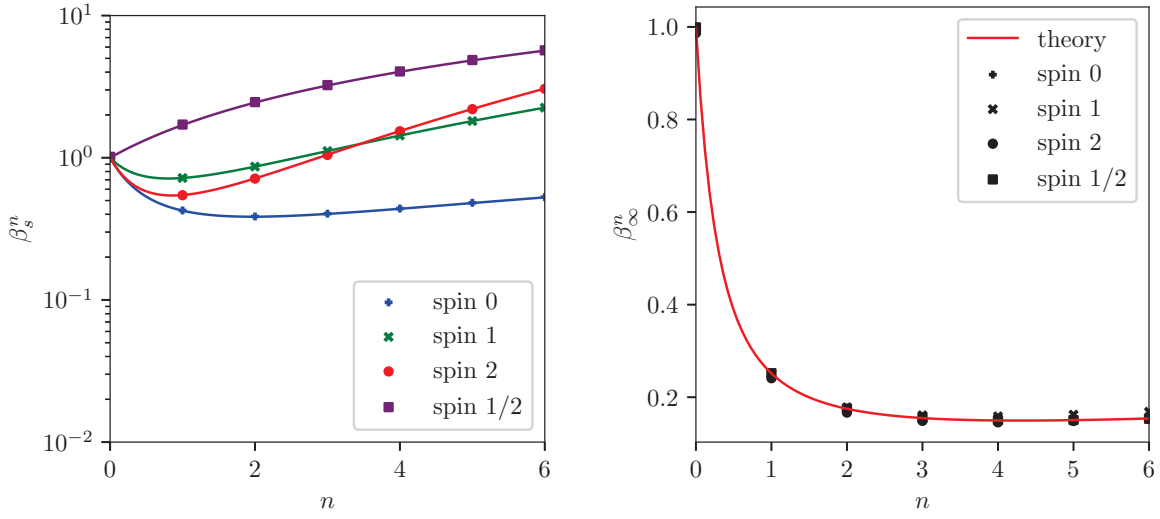

Figure 2.5: Comparison of the numerical HDBH cross-sections with the low-energy limits of Eqs. (2.130) (**left**) and with the high-energy limit of Eq. (2.129) (**right**). Data points are shown as markers and theoretical formulas as solid lines. [taken from [150]]

step of deriving the short-ranged potential. Concerning the massless spin 2 perturbations (and other spins as well), they were only studied in the case of QNMs [164, 214]. These studies invoke the same kind of potentials as in Eqs. (2.83), but solve the Schrödinger-like wave equation with different boundary conditions to find the quasi-normal frequencies. It was not possible to compare my numerical cross-sections for low values of ε for spins 0 and $1/2$ to those of [213] due to unspecified normalization factors in their Figs. 2, 3 and 4.

The high energy limit of the cross-section for polymerized BHs had not yet appeared in the literature. Using conditions (2.118), I obtain the value for the radius of the photon sphere in the limit $a_0 \to 0$. This is

$$r_{\rm c}^{\rm LQG} = \frac{r_+}{6}\left(3P^2 - 4P + 3 + \frac{9 + P\left(6 + P(10 + 6P + 9P^2)\right)}{z} + z\right), \tag{2.131}$$

where z is

$$z \equiv \Bigg[27 + 27P - 63P^2 - 190P^3 - 63P^4 + 27P^5 + 27P^6 + 3P(1+P)\sqrt{-675 + 3P(-238 + P(49 + P(636 + P(49 - P(238 + 225P)))))}\Bigg]^{1/3}. \tag{2.132}$$

The high energy limit of the cross-section is therefore given by

$$\beta_{\infty}^{\mathrm{LQG}} = \left(\frac{r_{\mathrm{c}}^{\mathrm{LQG}}}{r_{\mathrm{S}}}\right)^2 \frac{1}{G\left(r_{\mathrm{c}}^{\mathrm{LQG}}\right)} \,. \tag{2.133}$$

In the case where $a_0 \neq 0$, and in particular when taking the fiducial value $a_0 = \sqrt{3}\gamma/2 \simeq 0.11$ where $\gamma \equiv \ln(2)/\sqrt{3}\pi$ is the Barbero–Immirzi parameter [213], one cannot use the approximate formula (2.133). However, a numerical estimation of the photon sphere radius r_{c} can be performed and the resulting high-energy cross-section can be compared to the numerical one. The effect of taking $a_0 \neq 0$ is small anyways. It was proven by [203] that at low energy the scalar wave has a cross-section

$$\beta_{0}^{\mathrm{LQG}} = \frac{4m^2(1+P^2)}{r_{\mathrm{S}}^2}\left(1+\frac{a_0^2}{16m^4}\right) = \frac{r_+(r_+ + r_-)}{r_{\mathrm{S}}^2}\left(1+\frac{a_0^2}{r_+^4}\right). \tag{2.134}$$

The comparison to the numerical results is shown in Fig. 2.6, with very good agreement when analytical derivation is available, showing that the short-ranged potentials for this non-tr-symmetric example are efficient. For the spin 0 field, the low ε regime is correctly reproduced, but a discrepancy between the analytical limit and the numerical calculation is found at high values of ε. This difference is small, and concerns only the very low energy asymptotic behaviour. It is not clear whether the derivation of the formula (2.134) is valid at high values of ε. There is, to my knowledge, no literature giving the asymptotic limits at low energy for the other spins, and a "matching procedure" between "far field" and "horizon" analytical solutions as described above is very tedious

2.4 Primary spectra

In the above Section, I have derived the numerical value of the cross-sections for massless fields of spin 0, 1, 2 and 1/2 for relevant BH solutions. I have also compared the high- and low-energy limits to analytical formula, showing very good agreement that reinforce my confidence in the short-ranged potentials (2.83). Below, I obtain the primary HR spectra for all fields.

2.4.1 Hawking temperature

The master formula for the emission rate of HR is

$$\frac{\mathrm{d}^2 N_{slm}}{\mathrm{d}t\mathrm{d}E} = \frac{1}{2\pi}\frac{\Gamma_{Eslm}(x_j)}{e^{E'/T(x_j)} - (-1)^{2s}} \,, \tag{2.135}$$

where I have made explicit the dependency of the emission rate on, in general:

- field parameters: the energy E, the spin s and the angular momentum parameters (l, m);
- BH parameters: the set of quantities $\{x_j\}$ that contains at least the mass M, but also the parameters of the KBH (angular momentum a^*), RNBH (charge Q^*), HDBH (number of extra dimensions n and effective Planck mass M_{eff}) or LQGBH (deformation parameter ε and area gap a_0).

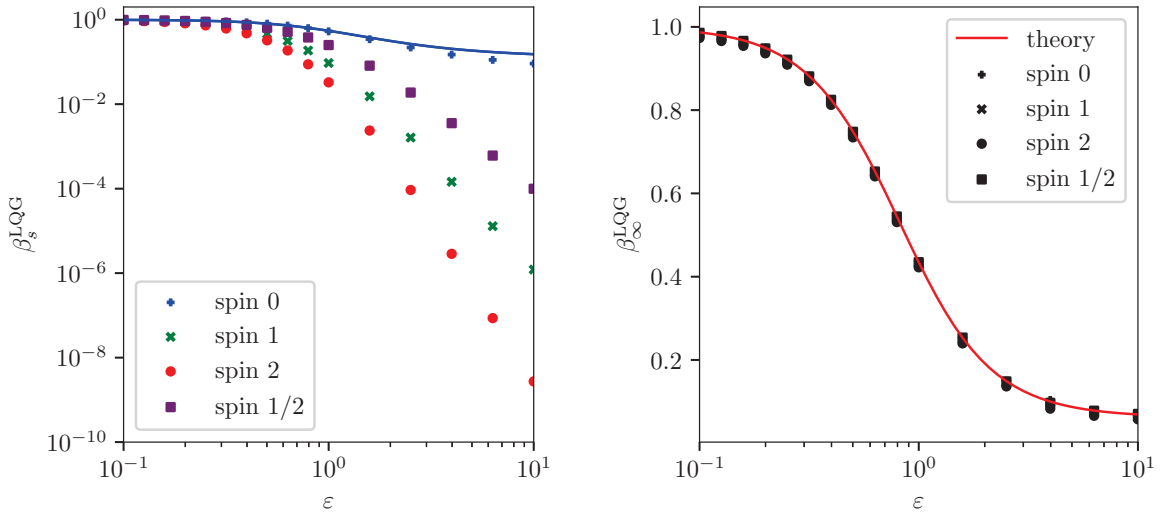

Figure 2.6: Comparison of the numerical LQGBH cross-sections with the low-energy limits of Eqs. (2.130) (**left**) and with the high-energy limit of Eq. (2.129) (**right**). Data points are shown as markers and theoretical formulas as solid lines. [taken from [150]]

The total rate of emission of a field with spin s is obtained by summing over the angular d.o.f.

$$Q_s(E) \equiv \frac{\mathrm{d}^2 N_s}{\mathrm{d}t\mathrm{d}E} = \sum_{l,m} \frac{\mathrm{d}^2 N_{slm}}{\mathrm{d}t\mathrm{d}E}\,, \tag{2.136}$$

The (Bekenstein-)Hawking temperature $T(x_j)$ depends only on the BH parameters. Its calculation is quite simple as

$$T = \frac{\kappa}{2\pi}\,. \tag{2.137}$$

In the spherically-symmetric case, it can be shown that [150]

$$\kappa^2 \equiv -\frac{1}{2}\nabla_\mu k_\nu \nabla^\nu k^\mu\Big|_{\mathrm{hor}} = \frac{1}{4}\frac{FG'^2}{G}\Big|_{\mathrm{hor}}\,, \quad \Longrightarrow \quad T = \frac{1}{2\pi}\sqrt{\frac{1}{4}\frac{FG'^2}{G}}\Big|_{\mathrm{hor}}\,. \tag{2.138}$$

Once applied to the RNBH case, I obtain

$$T_{\mathrm{RN}} = \frac{r_+ - r_-}{4\pi r_+^2}\,, \tag{2.139}$$

while for the HDBH I get

$$T_{\mathrm{HD}} = \frac{n+1}{4\pi r_{\mathrm{H}}}\,. \tag{2.140}$$

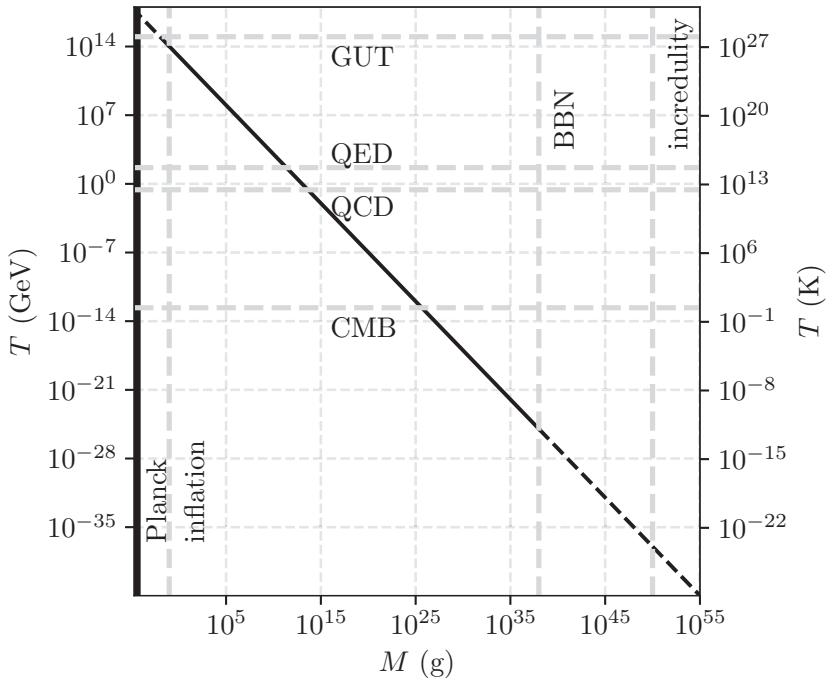

Figure 2.7: Temperature of a SBH as a function of its mass. The vertical lines have the same meaning as in Fig. 1.1. The horizontal lines give the energy scales of: the CMB ($T \sim 2.7\,\mathrm{K}$), the QCD phase transition ($\Lambda_{\mathrm{QCD}} \sim 250\,\mathrm{MeV}$), the QED phase transition ($\Lambda_{\mathrm{QED}} \sim 45\,\mathrm{GeV}$) and the GUT scale ($T \sim 10^{14} - 10^{16}\,\mathrm{GeV}$).

and finally for the LQGBH

$$T_{\mathrm{LQG}} = \frac{r_+^2 (r_+ - r_-)}{4\pi (r_+^4 + a_0^2)} \,. \tag{2.141}$$

In the KBH case, one can prove that [199]

$$T_{\mathrm{K}} = \frac{1}{2\pi} \left(\frac{r_+ - M}{r_+^2 + a^2} \right) . \tag{2.142}$$

These formulas reduce to the well-known SBH result in the limit where all the additional parameters go to 0

$$T_{\mathrm{S}} = \frac{1}{8\pi M} \,. \tag{2.143}$$

The Schwarzschild temperature is plotted in Fig. 2.7 together with relevant energy scales, and the non-standard temperatures are shown in Fig. 2.8. The behaviour of the Schwarzschild temperature is quite simple as it is inversely proportional to M. The behaviour is more complicated for the other

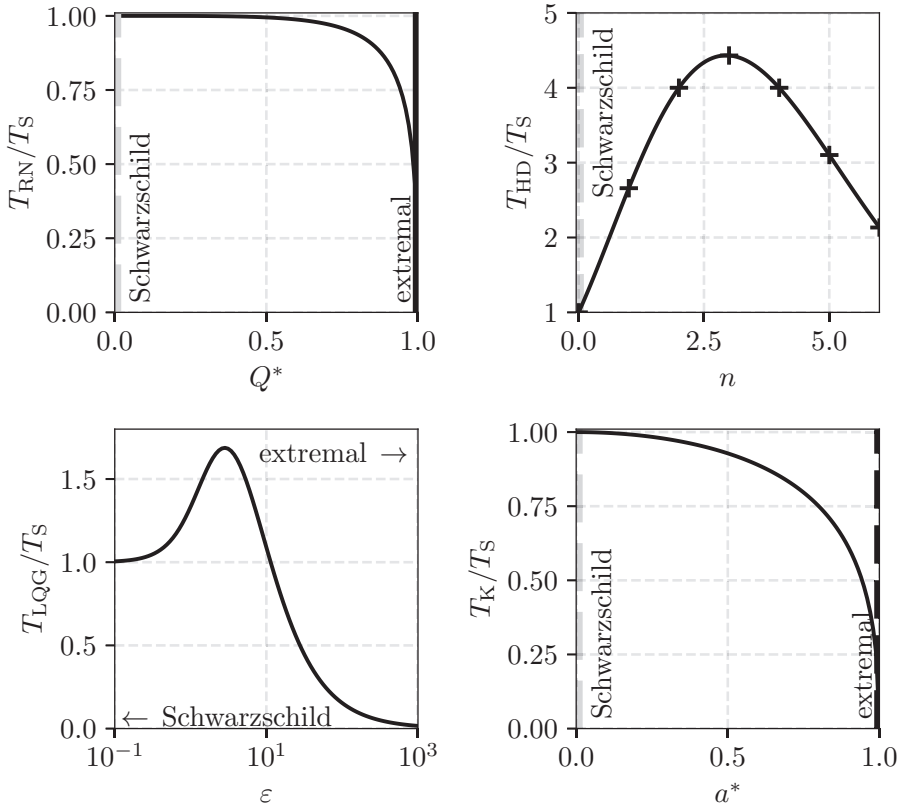

Figure 2.8: Temperatures of a RNBH (**upper left**), HDBH (**upper right**), LQGBH (**lower left**) and KBH (**lower right**) relative to the SBH, as a function of the relevant metric parameters Q^*, n, ε and a^*. The vertical lines represent the Schwarzschild limit (grey dashed) or the extremal limit (black).

temperatures. In the RNBH case, as Q^* increases at fixed M, the temperature decreases to reach the extremal limit $T \to 0$ when $Q^* \to 1$—just like for the KBH. In the LQG case, there is also an "extreme" limit $T \to 0$ when $\varepsilon \to +\infty$, but it is not attained in a monotonic fashion. Finally, the HDBH is more involved as at fixed n, the radius of the BH depends on the ratio M/M_{eff}. In Fig. 2.8, I have fixed this ratio to 1. Thus, one could naïvely expect that for the RNBH, LQGBH and KBH, the emission rate will decrease when approaching the "extremal" limit. The behaviour is not clear at first sight for the HDBH.

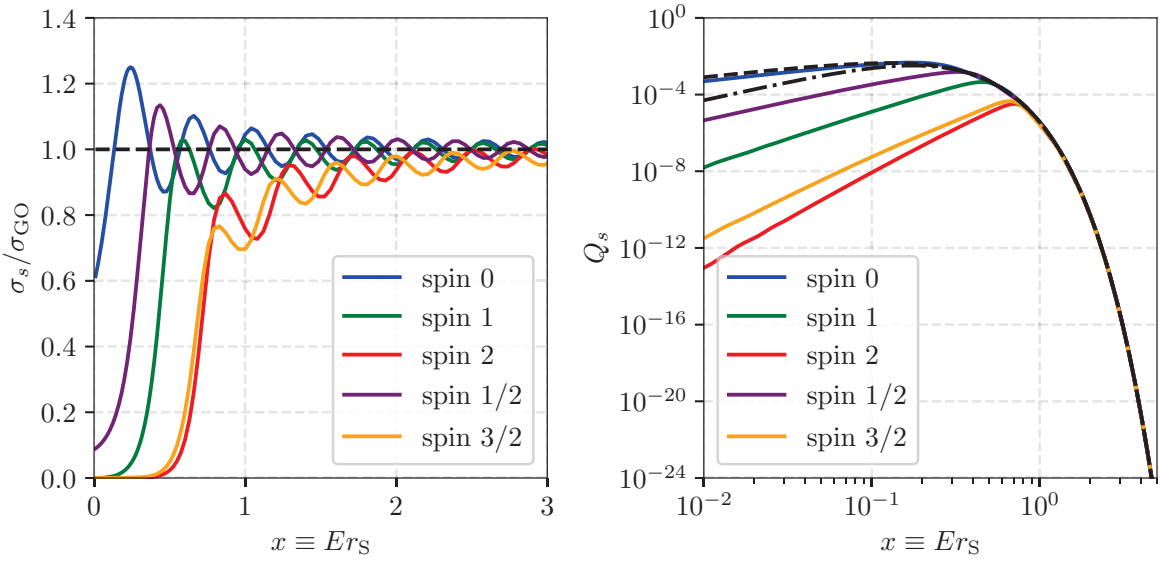

Figure 2.9: Left: Cross-section σ_{sE} of massless fields of spins 0 (blue), 1 (green), 2 (red), $1/2$ (purple) and $3/2$ (orange) relative to the GO approximation (dashed black line). **Right:** Corresponding instantaneous primary spectra. The GO approximation is indicated by black lines for a boson (dashed) and a fermion (dot-dashed).

2.4.2 Spectra

The Hawking primary spectrum, that is the instantaneous energy spectrum of emission of all fundamental d.o.f. (2.146), depends on the product of the Fermi–Dirac or Bose–Einstein temperature factor and of the GF. Let's consider first particles of spin 0, 1, 2, and $1/2$ with a single internal d.o.f.

SBH spectra. The total cross-sections σ_s for each spin s of a SBH are shown in Fig. 2.9 (left panel). The corresponding total primary spectra Q_s are displayed in Fig. 2.9 (right panel). Both figures are drawn as functions of the dimensionless parameter $x \equiv Er_{\rm S}$ as it was shown that the primary spectra are scale-invariant in that parameter for SBHs [107]. The results for the spin $3/2$ are entirely new and were implemented in `BlackHawk v2.0` for DM studies (for an application, see Section 4.5).

The first thing one remarks on the cross-section figure 2.9 is the oscillatory behaviour around the GO limit which is attained quite rapidly at $x \gtrsim 5$. These oscillations originate from the higher angular momentum modes in the sum (2.113) [115]. The second remark is that at low energy, all $s > 1/2$ cross-sections go to 0 as some power-law of E, as one can deduce from Eqs. (2.11). Hence, there is a hierarchy between fields in the peak value of the cross-section at $x \sim 1$ where the emission is expected to be concentrated.

In Fig. 2.9, the primary spectra for a spin s field with a single internal d.o.f. for a SBH shows

exactly the spin hierarchy intuited above, that is

$$Q_0 > Q_{1/2} > Q_1 > Q_{3/2} > Q_2 \,. \tag{2.144}$$

The peak of the emission spectra are not exactly located at $E \sim T$ but at slightly higher values, whose numerical realization depends on the particle spin, as was thoroughly studied by MG&W [121, 133]. The spin $^3/_2$ behaviour is very close to that of the spin 2.

RNBH spectra. The cross-sections and primary spectra of a RNBH are shown on Fig. 2.10. An increase in the charge Q^* leads to a monotonic decrease in the temperature and thus of the emitted power: the higher the BH charge, the smaller the HR rate; with the emission peaking at a smaller energy. It seems thus that when $T \to 0$ in the extremal limit, the evaporation should stop altogether, which led various people to consider PBHs stabilized by (dark) EM charge [215, 216].

HDBH spectra. The cross-sections and primary spectra of a RNBH are shown on Fig. 2.11. The HDBH exhibits a far more powerful HR that the Schwarzschild BH of the same radius. This is due to the fact that at equivalent mass, the HDBH has a larger radius. This causes the emission rates, and thus the lifetimes, to vary by orders of magnitude with the number of dimensions, effectively resulting in a mass shift of the PBH constraints [170, 171, 217, 218] (these are further modified by enhanced accretion processes [219]). The amount of HR that goes preferentially in the brane (SM fields) or in the bulk (gravitons) has been the subject of intense debate in the early 2000's [220–223] until Kanti & collaborators settled the problem [178, 179]. One unusual feature is that the oscillatory behaviour of the cross-section at high energies is completely damped.

LQGBH spectra. The cross-sections and primary spectra of a RNBH are shown on Figs. 2.12 (low values of ε) and 2.13 (high values of ε). To my knowledge, our paper [150] was the first to present primary spectra for LQGBHs for all field spins. The cross-sections for spins 0 and $^1/_2$ were given in [213] but the comparison is not possible due to unspecified normalization. Moreover, it seems that I find results differing from theirs for massless fields of spin $^1/_2$: they predict a distortion of the spectra at high energies that one does not observe in the right panel of Fig. 2.12 corresponding to the fermionic field. The height of the first peak in the fermionic cross-section seems to follow a different tendency in the present results compared to theirs when ε increases. However we both observe that increasing the parameter ε leads to a decreasing HR rate. A linear scale has been used in the left panels of Fig. 2.12 to make this statement more obvious, while a logarithmic scale was used for high values of ε in Fig. 2.13 as the HR is much more decreased. I also note that the parameter a_0 plays no particular role in the rates of emission, at least when varying between 0 and the often-used value $a_0 = \sqrt{3}\gamma/2 \simeq 0.11$ where $\gamma \equiv \ln(2)/\sqrt{3}\pi$ is the Barbero–Immirzi parameter [164], causing only a very slight decrease in the high energy tail due to the different temperatures. The differences are at the percentage level and not shown here. The effect of small values of ε on the HR rates is small altogether.

The results are much more intriguing for high values of ε, and are reported on Fig. 2.13. With values of $\varepsilon = \{1, 4, 10\}$ a reduction in the temperature of a factor $\sim \{1, 1.6, 3.2\}$ (respectively) is

obtained. The associated decrease in the emission rate is strongly spin-dependent, a feature that could be explained with an analysis of the precise dependency of the potentials in ε: the emission is more and more damped for high values of ε as the particle spin increases. This is a major result which has important consequences on the HR constraints discussed in Section 4.6. Note that the high-ε damping of the HR rate is very clear for spins $s > 0$, while the spin 0 emission rate is mildly affected.

KBH spectra. The primary spectra of a KBH are shown on Fig. 2.14 (the cross-sections cannot be easily isolated due to the angular momentum projection dependency).[26] For KBHs, even if the temperature decreases $T \to 0$ as the angular momentum approaches the extremal limit $a^* \to 1$, the BH-field spin coupling will compensate so much that the emission rate in fact increases with increasing a^*. Carter [111] wrongly identified that with the "superradiant" process. The enhancement due to a high KBH spin is non trivial and depends critically on the field spin (see *e.g.* [224]). Page already observed that the hierarchy between emission rates is totally reversed for near-extremal KBHs, with

$$Q_2 > Q_1 > Q_{1/2}\,, \tag{2.145}$$

as $a^* \to 1$. Numerically, the rate is multiplied by ~ 10 for spin $1/2$, by $\sim 10^2$ for spin 1 and by $\sim 10^4$ for spin 2 [119] (see also [199]). This behaviour is thus much less trivial than the RNBH one, and has interesting consequences on the Kerr PBH constraints from HR (see Sections 4.3 and 4.4).

[26] The emission rates for the SBH and the KBH have been double-checked by Cheek *et al.* [138], showing percent level agreement.

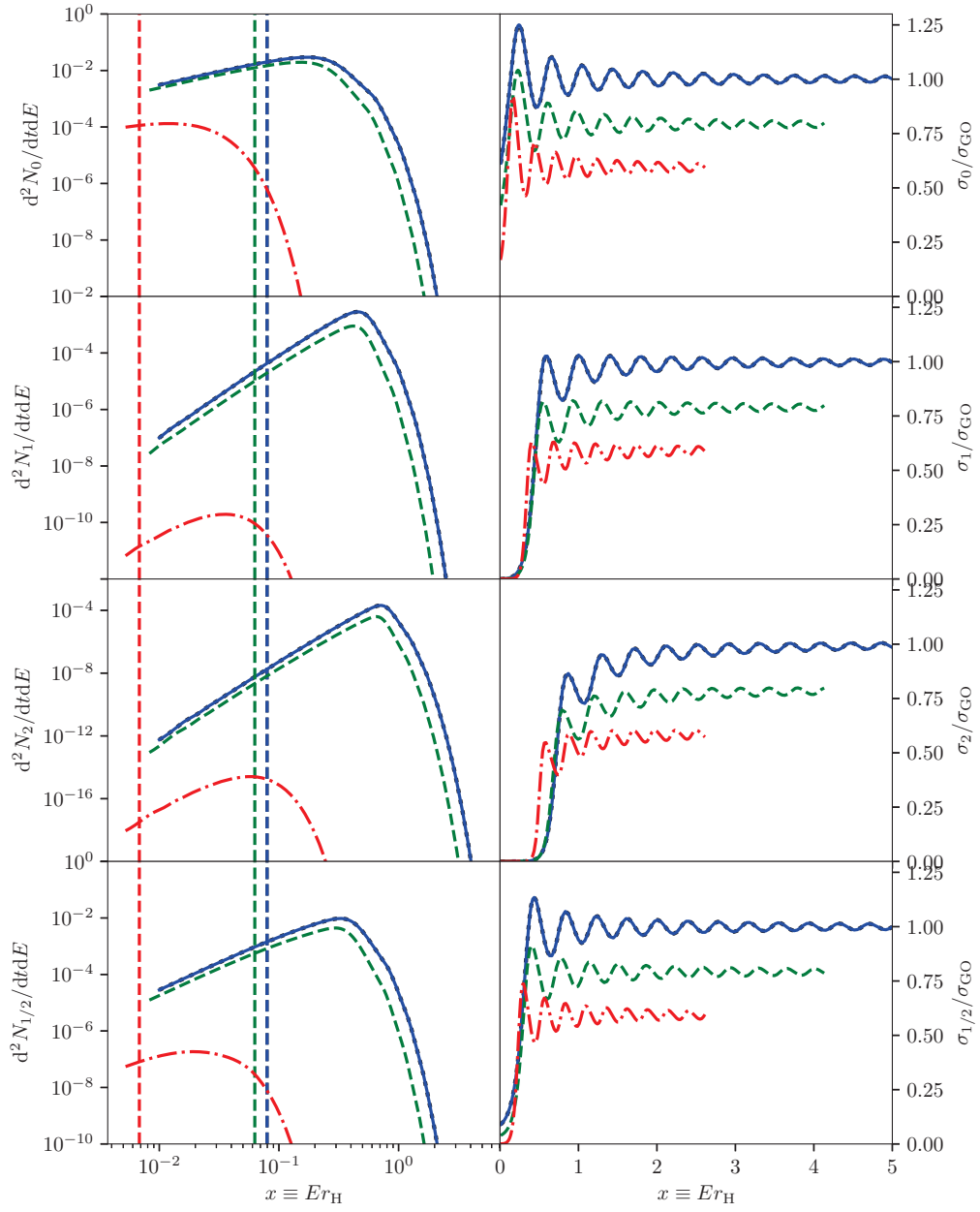

Figure 2.10: Primary spectra (**left**) and cross-sections (**right**) for spins 0, 1, 2 and 1/2 for a RNBH with $Q^* = \{0.01, 0.758, 0.999\}$ (resp. solid blue, dashed green, dot-dashed red) compared to the SBH (dotted black). The vertical lines represent T_{RN}. [taken from [150]]

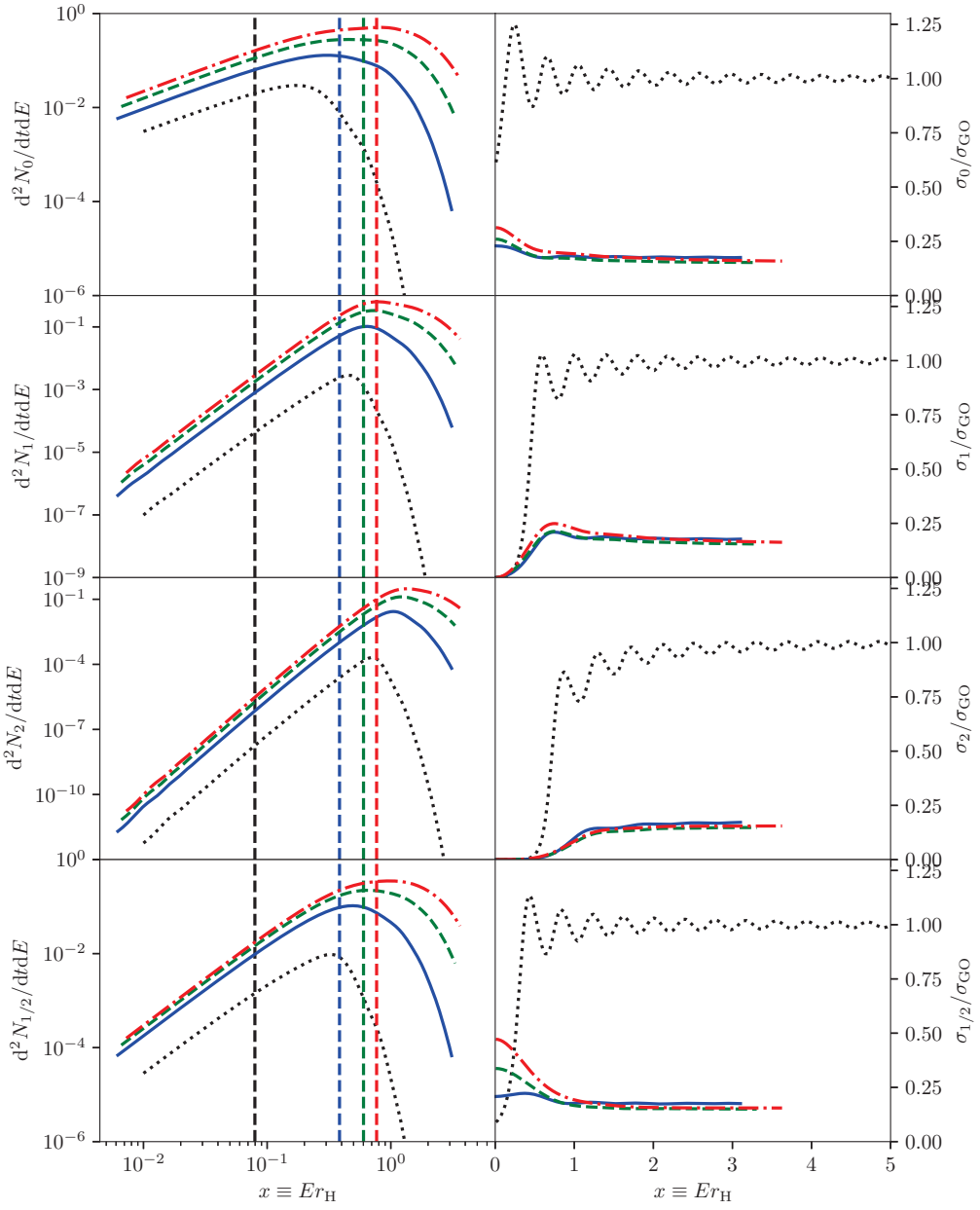

Figure 2.11: Primary spectra (**left**) and cross-sections (**right**) for spins 0, 1, 2 and 1/2 for a HDBH with $n = \{2, 4, 6\}$ (resp. solid blue, dashed green, dot-dashed red) compared to the SBH (dotted black). The vertical lines represent T_{HD}. [taken from [150]]

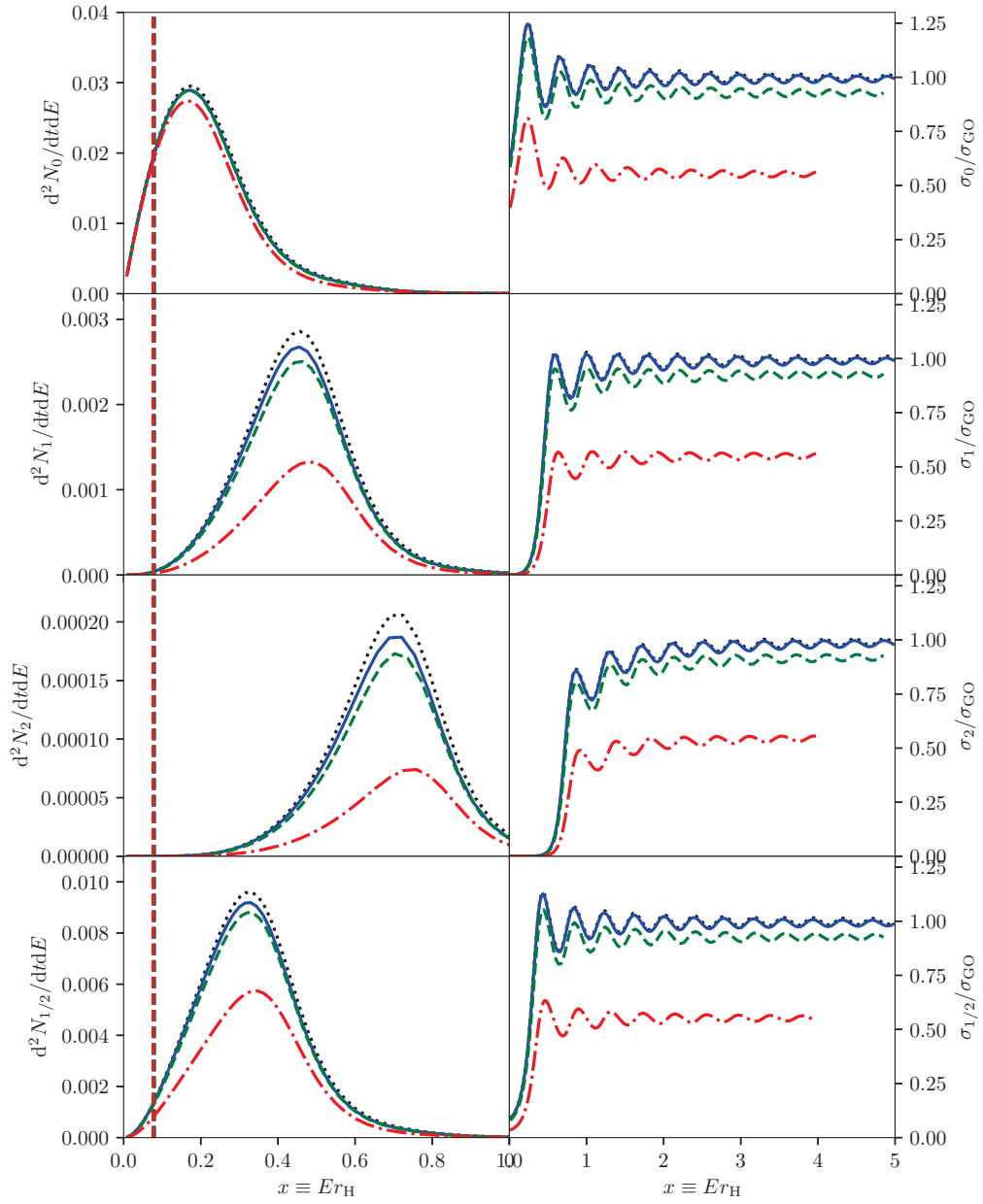

Figure 2.12: Primary spectra (**left**) and cross-sections (**right**) for spins 0, 1, 2 and 1/2 for a LQGBH with low values of $\varepsilon = \{10^{-1}, 10^{-0.6}, 10^{-0.1}\}$ (resp. solid blue, dashed green, dot-dashed red) compared to the SBH (dotted black). The vertical lines represent T_{LQG}. *Please note the linear vertical scale.* [taken from [150]]

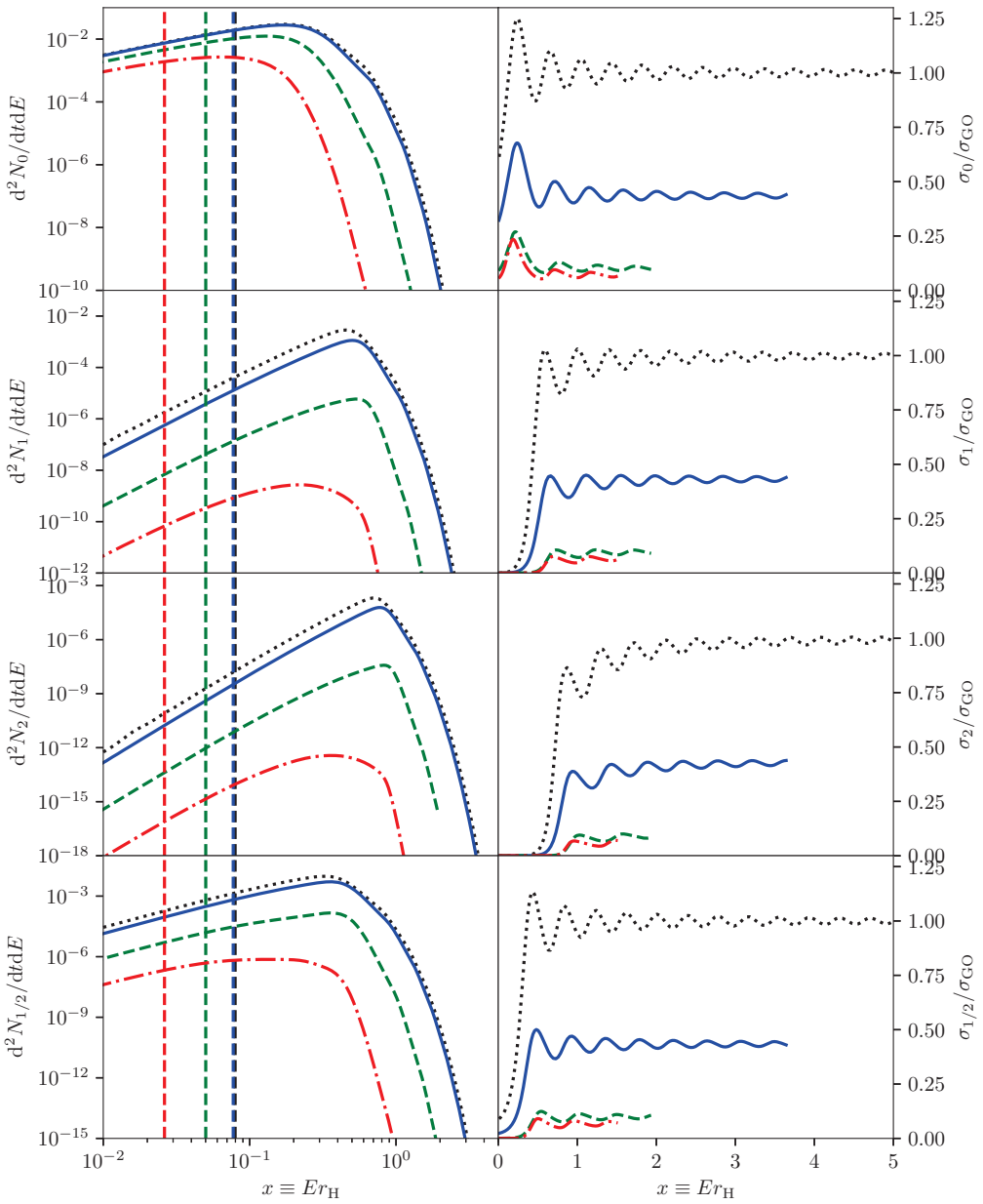

Figure 2.13: Same figure for a LQGBH with low values of $\varepsilon = \{1, 4, 10\}$ (resp. solid blue, dashed green, dot-dashed red) compared to the SBH (dotted black). [taken from [150]]

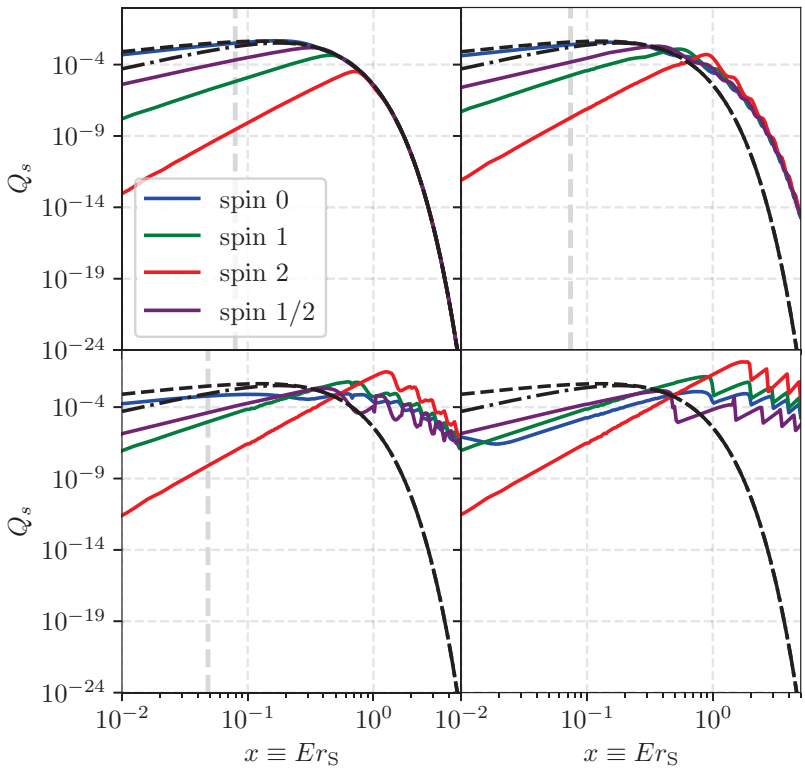

Figure 2.14: Primary spectra for spins 0, 1, 2 and 1/2 (resp. blue, green, red and purple lines) for a KBH with $a^* = \{0.5, 0.9, 0.9999\}$ (resp. **upper right**, **lower left** and **lower right**) compared to the SBH (**upper left**). The GO optics approximation is indicated for a boson (black dashed) and a fermion (black dot-dashed). The vertical lines represent $T_{\rm K}$ (the temperature $T_{\rm K}(a^* = 0.9999)$ is outside the plot).

2.5 Secondary spectra

Of course, the primary spectra of fundamental SM particles are not the final output of a BH. As developed in Section 2.2, there was a great deal of numerical work done in the 1990's to obtain the secondary spectra of BHs at all temperatures, taking into account:

- the emission cutoffs at $E < \mu$ where μ is the rest mass of a particle, meaning that more and more SM d.o.f. are emitted as the BH temperature increases;
- the precise composition of the primary emission, particularly at $E \sim \Lambda_{\rm QCD}$, where pions are emitted directly instead of free quarks and gluons;
- the subsequent evolution of the primary spectrum due to hadronization of the QCD particles into jets and the decay of massive particles into stable ones.

These calculations are the second main purpose of the public code `BlackHawk` presented in the next Chapter 3; the first being the calculation on the GFs.

The primary emission of a SM particle i of spin s_i and mass μ_i reads

$$Q_i(E) = g_i \Theta(E - \mu_i) Q_s(E)\,, \tag{2.146}$$

where the emission rate of a single d.o.f. of spin s is given by Eq. (2.136), Θ is the step function and g_i counts the number of internal d.o.f., that is color, helicity and antiparticle multiplicities given in Table 2.1 for all the SM fields. To obtain the secondary spectra, I follow the procedure introduced by MG&W [121, 133] using arguments of Oliensis & Hill [132]: the secondary spectra of fields j are obtained by hadronizing and decaying the primary spectra thanks to a convolution of the primary spectra with particle physics codes

$$Q_j \equiv \frac{{\rm d}^2 N_j}{{\rm d}t{\rm d}E} = \int_0^{+\infty} \sum_i \frac{{\rm d}N_{i\to j}}{{\rm d}e} Q_i(e)\,{\rm d}e\,, \tag{2.147}$$

where ${\rm d}N_{i\to j}/{\rm d}e$ are the branching ratios from primary to secondary particles; the numerical procedures are developed in Chapter 3.

When performing the convolution, one needs to know which particles are "stable" in the secondary emission, *i.e.* which particles have the time to interact with the environment (or the detector) before decaying. It was argued *e.g.* by Kohri & Yokoyama [225] that in the context of BBN studies, all particles with a lifetime $\tau \gtrsim 10^{-8}\,$s interact with the plasma. These particles are listed in Table 2.2. On the other hand, the only SM particles that can travel on cosmological scales to reach terrestrial detectors are "stable" in the usual manner. These are listed in Table 2.3.

In Fig. 2.15, I present the secondary spectra for a Schwarzschild PBH evaporating at BBN epoch, while in 2.16 I present the spectra of stable particles. All figures have been obtained with `BlackHawk` with the aid of hadronization tables computed with `PYTHIA`. These spectra would be of course non-trivially modified in the case of a non-Schwarzschild PBH. The general shape of the spectra can be compared to that obtained by MG&W (which considers only usual "stable" particles). The scale-invariance of the primary spectra as functions of $x \equiv E r_{\rm S}$ is lost for secondary spectra,

particle	symbol	lifetime (s)
photon	γ	∞
electron	$e^{\pm}$	∞
muon	$\mu^{\pm}$	$(2.1969811 \pm 0.0000022) \times 10^{-6}$
neutrinos	$\nu_{e,\mu,\tau}, \overline{\nu}_{e,\mu,\tau}$	∞
charged pions	$\pi^{\pm}$	$(2.6033 \pm 0.0005) \times 10^{-8}$
neutral "long" kaon	$K^0_{\rm L}$	$(5.099 \pm 0.021) \times 10^{-8}$
charged kaons	$K^{\pm}$	$(1.2379 \pm 0.0021) \times 10^{-8}$
proton	p,$\overline{\rm p}$	∞
neutron	n,$\overline{\rm n}$	880.2 ± 1

Table 2.2: Particles with a lifetime longer than 10^{-8} s, relevant for early universe/BBN studies [81].

particle	symbol	lifetime (s)
photon	γ	∞
electron	$e^{\pm}$	∞
neutrinos	$\nu_{e,\mu,\tau}, \overline{\nu}_{e,\mu,\tau}$	∞
proton	p,$\overline{\rm p}$	∞

Table 2.3: Stable particles, relevant for evaporating BH on cosmological time scales [81].

as the SM interactions of course depend on the energy of the particles. As shown by MG&W, the secondary particles produced by jet decays totally dominate in the lower energy part of the spectra. The (anti)protons are uniquely secondary particles.

2.6 Extended distribution

PBHs are formed in general with an extended distribution of mass, and possibly secondary parameter x (*e.g.* spin, charge) $\mathrm{d}^2 n/\mathrm{d}M\mathrm{d}x$ (see the discussion in Section 1.3). In this case, Eq. (2.146) to obtain the primary spectra for the complete distribution becomes

$$Q_i = \int_{M_{\rm min}}^{M_{\rm max}} \int_{x_{\rm min}}^{x_{\rm max}} g_i \Theta(E - \mu_i) Q_{s_i}(E) \frac{\mathrm{d}^2 n}{\mathrm{d}M \mathrm{d}x} \, \mathrm{d}x \, \mathrm{d}M \,. \tag{2.148}$$

This equation is simplified in the case where the two distributions for mass and secondary parameter are marginal $\mathrm{d}^2 n/\mathrm{d}M\mathrm{d}x = \mathrm{d}n/\mathrm{d}M \times \mathrm{d}\tilde{n}/\mathrm{d}x$ and it is further reduced if one of the distributions is monochromatic

$$Q_i = \begin{cases} \displaystyle\int_{x_{\rm min}}^{x_{\rm max}} g_i \Theta(E - \mu_i) Q_{s_i}(E) \frac{\mathrm{d}\tilde{n}}{\mathrm{d}x} \, \mathrm{d}x \,, & \text{mass,} \\ \displaystyle\int_{M_{\rm min}}^{M_{\rm max}} g_i \Theta(E - \mu_i) Q_{s_i}(E) \frac{\mathrm{d}n}{\mathrm{d}M} \, \mathrm{d}M \,, & \text{secondary parameter.} \end{cases} \tag{2.149}$$

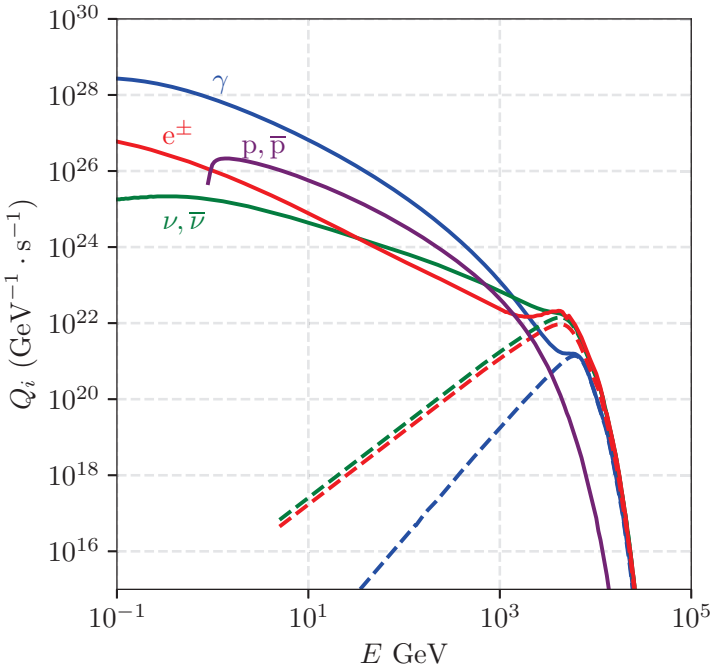

Figure 2.15: Primary (dashed) and secondary (solid) spectra of photons (γ), all flavors of neutrinos ($\nu, \overline{\nu}$), electrons and positrons ($e^{\pm}$) and (anti)protons ($p,\overline{p}$) from a 10^{10} g PBH (corresponding to ~ 1 TeV), with "stable" particles from BBH epoch (Table 2.2).

2.7 Black hole evolution

The major consequence of the HR process is that it makes BHs *evolve* in the counter-intuitive way of progressively *losing* mass. This is grasped by the Page coefficients already discussed above. Restricting the discussion to a KBH, recall that the Page coefficients are

$$\begin{pmatrix} -f(M,a^*)/M^2 \\ -g(M,a^*)a^*/M \end{pmatrix} \equiv \frac{\mathrm{d}}{\mathrm{d}t}\begin{pmatrix} M \\ J \end{pmatrix} = \sum_i g_i \sum_{s_i lm} \int_0^{+\infty} \frac{1}{2\pi} \frac{\Gamma_{Eslm}(a^*)}{e^{(E-m\Omega)/T(a^*)} - (-1)^{2s_i}} \begin{pmatrix} E \\ m \end{pmatrix} \mathrm{d}E\,, \quad (2.150)$$

They are obtained by integrating the instantaneous emission rate, multiplied by the field energy E (resp. angular momentum m) for the mass loss rate $f(M,a^*)$ (resp. angular momentum $g(M,a^*)$). These Page coefficients simplify neatly the equations of evolution of M and a^*

$$\begin{aligned} \frac{\mathrm{d}M}{\mathrm{d}t} &= -\frac{f(M,a^*)}{M^2}\,, \\ \frac{\mathrm{d}a^*}{\mathrm{d}t} &= \frac{a^*(2f(M,a^*) - g(M,a^*))}{M^3} = \frac{-a^* f(M,a^*) h(M,a^*)}{M^3}\,. \end{aligned} \quad (2.151)$$

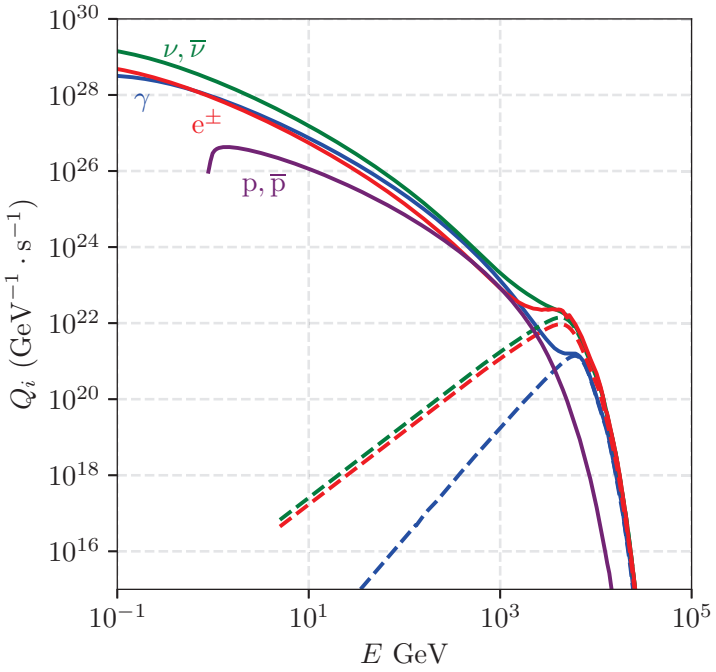

Figure 2.16: Primary (dashed) and secondary (solid) spectra of photons (γ), all flavors of neutrinos ($\nu, \overline{\nu}$), electrons and positrons ($e^{\pm}$) and (anti)protons ($p,\overline{p}$) from a 10^{10} g PBH (corresponding to ~ 1 TeV), with the usual "stable" particles (Table 2.3).

The set of coupled equations (2.151) can be solved numerically to obtain the mass and spin evolution of a BH by emission of a bunch of fundamental particles.[27] Some comments are of order. The SBH lifetime τ is given in general by [25]

$$\tau(M, a^*) = \int_0^M \frac{M^2}{f(M, a^*)} \mathrm{d}M \,. \tag{2.152}$$

If one considers that the Page coefficient $f(M, a^* = 0)$ is a constant, the lifetime of a SBH is

$$\tau_{\mathrm{S}} = \frac{1}{3 f(M_{\mathrm{i}})} M_{\mathrm{i}}^3 \,, \tag{2.153}$$

where M_{i} is the initial mass, while at each time t

$$M(t) = M \left(1 - \frac{t}{\tau_{\mathrm{S}}}\right)^{1/3} . \tag{2.154}$$

[27] Numerical fits of these functions have been obtained recently in [138].

First, it is obvious from the definition of $f(M, a^*) > 0$ that the mass decreases because of the evaporation process. Hence, a BH subject to HR is not strictly speaking *static* but backreaction of the emission on the BH metric should be taken into account. In fact, on mass scales safely above the Planck mass, the process can be considered as quasi-static and the backreaction problem alleviated. This breaks down at $M \sim M_{\rm Pl}$ where the semi-classical treatment of quasi-static HR is out of its regime of validity and quantum corrections must be taken into account. The result can be that a stable Planck-mass remnant (PMR) lingers, or that the BH disappears in a final flash. The PMR has very interesting properties as it is in fact a very compelling candidate for DM (see the discussion in Section 4.1.3).

Second, it is not obvious what is the sign of $g(M, a^*)$ because $m = -l, ..., +l$, plus the quantity $h(M, a^*)$ may be positive or negative depending on the relative importance of $f(M, a^*)$ and $g(M, a^*)$. This led Page [119] to postulate that for a BH only subject to scalar emission, for which they suspected $h(M, a^* \sim 0) < 0$ and $h(M, a^* \sim 1) > 0$ based on rough interpolations, the spin could in fact stabilize at a non-zero value given by the 0 of $h(M, a^*)$. This can be understood as follows: as the BH evaporates, its mass always decreases, but its spin is mass-dependent because $a^* \equiv J/M^2$. Hence, the spin can increase if the decrease in J due to spin-aligned mode emission is slower than the decrease in M^2 due to energy emission. This intuition was numerically confirmed by Chambers, Hiscock & Taylor [226, 227] and studied recently by [228] where they added numerous axion (scalar) fields to the modern SM content.[28]

Third, these evolution equations rely on the fact that PBHs are only subject to HR. This is not the case in general, as PBHs evolve in a complex environment from the time of their formation (radiation, then matter-dominated). They may accrete great amounts of material, in fact at a rate larger than their evaporation rate, at least for an initial period. The general formulation of the mass evolution should be

$$\frac{{\rm d}M}{{\rm d}t} = \Gamma_{\rm acc}(M) - \Gamma_{\rm evap}(M)\,, \tag{2.155}$$

where the decay rate $\Gamma_{\rm evap}$ is given by the HR Page coefficient, and the accretion rate $\Gamma_{\rm acc}$ is quite uncertain and depends on the density of the surrounding environment, on the relative velocity of the PBH and on the efficiency of BH accretion (which itself depends on the geometry and composition of the in-falling material and on the BH metric). This uncertainty gave rise to claims ranging from the extremal situation where PBHs accrete all the causally available matter and grow as fast as the Hubble horizon,[29] to the other extreme where PBH accretion is totally negligible. The correct behaviour is probably between those and numerous studies have tried to estimate what would be the mass gain of PBHs due to accretion in the early universe. Sufficient mass gain could allow big PBHs to be the seeds of the SMBHs at the center of galaxies [33, 229–232]. Accretion is however generally believed to remain at $\mathcal{O}(1)$ scales for PBH masses relevant for the HR phenomenon. Nevertheless, when the density of the universe decreases, accretion should stop and evaporation alone should occur.

Fourth, PBHs can form binary systems in the same manner as all other celestial objects. If these binary systems are long-lived—that is, not disrupted by fly-bys—then the PBHs can merge before

[28] `BlackHawk` was recently modified to be able to deal with this kind of unusual behaviour.

[29] This was the original proposition of Zel'dovich & Novikov [21], debunked by Carr & Hawking [24].

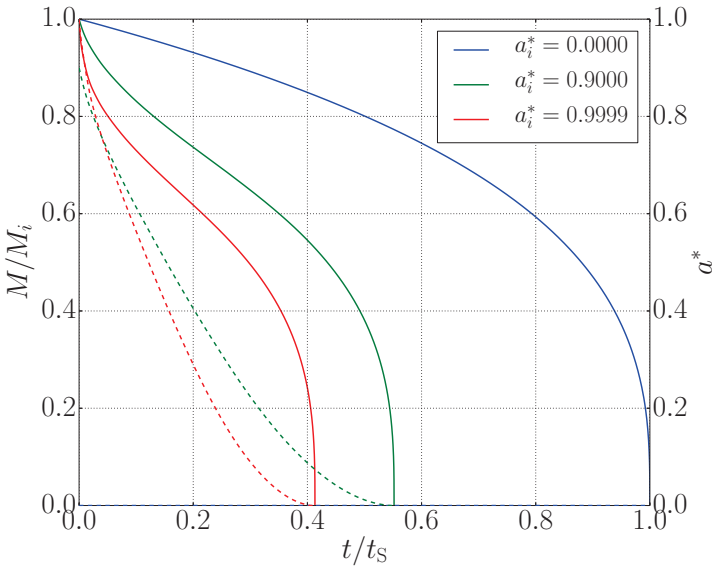

Figure 2.17: Evolution of a KBH mass M (plain curves, normalized to the initial mass $M_i = 10^{16}$ g which is the same for all curves) and spin a^* (dashed curves) as functions of time t (normalized to the SBH lifetime t_S), for different values of the initial spin $a_i^* = \{0, 0.9, 0.9999\}$. [taken from [236]]

they evaporate. This kindled interesting research in the GW experiments, as reviewed *e.g.* in [233, 234]. The relevant time scales were derived in [235].

[30]Letting all the above caveats aside, the evolution of a PBH mass and spin can be studied with Eqs. (2.151). An example is displayed in Fig. 2.17, where one observes that the lifetime of a KBH can be reduced by almost $\sim 60\%$ when going from the Schwarzschild case $a_i^* = 0$ to the near extremal case $a_i^* = 0.9999$ [199]. The higher the initial spin is, the stronger the initial mass loss will be due to the enhanced GFs, so the shorter the BH lifetime. After most of the spin is radiated away, all curves share the same shape as the Schwarzschild one.

The evolution of the lifetime of a KBH as a function of its initial spin is displayed in Fig. 2.18. There is a slight dependency on the initial mass that comes from the fact that the Page coefficient $f(M, a^*)$ is not a constant. Hence, depending on the available SM d.o.f. that a KBH is able to kinematically emit, the spin can be evaporated away more or less rapidly, before the universal Schwarzschild behaviour is attained.

These evolution curves allow one to determine what should be the initial PBH spin (taking only evaporation into account) such that its spin today is above some threshold value. This is particularly interesting in the eventuality of a BH detection with a spin above the "Thorne limit": for BHs with astrophysical origin, Thorne has shown that in the case of thin disk accretion, there is a limit to the reduced spin $a^*_{\rm lim} \approx 0.998$. This limit comes from accretion of the surrounding gas on a BH,

[30]This discussion is inspired from the paper "Evolution of primordial black hole spin due to Hawking radiation" [236] I wrote with A. Arbey and J. Silk.

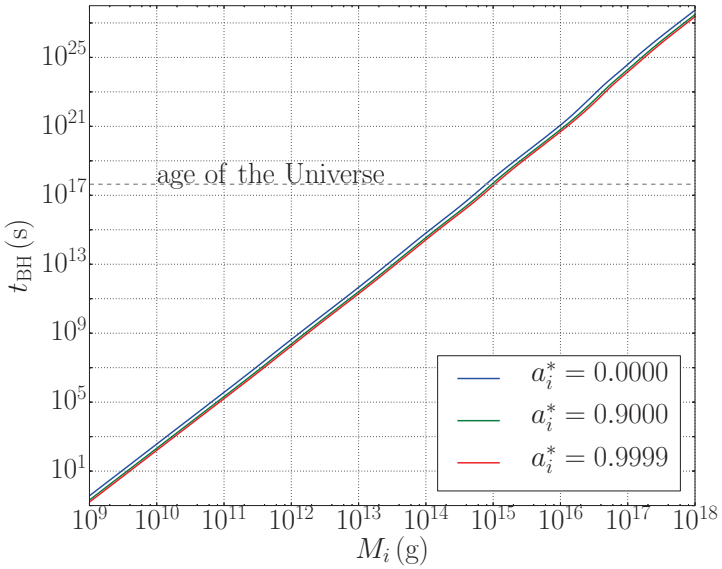

Figure 2.18: Kerr BH lifetimes $t_{\rm BH}$ (normalized to the Schwarzschild case $t_{\rm S}$) for different initial masses $M_{\rm i} = \{10^9, 10^{13}, 10^{18}\}$ g (resp. blue, green and red lines) as functions of the initial spin $a^*_{\rm i}$. *The x-axis is reversed to show* $1 - a^*_{\rm i}$ *in a logarithmic scale.* [taken from [236]]

and its balance with superradiance effects [237–239]. Surprisingly, the same $a^*_{\rm lim} \approx 0.998$ was found in [240] for BH mergers. This limit was recently generalized to other accretion regimes and disk geometries in [241], based on earlier work [242]; reaching somewhat higher values depending on the disk parameters. The overall state-of-art is that, except for really specific accretion environments, the spin of a BH of astrophysical origin should not exceed a generalized version of the Thorne limit [243]. Hence, detection of a near-extremal BH *e.g.* in GW experiments would be a smoking gun for PBH origin [236]. This goes the opposite way as the conventional view that merging BHs have *too low* spin to be of stellar origin.[31]

In Fig. 2.19, I give the spin of a PBH today as a function of its initial mass, for various initial spins. One can see that for a massive enough PBH, the spin is "protected" by the fact that the angular momentum and mass of a KBH decrease at approximately the same speed. Hence, a PBH with initial mass $M_{\rm i} \gtrsim 10^{16}$ g formed with an initial spin $a^*_{\rm i} > a^*_{\rm lim}$ would still have a spin $a^*_{\rm today} > a^*_{\rm lim}$. However, as shown in [197, 236], to have a spin today that is arbitrarily close to the extremal limit (and, once again, neglecting all the exterior influences) for currently evaporating PBHs of $M \sim M_*$ necessitates an initial spin even closer to the extremal limit, which could require dubious formation mechanisms. Furthermore, the existence of massive bosonic particles with a sufficiently long lifetime is a challenge for the existence of highly spinning PBHs. Coincidentally,

[31] A minimum spin should develop around these BHs due to material accretion, while the distribution of the posterior effective spin is centered around 0. This was a subject of debate at the CERN TH Institute "Primordial vs. Astrophysical origin of black holes". Future high statistics of mergers should disentangle that knot.

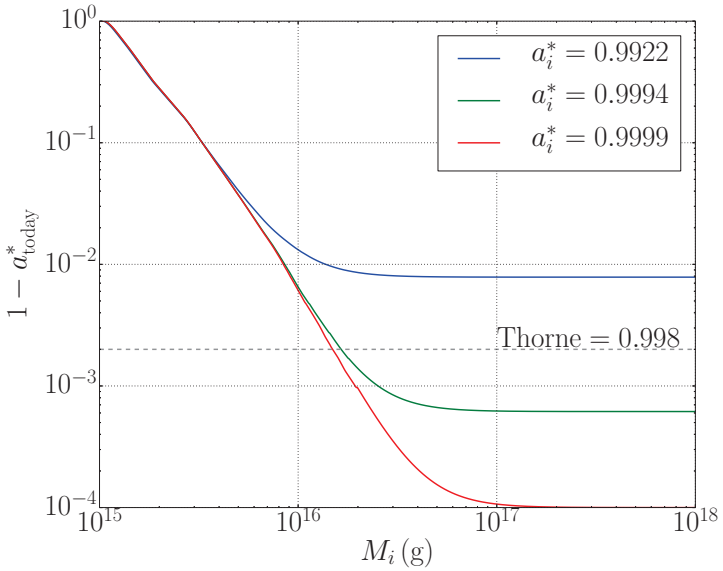

Figure 2.19: The value of the spin today $a^*_{\rm today}$ is plotted as a function of the initial mass $M_{\rm i}$ for different initial spins $a^*_{\rm i} = \{0.9922, 0.9994, 0.9999\}$ (blue, green and red lines, respectively). The "Thorne limit" $a^*_{\rm lim} \approx 0.998$ is shown as an horizontal dashed line. The y-axis is reversed to show $1 - a^*_{\rm today}$ on a logarithmic scale. [taken from [236]]

the superradiant instability of a PBH of mass $M \sim M_*$ is precisely triggered by pions, the latter initiating efficient "BH-bombs" [93, 244].

Chapter 3

BlackHawk

Contents

This Chapter is devoted to the code `BlackHawk`, which I present in Section 3.1. The main programs, options and output of the code are detailed in Sections 3.2, 3.3 and 3.4 respectively. Possible future developments are outlined in Section 3.5.

3.1 General presentation

[1]I describe `BlackHawk` [151, 152], a public `C` program for calculating the Hawking evaporation spectra of any BH distribution. This program allows the users to compute the primary and secondary spectra of stable or long-lived particles generated by HR of a distribution of BHs, and to study their evolution in time. The physics of HR has been extensively discussed in Sections 2.3 to 2.7. `BlackHawk` is available on the webpage `http://blackhawk.hepforge.org`.

3.1.1 Genesis

The subject of my Master's internship with A. Arbey was to study the interplay between PBH evaporation and BBN (see the discussion in Section 4.1.2.3). The idea was to compute the HR from PBHs and to inject the rate of emission of particles in a modified version of the public BBN code `AlterBBN` [245, 246], of which A. Arbey is the foremost developer. The little bibliography I did at that time showed to me that HR rates were already computed in the literature, and that the MG&W model could be used to predict the secondary spectra. Every ingredient seemed then in place to reproduce and ameliorate the results of *e.g.* [225, 247]. It has been $4^1/_2$ years since that time and I confess that I still haven't implemented PBH HR into `AlterBBN`.

It appeared to me very soon that most studies using PBHs as sources of particles during cosmological eras relied on very simplified versions of the MG&W model from the 1990's, sometimes even returning to primary Page spectra of the 1970's or using the "pure blackbody" approximation, instantaneous decay approximation, or an *ad-hoc* conversion between PBHs and decaying DM based on the PBH lifetime interpretation as a "decay rate". Thus, I searched for public numerical codes that would go beyond these approximations and found only `Charybdis` [186] and `BlackMax` [189–191] which were designed to compute the evaporation of BHs produced in collisions of energetic particles in accelerators within the context of HD theories. These computer programs indeed contained tabulated values of the GFs of HR and were interfaced with `PYTHIA` [248] to compute the hadronized secondary spectra, but starting only at $n = 1$ supplementary dimensions. Nowhere in the literature did I find a computer program to compute the simple GFs of a SBH. Thus, I decided that I had to do it all over again from scratch, and A. Arbey convinced me to publish the resulting program as a public code, just like `AlterBBN`. From that moment, `BlackHawk` was born. I had to recompute the GFs, compute up-to-date hadronization tables on the model of those of PPPC4DMID for DM indirect detection [249, 250][2] and embed everything into a user-friendly modular interface that users could modify at their will. `BlackHawk` is now at version `v2.1` with many more features than what I imagined in the beginning.

[1]This Chapter is mostly inspired from the latest arXiv version of the `BlackHawk` manual "BlackHawk: a public code for calculating the Hawking evaporation spectra of any black hole distribution" [151] and the release note of `v2` "Physics beyond the standard model with BlackHawk v2.0" [152].

[2]The material is available at `http://www.marcocirelli.net/PPPC4DMID.html`.

3.1.2 Scope

`BlackHawk` was originally designed to compute the HR rates of a SBH as a function of time, following the SBH evaporation. It was very early extended to extended mass functions of PBHs. J. Silk, with whom I collaborated during an internship at the Institut d'Astrophysique de Paris (IAP), suggested to compute the emission rates for spinning KBHs. It was then straightforward to incorporate extended spin distributions.We had the long-standing idea with A. Arbey to find a mean of going straight from the metric of a BH solution to its HR rates, in order to predict different signals for different BHs. This gave rise to the work produced in collaboration with M. Geiller, E. R. Livine and F. Sartini described in Section 2.3 where we found the general equations describing the emission rates of a spherically symmetric and static BH for spins 0, 1, 2 and $1/2$. The 3 examples listed in the previous Chapter, namely RNBH, HDBH and LQGBH were thus implemented in version `2.0`. A collaboration with I. Masina and G. Orlando, and another one with P. Sandick, B. Shams Es Haghi and K. Sinha, finally supported the need for BSM particle emission rates, such as the spin $3/2$ particle and the possibility to add supplementary d.o.f. to the SM. All the scripts used in building `BlackHawk` have been made publicly available together with the code. The features of `BlackHawk v2.1` are described below, and a complete list of the publications relying on the code is given in Appendix A.2.

3.2 Programs

The `BlackHawk` code is split into two programs, which are presented in this Section:

- `BlackHawk_tot`: full time-dependent Hawking spectra,
- `BlackHawk_inst`: instantaneous Hawking spectra.

A quick reminder of the compilation and launch procedure is given in Appendix A.1.

BlackHawk_inst. `BlackHawk_inst` computes the instantaneous primary and secondary HR rates of a distribution of BHs. It is convenient to visualize the rates of emission before launching a more computationally involved run of `BlackHawk_tot`. Furthermore, as PBHs with mass $M \gtrsim M_*$ barely evolve in a timescale equal to the age of the universe, using `BlackHawk_inst` is sufficient when one wants to compute the present emission of PBHs of $M \gtrsim M_*$. I emphasize however at this point that strictly speaking, PBHs today have lost a sizeable fraction of their initial mass and spin even if $M \gtrsim M_*$. For the spin part, it is described in detail in Section 2.7. For the mass part, and in the particularly sensitive case of an extended mass distribution, where the low mass tail of the distribution is particularly distorted by evaporation; I refer the interested reader to the analytical treatment in [57, 247] and the very recent numerical ones in [251, 252].

BlackHawk_tot. `BlackHawk_tot` computes the time-dependent primary and secondary HR rates, that is the instantaneous spectrum at each time step of the evolution of the BH distribution, from the initial conditions $(M_{\rm i}, \{x_{\rm i}\})$ of mass and secondary parameters (*e.g.* spin $\{x_{\rm i}\} = a_{\rm i}^*$ for a

KBH) down to the Planck mass (or the PMR mass if evaporation is incomplete). This program takes a longer time to execute because for a single set of initial conditions, a thousand of instantaneous time steps are required to achieve good accuracy. Thus, for a distribution of PBHs with an extended set of initial conditions, the computation is accordingly longer. Inside `BlackHawk`, efforts have been made to optimize the execution time. As estimation of the memory usage of a run is given *before* it actually starts to avoid memory overflows. A tiny script has been provided together with the code to automatically stack the redshifted emitted spectrum of a PBH with different expansion histories. An example displayed in Fig. 3.1. The script computes the integrated spectrum $\tilde{Q}_i$ of particle i from PBH formation $t_{\rm form}$ to the final time $t_{\rm end} = t_{\rm eva}$ for total evaporation or $t_{\rm end} = t_{\rm today}$ for the present time

$$\tilde{Q}_i(E) = \int_{t_{\rm form}}^{t_{\rm end}} (1+z(t)) Q_i\left(t, (1+z(t))E\right) \, {\rm d}t \,. \tag{3.1}$$

The redshift between running time t and the evaporation time $t_{\rm end}$ is taken into account to dilute the energies as well as the PBH distribution. This results in the two factors $1+z(t)$ where the redshift is given as a function of time by

$$1+z_{\rm RD}(t) = \left(\frac{t_{\rm end}}{t}\right)^{1/2}, \quad \text{or} \quad 1+z_{\rm MD}(t) = \left(\frac{t_{\rm end}}{t}\right)^{2/3}, \tag{3.2}$$

for full RD and MD respectively. In the standard cosmology (SC) scenario, the redshift is given by

$$1+z_{\rm SC}(t) = \begin{cases} \left(\dfrac{t_{\rm end}^{4/3}}{t \times t_{\rm eq}^{1/3}}\right)^{1/2}, & t < t_{\rm eq} \,, \\ \left(\dfrac{t_{\rm end}}{t}\right)^{2/3}, & t > t_{\rm eq} \,, \end{cases} \tag{3.3}$$

where $t_{\rm eq}$ is the time of matter-radiation equality. A more sophisticated or non-standard case of a mixed or alternate domination of radiation and matter could be straightforwardly implemented inside that script.

3.3 Options

`BlackHawk` is a totally transparent code, meaning that all the parameters can be modified by the user to obtain a non-standard behaviour. The parameters of a run are listed in a `parameter.txt` file that is saved in the output folder to allow for later examination. Below, I list the main options of the code.[3]

[3] More details about the routines, parameters and internal structure of the code can be found in the latest `BlackHawk` manual [151], to which I refer the interested reader.

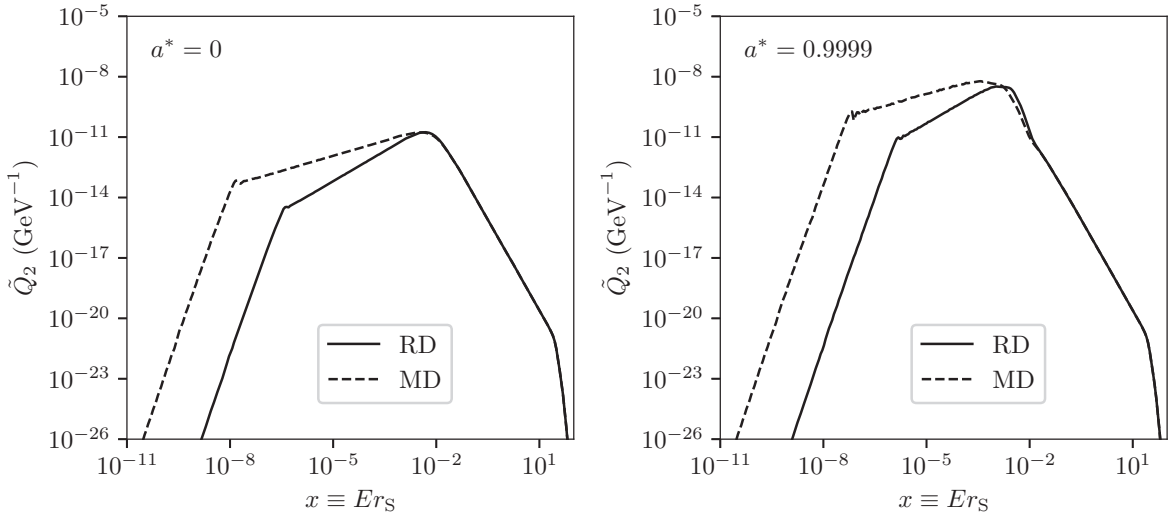

Figure 3.1: Stacked graviton spectrum emitted by a $M_{BH} = 10^{-1}$ g Schwarzschild BH (**left**, with $a^* = 0$) or near extremal Kerr BH (**right**, with $a^* = 0.9999$), in the case of RD (solid black) or MD (dashed black). [taken from [152]]

3.3.1 Black hole metric

Four types of BH metrics are implemented inside `BlackHawk`: the KBH, the RNBH, the HDBH and the LQGBH. The SBH is the trivial limit of any of those metrics with vanishing secondary parameters. The scripts used to compute the GFs are given in the code. They are written in `Mathematica`, which is a non-open source formal calculation language. I still keep the hope to rely only on public and free codes in all the parts of `BlackHawk`, but did not have the opportunity to write a differential solver for the Teukolsky equations. The scripts used to compute the Page coefficients are also furnished, and are written in `C`. The GFs are computed for 200 values of $x \equiv Er_S \in [10^{-2}, 5]$, corresponding to regimes where the low- and high-energy limits are reached to good accuracy. Outside this range, numerical fits have been performed to prolong the GFs, these being confronted to the analytical formulas derived in Section 2.3.3.2.

KBH metric: 50 values of $a^* \in [0, 0.9999]$ have been used to tabulate the GFs and the Page coefficients;

RNBH metric: 50 values of $Q^* \in [0, 0.999]$ have been used;

HDBH metric: 7 values of $n \in [\![0, 6]\!]$ have been tabulated;

LQGBH metric: 20 values of $\varepsilon \in [0, 100]$ for 2 values of $a_0 = \{0, 0.11\}$ have been used.

The modified GFs result in modified Page coefficients, thus the evolution equations (2.151) are adapted to the metric; with ε being a constant for LQGBHs. The evolution of RNBHs and

HDBHs are not yet available in the code. For an example of constraint on LQGBHs obtained with `BlackHawk`, see Section 4.6.

The computation of the GFs is one of the non-trivial parts of `BlackHawk`. In particular, the KBH case is extremely tricky as the potentials given in Eqs. (2.95) present diverging behaviour at some value of $r_{\rm div} > r_+$. This behaviour appears only for the "superradiant" modes, which are the dominant ones. Their numerical treatment requires solving the Schrödinger wave equation in two distinct regions $r < r_{\rm div}$ and $r > r_{\rm div}$, with an analytical matching procedure developed by Chandrasekhar & Detweiler [125–128]. The case of the spin 2 potential is even worse as for some of the 4 versions of the potential V_2, there is another divergence that is not possible to predict analytically. The 4 potentials are tried until the non-divergent one is found.[4]

3.3.2 PBH distribution

The user can choose to simulate a *purely* monochromatic distribution of PBHs, that is a single set of initial conditions $(M_{\rm i}, \{x_{\rm i}\})$, or to use built-in distributions for the mass and secondary parameters. It is of course possible to combine both extended distributions, with automatic re-scaling in that case to keep the normalization.

Dirac: a monochromatic mass and secondary parameter distribution;

Uniform: a uniform distribution of the form

$$\mathrm{d}n = \frac{A}{M_{\rm max} - M_{\rm min}}\mathrm{d}M\,, \quad \text{or} \quad \mathrm{d}\tilde{n} = \frac{\mathrm{d}x}{x_{\rm max} - x_{\rm min}}\,, \tag{3.4}$$

where $M_{\rm min,max}, x_{\rm min,max}$ are the distribution bounds;

Log-normal: the mass distribution can be log-normal either for the PBH mass density

$$\mathrm{d}n = \frac{A}{\sqrt{2\pi}\sigma M^2}\exp\left(-\frac{\ln(M/M_{\rm c})^2}{2\sigma^2}\right)\mathrm{d}M\,, \tag{3.5}$$

or number density

$$\mathrm{d}n = \frac{A}{\sqrt{2\pi}\sigma M}\exp\left(-\frac{\ln(M/M_{\rm c})^2}{2\sigma^2}\right)\mathrm{d}M\,, \tag{3.6}$$

with both appearing in the literature, where σ is the variance and $M_{\rm c}$ is a characteristic mass;

Power-law: this "scale-invariant" mass distribution is given by

$$\mathrm{d}n = AM^{\gamma-2}\mathrm{d}M\,, \tag{3.7}$$

where γ is related to the equation of state of the universe;

[4] This complicated mathematical behaviour, which is the price of having obtained short-range potentials, has for now prevented me to obtain the KBH GFs for the spin $^3/_2$ field.

Peak theory: this distribution is a refined form of the "scale-invariant" model [53, 54]. Assume that the perturbation power spectrum at scale k is

$$P(k) = R_{\rm c}\left(\frac{k}{k_0}\right)^{n-1}, \tag{3.8}$$

where the spectral index from the CMB is $n \approx 1.3$ and $R_{\rm c} = (24.0 \pm 1.2) \times 10^{-10}$ at the scale $k_0 = 0.002\,{\rm Mpc}^{-1}$; the resulting PBH distribution is

$$\mathrm{d}n \approx \frac{1}{4\pi^2 M}\left(\frac{X(n-1)}{6M}\right)^{3/2}\frac{(n-1)}{2}\nu^4 e^{-\nu^2/2}\mathrm{d}M\,, \tag{3.9}$$

where

$$\nu(M) \equiv \left(\frac{2(k_0^2 M/X)^{(n-1)/2}}{R_{\rm c}\Gamma((n-1)/2)}\right)^{1/2}\zeta_{\rm th}\,, \quad \text{and} \quad X \equiv \frac{4\pi}{3}\left(\frac{8\pi G}{3}\right)^{-1}\left\{\frac{H_0^2\Omega_{\rm m}}{1+z_{\rm eq}}\left(\frac{g_{*,\rm eq}}{g_*}\right)^{1/3}\right\}^{1/2}, \tag{3.10}$$

in which $\Omega_{\rm m} \approx 0.31$ is the matter energy density, $z_{\rm eq} = 3200$ is the redshift of matter-radiation equality with relativistic number of d.o.f. $g_{*,\rm eq} = 3.36$ while $g_* = 106.75$ is the same number at PBH formation and $\zeta_{\rm th} = 0.7$ is the threshold for PBH formation [53, 253];

Critical collapse: this mass distribution is

$$\mathrm{d}n = AM^{1.85}\exp\left(-\left(\frac{M}{M_{\rm f}}\right)^{2.85}\right)\mathrm{d}M\,, \tag{3.11}$$

where $M_{\rm f}$ is a characteristic mass;

Gaussian: this is a distribution for the secondary parameter

$$\mathrm{d}\tilde{n} = \frac{1}{\sqrt{2\pi\sigma^2}}\exp\left(-\frac{(x-x_{\rm c})^2}{2\sigma^2}\right)\mathrm{d}x\,, \tag{3.12}$$

where σ is the variance and $x_{\rm c}$ is a characteristic parameter value.

The mass distribution depends on a normalization factor A while the secondary parameter distribution is normalized to 1. It is also possible to provide a user distribution to `BlackHawk` by mean of an external file. For the physical justification of these distributions, see the discussion on PBH formation mechanisms in Section 1.3. The user can choose the discretization step of those distributions; then each bin of mass/secondary parameter is evolved independently with the evolution equations (2.151) using the relevant Page coefficients (2.150). For constraints on non-trivial PBH distributions, see Sections 4.3 and 4.4.

3.3.3 Initial time

The initial time at which PBHs form can either be automatically fixed by Eq. (1.17) or be provided by the user manually. There is no absolute time dependency inside `BlackHawk` (the stacking script described above is external), but it simplifies interpretation to have the relevant universe cosmological time in the output files.

3.3.4 Remnant

The user can fix a mass $M_{\rm PMR} > M_{\rm Pl}$ at which the evaporation stops and leaves a PMR. This is of interest if one desires to examine what is the integrated final burst spectrum of an exploding PBH in modified HR theories.

3.3.5 Additional particles

The user can add particles to the canonical SM ones listed in Table 2.1 to the emission spectrum. These additional particles can be DM particles, or the graviton. The main effect is to modify the Page coefficients by increasing the evaporation rate of the PBH. Built-in Page coefficients are computed for a single additional DM d.o.f. of spin 0, 1, 2, $1/2$ or $3/2$ but they can be recomputed for an arbitrary number of d.o.f. with arbitrary mass spectrum thanks to the provided scripts. See Section 4.5 for a study with DM emission by PBHs.

3.3.6 Hadronization

As discussed in Section 2.5, the primary Hawking spectra of (B)SM particles are not the end of the game, but particles must be hadronized and decayed before they can interact with the PBH environment or the detectors. This is performed by convolving the primary spectra with various particle physics codes, as listed below. Each code must be used in its range of validity to avoid spurious extrapolation.

PYTHIA: The particle physics code `PYTHIA v8.2` [248] was used to build hadronization tables that can be regarded as updates of the ones given by PPPC4DMID [249, 250]. `PYTHIA` has been confronted to accelerator data from $\sim 5 - 10^4$ GeV, and allows hadronization to be performed up to 100 TeV with no experimental check. Inside `PYTHIA`, one can force or cancel the decay of particles, thus it has been used to obtain the secondary spectra of "BBN stable" particles as well as "cosmologically stable" particles listed in Tables 2.2 and 2.3;

HERWIG: The particle physics code `HERWIG v7.0` [254] was used with the aid of P. Richardson during my 3-month stay at CERN to generate hadronization tables complementary to those of `PYTHIA` for the energy range $\sim 25 - 10^5$ GeV, showing good agreement with `PYTHIA`;

Hazma: It was pointed out in Ref. [255] that the extrapolation of the `PYTHIA` tables below the GeV scale that was automatically done in `BlackHawk v1.2` produced inaccurate results and that low-energy (MeV) hadronization and decay functions should be used instead. This was

particle	PYTHIA	HERWIG
gluons	$e^+e^- \to h^0 \to g\bar{g}$	$e^+e^- \to h^0 \to g\bar{g}$
Higgs boson	$e^+e^- \to h^0$	$e^+e^- \to h^0$
W bosons	$e^+e^- \to Z^0/\gamma^* \to W^+W^-$	$e^+e^- \to Z^0/\gamma^* \to W^+W^-$
Z boson	$e^+e^- \to h^0 \to Z^0Z^0$	$e^+e^- \to Z^0/\gamma^* \to Z^0Z^0$
leptons	$e^+e^- \to h^0 \to l^+l^-$	$e^+e^- \to Z^0/\gamma^* \to l^+l^-$
quarks	$e^+e^- \to Z^0/\gamma^* \to q\bar{q}$	$e^+e^- \to Z^0/\gamma^* \to q\bar{q}$

Table 3.1: List of the channels used to compute the hadronization tables for the Monte-Carlo codes PYTHIA and HERWIG.

done by tabulating results from the public code `Hazma` [256] in the energy range $\sim 10^{-6}-5\,\text{GeV}$, as explained in the `v2.0` release note [152].[5]

HDMSpectra: In order to study the final burst of PBHs in a precise manner, one needs a complete understanding of the ultra-high energy BSM behaviour [257]. While this is of course out of reach for now, known effects of the $\sim$ TeV energy SM must be implemented, such as massive weak boson couplings. This is done by the package `HDMSpectra` [258], which extends the regime of validity of `PYTHIA` up to the Planck scale.

The artificial collision channels used inside `BlackHawk` to produce the `PYTHIA` and `HERWIG` tables are presented in Table 3.1; example plots have already been given in Figs. 2.9, 2.15 and 2.16.[6] The channels used in `Hazma` are listed in [152, 255], with example plots given in Figs. 3.2 and 3.3. The `HDMSpectra` implementation is straightforward from the manual [258].[7] In all these packages, the branching ratio of a primary stable particle i to itself $i = j$ is a Dirac function $\mathrm{d}N/\mathrm{d}e = \delta(e - E)$ in Eq. (2.147).

3.4 Output

All the output files generated by a run of `BlackHawk` are stored in a folder:

```
>>> results/destination_folder/
```

In this Section I describe the files created by each program. The parameter file `parameters.txt` used for a run is always copied in the output folder in order to allow for subsequent data interpretation. Simple `Python` visualization scripts are provided with `BlackHawk` in order to plot the data produced by both programs. The user can of course modify these scripts or use any other plotting program.

[5] I am in discussion with the `Hazma` package authors to implement secondary neutrinos in their code which only includes secondary electrons and photons for now.

[6] While this manuscript was written, I became aware of the latest `PYTHIA v8.3` [259] and `HERWIG v7.2` [260] releases; the hadronization tables should be re-computed accordingly.

[7] The new `HDMSpectra` feature for high energy hadronization in `BlackHawk` has not yet been published in a release note. These are very time-consuming to write and I wait for more updates before moving on to `v3.0`.

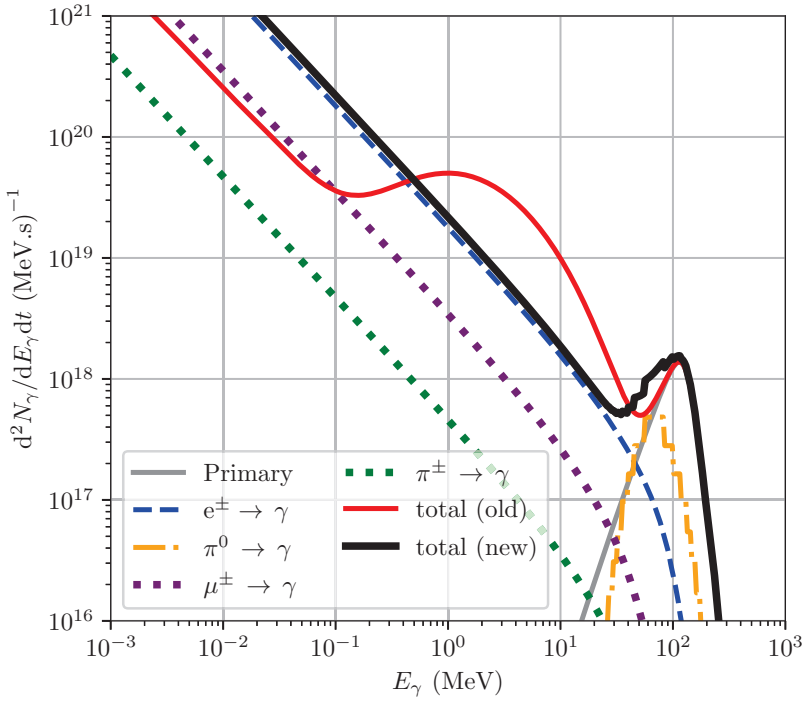

Figure 3.2: Comparison between the old `PYTHIA` extrapolated (solid red) and new `Hazma` computed (solid black) `BlackHawk` instantaneous total photon spectrum for a $M = 5.3 \times 10^{14}$ g PBH. From left to right: primary photon spectrum (grey solid); neutral pion decay (orange dot-dashed); electron FSR (blue dashed); muon decay+FSR (purple dotted); charged pion decay+FSR (green dotted). *To be compared with Fig. 2 upper left panel of [255]. FSR stands for "final state radiation".* [taken from [152]]

BlackHawk_inst program. Running `BlackHawk_inst` produces a set of output files:

- `BH_spectrum.txt`: this file contains the initial density spectrum of BHs and is 2-dimensional: the first column is a list of the BH initial masses, the first line a list of the initial secondary parameters and the bulk is the associated comoving number densities.
- `instantaneous_primary_spectra.txt`: this file contains the emission rates of the primary particles for each simulated initial energy. The first line is the list of primary particles, the first column is the list of energies, and each other column is the emission rate Q_i of Eq. (2.148).
- `instantaneous_secondary_spectra.txt`: this file contains the emission rates of the secondary particles for each simulated final energy. The first line is the list of secondary particles, the first column is that of energies, and each other column is the emission rate Q_j of Eq. (2.147).

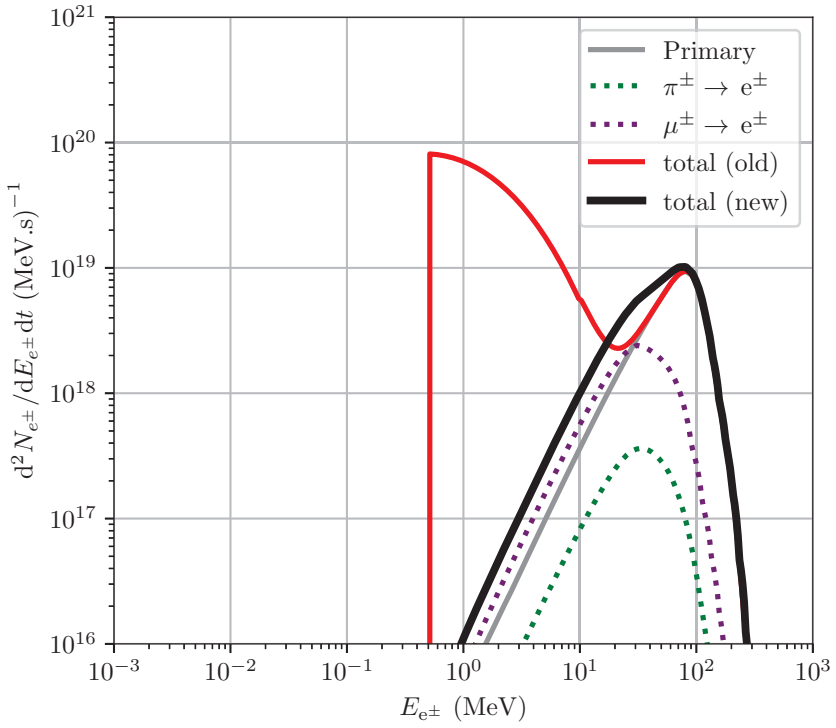

Figure 3.3: Comparison between the old `PYTHIA` extrapolated (solid red) and new `Hazma` computed (solid black) `BlackHawk` instantaneous total electron spectrum for a $M = 5.3 \times 10^{14}$ g PBH. From left to right: primary electron spectrum (grey solid); muon decay (purple dotted); charged pion decay (green dotted). [taken from [152]]

BlackHawk_tot program Running `BlackHawk_tot` produces a different set of output files:

- `BH_spectrum.txt`: this file is the same as for `BlackHawk_inst`.
- `life_evolutions.txt`: this file contains all the integrated time steps for each PBH initial condition $(M_\mathrm{i}, \{x_\mathrm{i}\})$, under the form of tables in which the first column gives the time, and each other pair of columns is the evolution of the mass and secondary parameter of PBHs as a function of time for a fixed initial mass.
- `dts.txt`: this file contains the integrated time steps t (first column) and the corresponding time intervals $\mathrm{d}t$ (second column). It is useful for precise time integration of the spectra.
- `*_primary_spectrum.txt`: these files contain the emission rates of each primary particle at each time step and for each simulated initial energy. The first line gives the list of energies, the first column gives the list of times, and each further column is the emission rate Q_i of Eq. (2.148).

- `*_secondary_spectrum.txt`: these files contain the emission rates of each secondary particles at each time step and for each simulated final energies. The first line gives the list of energies, the first column gives the list of times, and each other column is the emission rate Q_j of Eq. (2.147).

3.5 Perspectives

`BlackHawk` is surely the greatest achievement of this thesis work—it is at least the one that occupied most of my working time. Coding is a never-ending task, as there are always new features to implement, new bugs to solve and a better way of arranging (and naming) the functions and variables. `BlackHawk` is the first public code generating both primary and secondary Hawking evaporation spectra for any distribution of BHs, and their evolution in time.[8] The primary spectra are obtained using GFs, and the secondary ones result from the decay and hadronization of the primary particles thanks to particle physics codes. The BHs and spectra evolution are obtained by considering the energy (and angular momentum for KBHs) losses via HR and the quasi-static modification of the temperature of the BH.

`BlackHawk` is designed in a user-friendly way and modifications can be easily implemented; many people already took over the code for their own needs. The primary application is to study the effects of particles generated by Hawking evaporation on observable quantities and thus to disqualify or set constraints on cosmological models implying the formation of PBHs, as well as to test the HR assumptions and study BH general properties.

`BlackHawk v2.1` embeds new features compared to the previous versions, most of which deal with BSM physics: emission of DM, spin $3/2$ particles or BH solutions beyond standard general relativity and usual formation mechanisms (RNBH, HDBH and LQGBH). The code has thus been extended to allow for BSM studies, as described in the release note [152]. Moreover, I have designed the public tool `Isatis` to automatically compute the PBH HR constraints, with a built-in automatic `BlackHawk` launcher [262]. An application of this tool is presented in Section 4.2.

Future versions of `BlackHawk` could be extended in multiple directions, from other non-standard BH metrics to modified HR processes, as well as complete PBH evolution (accretion and/or mergers) in given cosmological scenarios. BSM particle interactions could also be implemented in the hadronization tables, and low-energy processes such as inner Bremsstrahlung should be added. Indeed, at MeV energies, Ref. [263] (see also [148]) demonstrated that the final state radiation of charged particles, as implemented inside `Hazma`, is not relevant for HR as BHs emit independent particles and not pairs of charged particles. Hence, the single vortex effect of inner Bremsstrahlung should dominate, which would be of particular interest for future MeV constraints on PBHs (see *e.g.* the discussion in Section 4.2.7). To my knowledge, no recent PBH study includes this effect.[9]

[8] While the latest version of the manual was being written, Refs. [138, 261] appeared, describing the code `ULYSSES` aimed at leptogenesis, in which HR of PBHs is computed in a similar way as in `BlackHawk`. Ref. [171] also appeared, describing the code `CosmoLED` aimed at all kinds of HDBH constraints. Both authors have checked for consistency with the results from `BlackHawk`; and both codes will be made publicly available.

[9] This fact has been pointed out to me by J. MacGibbon [private communication].

Chapter 4

Constraints

Contents

This Chapter contains the main results obtained with `BlackHawk`. In the first Section 4.1, I overview all the existing constraints on PBHs focusing on those related to evaporation. I present the `Isatis` tool and discuss constraint caveats in Section 4.2. I show the constraints obtained for Kerr primordial black holes in Section 4.3 for γ-rays and Section 4.4 for dark radiation; for other non-standard primordial black holes in Section 4.6 and finally for beyond standard model particles in Section 4.5.

4.1 Existing constraints

[1]PBHs cannot have arbitrary density as their presence at different stages of the evolution of the universe leaves distinct imprints that one should be able to measure today. Hence, constraints can be deduced on the abundance of PBHs from various astronomical and cosmological observations. Assuming that all PBHs have the same initial mass M (monochromatic distribution, I drop the "i" subscript hereafter in this Chapter) and that they form at the same time t_f during RD, one can express the constraints on the initial fraction of the mass density of the universe that collapsed into them as

$$\beta(M) \equiv \rho_{\mathrm{PBHs}}(t_\mathrm{f})/\rho_\mathrm{R}(t_\mathrm{f}) = M(t_\mathrm{f}) n_{\mathrm{PBH}}(t_\mathrm{f})/\rho_\mathrm{R}(t_\mathrm{f}), \tag{4.1}$$

where the last equality holds for monochromatic distribution only, which is assumed in this Section. If these PBHs are still around, one relates their abundance Ω_{PBH} today to the fraction β at formation by [28]

$$\beta(M) \approx 7.1 \times 10^{-10}\, \Omega_{\mathrm{PBH}} \left(\frac{\gamma}{0.2}\right)^{-1/2} \left(\frac{h}{0.67}\right)^{2} \left(\frac{g_*(t_\mathrm{f})}{106.75}\right)^{1/4} \left(\frac{M}{M_\odot}\right)^{1/2}. \tag{4.2}$$

In this formula, $g_*(t_\mathrm{f})$ is the number of relativistic d.o.f. at PBH formation and h is the reduced Hubble parameter today such that $H_0 = 100\, h\, \mathrm{km{\cdot}s^{-1}{\cdot}Mpc^{-1}}$. The values of the cosmological parameters were taken from Planck [29]. Note that the mathematically convenient parameter

$$\beta' \equiv \gamma^{1/2} \left(\frac{h}{0.67}\right)^{-2} \left(\frac{g_*(t_\mathrm{f})}{106.75}\right)^{-1/4} \beta\,, \tag{4.3}$$

is sometimes used in the constraint plots (see *e.g.* the review [28]), while it does not bear the same simple meaning as β. If one further assumes that the PBHs are a constituent of the CDM, which automatically assumes that they have not evaporated yet, one can express the constraints on the fraction of DM they represent

$$f_{\mathrm{PBH}} \equiv \frac{\Omega_{\mathrm{PBH}}}{\Omega_{\mathrm{DM}}}\,, \tag{4.4}$$

where $\Omega_{\mathrm{DM}} h^2 = 0.1188 \pm 0.0010$ [29]. In this thesis work, I alternatively use β for PBHs evaporated in the early universe and f_{PBH} for those that survived until today.

Since the first proposal of PBH existence, the constraints have continuously changed. In most cases, as for the constraints linked to HR or the CMB distortions, they have strengthened: the observations have become more and more precise, allowing less parameter space for PBHs. In some peculiar cases, they have been relaxed, as for microlensing or stellar disruption constraints: new theoretical developments have downgraded the expected PBH influence. Thus, it is quite interesting to have a look at the evolution of the general plot of constraints on $\beta(M)$ at different epochs, as shown on Fig. 4.1. The lower panel plot is taken from the most recent Carr *et al.* review [28] and shows that a window for all DM into PBHs is still open in the $\sim 10^{17} - 10^{23}\,\mathrm{g}$ mass range. This corresponds to the black Ω constraint in the lower panel of Fig. 4.1. In this particular spot, the only

[1]This Section is inspired from the review article "Primordial black hole constraints with Hawking radiation – a review" [8] under writing.

constraint comes from the fact that PBHs must not overclose the universe, that is $\Omega_{\rm PBH} < \Omega_{\rm DM}$ (or equivalently $f_{\rm PBH} < 1$). I hereafter denote this window as the "HR window".

In the following subsections, I describe briefly in that order:

- constraints on PBHs that do not involve HR (Section 4.1.1), including lensing constraints, dynamical (structure) constraints and GW constraints;
- constraints on PBHs that rely on HR (Section 4.1.2, including baryogenesis scenarios, BBN constraints, CMB constraints, cosmological background constraints and present background constraints;

where the denominations are described at the relevant places. For more detailed reviews and numerical estimation of the constraints, I refer the reader to [28, 35, 266].[2] Prospective constraints are discussed *e.g.* in the Snowmass 2021 white paper on PBHs [268].

4.1.1 Without Hawking radiation

In this Section, I review the PBH constraints that do not rely on the Hawking process.

4.1.1.1 Lensing constraints

PBHs of any mass behave as gravitational lenses that deviate light rays due to their strong gravitational field (for a review of this effect and its implications in cosmology, see [269]). PBHs should have a sensible proper motion with respect to the sources they lense the light of. Their radius is so small that they only behave as very transient lenses, that is called millilensing, microlensing, femtolensing or picolensing depending on the duration of the effect.

The visible effect on Earth is that the light from remote sources is suddenly brightened by the passing of a PBH due to the focusing effect [269]. This applies to the light of quasars, supernovae, stars, and γ-ray bursts (GRBs). The most famous studies are that of MACHO [270], EROS [271],[3] OGLE [272][4] and Subaru-HSC [274], which exclude $f_{\rm PBH} = 1$ in the range $\sim 10^{23} - 10^{35}\,$g. The original Subaru-HSC constraint was initially much more stringent and excluded PBHs as DM down to $\sim 10^{21}\,$g [275] but it was shown recently that this was due to a simplistic treatment of the source spatial extension [274].[5]

There is a disputed constraint on GRB femtolensing [276, 277] in the $10^{17} - 10^{19}\,$g mass range which would close a good deal of the HR window, and an ongoing search for fast radio burst lensing [278]. Microlensing constraints are the ones with the most expected improvement in the Snowmass PBH white paper [268].

[2] A user-friendly tool to draw customized constraints can be found on the GitHub page of B. Kavanagh [267].

[3] The names of these two collaborations are obviously irrespective.

[4] OGLE might have observed microlensing events compatible with planetary mass PBH origin [273].

[5] This was the subject of vehement debate at the CERN TH Institute "Primordial vs. Astrophysical origin of black holes".

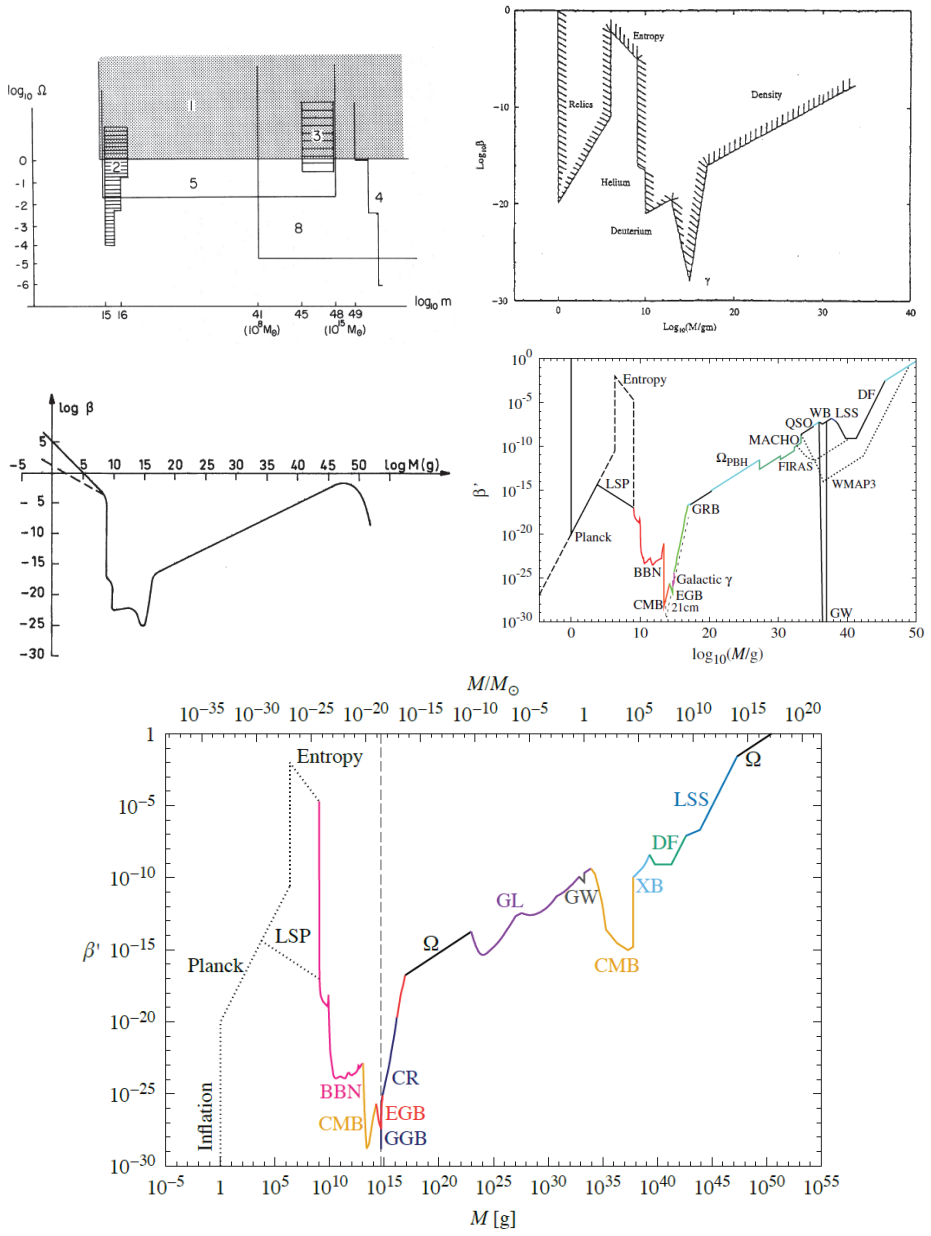

Figure 4.1: Constraints on PBHs taken from the reviews by Carr (1975) [47] (**upper left**), Novikov *et al.* (1979) [264] (**upper right**), Carr *et al.* (1994) [265] (**center left**), Carr *et al.* (2010) [247] (**center right**) and Carr *et al.* (2020) [28] (**bottom center**). The constraints are described in the text. All panels show constraints expressed in terms of $\beta(M), \beta'(M)$ for monochromatic Schwarzschild PBH distributions, except the oldest one which shows constraints as limits on $\Omega_{\rm PBH}$.

4.1.1.2 Dynamical constraints

PBHs are massive objects, and thus they exert gravitational attraction on the nearby material. This results: *i*) in gravitational friction that make them settle down in compact objects that they can subsequently absorb or destruct, *ii*) in gravitational disturbance of bound systems like stellar binaries, and *iii*) in gravitational heating of the interstellar medium (ISM) gas. The most severe constraints in the $10^{36} - 10^{47}$ g come from gas heating and galaxies, globular clusters and stellar binaries stability [279, 280] (see [33] for a review). "Stupendously" large PBHs would also accrete surrounding material with too much efficiency if formed in the early universe; depleting structure formation [33]. There could be constraints on the disruption of neutron stars and white dwarfs (the most compact non-BH objects) in the range $10^{18} - 10^{23}$ g [281, 282] (effectively closing all the HR window), but these were recently debunked [283–285] and await more rigorous theoretical treatment.

4.1.1.3 Accretion constraints

PBHs could also accrete gas and dust material into disks like any other celestial object. These disks could radiate in the X-ray band and heat the surrounding ISM or the CMB [286, 287], or the PBHs could be so massive that their gravitational potential distorts the CMB [288] (μ-distortions). These constraints exclude all DM into PBHs in the super-Solar mass range $M \gtrsim M_\odot$. Accretion indirectly takes a part in all other constraints as it modifies the PBH mass spectrum.

4.1.1.4 Gravitational wave constraints

As GWs propagate in space with no measurable alteration, they are the most precise probes of gravitational events back to the early universe. The stochastic GW background encompasses the GWs generated by PBH formation, by the statistical distribution of PBHs (scalar-induced GWs), by their sudden evaporation and modification of the equation of state, and by their continuous mergers since the early era. This may be the set of constraints totaling the greatest number of publications since 2015 and the first observation of the merger of BHs by the LIGO instrument [289, 290]. It was immediately suggested that the BH components of the binary merger were PBHs [291, 292], and the background of GWs from PBH mergers was predicted in [293]. The associated constraints are model-dependent but exclude PBHs in the $10^{30} - 10^{34}$ g mass range [294, 295] (observations by the LIGO/VIRGO instruments and the NANOGrav experiment). For a review about the GW perspectives of PBH studies, please refer to [234].[6] GWs from mergers are also one of the only positive evidence for PBHs, as even if they represent just a percent of the DM density, their mergers are still in the range of detectability at LIGO/VIRGO and future detectors [297].

Peculiar GW events such as very heavy $M \gtrsim 100\,M_\odot$ or light $M \lesssim M_{\rm TOV}$ BH binary mergers (*e.g.* [298, 299]) would be smoking guns towards PBH origin (see however [300]). A stochastic GW background should also be generated by PBH formation [301–303], and most interestingly it depends on the spin of the PBHs, giving access to a double-check of the PBH origin of BH mergers [304]. It could be the only way of constraining the PBH abundance in the remote $M \lesssim 10^9$ g mass range

[6] For a more general review about GWs and the early universe, see [296].

for which PBHs evaporate before BBN (see also Sections 4.4 and 4.5). The forthcoming LISA instrument is expected to shed some light on these yet unmeasured features [305].

4.1.2 With Hawking radiation

In this Section, I review the PBH constraints that somehow rely on the Hawking process. The remarkable thing with PBHs is that as they were born in the early universe, just after the inflation period, they may have had a measurable impact on *every* cosmological step of the universe evolution until today. That includes baryogenesis, the reheating of the universe, BBN, the CMB emission, generation of diffuse cosmological or local backgrounds and CRs, point-like sources (due to *e.g.* final explosions) and more spurious features like DM or DR emission and Planck-mass relics.

While studying the HR constraints, I have noticed that there is a gap in the publications on the subject from the early 1980's to the early 1990's. This gap corresponds more or less to the development of the WIMP paradigm in the 1980's that supplanted the PBH models for DM, and by the fact that the experimental description of HR seemed hindered by unknown behaviour at high energy. A combination of new particle accelerator data and astronomical observations permitted to MG&W to make a milestone advance in the PBH studies. The theoretical framework was clear then: PBHs emit particles in the form of well-defined QCD jets at high energy.

All the constraints put on PBHs in the 1970's were re-evaluated in the light of the MG&W model. These constraints also benefited from the great advances made in DM direct and indirect searches; in fact most of the subsequent studies on PBH evaporation took advantage on the fact that the HR process resembles DM decay. This went as far as directly converting DM constraints into PBH constraints by assuming that PBHs have a "decay rate" equal to the inverse of their lifetime $\Gamma \sim 1/\tau$.

A thorough account of the HR constraints on PBHs is given in the review [8].

4.1.2.1 Baryogenesis

The universe is not symmetric in (anti)baryon content.[7] For baryogenesis to take place, the three conditions of Sakharov [307] must be fulfilled:

Cond. 1: C and CP symmetry violation;

Cond. 2: baryonic number violation;

Cond. 3: thermodynamic equilibrium violation.

PBH interference in baryogenesis may proceed by four main scenarios:

- the "Hawking model" [105] where baryogenesis is the direct result of an asymmetry in the GFs (*e.g.* an effective chemical potential);

[7] See *e.g.* Ref. [306]:

> *That the Milky Way is essentially made of matter is evident [...] from the landings of space probes on the Moon and other planets without any disastrous consequences.* [306]

- the "Weinberg model" [308–310] where heavy (GUT) bosons emitted by HR of PBHs decay asymmetrically into (anti)baryons [311, 312];
- the "Dolgov model" [310, 313, 314] where a mass asymmetry between (anti)baryons cause asymmetric re-absorption probability by PBHs;
- the "Nagatani model" [315] where an EW symmetry-restored region exists around high-temperature PBHs and baryon asymmetry develops by sphaleron processes [316].

These four models check all the Sakharov conditions: condition 1 is satisfied because as PBH explosion manifestly violates the T symmetry, it should violate C/CP as well in order to conserve the CPT symmetry resulting from the global Lorentz invariance [131]. CP symmetry violation is also present in the SM as seen *e.g.* in neutral kaon decay [81, 317]; condition 2 is satisfied because PBHs don't conserve the baryon number—they can form from arbitrary material (say, only baryons) and evaporate in equal number of (anti)particles; condition 3 is satisfied because the evaporation of PBHs is a out-of-equilibrium process—PBHs can inject very high-energy particles in a low-temperature universe.

The PBH-generated asymmetry is protected from wash-out by subsequent interactions because they can evaporate *after* these interactions have frozen out. A small amount of asymmetry could also originate in the randomness of the HR process, with a fluctuation of the baryon number of the emitted flux of the same form as that of the emitted charge [120, 131, 318]. The GUT "Weinberg" model was greatly improved by Barrow & collaborators [319–323] (for dated but thorough reviews of the phenomenon, see [321, 324, 325]).

If PBHs generate the baryon asymmetry of the universe, this constitutes a major positive evidence for their existence. However, it would require an exponentially precise fine-tuning in the PBH (and/or GUT) parameters to obtain the observed baryon-to-photon ratio $\eta \equiv n_{\rm B}/n_\gamma \sim 10^{-9}$ [326, 327]. The parameter space is tightly constrained, but PBHs could be a viable *subdominant* source of asymmetry. These scenarios mainly rely on the fact that PBHs of mass $M \lesssim 10^{-9}$ are almost not constrained and that PBHs with $M \gtrsim 10^4$ g evaporate after the EW phase transition. Thus, they can dominate the energy density of the universe after formation and provide the baryon asymmetry as well as reheat the universe. The distinctive signature of such models is that they predict a stochastic GW background of multiple origins: PBH evaporation into gravitons, or PBH formation/Poisson distribution (scalar-induced GWs).

For a modern realization of the "Hawking model", see [328, 329]; for the "Weinberg model", see [330]. The "Nagatani model" seems deprecated since PBHs may not form symmetry-restoring fireballs [148]. A supplement of the "Weinberg model" where heavy right-handed νs take the place of GUT bosons is developed in [331–333]. As all these processes rely on the existence of BSM physics/particles, they provide no definitive constraint on the PBH fraction β in the early universe.

4.1.2.2 Reheating

At the end of the inflation period, the universe must be "reheated", meaning that some process should generate the radiation content of the universe. This "reheating" could result from the inflaton decay—the scalar field responsible for the inflation. Zel'dovich *et al.* [334] were the first to compute

explicitly the amount of entropy injected in the early universe by PBH evaporation, should them dominate the energy density at some point after formation. This results in a constraint on β for PBHs evaporated before BBN with $M \lesssim 10^9\,\mathrm{g}$, the first of its kind, though it is quite mild. García-Bellido *et al.* [335] went one step further by arguing that:

> [PBH reheating] *opens up an interesting possibility of connecting the origin of matter in the universe with black hole physics.* [335]

by which they mean, without invoking an *ad hoc* inflaton field. Reheating by PBHs is still a perfectly viable scenario. Some aspects of PBH reheating are discussed in Section 4.4.

4.1.2.3 BBN

The BBN constraints were among the first to be set from PBH evaporation [336–340]. The effects of PBHs on BBN are numerous:

- early hadron/neutrino injection modify the ratio $n_\mathrm{n}/n_\mathrm{p}$ at the onset of BBN [336, 337, 340] ($\mathrm{p} \longleftrightarrow \mathrm{n}$ inter-conversion);
- energetic hadron/photon/neutrino injection during BBN participates in the nuclear reaction chains [338, 339, 341, 342] (hadro-dissociation) or in EM cascades [343, 344];
- late energetic photons can break light nuclei at the end of/after BBN (photo-dissociation);
- PBHs participate in the energy density of the universe and inject entropy (modification of the Friedmann equations);

All these processes result in different light element abundances [345], which are tightly constrained by modern observations (see *e.g.* the review [346]). Already in their review of PBH constraints in various cosmologies of 1998, Liddle & Green [37] noted that:

> *[. . .] nucleosynthesis is well enough understood to tolerate only modest interference from black hole evaporation by-products.* [37]

but also:

> *[. . .] nucleosynthesis* [is] *the earliest time that we have any secure knowledge concerning the evolution of the universe.* [37]

All processes injecting more neutrons result in overproduction of ^{4}He while an effective spallation of heavy nuclei overproduces D. There is also a problem with the ^{7}Li primordial abundance, deduced from the so-called "Spite plateau" of metal-poor stellar composition [347]. BBN codes that predict other abundances with remarkable precision fail to produce the correct ^{7}Li abundance by a factor of ~ 3. Stellar mechanisms were proposed to reduce this discrepancy, with no success so far [348]. Modifications of BBN are another route toward a solution: fine-tuned decaying particles during BBN could destroy some ^{7}Li but this overproduces D as a general outcome [349, 350]. It is

tempting to apply this procedure to PBHs evaporating during BBN [351]. However, this is where the PBH HR/decaying DM analogy breaks down: it is not possible to fine-tune the PBH evaporation. Once the PBH mass and abundance is fixed, all decay products, time and energy scales flow from HR formulas immediately. I checked with J. Pradler during my presence in Vienna that no monochromatic PBH decay could solve the ^{7}Li discrepancy; while Carr *et al.* [28] claimed that a fine-tuned extended mass function could be a solution.

In fact, BBN constraints prevent sizeable PBH density in all the mass range $10^9 - 10^{13}\,$g. The precise assessment of PBH impact on BBN is quite difficult to handle analytically due to the complex Boltzmann equations involved. Very early in the BBN studies, numerical codes have been developed to compute the light element abundances (like the seminal Wagoner code [352–354] updated by Kawano [355, 356]). These codes have then been adapted to out-of-equilibrium BBN perturbed by all kinds of PBH models, but:

> *An exact calculation of the observational consequences* [on BBN] *of the evaporation of PBHs with a mass* $M < 10^{15}\,g$ *would require a detailed knowledge of the production of leptons, baryons and other particles [...]* [340]

This denotes a strong difficulty in high-energy PBH constraints—they rely on complex particle physics. The MG&W model deciphered the situation by giving the framework of high-energy PBH evaporation.

Sedel'nikov returned to the problem of standard BBN alterations by evaporating PBHs into energetic hadrons in 1996 [357]. All the ingredients were finally put together by Kohri & Yokoyama [225], with subsequent refinements in the reviews by Carr *et al.* [28, 247]. The constraints were revisited with the latest observational and theoretical developments in [358–360].[8] Notably, BBN is one of the few constraints computed for HDBHs [171, 217]. `AlterBBN` would probably benefit from an interface with `BlackHawk` in that context.

4.1.2.4 CMB

Nartikar & Rana checked early in the PBH story that they cannot generate the CMB light by direct HR [361]. However, the more and more precise measurements of the CMB, first by Penzias & Wilson [362] and then by the COBE [363–366], WMAP [367, 368] and Planck [369–371] satellites, yielded stringent constraints on the thermal history of the universe after BBN. The amount of exotic EM energy injected at that time is particularly constrained as it results in distortion of the CMB spectrum [334, 372]; while damping the CMB anisotropies [373–375] (for a review of the physical processes in the context of PBH evaporation, see *e.g.* [376]).

After the CMB, come the Dark Ages where the universe is neutral but the first stars are about to start shining. At that time, a reionization of the universe is expected because of X-ray emission of gas clouds and of the light of the first stars. PBHs can alter the reionization history by injecting energetic EM particles at late times. This was studied analytically by [377, 378], but the Boltzmann

[8] Ref. [359] relies on the public code `AlterBBN` [245] to compute the light elements abundances in the modified PBH cosmology. This code was developed by A. Arbey and collaborators and its updating was part of my early thesis challenges [246].

equations require precise solving through numerical methods. Most recent studies use the public codes `CLASS` [379–382][9] and `HYREC` [384] to compute the CMB observables in modified recombination histories with some PBH population [385].

The CMB is one of the few constraints that has been extended to non-monochromatic PBH distributions [386] and HDBHs [171, 217]. Recent work include [358, 387] and prospective limits can be found in [388]. CMB constraints exclude significant PBH density in the $10^{13} - 10^{16}$ g mass range.

A very important measurement has been performed recently by the EDGES collaboration, that is the 21 cm radio line of hydrogen hyperfine transition. This line is particularly sensitive to the ISM characteristics after the CMB and *during* the Dark Ages, which makes it a unique probe. A "trough" has been measured in the redshifted spectrum of the 21 cm line that could indicate a period of *cooling*, various astrophysics explanations [389, 390].[10] This places the strongest constraints on PBHs of mass $M \sim 10^{15} - 10^{18}$ g to date, as PBHs can only *heat* the ISM through energy injection. This constraint was intuited by Mack & Wesley in 2008 [392] but the EDGES data opened a new window on precision constraints [393–396]. Constraints were calculated for spinning PBHs as well [391, 397, 397, 398], and used to construct a fine-tuned PBH mass function in [399].

4.1.2.5 Cosmological backgrounds

Photons. This set of constraints will be discussed in detail in Section 4.2.

Neutrinos. Neutrinos have long escaped direct detection, due to their very small interaction rates with nuclei and electrons [400]. However, it is predicted by nuclear reaction models inside the Sun that a tremendous amount of neutrinos should traverse the Earth continuously. Furthermore, CR spalliation in the upper atmosphere should result in densely populated EM showers with a high-energy neutrino component [401]. Carr [131] was the first to estimate the neutrino background limits on PBHs, recomputed later in the MG&W model [402]. The fact that neutrinos interact so little with the other SM particles makes them excellent probes for the early universe physics, because they decouple from the plasma at $t \sim 1$ s and propagate almost freely until today [403].

The hadronization and decay processes in the secondary spectrum calculations cause different neutrino flavors to exhibit different fluxes, as noted by [404]. Neutrino flavor oscillations predicted by Pontecorvo [405, 406] and experimentally confirmed much later by flux measurement of neutrinos from nuclear reactors further mix up the different fluxes. These oscillations are interpreted as the consequence of the different bases for neutrino flavor eigenstates and mass eigenstates, the latter being the relevant d.o.f. for HR [407]. There is also an uncertainty on the neutrino nature: Dirac or Majorana, with different mechanisms to gain a (very small but) non-zero mass [408]. Recent neutrino background studies include [409–411]. Prospective limits have been set in [412–414] and are reviewed in [415].

[9] `CLASS` is the successor of `CAMB` [383], see also `http://class-code.net`.

[10] The SARAS 3 experiment has mitigated the magnitude of this measurement and new data are needed [391].

Gravitons. Gravitons are spin-2 massless particles that are the quanta of the gravitational interaction. They arise naturally in particle interpretation of GWs. At the beginning of HR studies, graviton emission was considered self-evident, but this particle has in fact never been formally identified and a coherent quantum theory of gravitation is yet to be found. Thus, most of the later studies have deprecated the graviton emission by PBH HR.

Yet, gravitons are the ultimate probe to early universe physics. They are the particles with the smallest cross-section with other SM particles, so that they can propagate freely and transport information from the earliest periods of the universe. Hence, graviton emission is one of the only distinctive signature of *e.g.* PBH baryogenesis scenarios (see the discussion above and *e.g.* [416]). Alas, those gravitons would have had very high frequency $f \propto T(M \sim 10^4\,\mathrm{g})$ at emission and the subsequent redshift leaves them with still very high frequency $f \sim 10^{14} - 10^{16}\,\mathrm{Hz}$ today [340, 417, 418]. Detection of these high-frequency GWs is a technical challenge, and some proposals were made in that direction [335]. Most of them rely on the Gertsenshtein effect that converts high-frequency gravitons into photons [419, 420] (GRAPH mixing).

As discussed in Section 2.4, KBHs exhibit highly enhanced primary spectra for high-spin particles, with the strongest enhancement for the spin-2 graviton [199], which could facilitate their detection. Gravitons could also participate in the DR content at BBN and CMB epochs, a constraint that is reviewed in Section 4.4. I show in Fig. 4.2 the redshifted graviton background as computed by `BlackHawk`.[11] The most promising PBHs are those with $M \sim 10^9\,\mathrm{g}$, just at the edge of the BBN constraint, because their radiation is less redshifted than the smaller ones, that evaporate earlier. The spectrum of GWs shows features that depend on the expansion history of the universe, particularly the inflation period.

4.1.2.6 Electrons & positrons

The fact that CR measurements show that the ratio $n_{\mathrm{e}^+}/n_{\mathrm{e}^-} \ll 1$ while PBHs should produce both in equal quantity advocates for use of e^+ flux as a limiting constraint [422]. However, Page & Hawking noted very early that:

> *The* [HR] *charged particles would be deflected by magnetic fields and so would not propagate freely to Earth.* [423]

This difficulty, related to $\mathrm{e}^\pm$ and $\mathrm{p}/\overline{\mathrm{p}}$ emission by PBHs, has long prevented precise assessment of the corresponding constraints. The origin of the "deflection" is twofold: *i*) Galactic magnetic fields deviate charged particles, which are trapped for some time in the Galaxy and may escape after a "leaking time" τ_{leak} (this is the "leaky box" model), this model was further complicated by the structure of the Galaxy with a disk and a halo region [422]; *ii*) the Solar wind screens low-energy particles from reaching the Earth, resulting in a strong "modulation" of their spectrum (this is the "force field" model). Furthermore, the determination of the PBH CR flux depends on their *local*, rather than cosmological, density, and thus on the distribution of PBHs inside the Galaxy—that is, the halo profile [422]. This density is either the same as the *global* PBH density, or PBHs could be

[11] These are part of the preliminary results presented at the 40th International Conference on High Energy Physics [421].

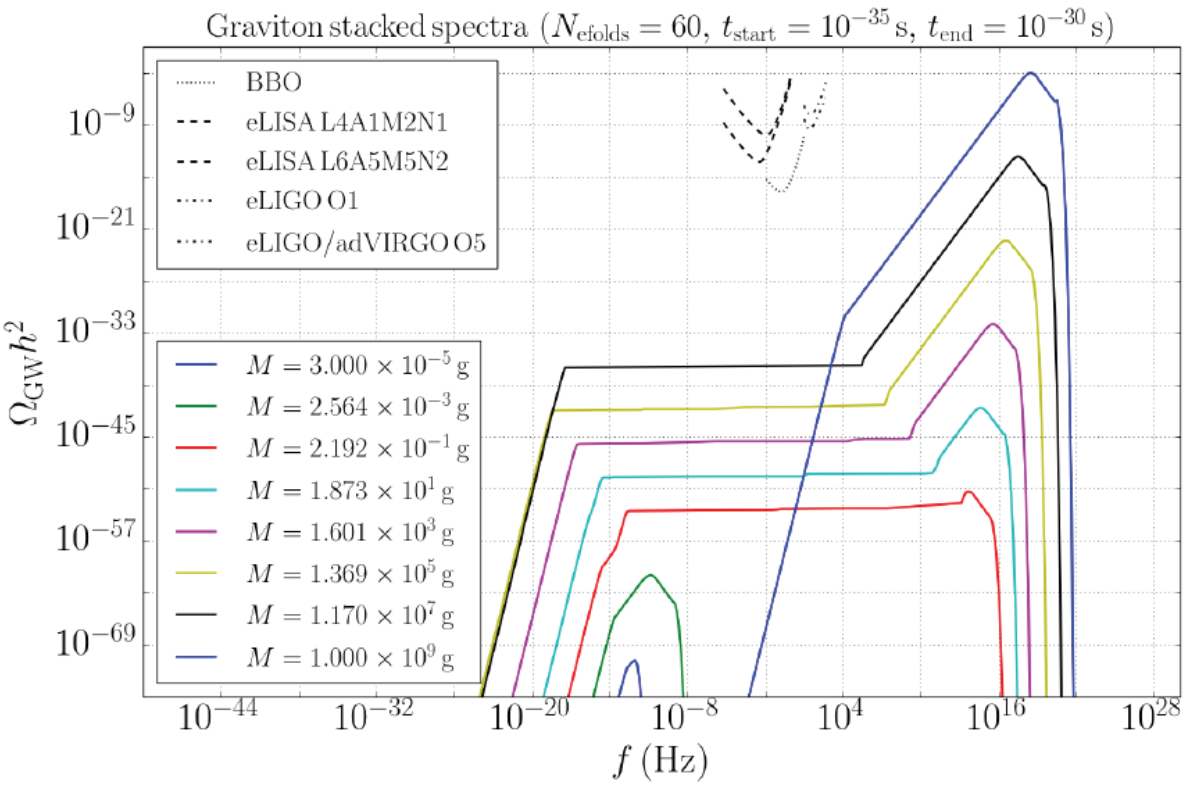

Figure 4.2: Redshifted graviton background from PBH evaporation of different masses and $\beta = 1$, compared to different instrument sensitivities. The characteristics of the inflation period are listed in the plot header. The background for realistic values of $\beta < 1$ is obtained straightforwardly. [taken from [421]]

clustered in galaxies like DM so that their "local clustering" factor of $\zeta \equiv \rho_{\rm gal}/\rho_{\rm tot}$ would increase in proportion their contribution to the CR flux [131]. Carr [131] compared the flux of PBH $e^{\pm}$ to the background flux at $\sim 100\,$MeV [424, 425] to show that this bound was not competitive with the γ-ray one. This bound was subsequently revised within the MG&W model [402]. Propagation models were refined over the years since the Ginzburg proposal [426], while still suffering from great theoretical uncertainties [427].[12]

An indirect positron constraint arises from the 511 keV feature detected some 50 years ago in the direction of the Galactic center (GC) [428–430]. This line could be the result of HR positron annihilation on background electrons in the Galactic bulge, which should be enriched in PBHs if those cluster like DM. This was first suggested by [431] and numerically estimated in [432, 433]. In fact, the 511 keV line constraints proved competitive with γ-ray constraints for $M \sim 10^{14} -$

[12]Numerical tools and programs can be found in the PPPC4DMID package http://www.marcocirelli.net/PPPC4DMID.html.

10^{17} g PBHs [434]. It was reinforced with new $e^{\pm}$ data [435] in the PBH CR review of Carr & MacGibbon [436]. Recent studies include [411, 437–439], with a HDBH extension in [171].

In the context of antiproton detection, Wells *et al.* [440] claimed that should a probe escape the heliopause, it would be ridden of the Solar modulation and have a direct access to the local ISM flux of charged particles. Voyager 1 was the first human-made probe to reach the fell regions of the Solar System and to finally measure the ISM $e^{\pm}$ since 2012 [441]. Boudaud & Cirelli [442] thus obtained a local PBH constraint that is less subject to uncertainties due to Solar modulation, while it still depends on the physics of the Galactic propagation.

Electrons, and EM energy in general, emitted in contemporary (PBH) DM-dominated objects heat up the ISM. This results in strong constraints on the PBH abundance in dwarf spheroidal galaxies (dSphs) such as Leo T [443, 444] or in cool-core galaxy clusters [445].

4.1.2.7 Antiprotons

PBH generation of an antiproton flux was first discussed by Kiraly *et al.* [446]. Considering the models of CR propagation in the Milky Way at the time, it was estimated that $\overline{\mathrm{p}}$ were 3 times more abundant than what was expected [447, 448]. They remarked that γ-ray, 511 keV and $\overline{\mathrm{p}}$ constraints were of the same order of magnitude, which suggested a common PBH origin. The constraint was refined in [449] which found it to be more stringent than the γ-ray limit due to local clustering with factor ζ. The $\overline{\mathrm{p}}$ flux was recomputed in the MG&W model by [402]. The BESS experiments [450] allowed for precise low-energy antiproton measurements thanks to Solar minimum activity in the 1990's; these data were used by Maki, Mitsui & Orito [451, 452] to strengthen the antiproton constraints with their own PBH jet hadronization code based on `JETSET` [453] (embedded in `PYTHIA`).

4.1.2.8 Final bursts

The final burst of PBHs is assuredly the type of constraint that has received the most attention in the early times. The competition between the different evaporation models listed in Section 2.2.3.3 (EP and CP models for the primary spectra, photosphere or no photosphere for the secondary ones) gave rise to various observational signatures, ranging from final bursts with μs duration and low-energy MeV γ-ray signature (CP model, photosphere) to "bursts" of $1 - 1000$ s duration with increasing γ energy up to the Planck scale (EP model, no photosphere) [454]. This resulted in order of magnitude spacing in the corresponding limits [455, 456].

PBH explosions could be detected if the source is close enough to Earth $D \lesssim 10$ pc, and if the PBH lifetime is exactly the age of the universe. The combination of both considerations limits the observable bursts to a narrow mass range around M_*, which is already strongly constrained by the diffuse γ-ray background. The conversion of the diffuse constraint to the local density of exploding PBHs gives a rate estimate of $10^{-2} - 1\,\mathrm{pc}^{-3}\cdot\mathrm{yr}^{-1}$ depending on the local clustering of PBHs ζ and of their mass distribution, while the best instruments to date, namely HAWC [457] and HESS [458, 459], put upper limits of $\sim 10^3 - 10^4\,\mathrm{pc}^{-3}\cdot\mathrm{yr}^{-1}$, with Fermi-LAT being a bit less constraining [460]. There is no great hope to observe a PBH explosion one day, even with prospective instruments such as SWGO [461].

The MG&W model settled down the basic features of PBH explosion, making it easier to compare the limits on the rate of PBH explosions from different studies [462–465], and the different observational techniques are now well described [466]. Interestingly, the MG&W model predicts that PBH explosions could generate CRs up to the Planck energy scale [467], which could explain the EeV CRs that challenged the expected Greisen–Zatsepin–Kuz'min (GZK) cutoff [468–470].

Maybe the most important stake of PBH final burst detection is that it would give a privileged access to ultra-high energy physics, possibly exposing new BSM d.o.f. like supersymmetric particles [139, 471]. Kapusta [142] noted that:

> *The fact that temperatures of* $[T > 100\,\mathrm{GeV}]$ *will never be achieved in a terrestrial experiment motivates me here to study the fate of primordial black holes during the final minutes of their lives* [142]

and predicted that:

> *Experimental discovery of exploding black holes will be one of the great challenges of the new millennium.* [142]

A way of testing BH quantum properties against theoretical models would be to detect a neutrino counterpart [139, 143, 404, 472] (or antiprotons [451]) and to examine the relative fraction of the different particles (γ, ν's, gravitons) reaching a detector [257]. Multimessenger PBH searches are one of the aims of the AMON program [473, 474]. Limits were also placed on the HDBHs explosion rate [475, 476].

4.1.3 Speculative constraints

Planck-mass remnants. The idea of BH remnants dates back to the review by Carr [131]. Based on the argument that BHs could have a non-zero baryon number (if protected by a $U(1)$ global symmetry) due to either collapse from a baryonic environment or to the random fluctuation of their $\mathrm{B}/\overline{\mathrm{B}}$ yield, they proposed that a BH "would stop evaporating altogether" when its baryonic charge is of the order of its mass and that all PBHs with initial mass $M < M_*$ would then have "evolve[d] into a remnant". The density of these remnants must not overclose the universe, which results in a constraint on the abundance of PBHs with $M < M_*$.

It was however MacGibbon [477] who gave for the first time a coherent picture of PBH evaporation where a scale-invariant PBH spectrum compatible with γ-ray observations and which provides the observed $\overline{\mathrm{p}}$ and e^+ CR fluxes leaves a population of PMRs with density precisely of that of the "cosmological dark matter" $\Omega_{\mathrm{PMR}} \sim \Omega_{\mathrm{DM}}$. This could explain in a very natural way the fact that the "hidden mass" required to bound galaxies and galaxy clusters as well as the "cosmological DM" are in fact the same thing (as proposed just before by Davis *et al.* [478] based on numerical simulations of the expanding universe and structure formation). This numerical coincidence could be referred to as a "PBH miracle", in analogy with the "WIMP miracle".

Barrow *et al.* [479] thoroughly studied the cosmological consequences of the existence of PMRs and conclude that if all PBHs have evaporated before BBN, then this DM scenario is perfectly viable. In 2000, Dolgov *et al.* [416] proposed a unified scenario of DM and baryogenesis by PBHs.

PBHs that dominate in the early universe give rise to the $\mathrm{B}/\overline{\mathrm{B}}$ asymmetry through the "Dolgov model" (see the discussion above). The PMRs of those PBHs subsequently dominate the universe after the PBH reheating, forming the CDM. The observational signature would be a background of gravitons with energy of $100\,\mathrm{eV} \longleftrightarrow 10^{16}\,\mathrm{Hz}$ radiated in the early universe and redshifted to today. Due to the progressive "hiding" of the antibaryons into PBHs, the PMRs would have today a gigantic antibaryonic charge.

This raises the question of the detection of the PMRs, as they would be a perfectly elusive DM candidate, interacting purely gravitationally with the SM and never decaying. Doroshkevich & Nasel'skii [480] argue that PMRs could merge and subsequently decay in the contemporary universe, giving rise to CRs beyond the GZK cutoff. On the other hand, PMRs stabilized against evaporation by (dark) EM charge [318] could be detected as they would interact electrically in terrestrial detectors.

Mixed DM-PBH models. If there exists a particle DM (PDM) candidate on top of a PBH component, then new constraints appear. The first, trivial, is that both components must share the total DM density $\rho_{\mathrm{DM}} = \rho_{\mathrm{PDM}} + \rho_{\mathrm{PBH}}$. There is also a totally non-trivial constraint arising from the fact that PBHs are early cores of accumulation of PDM [481–483]. The continuous accretion of DM can even form "ultra-compact mini halos" (UCMHs) around PBHs in the mass range $M \gtrsim 10^{20}\,\mathrm{g}$. Then, these UCMHs would be the location of very effective DM annihilation and decay, which would turn them into bright point sources for photons, neutrinos or electrons, just like smaller evaporating PBHs [484–487]. A PBH+UCMH system would also participate in microlensing events, being a more efficient lens than a PBH of the same mass if it were alone.

Hence, the PDM parameter space reduces that of PBHs, and *vice versa*. In fact, the combined constraints are so tight that PBHs and weakly interacting massive particle (WIMP) DM are mutually exclusive [488, 489], which has caused the mixed model to be denoted as "All or nothing" [490, 491]. If *some* subdominant WIMP density exists, then PBHs are excluded as a DM component down to $f_{\mathrm{PBH}} \sim 10^{-10}$ depending on the DM mass, which would be—by far—the strongest bound in the whole $M \gtrsim 10^{18}\,\mathrm{g}$ mass range [491]. Of course, if DM is not self-interacting then these limits do not apply. The complementary interplay with PBH direct emission of DM described in Section 4.5 is negligible for $M > M_*$.

DM/DR production. The literature about DM and DR production by PBHs is prolific and is reviewed in the dedicated Sections 4.4 and 4.5.

4.2 Schwarzschild primordial black holes

[13]In this Section, I discuss in detail the general (hidden) assumptions necessary to obtain the easiest kind of PBH constraint, that is the γ-ray background constraint.

[13]This Section is based on my paper "Limits on primordial black holes detectability with Isatis: A BlackHawk tool" [262].

4.2.1 A little bit of history

Evaporation of PBHs with emission of photons has been historically the first HR constraint imposed on the PBH abundance around M_*. This is the range where HR is the strongest today. Chapline [492] described the redshifted cosmological photon background from PBHs:

> *[...] as a continuation of the 3 K blackbody spectrum and* [rising] *slowly to peak at an energy determined by the smallest black hole mass now existing.* [492]

This limit was refined by Page & Hawking in 1976 [423] using their numerical GFs and the 100 MeV measurement of the diffuse background by Fichtel *et al.* [493]. This energy scale corresponds precisely to that of the hottest PBHs today, those with $M \sim M_*$. It yielded a constraint $\Omega_{\rm PBH} \lesssim 10^{-8}$; this "Page-Hawking limit" (PHL) remained the strongest one until recently. Page & Hawking focused on photons because they are easy to detect. Neutrinos have a greater emission rate (more d.o.f. and $Q_{1/2} > Q_1$), and gravitons are not screened by the ISM content, but:

> *It would be very difficult to detect the gravitons or neutrinos because they have such small interaction cross-section.* [423]

The PHL has not received any new contribution until the MG&W model permitted to compute precisely the total secondary spectrum of photons [402, 462], with the conclusion that the PHL—of magnitude closer to $\Omega_{\rm PBH} \sim 10^{-9}$—excluded PBHs as 100% DM for $M \lesssim 10^{16}$ g. However, these used the same 1970's data [493, 494]. In 1992, Overduin & Vesson published an important paper [495]. It is the first time, to my knowledge, that a general study is made to:

> *[...] draw together constraints that can be set on an important class of dark matter candidates; namely, those which are unstable to decay over cosmological timescales, and whose photon decay products therefore provide a well-defined way to identify their nature.* [495]

DM existence was intuited for a long time, but the only confirmed interactions with normal matter were of gravitational nature [7]. Therefore, DM could be of a totally elusive nature, preventing its detection and identification in any kind of experiment. The only hope was that, somehow, DM had a link with the SM particles. The simplest possibility is that DM decays, and that this decay involve the simplest form of energy in the SM, photon radiation. This paradigm applies directly to unstable PDM, and to PBHs that produce (among others) γ-rays via HR, which can be understood as some kind of progressive decay. Overduin & Vesson based their constraining program on the newly published "Grand unified photon spectrum" [496], that was a complete recollection of the diffuse photon background in all wavelengths from long radio to short γ-rays. A state-of-the art of the DM indirect detection program with this method was given in [497].

The diffuse photon background was definitively improved in the MeV-GeV range by the COMPTEL [498] and EGRET [499] instruments. Kim *et al.* [500] fitted these 0.8 MeV−30 GeV data with a power-law and deduced constraints on the integrated photon flux from PBHs of mass $2 \times 10^{13} - 5 \times 10^{14}$ g. This was refined by [49, 501] for critical collapse mass distributions, and

[436] who remarked that PBHs cannot be the sole source of background due to different spectrum power-laws. Modern derivations of this limit include [57, 247, 255, 502–510].

The PHL was adapted to HDBHs in [170, 171, 217, 218, 223, 511]. Adaptation to KBHs is the object of Section 4.3 while non-standard PBHs are discussed in Section 4.6. The PHL was in fact derived so much times that it has become difficult to compare the different PBH bounds due to the great number of different underlying assumptions. This is the subject of the present Section.

4.2.2 General paradigm

PBHs are convenient candidates to explain the elusive DM. However, years of constraints from various astronomical observations have constrained their abundance over a wide range of masses, leaving only a narrow window open at $10^{17}\,\mathrm{g} \lesssim M \lesssim 10^{22}\,\mathrm{g}$ for all DM in the form of PBHs. This disputed window must be examined with a critical eye, interrogating the general hypotheses underlying the γ-ray constraints. I review 4 levels of assumptions: *i)* instrument characteristics, *ii)* prediction of the (extra)galactic photon flux, *iii)* statistical method of signal-to-data comparison and *iv)* computation of the HR rate.

As an improvement over previous studies I developed `Isatis`, a new tool designed for `BlackHawk`. I discuss the existing and prospective constraints on the PBH abundance in Section 4.2.4 and investigate the impact of assumptions *i)-iv)* in Section 4.2.5. I show that the constraints can vary by several orders of magnitude, advocating the necessity of a reduction of the theoretical sources of uncertainties. I then consider an "ideal" instrument in Section 4.2.6 and I demonstrate that the PBH DM scenario can only be constrained by the direct photon HR phenomenon below $M_{\rm max} \sim 10^{20}\,\mathrm{g}$. The upper part of the mass window should therefore be closed by other means.

Because all BHs evaporate due to HR, losing their mass in a time related to their initial mass by $\tau \sim M^3$, their contribution to DM today implies that their initial mass was more than $M_* \gtrsim 10^{14}\,\mathrm{g}$. Ref. [512] returned recently to the PBH accretion problem, arguing that accretion may overcome HR during the RD era, causing PBHs to grow during this period, so that the mass of PBHs evaporating just now is reduced from $M \lesssim 10^{15}\,\mathrm{g}$ to $M \sim 10^{14}\,\mathrm{g}$. This justifies that I safely show the constraints down to $M \geq M_{\rm min} = 10^{14}\,\mathrm{g}$. PBHs with mass $M \sim 10^{20}\,\mathrm{g}$ emit in the keV band; as the mean energy of HR is inversely proportional to the PBH mass $\langle E \rangle \propto 1/M$, heavier PBHs $M \geq M_{\rm max} = 10^{20}\,\mathrm{g}$ are very hard to see through their photon HR, as will be shown in the following.

During the last years, numerous constraints have been established on the PBH abundance in the disputed mass range $[M_{\rm min}, M_{\rm max}]$, with at stake the answer to the question of whether light PBHs are indeed the elusive DM. What I will henceforth call *direct* photon constraints are set by comparing the PBH emission spectrum to some target photon flux [255, 505, 513] (*e.g.* the GC), to the stacked isotropic X-ray or γ-ray backgrounds (denoted together as EXGB; this is the PHL) [247, 503, 509, 514, 515] or to a combination of the two [504, 506, 507]. *Indirect* photon constraints as well as other particle backgrounds and other kind of HR constraints are reviewed above in Section 4.1.

Most of the recent studies now take into account the effect of having a non-zero PBH spin, which enhances the photon emission and thus results in more stringent constraints for KBHs, or an extended PBH mass distribution, that should be more realistic regarding the channels of PBH

formation (see the next Section 4.3). More exotic studies derived constraints on non-standard PBHs (see Section 4.6).

Photon constraints are handy thanks to several simplifications: photons are massless particles, thus any PBH mass is compatible with the emission of photons with the corresponding mean energy $\langle E \rangle \sim T$; photons travel in straight lines, so their detection does not rely on complex propagation models; and the detection of photons by all kinds of instruments is a mastered technique that does not suffer from large measure uncertainties and was already performed accurately in a very wide range of energies. This is why I focus on photons in this Section. I further restrict the scope of this analysis to most minimalist SBHs with a monochromatic mass distribution and unclustered spatial distribution.

As stated above, the fraction $f_{\rm PBH}$ is already strongly constrained in the $M_{\rm min} - 10^{16}\,$g range, leaving small doubt on the possibility that PBHs can constitute all of DM in the low mass part of the HR window, with constraints robustly set to $f_{\rm PBH} < 10^{-5}$. However, the high mass range $10^{16} - 10^{22}\,$g has been the subject of multiple studies that claimed exclusion of 100% PBH-DM up to 10^{17} and even $10^{18}\,$g (*e.g.* EXGB constraints in the case of an extended mass distribution of spinning PBHs [514], see below). The aim of this study is to make quantitatively explicit the underlying assumptions and approximations, to contextualize the claimed limit validity and to underline the way they can (or cannot) be compared to each other. This is of utmost importance because not the whole mass window that is currently scrutinized for 100% PBH-DM is accessible to HR constraints, as will be demonstrated; extended mass functions that are fitted to the available remaining window constrain back the fine-tuned PBH formation models (and thus the early universe conditions) used to derive them; and the robustness of the estimation of the limits can help design optical instruments that would be sensitive to the most extreme parameter space accessible to HR measures. I regroup the assumptions into 4 categories, all of which discussed in detail in the following:[14]

i) instrument characteristics,

ii) computation of the (extra)galactic photon fluxes,

iii) statistical treatment,

iv) computation of the HR.

4.2.3 Basic formulas

The emission rate Q_i of a massless particle i with spin s_i by a SBH is given by Eq. (2.146). The BH temperature is given by Eq. (2.143), so that when the mass decreases because of evaporation, the temperature increases. The emission rate is further cutoff at the particle rest mass $E > \mu_i$, which is trivial for massless photons. Once the instantaneous emission rates Q_i of all particles i are known, they can be integrated over to obtain the BH mass loss rate in the form of the Page coefficient (2.150), which then defines the BH evolution equation (2.151). All these quantities are computed using `BlackHawk v2.1`.

[14] The PBH nature (beyond Schwarzschild) and mass distribution, as well as the computation of the GFs and hadronization branching ratios, belong to the type *iv)* assumptions.

I would like to emphasize that the above calculations assume that the Hawking result holds throughout (most) of the PBH history. They may break down only at the very end of evaporation $t \sim \tau$, where τ is the usual BH lifetime, when $M \sim M_{\rm Pl}$ and quantum gravity effects become relevant. This has no effect on the constraints under discussion. However, it was claimed that the so-called "memory burden" of BHs [516]—their capacity to store information—can slow down the evaporation process to extremely low rates or even stop it, within timescales $t \ll \tau$. If that were true, the evaporation constraints set by *e.g.* photon background measurement would be dramatically alleviated even for SBHs and PBHs of mass $M \ll 10^{14}\,$g could represent a fraction or all of DM [517]. The same kind of effect arises in some calculations of HR taking backreaction into account [518]. The survival of M_* PBHs until today can reversely by used to test these modified HR calculations [519]. Hereafter, I assume that the usual paradigm holds until $M \sim M_{\rm Pl}$.

The quasi-thermal Hawking emission, that I called "primary", is not the final output of HR. Most particles in the SM are not stable (weak gauge bosons, charged leptons) or cannot exist outside confined hadrons (gluons and quarks). The primary emission must be convolved with analytical or numerical branching ratios to obtain the "secondary" spectra of stable particles that can be detected in instruments (photons, electrons, neutrinos, protons and their antiparticles). The secondary spectrum Q_j for particle j is then given by Eq. (2.147). In particular, Q_γ is the final rate of emission of *direct* photons from PBHs, meaning that no interaction with the ISM or with other astronomical objects has been considered (scattering, absorption...).

Inside `BlackHawk v2.1`, I use the `Python` package `Hazma` [256] for this study, which is relevant for low energy hadronization and decays ($E \lesssim$ some GeV). This package considers that pions are emitted as fundamental particles instead of single quarks and gluons, and subsequently decayed into photons and leptons, in accordance with the MG&W model. `Hazma`, which relies on analytical decay and FSR formulas, undoubtedly suffers from inherent approximations. I should also implement Bremsstrahlung effects for emitted charged particles [263] that may dominate at very low energy, around the keV scale. Using `Hazma`, Ref. [255] showed that the emission of all the massive particles (the lightest being the electron) is exponentially suppressed for PBHs with mass $M \gtrsim 10^{17}\,$g, and only primary photons, neutrinos and maybe gravitons are radiated. Secondary photons however dominate the spectrum for PBHs with lower masses, with a mean energy $\langle \tilde{E} \rangle$ well below the PBH temperature.

In the following, I give the basic formulas for (extra)galactic PBH photon flux computation, together with a discussion of related type *ii)* assumptions. Both (extra)galactic contributions are important because coincidentally, they are of the same order of magnitude at MeV energies for PBHs right in the relevant HR window $M \sim 10^{15} - 10^{18}\,$g (a fact that was first noted by Ref. [520]). Low energy photons principally come from the redshifted extragalactic spectrum while high energy photons originate from the Galaxy [504, 506, 507].

4.2.3.1 Galactic flux

If PBHs represent some fraction of DM, then they are present in the Milky Way halo with some spatial distribution $\rho_{\rm gal}(r)$ (in galactocentric coordinates) which I take as spherical for simplicity. The photons they emit through HR propagate in straight lines from their origin PBH to Earth.

Thus, the flux of GC PBH photons received by an instrument on Earth per unit energy, time, surface and solid angle is [255, 255, 504–506, 513]

$$\frac{\mathrm{d}\Phi_\gamma^{\mathrm{gal}}}{\mathrm{d}E} = \frac{1}{A_{\mathrm{gal}}}\frac{J_{\mathrm{gal}}}{4\pi}Q_\gamma(E)\,, \tag{4.5}$$

where

$$J_{\mathrm{gal}} \equiv \frac{1}{\Delta\Omega}\int_{\Delta\Omega}\mathrm{d}\Omega\int_{\mathrm{LOS}}\rho_{\mathrm{gal}}(r(l,\Omega))\,\mathrm{d}l\,, \tag{4.6}$$

with $\Delta\Omega$ the field of view (f.o.v.) considered and $A_{\mathrm{gal}} \equiv M$ is the normalisation constant for a monochromatic mass M distribution of SBHs. Note that this formula could be adapted to any compact source other than the GC with the relevant surface factor J integrated over the volume of that source. I remark that the flux depends on the mass distribution of DM in the Milky Way halo and on the precise location R_0 of the Solar System in this halo, contained in the definition of the line of sight (LOS) [506].

4.2.3.2 Extragalactic flux

PBHs form in the early universe, with a formation time t_{f} related to their initial mass by Eq. (1.17). Hence, they emit particles via HR during all cosmological eras until today, and this continuous flux piles up with a dilution factor $a(t) = 1 + z(t)$. The flux on an instrument today per unit energy, time, surface and solid angle is given by [503, 504, 506, 507, 509, 514, 515]

$$\frac{\mathrm{d}\Phi_\gamma^{\mathrm{egal}}}{\mathrm{d}E} = \frac{1}{4\pi A_{\mathrm{egal}}}\int_{t_{\mathrm{min}}}^{t_{\mathrm{max}}}\mathrm{d}t\int_0^{+\infty}a(t)\,Q_\gamma(t, E = a(t)E')\,\mathrm{d}E'\,, \tag{4.7}$$

with $t_{\mathrm{min}} = t_{\mathrm{CMB}}$ for photons, because the universe is opaque to light before that, and $t_{\mathrm{max}} = \min(\tau, t_{\mathrm{today}})$. The normalization constant for a monochromatic mass M distribution of SBHs is $A_{\mathrm{egal}} \equiv M/\rho_{\mathrm{DM}}$ where $\rho_{\mathrm{DM}} \equiv \Omega_{\mathrm{DM}}\rho_{\mathrm{c}}$ is the global density of DM today. I remark that the flux depends on the value of the cosmological DM density fraction, but also on the redshift history of the universe; I have further neglected the optical depth of the ISM (line absorption of light) apart from the cutoff at the CMB time in integral (4.7).[15]

4.2.4 A nomenclature of constraints

Now, I detail how the fluxes (4.5) and (4.7) are compared to different sets of data to derive PBH abundance constraints. This discussion is quite trivial and cumbersome but I think that it is of central importance to recall the basics. Altogether, this Section deals with type *iii)* assumptions.

[15] A more sophisticated description of t_{min} could be implemented by an additional factor $e^{-\tau_{\mathrm{OD}}(E,z)}$ where τ_{OD} is the "optical depth" taking ISM interactions into account. This in fact results in a strong cutoff at $t = t_{\mathrm{CMB}}$ in the case of photons [247].

4.2.4.1 Existing data

The first and very classical method to obtain a constraint on the PBH abundance from HR consists of directly comparing the predicted flux for some PBH mass and abundance—I recall that I focus here only on a monochromatic distribution of SBHs—and some set of data measured by an instrument. Photon data are either presented in a differential (energy or number of events per unit time) or integrated (total energy or number of events) form, as a function of photon energy. Both should be equivalent as one does not expect the PBH signal to vary during the time of observation. Then, to constrain a signal, one can compare the spectrum to each energy bin of the data set, asking that the PBH photon flux does not overrun the measured flux. One can also consider the whole instrument energy band and compare the integrated quantities. This is a model independent method, but there are already two ways to compare the signal to the data, and there remains a choice to make as for the confidence level (CL) one choses to exclude PBHs at (data, data $+\sigma$, data $+2\sigma$, ...). One can also fit the data with some function (from a simple segmented function to a complex analytical formula), motivated by a physical interpretation or not. This is already a model dependent approximation, as it infers data in unmeasured energy bins from data in measured ones. One can finally go one step further, by assuming that some fraction of the measured signal comes from astronomical sources, as first pointed out by [502] in the context of the PBH constraints from the EGXB. Thus, there is even less available parameter space for the PBH abundance. This is highly model dependent, and contains a hidden feedback loop: most astronomical backgrounds are estimated (calibrated) thanks to the very same data. Furthermore, the data are often "cleaned" using catalogs of identified point-sources to obtain the diffuse components. This introduces a bias that I have overlooked in the present analysis: if PBHs are highly "clumped" inside the Galaxy [46, 521–523], they would resemble point-like sources and be cleaned away in the diffuse component search procedure. Constraints for clustered PBHs require a dedicated treatment (see *e.g.* [515, 524, 525]).[16]

4.2.4.2 Prospective instruments

When data is not yet available in some energy range, one can put a conservative constraint on the PBH signal by saying that if the prospective instrument designed to explore this particular energy range is built and measures nothing, then this means that the signal is below the sensitivity of the instrument, with some CL. When data is already available, it is very complicated to decide what to do. In fact, the more precise instrument to come can totally revolutionize the measures due to an error of appreciation of the functioning of the previous ones.[17] An independent conservative constraint would be to predict what sensitivity to a PBH signal some instrument can *in principle* reach, assuming that all the signal comes from PBHs or that some (model-dependent) background is to subtract beforehand. This is quite radical and nobody expects that all the measures taken by long-time working instruments are to be thrown away. A more reasonable method is to build a model of background, and to use it to estimate what would be the prominence of the PBH signal "above" the background (signal-to-noise ratio—SNR— method or χ^2 method). This also contains a

[16] The clustering of PBHs also modifies drastically their merger rate, which was at the center of debates at the CERN TH Institute "Primordial vs. Astrophysical origin of black holes".

[17] See *e.g.* the different slopes of the EGRET and Fermi-Lat data below.

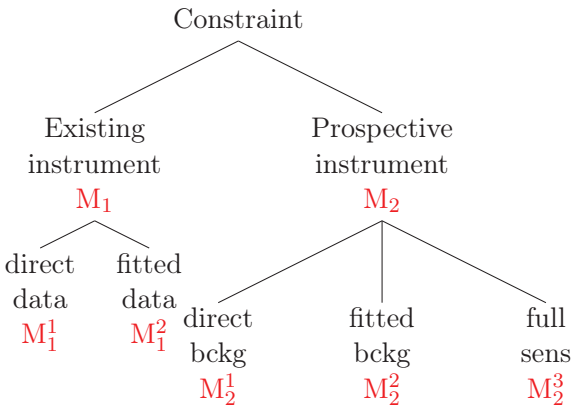

Figure 4.3: The different constraint methods. I have restricted the tree to methods we have encountered in the literature: for existing instruments, "direct data" means that the instrument data points are used, and "fitted data" that a fit running through the data points is chosen; for prospective instruments, "direct bckg" means that the data points used as agnostic background, "fitted bckg" that some fit is used and "full sens" that pre-existing data are ignored and the new detector maximal sensitivity is used. The designation we use in the text are: "type 1" methods M_1 with sub-methods M_1^1 and M_1^2 for existing instruments; "type 2" methods M_2 with sub-methods M_2^1, M_2^2 and M_2^3 for prospective instruments.

feedback loop: background models are often calibrated thanks to the older instrument data, thus a deviation from the expected background compensated by a PBH signal would appear as no signal at all. Once again, the PBH signal and the background can be compared over the whole energy range or inside each energy bin separately.

4.2.4.3 Summary

One therefore understands that even the simplest data-signal comparison method contains non-trivial features that complicate the comparison between constraints set with different choices. This is even worse for the prospective instrument methods as the dependency to the background modelling is complex. I do not intend here to build a hierarchy of the methods chosen by different authors but just to quantitatively highlight their differences. Ref. [255] is the first, to my knowledge, to compare the PBH constraints from different prospective instruments with rigorously the same statistical method. One must also check that instrument characteristics and theoretical choices for the PBH flux calculation are coherent from one study to another. I have built a tree in Fig. 4.3 to summarize the methods described above, restricted to the ones used in the recent literature (examples are listed in the Appendix of Ref. [262]). *Please refer to this tree for all the subsequent abbreviated method nomenclature.*

4.2.5 A numerical tool: the Isatis program

For the sake of this study, I have designed `Isatis`, a numerical public tool that relies on the `BlackHawk` PBH spectra to compute the constraints with a controlled set of assumptions. The code is presented in detail in the Appendix of Ref. [262]. The idea is to use `BlackHawk` to obtain the *direct* PBH photon spectrum, and then to derive the constraint on the PBH abundance for a list of optical instruments, existing or prospective. All constraint assumption types *i)-iv)* listed above, with different statistical methods from the nomenclature given in Fig. 4.3 available, can be modified. Hence, the quantitative individual impact of the assumptions on the PBH *direct* photon constraints can be investigated. This allows to compare consistently the constraints from the literature. Identifying the dominant parameters further gives an insight on where to look for improvements in the constraints. In this Section, I revisit the literature constraints from GC and EXGB PBH photon fluxes and examine type *iii)* assumption impact.

4.2.5.1 Existing instruments

In Fig. 4.4 (left panels), I show the photon flux measured by 4 instruments in the GC direction (latitude b and longitude l close to 0 in galactocentric coordinates), spanning the $10\,\mathrm{keV} - 100\,\mathrm{GeV}$ energy range: INTEGRAL [526], COMPTEL [526, 527], EGRET [528, 529] and Fermi-LAT [530].[18] In the same figure (right panels), I display the EXGB measured by 4 instruments, spanning the $1\,\mathrm{keV} - 1\,\mathrm{TeV}$ energy range: HEAO+balloon [533], COMPTEL [534], EGRET [535] and Fermi-LAT [536] (model A). I also draw various fitting models (see legend), quite accurate in some energy ranges but unsuccessful in reproducing the whole set of data.[19]

To obtain the PBH constraints, I must here use method M_1. I give the results for the submethod M_1^1 in Fig. 4.5: direct comparison of the signal to the data requiring that

$$f_{\rm PBH} \int_{E^{\rm X}_{\rm low}}^{E^{\rm X}_{\rm up}} \frac{\mathrm{d}\Phi^{\rm PBH}_{\rm gal/egal}}{\mathrm{d}E}\,\mathrm{d}E \leq (E^{\rm X}_{\rm up} - E^{\rm X}_{\rm low}) \times \left[\frac{\mathrm{d}\Phi^{\rm X}_{\rm gal/egal}}{\mathrm{d}E} + \mathrm{CL} \times \Delta\Phi^{\rm X}\right], \tag{4.8}$$

in each energy bin, where the fluxes $\mathrm{d}\Phi_{\rm gal/egal}/\mathrm{d}E$ are given by Eqs. (4.5) and (4.7), $E^{\rm X}_{\rm low/up}$ are the bounds of the energy bins of instrument X and $\mathrm{d}\Phi^{\rm X}_{\rm gal/egal}/\mathrm{d}E$ (resp. $\Delta\Phi^{\rm X}$) is the photon flux (resp. error bar) measured by X and shown in Fig. 4.4. CL is the confidence level, translated in the number of error bars considered above or below the central value of the data points. I have chosen a Navarro–Frenck–White (NFW) DM profile [546] with the "convenient" set of parameters from [547] for the galactic flux, and the standard MD from CMB ($t \approx 1.2\times10^{13}\,\mathrm{s}$) to today ($t \approx 4.4\times10^{17}\,\mathrm{s}$) for the extragalactic flux, with $\Omega_{\rm DM}$ given by Planck [253]. In Fig. 4.5, I have performed an empirical power-law fit to the most stringent constraints, with parameters

$$f_{\rm PBH} \sim (M\,(\mathrm{g})/2\times10^{17})^{2.8}\,, \tag{4.9}$$

[18] Be careful that the f.o.v. around the GC on which the data has been averaged is not the same for each instrument, causing probable normalization incompatibilities on that plot.

[19] Other instruments or models could be easily implemented, such as the background models of [539–541] discussed in [510] or the Swift-BAT [542], SMM [543] and XMM-Newton [544] instruments. The X-ray sky has been explored by several more recent instruments, as reviewed *e.g.* in [545].

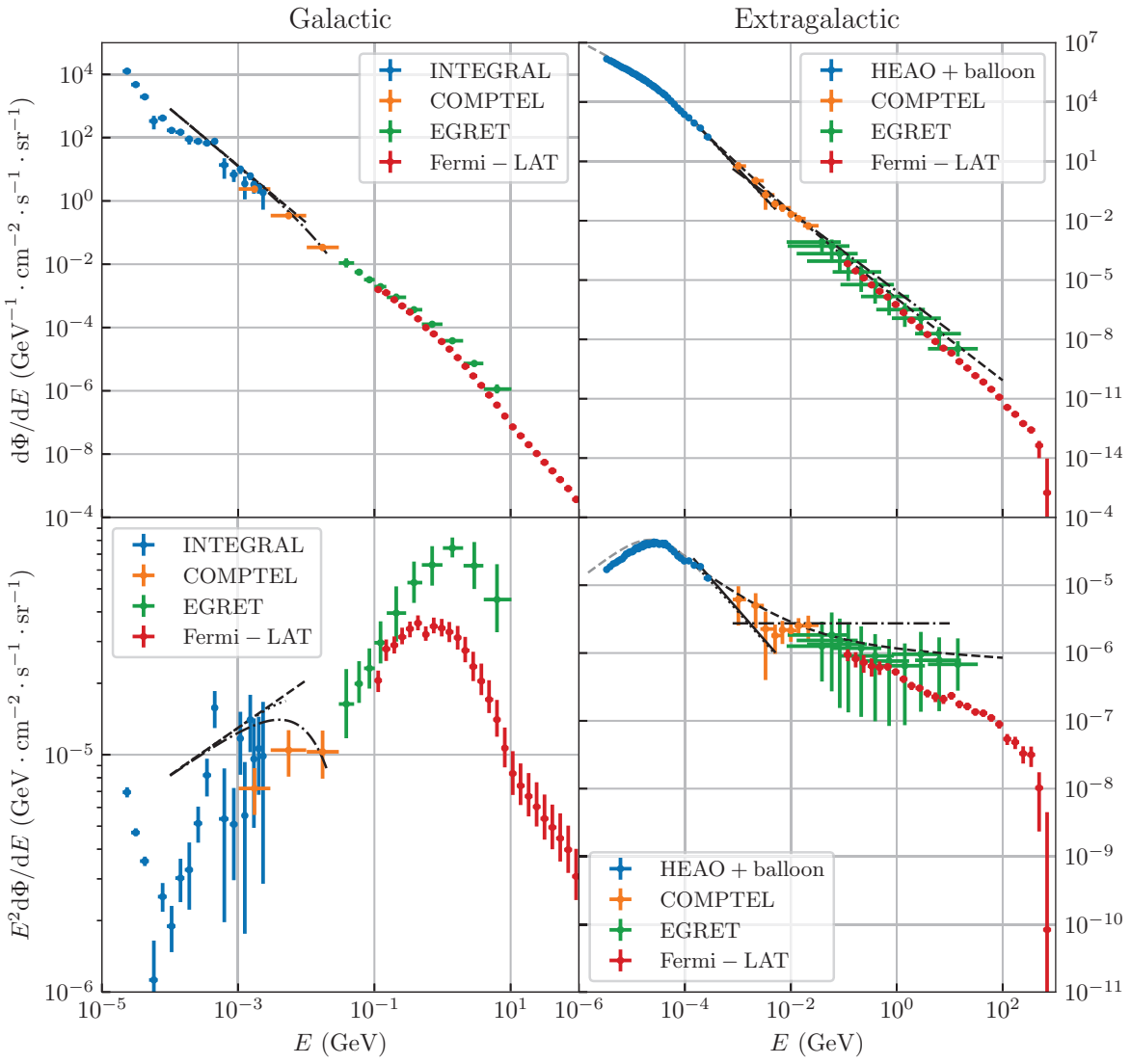

Figure 4.4: Left: GC photon flux measured by INTEGRAL [526] ($l \in [-30, +30]$, $b \in [-15, +15]$), COMPTEL [526, 527] ($l \in [-30, +30]$, $b \in [-15, +15]$), EGRET [528, 529] ($l \in [-30, +30]$, $b \in [-5, +5]$) and Fermi-LAT [530] ($l \in [-30, +30]$, $b \in [-10, +10]$). For completeness, I draw the following background models: [531] (dashed), [532] (dot-dashed) and [507] (dotted). **Right:** Isotropic extragalactic photon flux measured by HEAO+balloon [533], COMPTEL [534], EGRET [535] and Fermi-LAT [536] (model A). For completeness, I draw the following background models: [533] (dashed, black), [537] (dashed, grey), [538] (dot-dashed), [503] (dotted), [507] (solid). **Upper** and **lower** panels show $\mathrm{d}\Phi/\mathrm{d}E$ and $E^2\mathrm{d}\Phi/\mathrm{d}E$. [taken from [262]]

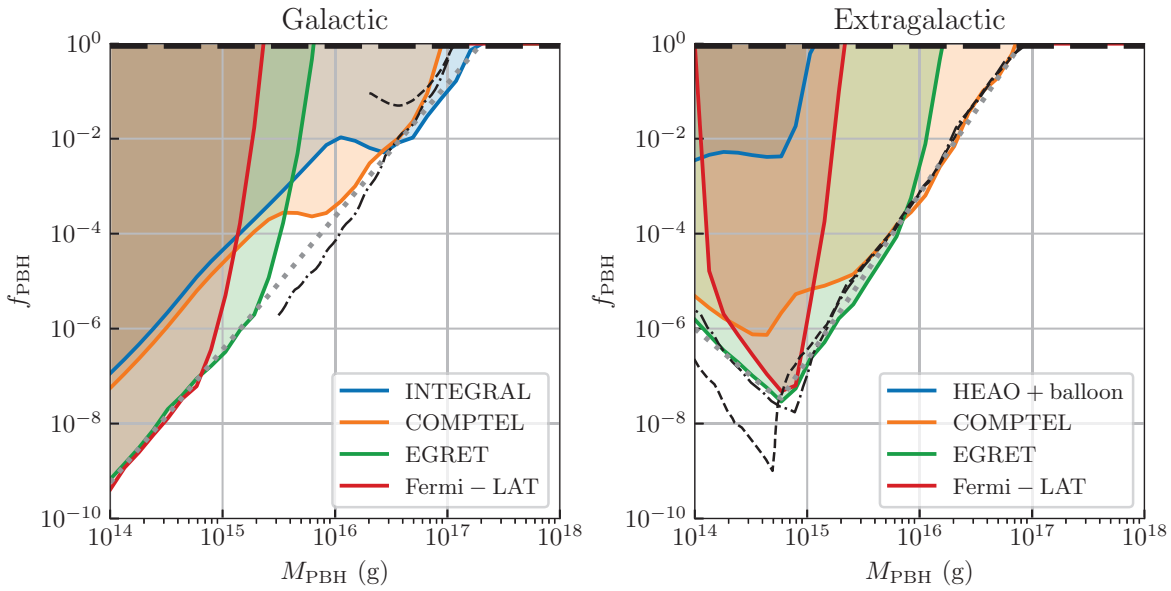

Figure 4.5: Left: PBH constraints from GC observations of the 4 instruments of Fig. 4.4. For comparison, I show the limits set by Ref. [513] for INTEGRAL (dashed) and Ref. [255] for COMPTEL (dot-dashed), stressing the fact that the statistical method is not the same as here. **Right:** PBH constraints from EXGB observations of the 4 instruments of Fig. 4.4. For comparison, I show the limits set by Ref. [247] (dashed) and Ref. [514] (dot-dashed). **Method:** Limits from this work (shaded areas) are computed with method M_1^1 using the central values of the Fig. 4.4 fluxes (CL = 0 in Eq. (4.8)). [taken from [262]]

for the GC, which overestimates the results at $\sim 5 \times 10^{15}\,$g and

$$\begin{cases} f_{\rm PBH} \sim (M\,({\rm g})/10^{11})^{-2}\,, & M \lesssim 8\times 10^{14}\,{\rm g} \\ f_{\rm PBH} \sim (M\,({\rm g})/8\times 10^{16})^{3.5}\,, & M \gtrsim 8\times 10^{14}\,{\rm g} \end{cases} \tag{4.10}$$

for the EXGB, which can be compared to [266].

As an example, let me now examine the impact of the CL parameter, which takes into account the error bars of the photon fluxes. This is a type *iii)* assumption. To do so, i repeat the analysis of Fig. 4.5 with CL $= \{-1, 1, 2\}$ (lower error bar, upper error bar and twice the upper error bar), and present in Table 4.1 the maximum relative discrepancy in $f_{\rm PBH}$, as compared to the case CL = 0 (central values). Obviously, instruments with large error bars are the most affected: looking at Eq. (4.8), one easily deduces that an increase of the instrument flux by a factor α results in a constraint relieved by the same factor α. This is directly shown by the linearity between CL and the relative increase in $f_{\rm PBH}$ in Table 4.1 (slightly broken for asymmetric error bars). I observe that the CL parameter can have an impact of up to a factor of a few on $f_{\rm PBH}$ for instruments with very large error bars.

instrument		−1	0	+1	+2
galactic	HEAO + balloon	−0.68	0	+0.68	+1.36
	COMPTEL	−0.21	0	+0.21	+0.44
	EGRET	−0.40	0	+0.40	+0.81
	Fermi − LAT	−0.10	0	+0.10	+0.20
extragalactic	INTEGRAL	−0.08	0	+0.05	+0.11
	COMPTEL	−0.80	0	+0.80	+1.61
	EGRET	−0.70	0	+1.30	+2.59
	Fermi − LAT	−0.24	0	+0.20	+0.40

Table 4.1: Relative maximum increase in $f_{\rm PBH}$ for CL $= \{-1, 0, +1, +2\}$ relative to the case CL $= 0$ for the instruments of Fig. 4.5.

The impact would be exactly of the same kind if the flux data are replaced by some fitting function: the relative discrepancy in the constraint would be directly proportional to the relative discrepancy between the data and the fit. On the other hand, an increase of the PBH signal by a factor α results in a constraint more stringent by the same factor α.

4.2.5.2 Prospective instruments

A large set of prospective instruments, among which AdEPT [550], AMEGO [551, 552], AS-TROGRAM [553, 554] (results for the AS-ASTROGRAM design [555] are new to Ref. [262]), GECCO [556], GRAMS [557–559], MAST [549], PANGU [560, 561] and XGIS-THESEUS [562, 563], are designed to explore the MeV energy range more accurately than previously done with COMPTEL and EGRET, which will improve both the description of the EXGB and the diffuse GC emission.[20] This energy scale is crucial to set constraints on the fraction of DM $f_{\rm PBH}$ in the disputed mass range $10^{15} - 10^{18}$ g. Data is already available in this energy band, so new instruments will only reduce the error bars. The total number of photons—background plus PBH signal—observed by a prospective instrument X is given by [255, 505, 506]

$$N^{\rm X}_{\rm tot} = T_{\rm obs} \Delta\Omega \int_{E_{\rm min}}^{E_{\rm max}} A^{\rm X}_{\rm eff}(E)\, {\rm d}E \int W(E, E')\, \frac{{\rm d}\Phi^{\rm X}_{\rm tot}}{{\rm d}E'}\, {\rm d}E' \,, \tag{4.11}$$

where $T_{\rm obs}$ is the duration of observation, $\Delta\Omega$ is the solid angle f.o.v., $A_{\rm eff}$ is the effective area (which defines the energy band probed, see Fig. 4.6, left panel) and $W(E, E')$ is a window function accounting for the finite energy resolution of the instruments. Following the literature, I take this to be a Gaussian function [565].[21] All the useful references concerning these instruments are listed in Table III in the Appendix of Ref. [262]. I now consider the *total* photon flux from PBHs, that

[20] This field is under intense scrutiny right now, and PBH MeV γ-rays are mentioned as one of the chief goals of the future MeV instruments listed in the γ-ray Snowmass 2021 white paper [564] and PBH white paper [268].

[21] Inside `Isatis`, I have ensured that the relative energy resolution of the photon spectra matches at least that of the instruments, *i.e.* less than a percent.

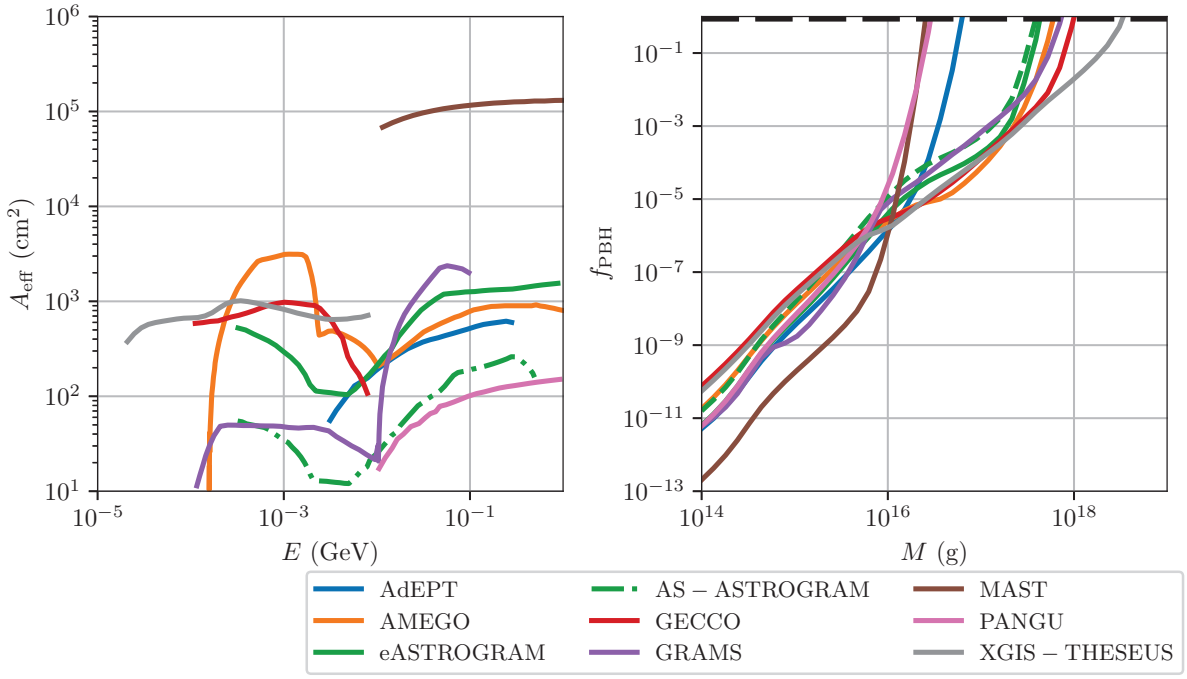

Figure 4.6: Left: Effective area for prospective optical instruments (see text), adapted from Refs. [255, 506, 548, 549]. I have truncated the effective area of MAST as I am not concerned in $>$GeV photons for the PBH mass range probed here. **Right:** PBH constraints from GC+EXGB observations using the method M_2^2 with the background of [532]. [taken from [262]]

is $\Phi_{\rm tot} = \Phi_{\rm gal} + \Phi_{\rm egal}$, and the *total* background flux. Following method M_2, the PBH constraint is obtained by requiring that the SNR stays below some detection threshold

$$\frac{f_{\rm PBH} N_{\rm PBH}}{\sqrt{N_{\rm bckg}}} \leq \mathrm{SNR}\,, \tag{4.12}$$

where I have separated the PBH and the background contributions to the total photon count. An alternative method would consist in demanding that this SNR is not attained in *any* energy bin of the background. I have checked with `Isatis` that this results in a relative change of the constraint $f_{\rm PBH}$ up to a factor of a few.

Most of the difficulty resides in the choice of background. As discussed above, backgrounds are calibrated to the data and thus automatically contain feedback loops. In Fig. 4.6 (right panel), I show the PBH constraints obtained by using the same fitted background as Ref. [255] (see [532] for details), *i.e.* method M_2^2; with SNR $= 5$, $T_{\rm obs} = 10\,$yr and $\Delta\Omega = 5^o \times 5^o$. The other parameters follow Section 4.2.5.1. While not reproduced here, I checked that I obtain results very close to that of Ref. [255] for AdEPT, GECCO and GRAMS (see also [566]), Ref. [507] for AMEGO and

instrument	Ref. [506]	data points
AdEPT	−0.28	−0.08
AMEGO	+0.17	+0.16
eASTROGRAM	+0.11	+0.17
AS-ASTROGRAM	+0.10	+0.16
GECCO	+0.82	+0.72
GRAMS	+0.38	+0.43
MAST	−0.47	−0.02
PANGU	−0.54	−0.02
XGIS-THESEUS	+3.19	+3.54

Table 4.2: Relative extremal variation in $f_{\rm PBH}$ when using the same background as [506] or the central values of the data points compared to the background of [532] for the instruments of Fig. 4.5.

Ref. [506] for XGIS-THESEUS. There are discrepancies with Ref. [505] for GECCO and Ref. [150] for AMEGO, probably linked to the different statistical treatment. Stranger though are the discrepancies I find with respect to Ref. [255] for AMEGO, eASTROGRAM, MAST and PANGU: the constraints obtained by [255] reach up to PBH masses that *cannot* be probed with those 4 instruments; $M \gtrsim 10^{18}\,$g (corresponding to $E \lesssim 100\,$keV) for AMEGO and eASTROGRAM, and $M \gtrsim 10^{17}\,$g (corresponding to $E \lesssim 1\,$MeV) for PANGU and MAST. The present constraints look more reasonable to this point of view: only the XGIS-THESEUS instrument can probe M up to several $10^{18}\,$g, as shown by the effective area plot in Fig. 4.6 (left panel).

As a second example, I explore the effect of the background choice, that is also a type *iii)* assumption. In Table 4.2, I display the extremal relative change in $f_{\rm PBH}$ when choosing the same background as Ref. [506] and the agnostic background consisting of the central values of the data points (*i.e.* method M_2^1), as compared to the background of [255]. I observe that the choice of background, for the 3 examples shown, can have an impact up to a factor of a few on $f_{\rm PBH}$ in the case of the instrument XGIS-THESEUS.

4.2.6 Reverse engineering the Hawking radiation constraints

In the previous Section, I have revisited existing constraints and exposed their robustness relative to some type *iii)* assumptions, namely the background choice and the statistical method of comparison between the PBH signal and data. In this Section, I examine thoroughly all the other assumptions. Indeed, changing the instrument characteristics at will inside `Isatis` gives an unprecedented access to a reverse procedure: what would be the capabilities of an "ideal" instrument if one could fix arbitrarily all the parameters? Answering this first question carefully could certainly give hints towards design choices for future instruments. But one can go deeper: whatever be the capabilities of the instruments, is there a limit to the PBH mass range one can constrain with *direct* photon PBH constraints? In other words, can the HR window for all DM into PBHs be closed? If the answer to this second question is *yes*, this will certainly weigh in the favor of dedicated instrument

designs. If it is *no*, theoretical efforts will need to be pursued to use other kinds of constraints in the (to be determined) remaining window.

As already stated, for a given PBH mass M, the constraint $f_{\rm PBH}(M)$ for an "ideal" prospective instrument is impacted by several assumptions regrouped in 4 categories: *i)* instrument characteristics, *ii)* uncertainties on the (extra)galactic fluxes, *iii)* different statistical treatments and *iv)* uncertainties on HR. Each of those can then be decomposed into several contributions, that I review in detail below. I define a test instrument with a given set of technical characteristics, along with fiducial parameters for the (extra)galactic fluxes and standard assumptions for the HR, and I fix the statistical method:

i) observation time $\overline{T}_{\rm obs} = 10\,{\rm yr}$, f.o.v. $\overline{\Delta\Omega} = 5^o \times 5^o$ around the GC, relative energy resolution $\bar{\epsilon}(E) = 1\%$, constant effective area $\overline{A}_{\rm eff}(E) = 10^3\,{\rm cm}^2$ for $E = 1\,{\rm keV} - 1\,{\rm GeV}$,

ii) standard MD from the CMB to today for the extragalactic flux and $\overline{\Omega}_{\rm DM}$ from Planck [253], NFW profile for the Milky Way halo with the "convenient" parameters of [547] resulting in $\overline{J}_{\rm gal}$ (cf. Section 4.2.5.1),

iii) statistical method M_2^2 (central values of the data points as background) which considered with point *ii)* gives $\overline{{\rm d}\Phi}_{\rm bckg}/{\rm d}E$, and $\overline{\rm SNR} = 5$,

iv) Schwarzschild PBHs with a monochromatic distribution, Hawking primary spectra $\overline{Q}_i$ computed by `BlackHawk` with the low-energy `Hazma` branching ratios $\overline{Br}_{i\to j}$ for the secondary spectra.[22]

These characteristics result in a fiducial constraint that I denote by $\overline{f}_{\rm PBH}(M)$. Any modification of some assumption results in a different constraint $f_{\rm PBH}(M)$ that I parametrize through

$$f_{\rm PBH}(M) = \overline{f}_{\rm PBH}(M) \left(\prod_{i),\ ii),\ iii),\ iv)} \alpha({\rm param.}) \right) \tag{4.13}$$

where the α's are the contributions from types *i)-iv)* assumptions. I detail the mathematical form of these in the following, and give quantitative results for the modified $f_{\rm PBH}$ thanks to `Isatis`.

4.2.6.1 Instruments parameters

A direct look at Eqs. (4.11) and (4.12) shows that

$$\alpha(T_{\rm obs}) = (T_{\rm obs}/\overline{T}_{\rm obs})^{-1/2}, \quad \text{and} \quad \alpha(A_{\rm eff}) = (A_{\rm eff}/\overline{A}_{\rm eff})^{-1/2}, \tag{4.14}$$

as the number of photons captured for both the background and the signal is directly proportional to these quantities. In the limit in which the f.o.v. covers only the desired target, one also has

$$\alpha(\Delta\Omega) \sim (\Delta\Omega/\overline{\Delta\Omega})^{-1/2}. \tag{4.15}$$

[22] In particular, I do assume that the semi-classical HR holds on throughout most of the PBH lifetime, see the discussion in Sec. 4.2.3.

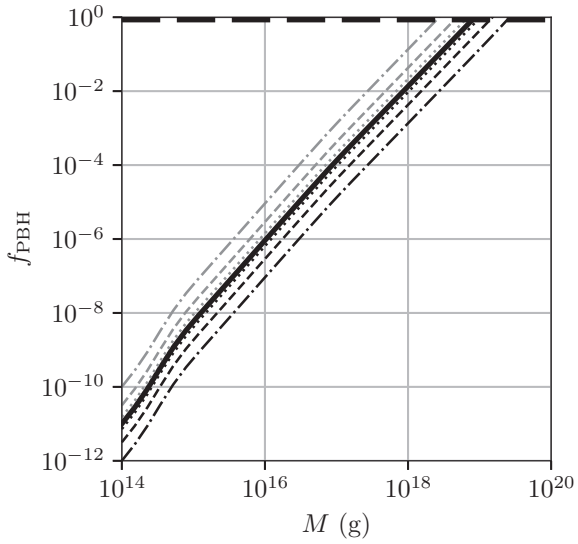

Figure 4.7: Modification of the constraint f_{PBH} for $T_{\mathrm{obs}} = \{1, 100\}\,\mathrm{yr}$ (dashed grey and black), $A_{\mathrm{eff}} = \{10^1, 10^5\}\,\mathrm{cm}^2$ (dot-dashed grey and black), $\epsilon = 10\%$ (solid grey, indistinguishable from the fiducial) and $\Delta\Omega = \{2^o \times 2^o, 10^o \times 10^o\}$ (dotted grey and black) compared to the fiducial set (solid black). "Test" instruments were implemented inside `Isatis` to obtain these constraints. [taken from [262]]

Energy resolutions are overall small and might get smaller in the future as detection techniques improve, so that the window function in Eq. (4.11) tends towards a Dirac distribution, reducing the pollution from neighbouring energy bins. Thus, changing the energy resolution should have a negligible impact $\alpha(\epsilon) \sim 1$.

All these estimations are confronted to quantitative results from `Isatis` in Fig. 4.7. First, I observe that the fiducial constraint extends up to $\sim 10^{19}\,\mathrm{g}$, because the energy coverage of that "ideal" instrument goes down to the keV scale. Second, I note that the constraint is close to a power-law of the PBH mass $f_{\mathrm{PBH}}(M) \sim (M\,(\mathrm{g})/8 \times 10^{18})^2$, a feature that comes from four facts: the primary emission peaks at an energy that is proportional to the PBH mass; the number density of PBH is inversely proportional to their mass; the background fit of [532] is approximately a power-law; and the fiducial effective area is a constant. The effect of the secondary spectra is somewhat visible in the slope breaking below $10^{15}\,\mathrm{g}$. The global variations of f_{PBH} compared to $\overline{f}_{\mathrm{PBH}}$ from the modification of the various parameters has precisely the behaviour expected from Eqs. (4.14) and (4.15). One verifies that the energy resolution has no visible impact.

4.2.6.2 Flux parameters

As the column density of the target impacts only $N_{\rm PBH}$, one can estimate

$$\alpha(J_{\rm target}) \sim (J_{\rm target}/\overline{J}_{\rm gal})^{-1}, \tag{4.16}$$

The precise impact is obviously more complex depending on the predominance of the target flux over the diffuse extragalactic flux, which also depends on the energy considered. As seen before, one expects the target flux to dominate at high energies, constraining low PBH masses, and the redshifted isotropic flux to dominate at low energies, constraining high PBH masses. In Fig. 4.8 I show the extremal change in $f_{\rm PBH}$ for different galactic DM profiles:

- the generalized Navarro–Frenk–White (NFW) profile defined by [546, 567]

$$\rho_{\rm DM}(r) = \rho_{\rm c} \left(\frac{r_{\rm c}}{r}\right)^{\gamma} \left(1 + \frac{r}{r_{\rm c}}\right)^{\gamma-3}, \tag{4.17}$$

  where the classical NFW is obtained for $\gamma = 1$

- the Einasto profile defined by [567–569]

$$\rho_{\rm DM}(r) = \rho_{\rm c} \exp\left\{-\frac{2}{\gamma}\left(\left(\frac{r}{r_{\rm c}}\right)^{\gamma} - 1\right)\right\}. \tag{4.18}$$

Both of these profiles depend on 3 independent parameters: a characteristic density $\rho_{\rm c}$, a characteristic radius $r_{\rm c}$ and a power γ. Even with modern measures, these parameters suffer from large uncertainties. I use the 68% CL parameters of [567] (Tables II and III corresponding to two baryonic models B1 and B2) to be as general as possible in Fig. 4.8.[23] Spanning the whole 68% CL range of the parameters results in constraints $f_{\rm PBH}$ varying by 2 (resp. 1) orders of magnitude inside the same profile and baryonic model for NFW (resp. Einasto) profile; by $\sim 50\%$ (resp. $\sim 1\%$) from one baryonic model to the other (B1 or B2) for NFW (resp. Einasto) profile; and by 20% (resp. 30%) from one profile to the other (NFW or Einasto) for model B1 (resp. B2). The largest variations are obtained with the generalized NFW profile. I am far from having explored the complete diversity of the DM halo profiles existing in the literature, but I can already predict that $\alpha(\text{gal}) \sim 10^{-1} - 10^{1}$. I do not consider targets other than the GC. Even if the density factor is determined more precisely in *e.g.* M31 or DM concentrated dSphs like Draco because they are observed as a whole, it is much smaller than that of the GC and results in less stringent constraints: 10^{-2} factor reduction for M31 and Draco [255].

A modified redshift history of the universe or DM density may have a small impact on the time stacked isotropic spectrum. I have checked that this is negligible regarding the small uncertainties on the cosmological parameters for the recent universe (after the CMB), resulting in $\alpha(\text{egal}) \sim 1$.

[23] Refs. [255, 567] use the incredibly precise radius of the Sun orbit $R_\odot = 8.122 \pm 0.031\,\text{kpc}$ recently obtained by the measurement of the orbit of S2 [570], which differs from the older "convenient" value of [547]. Ref. [255] further uses the central values of the NFW profile of Table III and maximizes the density parameter $J_{\rm gal}$ for the Einasto profile with the 68% CL values of Table III.

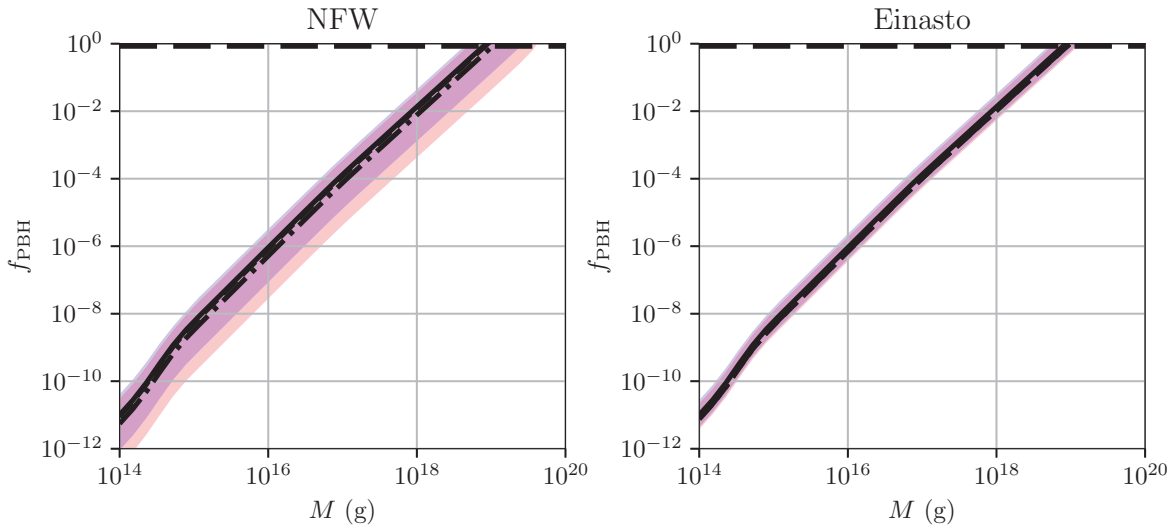

Figure 4.8: Modification of the constraint $f_{\rm PBH}$ for different galactic profiles, compared to the fiducial case (solid black line). **Left:** $f_{\rm PBH}$ for a generalized NFW profile. **Right:** $f_{\rm PBH}$ for a Einasto profile. Dashed (dot-dashed) black lines correspond to the central values of the parameters of [567] and baryonic model B1 (B2); shaded blue (red) areas correspond to a complete span of the 68% CL range for all the parameters for model B1 (B2). [taken from [262]]

4.2.6.3 Statistical treatment

As the photon background only affects $N_{\rm bckg}$, I have already concluded in Section 4.2.5.2 that

$$\alpha(\text{bckg}) = \left(\frac{\mathrm{d}\Phi_{\rm bckg}}{\mathrm{d}E} \Big/ \frac{\overline{\mathrm{d}\Phi}_{\rm bckg}}{\mathrm{d}E} \right)^{1/2} , \tag{4.19}$$

within method M_2. The different choices of backgrounds for prospective instruments in Table 4.2 result in $\alpha(\text{bckg}) \sim 0.5 - 3$ at most. This impact is completely equivalent to that of changing the CL parameter inside method M_1^1, as shown by Table 4.1. On the other hand, the SNR is directly proportional to $f_{\rm PBH}$, thus

$$\alpha(\text{SNR}) = (\text{SNR}/\overline{\text{SNR}})^1 . \tag{4.20}$$

As paper [262] was finalized, I became aware of Ref. [510], where the constraints from the EXGB are revisited with data from instruments different from those presented in Fig. 4.4. The contribution from the GC is included, as well as Hawking radiated electron-positron annihilation. Ref. [510] takes into account astrophysical contribution to the diffuse photon flux in order to obtain more stringent constraints on the PBH abundance, thus using what I denoted in the tree 4.3 as method M_1^2. They obtain constraints more stringent by 2 orders of magnitude in the mass range $10^{15} - 10^{17}$ g. Ref. [508]

also came out, which takes into account the precise spatial distribution of the GC signal in fitting the PBH signal, an effect that I overlooked here by averaging over the Galactic bulge.

4.2.6.4 Hawking radiation

Last but not least, there are uncertainties related to the very computation of the PBH HR spectra. These only affect $N_{\rm PBH}$ in Eq. (4.12), thus I predict

$$\alpha(Q_\gamma) = (Q_\gamma/\overline{Q}_\gamma)^{-1}, \quad \text{and} \quad \alpha(\mathrm{Br}_{i\to\gamma}) = \left(\mathrm{Br}_{i\to\gamma}/\overline{\mathrm{Br}}_{i\to\gamma}\right)^{-1}. \tag{4.21}$$

The uncertainties on the primary emission rates for Schwarzschild PBHs are directly related to the tables contained inside `BlackHawk`, which have been confronted to the literature with an accuracy of less than a percent, such that $\alpha(Q_\gamma) \sim 1$.

There could be large uncertainties in the branching ratios computed by the particle physics codes. At very high energy $E \gtrsim$ TeV `BlackHawk` relies on `HDMSpectra` [258], in the documentation of which is explained that the precise treatment of the EW cascades can alter the branching ratios into photons by several orders of magnitude compared to `PYTHIA`. This has not yet been confronted to accelerator data. At LHC energies $E \sim$ GeV $-$ TeV, `BlackHawk` relies on `PYTHIA` [248] or `HERWIG` [254] with good correspondence to the data, even with the QCD uncertainties [571].[24] At low energies $E \lesssim$ GeV, `BlackHawk` relies on `Hazma` [256], which is also based on accelerator data, but does not take into account *e.g.* the Bremsstrahlung radiation of charged particles specific to PBH radiation [263] which should dominate at the keV scale. The choice of the QCD scale $\Lambda_{\rm QCD}$ at which pions are emitted as primary particles and of the dynamical rest masses of the quarks and gluon introduces further uncertainties (see [228] for a recent discussion). Ref. [258] showed that the branching ratios for "low final energies" $E/e \lesssim 10^{-4}$ in Eq. (2.147) as computed with `PYTHIA` (and thus `HDMSpectra`) suffer from order-of-magnitude uncertainties linked to the difficult tracing of EW cascades on such stretched scales. Hence, I conclude that even with very precise primary spectra, the secondary spectra (integrated over primary energies from all scales) are associated with an order-of-magnitude possible variation from all these codes $\alpha(\mathrm{Br}_{i\to\gamma}) \sim 10^{-1} - 10^{1}$.

4.2.6.5 Summary

Summarizing the results from this Section, I recollect that compared to the fiducial case $\overline{f}_{\rm PBH}$, the value of the PBH constraint for all masses can vary within each set of assumptions:

i) $\alpha_{i)} = \alpha(T_{\rm obs}) \times \alpha(A_{\rm eff}) \times \alpha(\Delta\Omega)$, with extremal values $\alpha^{\rm min}_{i)} \approx 8 \times 10^{-4}$ for $T_{\rm obs} = 100\,{\rm yr}$, $A_{\rm eff} = 10^5\,{\rm cm}^2$ and $\Delta\Omega = 4\pi$ and $\alpha^{\rm max}_{i)} \approx 80$ for $T_{\rm obs} = 1\,{\rm yr}$, $A_{\rm eff} = 10\,{\rm cm}^2$ and $\Delta\Omega = 2^o \times 2^o$,

ii) $\alpha_{ii)} \approx \alpha({\rm gal})$ with extremal values $\alpha^{\rm min}_{ii)} \approx 0.1$ and $\alpha^{\rm max}_{ii)} \approx 10$ for the NFW profile,

iii) $\alpha_{iii)} = \alpha({\rm bckg}) \times \alpha({\rm SNR})$, with extremal values $\alpha^{\rm min}_{iii)} \approx 0.1$ for ${\rm SNR} = 1$ and $\alpha^{\rm max}_{iii)} \approx 6$ for ${\rm SNR} = 10$,

[24] Updated estimates of the QCD uncertainties will be released soon [572]; for an application of those to DM searches see *e.g.* [573].

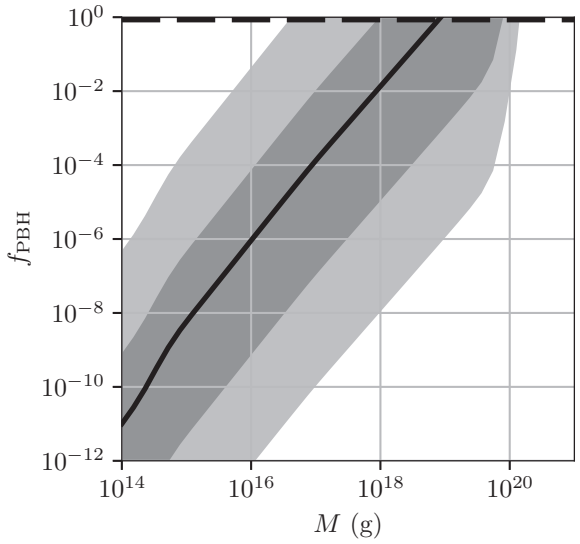

Figure 4.9: Schematic PBH constraints for all extremal assumptions $\alpha_{\rm tot}$ (light grey area) and with only the extremal fiducial instrument characteristics $\alpha_{i)}$ (dark grey area), compared to the fiducial case (dark solid line). [taken from [262]]

iv) $\alpha_{iv)} \approx \alpha(\overline{\rm Br}_{i\to\gamma})$ with extremal values $\alpha_{iv)} \approx 0.1$ and $\alpha_{iv)} \approx 10$.

Overall, I obtain

$$8 \times 10^{-7} \lesssim \alpha_{\rm tot} \lesssim 4.8 \times 10^{4}\,, \tag{4.22}$$

with all the sources of uncertainties and

$$10^{-3} \lesssim \alpha_{ii)} \times \alpha_{iii)} \times \alpha_{iv)} \lesssim 6 \times 10^{2}\,, \tag{4.23}$$

if I restrict to the fiducial instrumental parameters, which is still, as we say in French, *une sacrée fourchette*—a very large span—as it runs over 11 orders of magnitude for $\alpha_{\rm tot}$ and 5 orders of magnitude for $\alpha_{ii)-iv)}$. The extremal constraints are schematically shown on Fig. 4.9. The 100% PBH-DM scenario is excluded up to $M \sim 10^{20}$ g in the most favorable case but the open window goes down to $M \sim 10^{17}$ g in the less favorable one. Of course, the extremal values of the (independent) uncertainties *ii)-iv)* are presumably not attained at the same time, but nevertheless one sees that *PBH constraints from direct HR of photons are still highly model dependent* due to several sources of uncertainties. I conclude that modifying the prospective instrument characteristics allows to close the $M \lesssim 10^{20}$ g window, but I also note that the slope of $f_{\rm PBH}$ is nearly vertical in this region; I discuss this last feature below.

4.2.7 Very low energies

I observe on Fig. 4.9 that the constraint $f_{\rm PBH}$ saturates at high PBH masses. This is due to the exponential cutoff of Q_γ and thus of $\mathrm{d}\Phi_{\rm PBH}/\mathrm{d}E$ at energy $E \gtrsim E_{\rm max} \sim T_{\rm PBH} \approx 1\,\mathrm{keV}(M/10^{19}\,\mathrm{g})^{-1}$ for Schwarzschild PBHs. Hence, as my description of the background and of the secondary photon spectrum is limited to this keV lower energy bound in this study, I cannot obtain $f_{\rm PBH}$ at $M \gtrsim 10^{20}\,\mathrm{g}$. Increasing the capabilities of the prospective "ideal" instrument would only make the constraint steeper at $M \sim 10^{20}\,\mathrm{g}$. Thus, pushing the PBH constraint on *direct* photon emission up to lower energies and thus higher PBH masses, with the aim of constraining the whole (yet) open window $M \sim 10^{18} - 10^{22}\,\mathrm{g}$ for all DM into PBHs, would require both precise background description at $E \sim 10 - 1000\,\mathrm{eV}$ *and* precise particle physics codes to compute EM showers down to the eV energy range. One can suppose that the primary spectrum dominates below the keV scale as the emission of all particles except for photons, neutrinos and gravitons is exponentially suppressed at $M \gtrsim 10^{17}\,\mathrm{g}$. However, this energy range falls down right in the (very) far UV band ($\lambda \sim 10 - 1000\,\text{Å}$). To my knowledge, this band is not yet covered within a precise all-sky (resp. GC) survey that would give an access to the isotropic (resp. GC) component of the background. The GALEX [574] (and future UVEX [575]) instruments are sensitive only starting above $\lambda \sim 1000\,\text{Å}$.

Suppose that one extrapolates the "ideal" instrument capabilities, the PBH HR rates and the GC+EXRB background down to the eV energy scale: $\mathrm{d}\Phi_{\rm bckg}/\mathrm{d}E \propto E^{-2}$ and $A_{\rm eff}(E) = \overline{A}_{\rm eff}(E)$ at $E = 10 - 1000\,\mathrm{eV}$. For the fiducial values of the parameters *i)−iv)* I obtain $f_{\rm PBH} \sim 10^6$ at $M = 10^{22}\,\mathrm{g}$. Closing the window for all DM into PBHs with *direct* photons would then require to increase the capabilities of our "ideal" instrument by a factor 10^6 (or reduce $f_{\rm PBH}$ by a factor 10^{-6}), which is unrealistic as $\alpha_{i)}^{\rm min} = 8 \times 10^{-4}$ is already technically challenging. Plus, I expect the spectrum of light at these wavelengths to be overcrowded by astronomical sources (see *e.g.* Fig. 2 of [575]), further increasing the amelioration factor needed to obtain $f_{\rm PBH} \sim 1$ at $M = 10^{22}\,\mathrm{g}$. Thus, I conclude that the window for all DM into PBHs cannot be closed by *direct* photon detection from PBH evaporation.[25] Complementary constraints, relying on complex modelling, are thus needed: dynamical capture by or microlensing of stars (see the review by [285]), rare collisions with solid objects [576] or GRB lensing [577].

4.2.8 Conclusion

In this Section, I have computed the photon emission spectrum by HR of monochromatic SBHs. I restricted the study to the *direct* photons resulting from the primary emission of photons and the secondary emission resulting from EM interactions or decay of other primary particles. I obtained the flux on Earth of photons coming from the GC plus the isotropic redshifted emission from past ages. I identified all the assumptions underlying the computation of this flux and ended up with a clear nomenclature of the constraining methods M_i^j, classifying existing and prospective constraints.

Then, I used `Isatis`, a new public tool available inside `BlackHawk` to examine quantitatively how the constraints presented in the literature depend on those assumptions, regrouped in 4 categories:

[25] Note that Ref. [509] concludes similarly to impossible detection of direct 21 cm radio photons at μeV scale and PBH masses $10^{17} - 10^{28}\,\mathrm{g}$, see also Appendix B.2.1.

i) instrument characteristics, *ii)* (extra)galactic flux description, *iii)* statistical method used and *iv)* HR uncertainties. I have shown that, for a given instrument design *i)*, the constraint on the DM fraction into PBHs $f_{\rm PBH}(M)$ can span up to 5 orders of magnitude due to uncertainties *ii)-iv)*.

This has a direct impact on the size of the current and prospective available window for the 100% PBH-DM scenario and questions the robustness of the current constraints. *I underline the necessity of more precise galactic photon background and HR determination*, especially at low energies where high mass PBH constraints could close the remaining window. I emphasize that the very validity of the semi-classical computation of HR assumed throughout the study, that could be included as one of the *iv)* uncertainties, is a fundamental basis of the whole work.

Finally, I have examined to what extent a prospective "ideal" instrument could constrain $f_{\rm PBH} < 1$ from (currently) $M \sim 10^{18}$ g up to $M_{\rm max} \sim 10^{20}$ g by "reverse engineering" `Isatis`. I conclude that even if instrument characteristics *i)* allow for another 5 orders of magnitude variation of $f_{\rm PBH}(M)$, *above* $M_{\rm max}$*, direct photon constraints are not effective anymore so that complementary constraints should be developed instead.* I refer the reader to Section 4.1 for other means of constraining the PBH abundance in this mass range.

There are numerous ways to build up on this study and improve `Isatis`. First, I have only considered Schwarzschild PBHs, but some EMDE models predict PBHs born with high spin, which would increase their photon yield and result in more stringent constraints; this is the subject of next Section 4.3. Non-standard BH solutions, *e.g.* derived from effective loop quantum polymerization, also predict very different photon spectra; this is the subject of Section 4.6. Deviations from the semi-classical HR computation at mass scales greater than the Planck scale could also be explored. Second, I have considered a monochromatic mass distribution, which is obviously unrealistic and could be refined within a specific PBH formation model. The main effect is to "spread" the constraints towards higher and lower PBH masses due to the high and low mass tails of the distribution under consideration, as shown also in Section 4.3. Third, I have computed the *direct* photon spectrum from instantaneous HR, but I could go further and obtain the *indirect* photon spectrum after model dependent interactions of *direct* photons or electrons/positrons with the ISM [510]. One last possibility is to constrain PBHs through their *(in)direct* electron/positron, neutrino, graviton or (putative) DM particle yield. Some unpublished work has been pursued in order to reproduce the constraints of *e.g.* [411–413, 442] with an extended version of `Isatis`. Including the neutrino secondary spectra inside `Hazma` would allow for great improvement [415]. Finally, I have assumed that PBHs are not clustered when examining the Galactic constraints, but are rather smoothly distributed following the halo density function. Clustered PBHs would appear as point-like sources and would require a suited search.

4.3 Kerr primordial black holes – γ-ray constraints

[26]In this Section I present the constraints obtained for KBHs. Before `BlackHawk` was released, the KBHs constraints were almost unexplored. As discussed in Section 2.2, KBHs were at first of interest

[26]This Section is based on the paper "Constraining primordial black hole masses with the isotropic gamma ray background" [514] I wrote with A. Arbey & J. Silk.

mainly because they could be unstable due to superradiance and the "BH bomb" effect [93, 244, 578], that is the capacity of bosonic resonant scattering around BHs that would extract energy and angular momentum from KBHs until they totally disappear (stimulated emission). The GFs of KBHs were computed numerically by Page at the same time as the SBH and the RNBH [120], but they were not used to constrain PBHs at that time. Following the corresponding discussions in the previous chapters, I believe that is due to two main reasons:

- in the RD era, PBHs are supposed to be born with low spin;
- even if born with high spin, PBHs were (are) thought to lose their angular momentum faster than their mass.

It is striking to see that in the analytical study by Carter *et al.* [111], often cited to support the second argument, it is not proven that PBHs should lose their spin *faster* than their mass, but in fact at more or less the same rate. This is later supported by the Page numerical calculation of the KBH GFs and the associated Page coefficients [120]: PBHs initially near extremal still exhibit a strong angular momentum at $\sim 50\%$ of their lifetime; that is to say, PBHs with initial mass $M \gtrsim M_*$ that have strong HR rates but that have lifetime $\tau \gg t_0$ the age of the universe may still have a strong spin today (recall that $\tau \propto M^3$). This was further numerically studied by Chambers, Hiscock and Taylor [226, 227] that showed additionally that if numerous BSM scalar d.o.f. exist, then a PBH could stabilize its angular momentum at a non-zero value $a^*_{\rm eq} \sim 0.5$. I studied the former point with `BlackHawk` in [236], whereas the latter point has been confirmed very recently by Calza *et al.* [228] using modern computation means (see the discussion in Section 2.7).

Besides, PBHs could either be formed highly rotating, *e.g.* during an EMDE [65, 66] (see Section 1.3.3), or they could acquire spin by subsequent accretion [69] or mergers [70, 579]. Thus, observational limits linked to the spin of PBHs give a unique probe of non-standard inflationary models and binary evolution. The accretion mechanism is further motivated by the observation of stellar [580] and supermassive [581] BHs by X-ray emission, showing that they indeed have very high spins. Even if the formation mechanism disfavors spinning PBHs, statistically *some of them* could be highly rotating [68]. The spin measurement will become more and more precise with future detectors [582].

Finally, the near-extremal spin of PBHs may stabilize them against evaporation, making $M < M_*$ PBHs candidates for DM. This speculative thought is motivated by the fact that even if HR rates increase with increasing spin parameter a^*, they should drop to 0 somehow at $a^* = 1$. Continuity arguments thus suggest that PBHs with a^* very close but smaller than 1 should have negligible evaporation.[27]

All these arguments show that dedicated studies for spinning PBHs are needed. To my knowledge, the GFs of KBHs were used to constrain their abundance relatively to the HR effect only in two papers before `BlackHawk` was released: Ref. [199] computed the high-frequency GW background from small PBHs evaporated in the early universe, and Ref. [71] evaluated the contribution of BSM d.o.f. evaporated by small rotating PBHs to $\Delta N_{\rm eff}$. In this Section, I discuss an extension of the

[27] This is a work in progress with A. Arbey and J. Silk. Numerical and analytical exploration shows to this date no decrease of the evaporation rate, even if some kind of saturation is observed at $a^* = 0.9999$.

PHL to KBHs, and in Section 4.4 I show how precision calculation with `BlackHawk` refines the $\Delta N_{\rm eff}$ constraints. Since `BlackHawk` was released, many recent studies took advantage from its numerical GFs to (re-)evaluate PBH constraints for spinning PBHs, as shown in Appendix A.2.

I present an extension of the constraints on PBHs of masses $M \sim 10^{13} - 10^{18}\,$g arising from the EGXB. PBHs evaporate by emitting HR that should not exceed the observed background. Generalizing from monochromatic distributions of SBHs to extended mass functions of KBHs, I show that the lower part of this mass window can be closed for near-extremal BHs. If the PBHs were sufficiently numerous, that is to say if they contribute to a large fraction of DM, HR from PBHs may be the source of observable background radiation. In this study, I update the constraints on the number density of PBHs by observations of the diffuse EGXB (see the discussion above in Section 4.2), taking into account the latest Fermi-LAT data [536] and, as new parameters, the spin of PBHs and extension of the PBH mass function (in the case of a log-normal distribution). The assumption is that part of the EGXB comes from the time-stacked, redshifted HR produced by evaporating PBHs distributed isotropically in the extragalactic universe. Those PBHs must have survived at least until the epoch of CMB transparency for the HR to be able to propagate in the intergalactic medium. This sets the lower boundary on the PBH mass $M_{\rm min} \sim 5 \times 10^{13}\,$g. Furthermore, the HR peaks at an energy which decreases when the PBH mass increases. This sets the upper boundary for the PBH mass $M_{\rm max} \approx 10^{18}\,$g as the EGXB emission does not constrain the photon flux below 100 keV.

4.3.1 Basic formulas

BHs emit radiation and particles similar to blackbody radiation with a temperature linked to their mass M and spin parameter $a \equiv J/M \in [0, M]$ (J is the BH angular momentum) through Eq. (2.142). The number of particles N_i emitted per unit energy and time is given by Eq. (2.146). For KBHs, the total energy of emitted fields in that equation is $E' \equiv E - m\Omega$, taking into account the BH horizon rotation velocity $\Omega \equiv a^*/(2r_+)$, where $a^* \equiv a/M \in [0, 1]$ is the reduced spin parameter and $m \in \{-l, ..., +l\}$ is the projection of the particle angular momentum $l = \{s, s+1, ...\}$. The GF values of `BlackHawk v1.2` were used in this study.

This emission can be integrated over all energies to obtain equations (2.151) for the evolution of both PBH mass and spin. There are two main effects coming from the PBH spin that play a role in the EGXB constraints. Firstly, a Kerr PBH with a near-extremal spin $a^* \lesssim 1$ radiates more photons than a Schwarzschild one ($a^* = 0$). This is due to the coupling between the PBH rotation and the particle angular momentum for high-spin particles, linked to the phenomenon of superradiance [119, 128, 224]. One thus expects the γ-ray constraints to be more stringent due to the more important photon flux. Secondly, a near-extremal KBH will evaporate faster than a SBH with the same initial mass due to this enhanced HR (see Fig. 2.18). Moreover, the photon peak emission of KBHs is located at higher energies than the SBH one (see Fig. 2.14). These two effects mimic the radiation of a PBH with zero spin and smaller mass. Hence, one expects that the constraints for KBHs will be shifted toward higher PBH masses when the initial reduced spin parameter a_i^* increases. Their amplitude in not trivial to forecast.

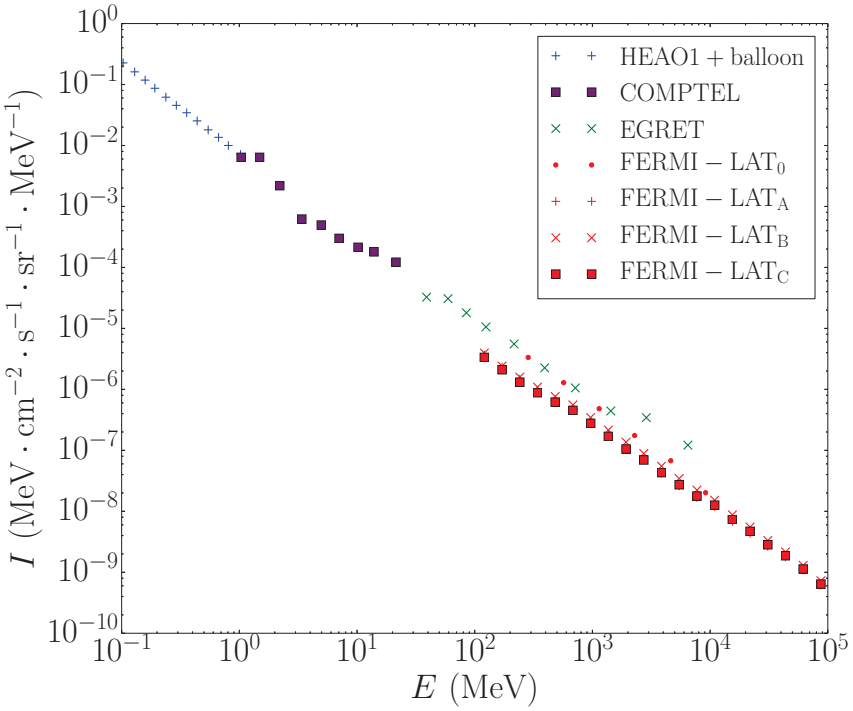

Figure 4.10: The EGXB as measured by HEAO-1+balloon, COMPTEL, EGRET and Fermi-LAT missions [28, 247, 536, 583]. The Fermi-LAT$_0$ marks correspond to the 1st year results and the Fermi-LAT$_{A,B,C}$ marks to 6-year measurements. [taken from [514]]

4.3.2 Isotropic γ-ray background

Many objects in the universe produce gamma rays, such as Active Galactic Nuclei and GRBs [536]. The EGXB is the diffuse radiation that fills the intergalactic medium once all point-sources have been identified and removed from the measured photon flux. This background might come from unresolved sources, or more speculatively from DM decays or annihilations. Fig. 4.10 shows the EGXB measured by four experiments (HEAO-1+balloon, COMPTEL, EGRET and Fermi-LAT) over a wide range of energies between 100 keV and 820 GeV.

If one considers the simplifying hypothesis that DM is distributed isotropically at sufficiently large scales, then its annihilations/decays should produce, at each epoch of the universe since transparency, an isotropic flux of photons. Thus, the flux measured along some LOS should be the redshifted sum over all epoch emissions. In the case of PBH HR and following Carr *et al.* [28, 247, 583] I estimate the photon flux at energy E to be

$$I \equiv E\frac{\mathrm{d}F}{\mathrm{d}E} \approx \frac{1}{4\pi} n_{\mathrm{PBH}}(t_0) E \int_{t_{\min}}^{t_{\max}} (1+z(t)) Q_\gamma \,\mathrm{d}t\,, \tag{4.24}$$

where $n_{\mathrm{PBH}}(t_0)$ is the number density of PBHs of a given mass M today, $z(t)$ is the redshift and the

time integral runs from $t_{\rm min} = 380\,000\,{\rm yr}$ at last scattering of the CMB to $t_{\rm max} = \max(\tau(M), t_0)$ where $\tau(M) \sim M^3$ is the PBH lifetime and t_0 is the age of the universe. As the universe is expanding, the number density of PBHs evolves as $(1+z(t))^{-3}$, and the energy of the emitted photons evolves as $(1+z(t))^{-1}$. A last factor $(1+z(t))$ comes from the change of integrand variable from the LOS to the present time. At $t > t_{\rm min}$, the universe expansion is dominated by the matter component so that

$$z(t) = (H_0 t)^{-2/3} - 1\,, \tag{4.25}$$

with H_0 the Hubble parameter today, given *e.g.* by Planck [253].

The HR emission spectrum Q_γ depends on the PBH mass and spin, and thus also on time as these quantities evolve through Eqs. (2.151). I also note the possibility that PBHs might be clustered at formation, leading to point-like γ-ray sources and anisotropic spatial distribution. An unknown part of the resolved point-like sources of Fermi-LAT could be composed of small PBHs emitting HR [525], but these are removed from the EGXB, thus evading the constraints set here. The anisotropic Galactic γ-rays from PBHs have not been included in this study, and data are compared to the background with method M_1^1 from Fig. 4.3. For other sources of uncertainties, see the detailed discussion in Section 4.2 above.

4.3.3 Monochromatic distribution

Ref. [514] used `BlackHawk v1.2` to compute the HR and the PBH evolution. I consider first monochromatic PBH distributions of masses comprised between $M_{\rm min} = 10^{13}\,{\rm g}$ and $M_{\rm max} = 10^{18}\,{\rm g}$ and initial spin parameters between $a^*_{\rm min} = 0$ and $a^*_{\rm max} = 0.9999$, and compute the integral of Eq. (4.24) over the redshift (matter-dominated era). The result of the integral is compared to the measured EGXB and the maximum allowed value of the present PBH number density $n_{\rm PBH}(t_0)$ at a given PBH mass M is found, with a conservative approach taking into account the most stringent constraints (*e.g.* Fermi-LAT$_{\rm C}$ at $E = 1\,{\rm GeV}$). The corresponding limit on the DM fraction $f_{\rm PBH}$ constituted of PBHs of mass M is obtained through $n_{\rm PBH}(t_0) = f_{\rm PBH}\rho_{\rm DM}/M$, where $\rho_{\rm DM} \approx 0.264 \times \rho_{\rm tot} \approx 2.65 \times 10^{-30}\,{\rm g{\cdot}cm^{-3}}$ is the current average DM density in the universe [253]. If the maximum allowed fraction $f_{\rm PBH}$ is greater than 1, I set it to 1 in order not to exceed the observed DM density, meaning that the EGXB does not constrain $f_{\rm PBH}$ for the given PBH mass.

Fig. 4.11 shows the resulting constraints for the DM fraction $f_{\rm PBH}$ in PBHs of mass M for initial spins $a^* \in \{0, 0.9, 0.9999\}$. First, one checks that the $a^* = 0$ constraints are comparable with those of [247]. The present results do not exhibit the feature just after the peak linked to primary/secondary photons domination explained in [247] because the secondary spectrum is numerically computed for all PBH masses. As a consequence, the peak is smoothed out. The "shifting effect" of the constraint toward higher masses as the initial PBH spin parameter a^* increases is manifest. This is due to the fact that KBHs with high initial spin evaporate faster. Thus, in order to have the same kind of HR time-distribution as a SBH, the PBH must have a higher initial mass. However, this is not accompanied with a more stringent constraint linked to the enhanced emission for KBHs. I understand this as follows: PBHs with a higher mass emit photons at lower energies (cf. the temperature-mass relation (2.142)); and the slope of the EGXB is steeper than that of integrated HR [436]. The two effects approximately cancel. The main result is that if PBHs have

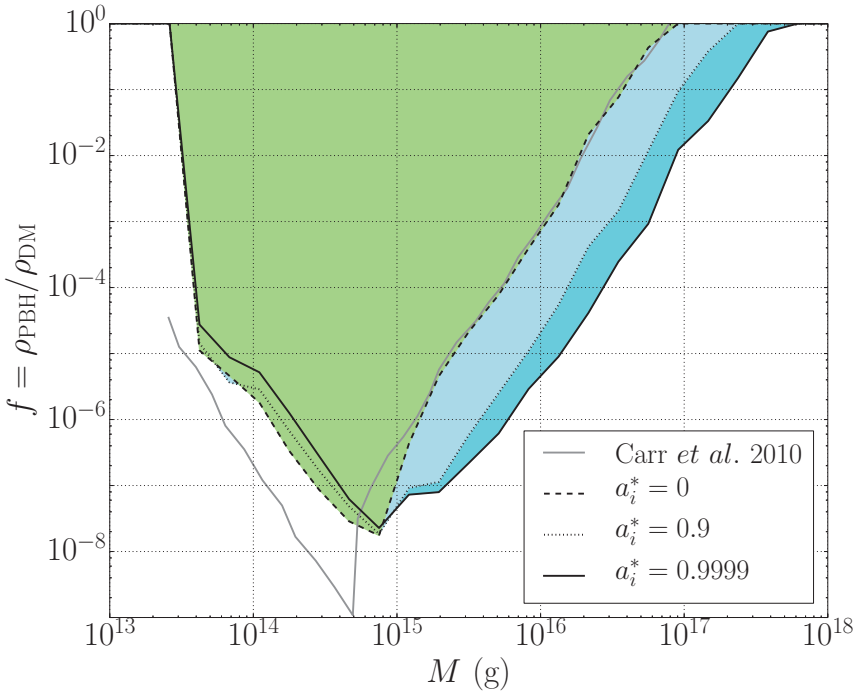

Figure 4.11: The new EGXB constraints on the DM fraction $f_{\rm PBH}$ in form of PBHs, for monochromatic distributions of PBHs of mass M and initial spins $a_i^* \in \{0, 0.9, 0.9999\}$. Color shaded regions are excluded. For comparison, the result of Carr *et al.* [247] ($a_i^* = 0$) has been superimposed as a gray line. [taken from [514]]

a high initial spin parameter $a^* \lesssim 1$, the "small-mass" window $10^{17} - 10^{19}$ g can be reduced by up to almost one order of magnitude on its lower boundary, giving a narrower window of $6 \times 10^{17} - 10^{19}$ g for all DM into PBHs.

4.3.4 Extended distribution

I also obtained constraints for extended mass functions to study the effects related to the width of a peak in the PBH mass distribution. The history of extended PBH distributions is more complex than that of spinning PBHs. Historically, as discussed in Section 1.3.2, PBHs were believed to form naturally with an extended spectrum, while monochromatic distributions were used only because analytically simplifying. Conversion from monochromatic constraints back to some extended distribution was then necessary to apply the constraint to some specific PBH model. However, a simple conversion from monochromatic to extended mass functions is not analytically trivial. I thus derive the constraints by computing the full Hawking spectra associated to the PBH distribution. In other recent studies, the Carr *et al.* [56] method is sometimes used, or people benefit from the capability of `BlackHawk` to generate directly the full HR spectrum of extended distribution.

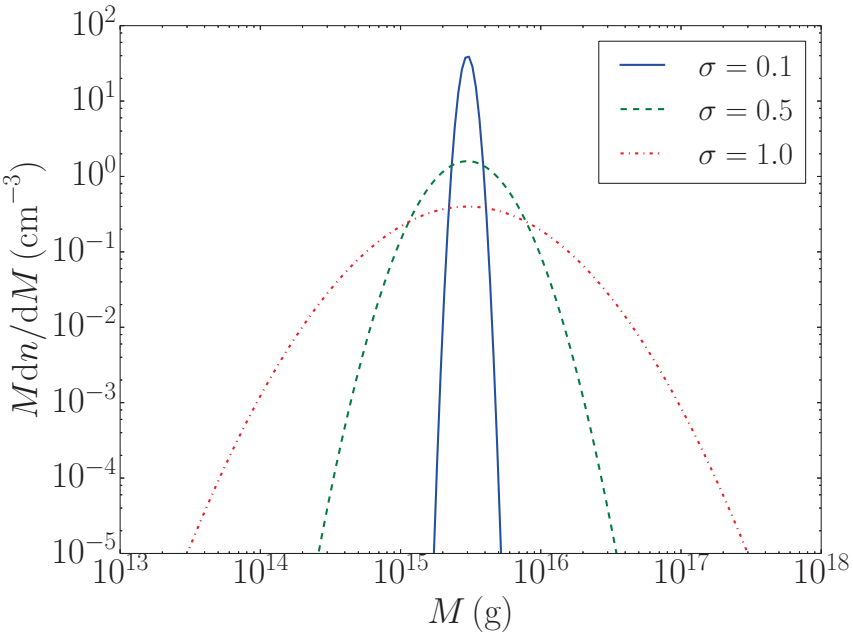

Figure 4.12: Examples of log-normal distributions (4.26) for values of $\sigma \in \{0.1, 0.5, 1\}$. The amplitude is $A = 1$ and the central mass is $M_\mathrm{c} = 3 \times 10^{15}\,\mathrm{g}$ for all distributions for clarity. [taken from [514]]

I considered extended mass functions of log-normal form

$$\frac{\mathrm{d}n}{\mathrm{d}M} = \frac{A}{\sqrt{2\pi}\sigma M} \exp\left(-\frac{(\ln(M/M_\mathrm{c}))^2}{2\sigma^2}\right), \tag{4.26}$$

i.e. a Gaussian distribution in logarithmic scale for the mass density. A is some amplitude, linked to the fraction of DM into PBHs. This distribution is normalized to 1 if $A = 1$. To compute the spectra, the `BlackHawk_tot` program was used with 10 different PBH masses scanning the whole peak width. I remain agnostic about the origin of this extended mass distribution: the log-normal distribution can accommodate a wide range of PBH formation mechanisms [55]. To test these distributions, I have scanned M_c the mean of the Gaussian distribution ranging from $10^{13}\,\mathrm{g}$ to $10^{18}\,\mathrm{g}$, and its width $\sigma \in \{0.1, 0.5, 1\}$. Fig. 4.12 shows examples of these distributions for $M_\mathrm{c} = 3 \times 10^{15}\,\mathrm{g}$.

Eq. (4.24) must be modified to obtain the fraction for an extended mass function, and use formula Eq. (2.148) for the primary flux. The fraction of DM in form of PBHs is obtained by maximizing the flux (increasing the normalization constant A) while respecting all the EGXB constraints

$$f_\mathrm{PBH} \equiv \frac{\rho_\mathrm{PBH}}{\rho_\mathrm{DM}} = \frac{A}{\rho_\mathrm{DM}\sqrt{2\pi}\sigma} \int_{M_\mathrm{min}}^{M_\mathrm{max}} \exp\left(-\frac{\log(M/M_\mathrm{c})^2}{2\sigma^2}\right) \mathrm{d}M\,. \tag{4.27}$$

Even if the EGXB constraints valid at $M \sim M_\mathrm{c}$ prevent A from exceeding its maximum value when $\sigma \to 0$ (monochromatic distribution), one expects that when the distribution width σ in-

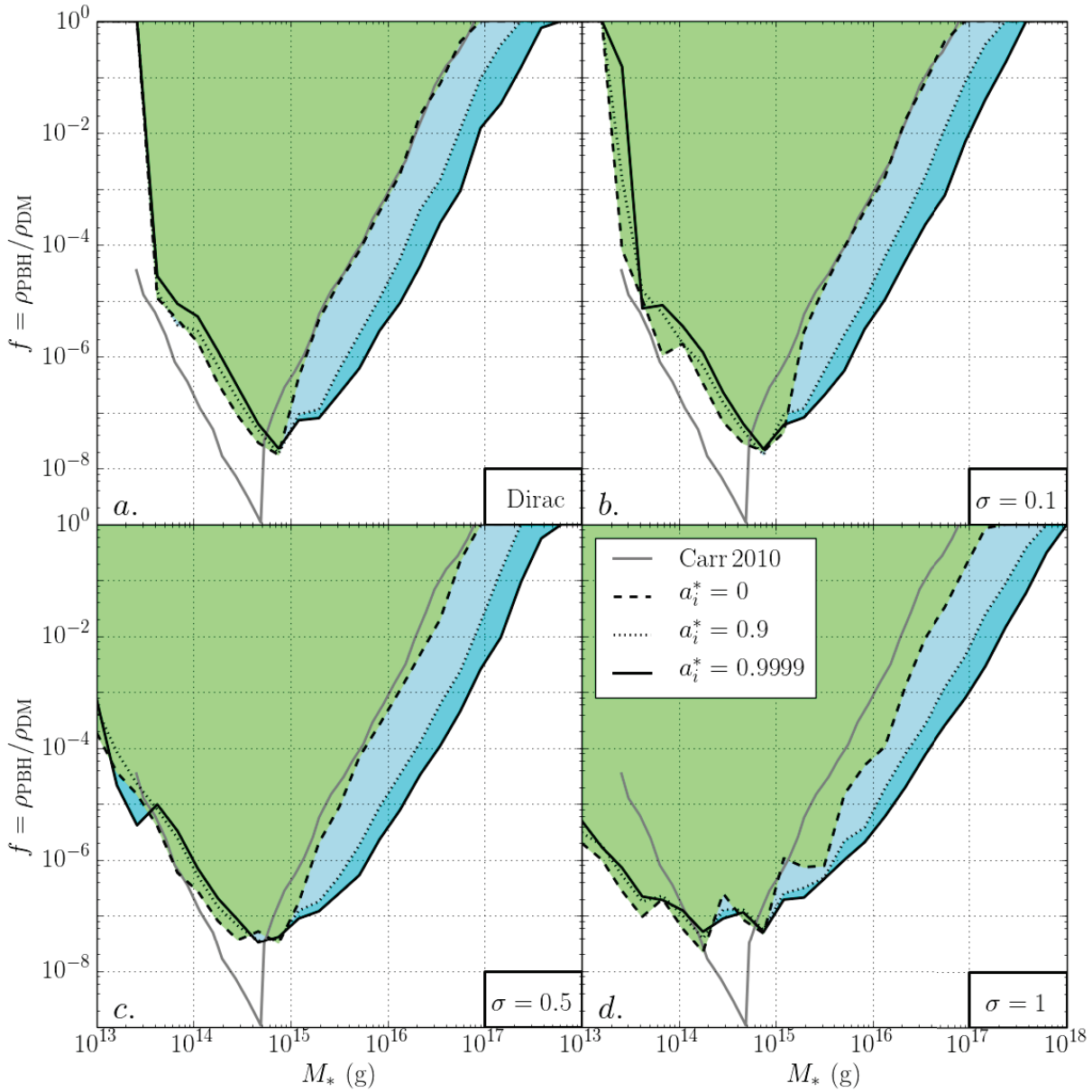

Figure 4.13: ***a.*** The same monochromatic plot as Fig. 4.11 for comparison (here $M_* \to M$ is the monochromatic mass). ***b., c., d.*** The EGXB constraints on the DM fraction $f_{\rm PBH}$ in form of PBHs, for distributions of PBHs of initial spins $a^* \in \{0, 0.9, 0.9999\}$ following Eq. (4.26), with central mass $M_* \to M_{\rm c}$ and widths $\sigma \in \{0.1, 0.5, 1\}$. Color shaded regions are excluded. [taken from [514]]

creases, monochromatic EGXB constraints from $M \lesssim M_{\rm c}$ and $M \gtrsim M_{\rm c}$ will become more and more important, thus limiting A. On the other hand, if σ increases, the full distribution integral that contributes to the DM fraction $f_{\rm PBH}$ increases as well because of the $M \lesssim M_{\rm c}$ and $M \gtrsim M_{\rm c}$ contributions. The competition between the two effects is difficult to forecast.

Fig. 4.13 (panels b, c and d) shows the constraints for distribution widths $\sigma \in \{0.1, 0.5, 1\}$ (respectively) and $a^* \in \{0, 0.9, 0.9999\}$. There are 3 kinds of observations to be considered:

1) For a fixed PBH initial spin a^*, when the width of the distribution σ increases, the excluded region widens. This effect is sensible when $\sigma \gtrsim 0.5$. This can be interpreted as follows. When the PBH distribution is sharp, that is to say when their number density is concentrated in the central part $M \sim M_{\rm c}$ of the distribution, then only the HR emitted by these central mass PBHs comes into play when applying the γ-ray constraints, the rest being negligible. Thus the constraints on $f_{\rm PBH}$ look very much like the monochromatic limit. When the distribution gets wider, the number density of PBHs is spread over $M \gtrsim M_{\rm c}$ and $M \lesssim M_{\rm c}$ and these high- and low-mass PBHs (compared to the central value $M_{\rm c}$) contribute more and more to the γ-ray emission as σ, the width of the distribution, increases. As the constraints are most severe for $M_* \sim 10^{15}\,$g, wide distributions centered on $M_{\rm c} \ll M_*$ and $M_{\rm c} \gg M_*$ for which the $M \sim M_*$ contribution is still important are severely constrained. At high σ, this extends the excluded region to $M_{\rm c} \ll M_*$ and $M_{\rm c} \gg M_*$ and closes the $10^{17} - 10^{18}\,$g window for all DM made of PBHs;[28]

2) For a fixed PBH initial spin a^*, when the width of the distribution σ increases, the constraint on $f_{\rm PBH}$ at the peak M_* becomes less stringent. This is easily explained as follows. For a distribution peaked at M_*, the HR emitted by the PBHs of mass $M \sim M_*$ are the one that constrain the most the authorized total amplitude of the mass distribution. Thus, adding PBHs with $M \lesssim M_*$ and $M \gtrsim M_*$ to the distribution does not result in new constraints, but the total density of PBHs integrated over the full distribution, and so the total fraction $f_{\rm PBH}$ of DM into PBHs increases;

3) For a fixed width of the distribution σ, when the initial spin a^* of the PBHs increases, the constraints are shifted toward higher central masses while being slightly more stringent. This is coherent with the results of Fig. 4.13 (panel a) for the monochromatic distributions presented in the previous section.

The oscillatory feature present on the constraint curves at $M \sim M_*$ is a numerical artifact due to the discrete evaluation of the PBH mass distribution. Taking the convex hull of each shaded region should give a more robust conservative constraint.

One can sum up these observations in the following way. For an extended PBH mass function, the overall constraint comes from the PBHs evaporating today in this distribution with initial mass $M \sim M_*$. Distributions centered away from M_* are more and more constrained as the tail of the distribution is important at M_*: $f_{\rm PBH}$ decreases as σ increases because the maximum value of A decreases. Distributions centered close to M_* are not much more constrained when the distribution

[28] This is precisely the effect predicted by [49].

expands, the maximum value of A remains the same: $f_{\rm PBH}$ increases as σ increases because the distribution integral increases. The very same effects can be observed *e.g.* in the right panel of Fig. 2 of [442] and on subsequent literature on extended mass distributions; see Appendix A.2.

With an extended mass function and no spin, the small mass window for all DM into PBHs reduces to $2 \times 10^{17} - 10^{23}\,$g, and the addition of a nearly extremal spin parameter shrinks it further to $10^{18} - 10^{23}\,$g, that is to say a loss of one order of magnitude compared to the previous zero spin monochromatic distributions.

4.3.5 Conclusion

In this study, I have updated the EGXB constraint on PBH evaporation for monochromatic SBH distributions, using the latest Fermi-LAT data and the public code `BlackHawk`. This has resulted in enhancing the constraint on the masses of presently evaporating PBHs, and reducing the constraint on $M_* \sim 10^{15}\,$g. The main result is the extension of the EGXB constraint from Schwarzschild to Kerr PBHs, and from monochromatic to extended mass functions. I have shown that increasing the initial spin parameter a^* of PBHs to near extremal values can close the mass window $10^{17} - 10^{18}\,$g (where PBHs could still represent all of the DM). I have also demonstrated that extended mass functions can allow a greater fraction of DM in the form of PBHs when they are centered close to the strongest monochromatic constraint M_*, while they are more severely constrained when centered away from this peak. In this case, the allowed mass window can be reduced even with Schwarzschild PBHs. This study would greatly benefit from the new `BlackHawk` tool `Isatis`, which can rapidly compare the constraints from different PBH distributions. Indeed, the above study depicted in Section 4.2 has focused on monochromatic SBHs. The PBH spin and mass distributions could be implemented as type *iv)* assumptions in that study, stretching further the error bars on Fig. 4.9. Numerous studies now use the extended spin and mass distributions of `BlackHawk` to compute refined PBH HR constraints, as listed in Appendix A.2.

4.4 Kerr primordial black holes – dark radiation constraints

[29]I present now precision calculations of DR in the form of gravitons coming from Hawking evaporation of spinning PBHs in the early universe. This is a precision study of HR of PBHs prior to BBN, incorporating a careful treatment of extended spin distributions of a population of PBHs, the PBH reheating temperature, and the number of relativistic d.o.f. I compare these precision results with those existing in the literature, and show constraints on PBHs from current bounds on DR from BBN and the CMB, as well as the projected sensitivity of CMB Stage 4 experiments (CMB-S4). As an application, I consider the case of PBHs formed during an EMDE. I calculate graviton production from various PBH spin distributions pertinent to EMDEs, and find that PBHs in the entire mass range up to $10^9\,$g will be constrained by measurements from CMB-S4 experiments, assuming PBHs come to dominate the universe prior to evanescence. I also find that for PBHs with monochromatic spins $a^* > 0.81$, all PBH masses in the range $10^{-1}\,{\rm g} < M_{\rm BH} < 10^9\,{\rm g}$ will be probed by CMB-S4.

[29]This Section is based on the paper "Precision calculation of dark radiation from spinning primordial black holes and early matter-dominated eras" [584] I wrote with A. Arbey, P. Sandick, B. Shams Es Haghi & K. Sinha.

4.4.1 General paradigm

The spin of the PBH population depends on the equation of state of the universe at their formation, as does the mass distribution (see Section 1.3). During the last two decades, constraints were placed on a wide range of PBH masses, assuming Schwarzschild (non-rotating) PBHs with monochromatic mass spectra [28]. Using a combination of numerical and analytical results for HR, recent studies have started to complete the constraints on PBHs with non-zero spin (see Section 4.3 above). Here I study the production of DR in the form of gravitons coming from Hawking evaporation of populations of spinning PBHs prior to BBN. I compute the primary and secondary spectra of SM particles and gravitons for realistic spin distributions of PBHs from an EMDE [41] as well as a hierarchical merger history [70]. The calculations are performed with `BlackHawk v2.0`; to my knowledge, Ref. [584] is the first precision calculation of HR with with non-trivial PBH spin distributions using this code.

The evolution of a given distribution of PBHs and the associated time-dependent spectrum of emitted gravitons are computed, allowing a straightforward determination of the total energy emitted in the form of DR. This affects the number of relativistic species, with the result characterized as the deviation from the SM expectation of the effective number of neutrino species, $\Delta N_{\rm eff}$. I compute $\Delta N_{\rm eff}$, and compare it to existing results in the literature and interpret it in the context of current limits on $\Delta N_{\rm eff}$ from BBN and CMB measurements. In particular, the BBN constraints on the DR density have been carefully calculated using `AlterBBN` [245, 246].

The main application of these results is the calculation of $\Delta N_{\rm eff}$ from PBHs that were formed during an EMDE and subsequently came to dominate the universe prior to evanescence. EMDEs are highly motivated due to the ubiquity of moduli in string theory and have been extensively studied in recent years in the context of DM [585–590] and baryogenesis [591]. PBHs that evaporated before BBN are harder to constrain because they leave no direct imprint on well-known cosmological eras (for PBH constraints from DM emission see Section 4.5 below; for other types of constraints see Section 4.1 above). Following the spin distributions used in [65] as benchmark examples, I find that PBHs formed during an EMDE with a spin distribution due to the "first-order effect" (see below) are constrained by current CMB bounds on $\Delta N_{\rm eff}$ in the mass range $10^8 - 10^9$ g; they are completely constrained in the mass range $10^{-1} - 10^9$ g by projections of CMB-S4. PBHs that formed with spin distribution due to the "second-order effect" (see below), on the other hand, are not constrained by current BBN or CMB bounds on $\Delta N_{\rm eff}$; they too would, however, be completely constrained in the mass range $10^{-1} - 10^9$ g by CMB-S4.

The fact that PBHs formed during an EMDE that evaporate before BBN will be completely probed by $\Delta N_{\rm eff}$ measurements from CMB-S4 experiments is the main result of this work. Physically, this happens because they are endowed with significant spin, which enhances their production of gravitons during evaporation. It should be noted that the $\Delta N_{\rm eff}$ constraints are only relevant if the PBHs come to dominate the universe. Generally, this is quite restrictive on the sector that causes the EMDE. A complete scenario, in terms of a modulus sector, is described in the Appendix A.1 of Ref. [584]; with the result that for a variety of PBH spin distributions and fractions β of the total energy density of the universe that is constituted by PBHs at formation time during an EMDE, moduli with masses larger than $\sim 10^8$ GeV will be constrained by CMB-S4 experiments (see Fig. 8

of [584]).

I also consider the case of a spin distribution due to inspirals of PBHs under a hierarchical merger history [70], obtaining, for the first time, precision predictions for $\Delta N_{\rm eff}$ in this scenario, which will be probed by CMB-S4. Finally, I apply these results to the case of PBHs with extremal spins regardless of origin, and find that PBHs with initial spin $a^* \gtrsim 0.99$ and mass $M \gtrsim 10^8\,{\rm g}$ are excluded by CMB stringent constraints (TT,TE,EE+low E) while those with even higher spin $a^* \gtrsim 0.999$ are constrained by the CMB conservative constraints (TT+low E), but only for masses $M \gtrsim 2 \times 10^8\,{\rm g}$. I further determine that the limiting value of the PBH initial spin that will be constrained by CMB-S4 for *all* PBH masses up to $M = 10^9\,{\rm g}$ is $a^*_{\rm min,\,all} \simeq 0.81$.

4.4.2 $\Delta N_{\rm eff}$ calculation

The rate of emission of one d.o.f. of a particle i per unit time and energy is given by Eq. (2.148). Due to the continuous emission of all d.o.f. (SM and beyond), KBHs lose mass and angular momentum as described by Eqs. (2.150) and (2.151). Any d.o.f. additional to the SM would be Hawking emitted as this process is purely gravitational. This would increase the Page coefficients and hasten the BH disappearance. In the case studied here, *i.e.* additional emission of spin 2 massless gravitons, the number of added degrees of freedom (2) compared to the SM is very small (see Table 2.1), and thus the effect on the Page coefficients is negligible, so the lifetime of PBHs remains essentially unchanged. Nonetheless this effect is taken into account in `BlackHawk`.

Recent studies have tried to constrain the fraction of ultra-light PBHs with masses $10^{-5}\,{\rm g} \lesssim {\rm M} \lesssim 10^9\,{\rm g}$ by considering that they emit dark sector particles before BBN. This mass range is unconstrained by current cosmological observations, though it may be probed by future GW experiments (*e.g.* [592]). This scenario would therefore be an elegant way of providing the DM content of the universe while evading PBH constraints (see Section 4.5 below). If sufficiently light, this energetic dark sector can provide DR that can measurably affect cosmology, which is reviewed now.

HR of PBHs in the early universe creates SM particles along with other particles that are either decoupled or feebly interacting with the SM. Here I outline the steps for calculating $\Delta N_{\rm eff} = N_{\rm eff} - 3.046$, where $N_{\rm eff}$ is the total number of relativistic d.o.f. and 3.046 is the SM expectation [253], from PBH evaporation.[30] The precision calculations involve two steps: taking into account the distribution of PBH spins and carefully defining the reheating temperature. I also use a precise expression for the number of accessible d.o.f.

Using conservation of entropy during the expansion of the universe, one can track the evolution of the energy density of DR from reheating to matter-radiation equality. For a population of PBHs with lifetime τ, the age of the universe at formation is small relative to τ such that the evaporation time is $t_{\rm eva} \simeq \tau$. Assuming instantaneous thermalization of SM particles at the end of PBH evaporation, the reheating temperature, $T_{\rm RH}$, can be obtained as

$$\rho_{\rm PBH}(\tau) - \rho_{\rm DR}(\tau) = \rho_{\rm SM}(\tau) \equiv \frac{\pi^2}{30} g_*(T_{\rm RH}) T_{\rm RH}^4\,, \tag{4.28}$$

where $\rho_{\rm PBH}(\tau)$ is the energy density of PBHs at the time of evaporation, $\rho_{\rm DR}$ ($\rho_{\rm SM}$) is the amount

[30] I kindly thank B. Shams Es Haghi for going through these calculations.

of energy PBHs emit in the form of DR (SM particles), and $g_*(T)$ denotes the total number of relativistic d.o.f. at temperature T, given by

$$g_*(T) = \sum_{rmB} g_{\rm B} \left(\frac{T_{\rm B}}{T}\right)^4 + \frac{7}{8} \sum_{\rm F} g_{\rm F} \left(\frac{T_{\rm F}}{T}\right)^4 . \tag{4.29}$$

Here the sum includes all bosonic (B) and fermionic (F) d.o.f. with temperatures of $T_{\rm B}$ and $T_{\rm F}$, respectively. The density of PBHs at evaporation is related to the density of PBHs at formation, usually expressed in terms of the fraction of the energy density of the universe that collapsed into PBHs at PBH formation time, which is denoted by β. In this work, it is assumed that β is sufficiently large such that the energy density of PBHs exceeds that of radiation at some time before evanescence (see the explicit scenario in Appendix A.1 of Ref. [584]). With this hypothesis, the density of PBHs at evaporation is fixed by the fact that radiation produced by HR constitutes the main component of SM radiation at reheating [593]. Thus, tracing the redshifted temperature of the CMB today back to reheating (from today back to the matter-radiation equality time with $a(t) \sim t^{2/3}$ and then to the reheating time, $t_{\rm RH} \simeq \tau$, with $a(t) \sim t^{1/2}$), one obtains the value of $T_{\rm RH}$. The values obtained for $\Delta N_{\rm eff}$ in this study should be considered as *upper limits* in the case of full PBH domination prior to evaporation. The constraints are generally weakened but must be recalculated if PBHs do not dominate the energy density of the universe before evanescence.

The energy density of SM radiation (all relativistic particles) is therefore diluted as

$$\frac{\rho_{\rm R}(t_{\rm EQ})}{\rho_{\rm R}(t_{\rm RH})} = \left(\frac{a_{\rm RH}}{a_{\rm EQ}}\right)^4 \left(\frac{g_*(T_{\rm EQ})}{g_*(T_{\rm RH})}\right) \left(\frac{g_{*,S}(T_{\rm RH})}{g_{*,S}(T_{\rm EQ})}\right)^{4/3} , \tag{4.30}$$

where $a_{\rm RH(EQ)}$ is the scale factor at reheating (matter-radiation equality), and $g_{*,S}(T)$ counts the number of relativistic d.o.f. contributing to the entropy, given by

$$g_{*,S}(T) = \sum_{\rm B} g_{\rm B} \left(\frac{T_{\rm B}}{T}\right)^3 + \frac{7}{8} \sum_{\rm F} g_{\rm F} \left(\frac{T_{\rm F}}{T}\right)^3 . \tag{4.31}$$

Similarly, the energy density of DR, $\rho_{\rm DR}$, also dilutes as

$$\frac{\rho_{\rm DR}(t_{\rm EQ})}{\rho_{\rm DR}(t_{\rm RH})} = \left(\frac{a_{\rm RH}}{a_{\rm EQ}}\right)^4 . \tag{4.32}$$

Therefore, the ratio of the energy density of DR to the SM radiation energy density at matter-radiation equality becomes

$$\frac{\rho_{\rm DR}(t_{\rm EQ})}{\rho_{\rm R}(t_{\rm EQ})} = \frac{\rho_{\rm DR}(t_{\rm RH})}{\rho_{\rm R}(t_{\rm RH})} \left(\frac{g_*(T_{\rm RH})}{g_*(T_{\rm EQ})}\right) \left(\frac{g_{*,S}(T_{\rm EQ})}{g_{*,S}(T_{\rm RH})}\right)^{4/3} , \tag{4.33}$$

which determines the effective number of neutrino species as [594]

$$\Delta N_{\rm eff} = \frac{\rho_{\rm DR}(t_{\rm EQ})}{\rho_{\rm R}(t_{\rm EQ})} \left[N_\nu + \frac{8}{7}\left(\frac{11}{4}\right)^{4/3}\right] . \tag{4.34}$$

4.4.3 Extended spin distributions

For the purpose of this study, I focus on single-mass, rotating PBHs with an initial spin number distribution $\tilde{n}$ normalized to unity,

$$\int_0^1 \frac{\mathrm{d}\tilde{n}}{\mathrm{d}a^*}\,\mathrm{d}a^* = 1\,. \tag{4.35}$$

Note that the assumption of a monochromatic mass distribution for PBHs is justified if the PBH production occurs at a precise time, leading to a very narrowly peaked mass distribution. The total energy that has been emitted in the form of DR by the reheating time $t_{\rm RH}$ can be expressed as a ratio over the SM emission, *i.e.* the ratio of the energy densities after evaporation is complete

$$f_{\rm DR} \equiv \frac{\rho_{\rm DR}(t_{\rm RH})}{\rho_{\rm SM}(t_{\rm RH})} = \frac{\rho_{\rm DR}(t_{\rm RH})}{\rho_{\rm PBH}(t_{\rm RH}) - \rho_{\rm DR}(t_{\rm RH})}\,, \tag{4.36}$$

where $\rho_{\rm DR/SM}(t_{\rm RH})$ is the total emission integrated over the history of the universe prior to reheating

$$\rho_{\rm DR/SM}(t_{\rm RH}) = \int_0^1 \mathrm{d}a^* \,\frac{\mathrm{d}\tilde{n}}{\mathrm{d}a^*} \int_0^{t_{\rm RH}} \mathrm{d}t \int_0^{+\infty} \mathrm{d}E\, E\, \frac{\mathrm{d}^2 N_{\rm DR/SM}}{\mathrm{d}t\mathrm{d}E}(M, a^*)\,, \tag{4.37}$$

and

$$\frac{\mathrm{d}^2 N_{\rm SM}}{\mathrm{d}t\mathrm{d}E} \equiv \sum_{i\,\in\,\rm SM} Q_i\,. \tag{4.38}$$

The emission rates for individual species Q_i come from Eq. (2.146). I stress that the ratio (4.36) takes into account the fact that for high DR emission, which for gravitons can occur for highly spinning BHs, the approximation $\rho_{\rm PBH} \simeq \rho_{\rm R}$ used in [71, 595] no longer holds. This could be one of the reasons the present results differ from those of [595] for high PBH spin. Recall that $\rho_{\rm SM} = \rho_{\rm R}$ at time $t_{\rm RH}$ (which occurs before matter-radiation equality), which allows to use the ratio (4.36) in Eq. (4.29) to determine $\Delta N_{\rm eff}$. Furthermore, note that the normalization of the density of PBHs $\rho_{\rm BH}$ is irrelevant to the computation of $\Delta N_{\rm eff}$, since it cancels out of the ratio $f_{\rm DR}$ in Eq. (4.36). It is straightforward to integrate over the spectrum calculated by `BlackHawk` to obtain the total energy emitted in the form of SM particles and additional DR and hence the ratio $f_{\rm DR}$ in Eq. (4.36).

The main effect of a spin distribution, relative to monochromatic spin, is to modify the rate of emission of DR, and thus its ratio to SM radiation, as in Eq. (4.36). Indeed, it is well known that spinning BHs emit more high spin particles ($s = 1$ or $s = 2$) than non-spinning (see Fig. 2.14). As I consider the emission of spin 2 massless gravitons, this effect can be quite sizeable, with the emission being enhanced by a factor of up to $\sim 10^4$ [119]. The effect of this enhancement on the ratio (4.36) is somewhat less dramatic, since the emission of spin 0, 1, and 1/2 SM particles also increases. Still, taking into account extended spin distributions of PBHs with significant high-spin component enhances $f_{\rm DR}$ and hence $\Delta N_{\rm eff}$, leading to more stringent constraints than one would find for simple single-spin distributions. The particular attention given in `BlackHawk` to full distributions of PBHs is a great improvement over previous studies of the abundance of PBHs. To my knowledge, this is the first precision calculation of HR from a population of PBHs with any non-trivial spin distribution.

4.4.4 Reheating temperature and degrees of freedom

When an extended spin distribution of PBHs is employed rather than a monochromatic spin distribution, there is some subtlety in defining the reheating temperature. As spinning BHs emit more radiation than non-spinning ones, with a continuous increase in the emission as a^* increases, they evaporate faster. Although initial nonzero spin has a small effect on BH lifetime (somewhat less than 60% diminution for extremal spin, see Fig. 2.18), it does influence the way one defines the reheating time. For PBHs with equal lifetime τ, assuming an instantaneous reheating in Eq. (4.28) is justified by the fact that PBHs emit most of their HR during a period of time that is negligibly small relative to their lifetime. However, since KBHs with higher spin evaporate faster than KBHs with lower spin, a distribution in initial spins causes a spread of the evanescence times and a non-instantaneous reheating scenario.

For simplicity, I consider two extreme possibilities for the definition of the reheating time:

1. the reheating time corresponds to the time at which the last PBHs (with the lowest spins) evaporate;

2. the reheating time corresponds to the average PBH lifetime, weighted by the spin distribution

$$\langle \tau \rangle \equiv \int_0^1 \tau(M, a^*) \frac{dn}{da^*} \, da^* \, . \tag{4.39}$$

In Ref. [584] it is argued that the second option is more physically realistic, as the averaged lifetime corresponds roughly to the peak of the emission of the HR. Both options are discussed in Section 4.4.5, where I present the results.

Finally, in order to obtain the ratio (4.29), it is necessary to specify the quantities $g_*(T)$ and $g_{*,S}(T)$. Precise determination of these numbers of d.o.f. are model-dependent, especially for the region of temperatures close to the QCD phase transition. Here, that corresponds to $M \sim 7 \times 10^8$ g ($T_{\rm RH} \sim 100$ MeV). Refs. [595, 596] use step functions which give results qualitatively similar to the present ones, while the model used in [71] is not made explicit and shows a significantly different behaviour. In this work, I use the tabulated values of $g_*(T)$ and $g_{*,S}(T)$ available within the public code `SuperIso Relic` [597–599].

4.4.5 Precision results for $\Delta N_{\rm eff}$

Now I present precision results for $\Delta N_{\rm eff}$ with improvements to the calculation as described above. In Section 4.4.5.1, I explore the effect of each of the three precision elements included here; spin distributions, reheating temperature, and d.o.f. In Section 4.4.5.2 I present explicit predictions for $\Delta N_{\rm eff}$ from PBH spin distributions expected from an EMDE.

In all cases, the results for $\Delta N_{\rm eff}$ are compared to current experimental limits and projected sensitivities of future experiments. There are three relevant CMB constraints/sensitivities: two are taken from the Planck Collaboration [253] and are denoted in the plots as CMB^1 (TT+low E, conservative) and CMB^2 (TT,TE,EE+low E, more stringent). The third one is the sensitivity of the future CMB-S4, and represents an order of magnitude improvement over current limits (see details

in [600–602]). Where relevant, the constraint on $\Delta N_{\rm eff}$ from `AlterBBN` is also included, while it is less stringent that the CMB ones (for details about this constraint, see Section V of Ref. [584]).

The results, as in Refs. [71, 595, 596], are presented as constraint on $\Delta N_{\rm eff}$ with respect to the monochromatic mass distribution of PBHs. Since I study scenarios in which PBHs come to dominate the universe prior to evaporation, the history of the universe before PBH domination has no impact on the constraints. Therefore β cannot be determined uniquely based on constraints on $\Delta N_{\rm eff}$; sufficiently large initial energy densities of PBHs which initiate a PBH-dominated era before evaporation lead to the same constraints.

4.4.5.1 Benchmark spin scenarios

I first compute $\Delta N_{\rm eff}$ for some benchmark PBH spin scenarios. The results calculated with an extended spin distribution are compared to those obtained from monochromatic spin distributions (*e.g.* the central/peak value of the extended distribution), as well as $\Delta N_{\rm eff}$ obtained with the two reheating temperature calculations. They are also compared to previous calculations in the literature for $a^* = 0$ and $a^* = 0.99$ to demonstrate the full effects of the precision calculation.

Let's first make a few comments about PBH masses in the low mass regime. In the present calculations, I find that changing the PBH mass in the range $10^{-1}\,{\rm g} < M < 10^{9}\,{\rm g}$ has a very small effect on the ratio $\rho_{\rm DR}/\rho_{\rm R}$ (less than 1% over the whole mass range). This is because, for a given spin distribution, the main variation in $\Delta N_{\rm eff}$ as the PBH mass is varied comes from the different reheating times (and thus reheating temperatures). Below $M \lesssim 10^5\,{\rm g}$, the reheating temperature is far above the mass of all the SM particles ($T_{\rm RH} \gg 10^2\,{\rm GeV}$), so $g_*(T)$ and $g_{*,S}(T)$ have already reached their asymptotic values. Thus, $\Delta N_{\rm eff}$ values for $M \lesssim 10^5\,{\rm g}$ can be safely extrapolated from their value corresponding to the case of $M = 10^5\,{\rm g}$. Note that those results also apply to the $M = 10^{-5} - 10^{-1}\,{\rm g}$ mass range for PBHs. This range is sometimes excluded from analyses due to model-dependent limits on the inflationary Hubble parameter [29]. Below, I present results only for $10^5\,{\rm g} \leq {\rm M} \leq 10^9\,{\rm g}$.

To show how the prediction for $\Delta N_{\rm eff}$ from an extended distribution of PBH spins compares to the monochromatic approximation, two benchmark extended spin distributions are used, along with the corresponding prediction assuming a monochromatic distribution. First, I consider the asymptotic spin distribution expected for multiple generation PBH inspirals [70]. The average spin in this case is $\langle a^* \rangle \simeq 0.7$, so I compare the results for the full spin distribution to those for the monochromatic spin distribution with $a^* = 0.7$. As discussed above, more gravitons are expected to be emitted because there are higher spin PBHs in the extended distribution, relative to the monochromatic case. This is borne out in the results shown in the left panel of Fig. 4.14. One sees that $\Delta N_{\rm eff}$ indeed does acquire greater values (by $\sim 25\%$) for the full distribution than for the monochromatic one. This discrepancy becomes critical for PBH masses above $7 \times 10^7\,{\rm g}$; in the case of the extended distribution, these PBHs will be probed by CMB-S4, while the average spin approximation leads to the conclusion that only PBHs with masses above $2 \times 10^8\,{\rm g}$ would be accessible to CMB-S4.

In the right panel of Fig. 4.14, I show the results for a benchmark extended distribution from

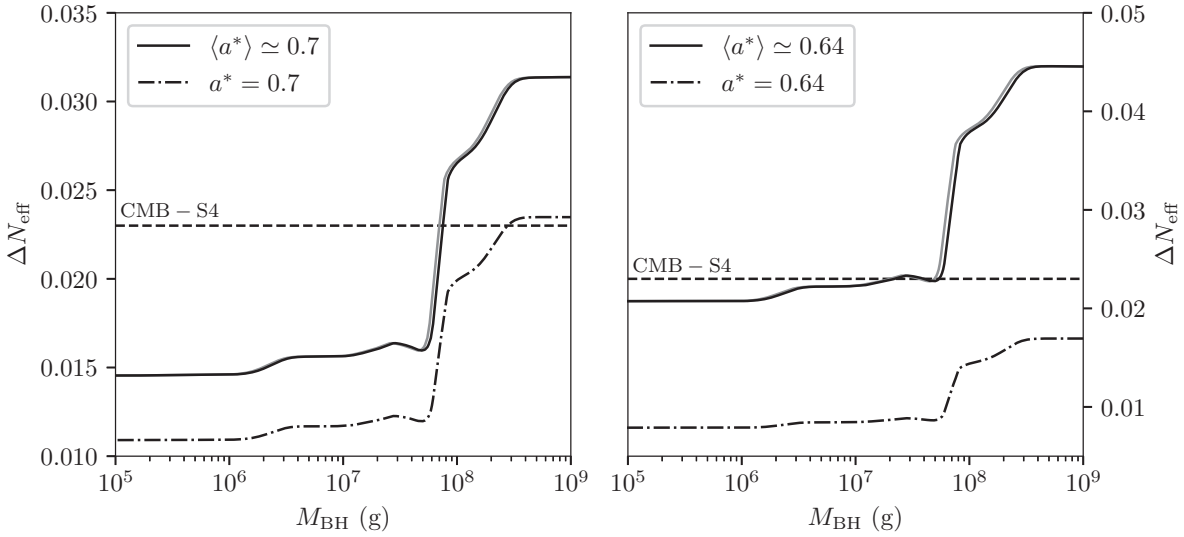

Figure 4.14: Left: Comparison of the results for $a^* = 0.7$ (dot-dashed line) and the full "inspiral" distribution with $\langle a^* \rangle \simeq 0.7$ (solid lines). The relative difference in $\Delta N_{\rm eff}$ between the solid and dashed curves is $\sim 25\%$. **Right:** Comparison of the results for $a^* = 0.64$ (dot-dashed line) and a benchmark extended distribution from an EMDE with $\langle a^* \rangle \simeq 0.64$ (solid lines). The relative difference in $\Delta N_{\rm eff}$ between the solid and dashed curves is $\sim 60\%$. The black (grey) curves correspond to instantaneous reheating at the weighted average value of the black hole lifetimes (last black hole evaporation). The prospective CMB-S4 constraint (horizontal dashed line) is extracted from [71]. [taken from [584]]

an EMDE with $\langle a^* \rangle \simeq 0.64$, along with a monochromatic distribution with $a^* = 0.64$.[31] The spin distribution in the right panel of Fig. 4.14 due to early matter domination is significantly different from that in the left panel due to inspirals. In particular, this EMDE spin distribution is less symmetric and much broader than the inspiral distribution. The relative discrepancy between the extended distribution and the monochromatic distribution is therefore even greater ($\sim 60\%$) in the right panel than in the left panel of Fig. 4.14. For this EMDE extended spin distribution, one finds that PBHs with masses above $\sim 7 \times 10^7\,$g will, in fact, be probed by CMB-S4. This conclusion stands in stark contrast to that inferred under the assumption of a monochromatic spin distribution at the peak or average spin.[32]

The results for the extended spin distributions in both panels of Fig. 4.14 are also shown for the two prescriptions for calculating the reheating temperature, as discussed above: (1) instantaneous reheating at the evaporation time of the last PBH (with the lowest spin) is shown in grey, and (2)

[31] The value $a^* = 0.63$ mentioned in [65] is the peak value of the distribution, not its average.

[32] A compact description of the physics of the two benchmark spin distributions as well as plots of $\mathrm{d}\tilde{n}/\mathrm{d}a^*$ in both cases can be found in Appendix A.2 and A.3 of Ref. [584].

the weighted average PBH evaporation time using Eq. (4.39) is shown in black. In both panels, one can see that prescription (2) results in a shift in the $\Delta N_{\rm eff}$ curve to higher PBH mass relative to the results assuming prescription (1). This can be understood on the basis of the reheating temperature from prescription (1) being smaller than the reheating temperature from prescription (2). Indeed, higher spin PBHs evaporate faster, and are better accounted for in prescription (2). Thus, one could achieve the same reheating temperature (and therefore the same $\Delta N_{\rm eff}$) with prescription (1) by assuming a higher PBH mass.

In Fig. 4.15, I compare the values of $\Delta N_{\rm eff}$ obtained with precision calculations using `BlackHawk` to recent calculations in the literature. In the left panel of Fig. 4.15, I consider $a^* = 0$ (SBH), and compare the $\Delta N_{\rm eff}$ from `BlackHawk` (solid) with those calculated in Refs. [71] (denoted as [H20], dashed) and Ref. [596] (denoted as [M20], dot-dashed) updated in Ref. [595] with the help of `BlackHawk` (denoted as [M21], dotted). The relative discrepancies in these cases are $\sim 10\%$. In the right panel of Fig. 4.15, I consider $a^* = 0.99$, and compare with the results of Ref. [71], where one finds a $\sim 20\%$ discrepancy. As discussed in Section 4.4.4, an important difference between the present results (solid) and other calculations in the literature is that the values for $g_*(T)$ and $g_{*,S}(T)$ are taken from the public code `SuperIso Relic` [597–599]. Near $M \sim 8 \times 10^7\,{\rm g}$ (corresponding to $T_{\rm RH} \sim 100\,{\rm MeV}$), the number of d.o.f. is very sensitive to the QCD equation of state, and the precise behavior of $\Delta N_{\rm eff}$ is evident. That said, using a simple step function for $g_*(T)$ and $g_{*,S}(T)$ gives results qualitatively similar to the ones described here [595, 596]. This precision calculation reveals that highly spinning PBHs with $a^* = 0.99$ and masses $M \gtrsim 2 \times 10^8\,{\rm g}$ that dominated the universe before BBN are, in fact, *already excluded* by CMB[2] constraints on $\Delta N_{\rm eff}$.

4.4.5.2 Early matter dominated era and extremal spins

Now I present the results of precision calculation of $\Delta N_{\rm eff}$ for PBH spin distributions from a period of early matter domination. This is the first time a prediction for $\Delta N_{\rm eff}$ from PBHs produced during an EMDE has been calculated. It is assumed that PBHs produced during the EMDE come to dominate the universe by the time of evanescence. The validity of this assumption depends on the physics behind the EMDE—as an example, see the scenario of an EMDE caused by a gravitationally coupled modulus field described in Appendix A.1 of Ref. [584].

I use the spin distributions from Ref. [65] as benchmarks. Angular momentum within a comoving region of space has two components; the first-order contribution ("the first-order effect") originating from deviation of the boundary of the volume from a sphere, and the second-order contribution ("the second-order effect") sourced by density fluctuations in the comoving region. The "first-order effect" usually dominates (when the initial deviation of the boundary of collapsing region from a sphere is large), but an almost spherical initial collapsing region can diminish the "first-order effect" and make the "second-order effect" the dominant one.

In Fig. 4.16, I present $\Delta N_{\rm eff}$ results for PBHs formed during an EMDE, with spin distributions due to first- and second-order effects in the upper and lower panels, respectively. In each panel, results are shown for three different values of $\sigma_{\rm H}$, the mean variance of the density perturbations at horizon entry

$$\sigma_{\rm H} = \langle \delta_s(t_{\rm H})^2 \rangle^{1/2}\,, \tag{4.40}$$

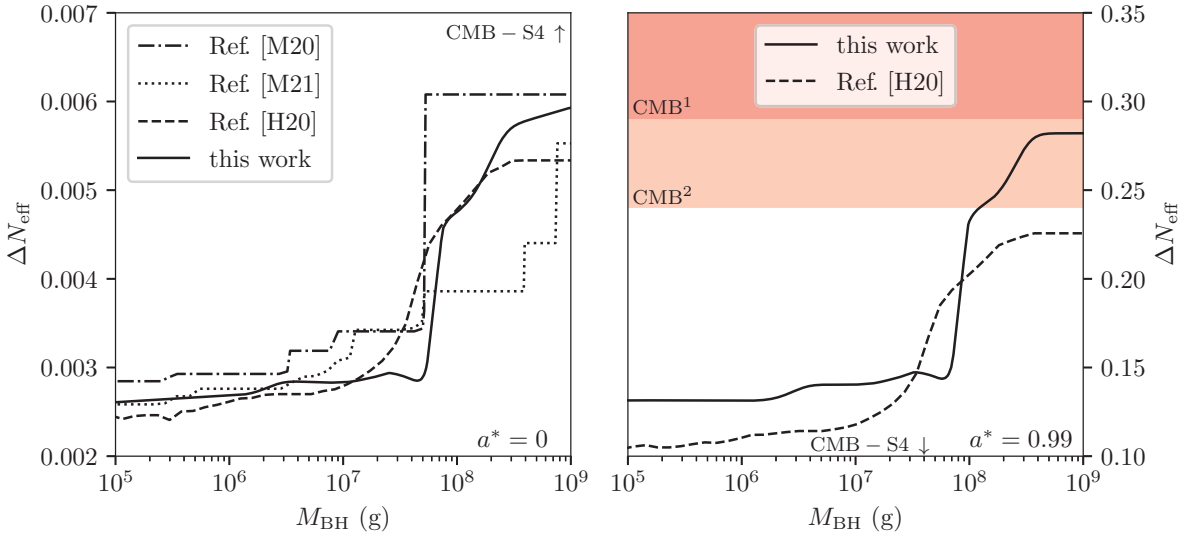

Figure 4.15: Left: Comparison between the precision calculation for $a^* = 0$ (solid) and the results of Ref. [M20] [596] (dot-dashed) updated in Ref. [M21] [595] (dotted) and Ref. [H20] [71] (dashed). **Right:** Comparison between the precision calculation for $a^* = 0.99$ (solid) and the results of Ref. [H20] [71] (dashed). The 95% CL CMB limits on $\Delta N_{\rm eff}$ (shaded areas) are taken from [253] (CMB^1: TT+low E, CMB^2: TT,TE,EE+low E); the CMB-S4 limits are the same as in Fig. 4.14. [taken from [584]]

where $\langle \delta_s^2 \rangle$ is the variance of the density perturbations integrated over the volume of a sphere and $t_{\rm H}$ is the time of horizon entry. $\sigma_{\rm H}$ controls the shape of the spin distribution, as well as the peak location. For both the first- and second-order effects, larger $\sigma_{\rm H}$ leads to broader spin distributions. Increasing $\sigma_{\rm H}$ also shifts the peak of the second-order distribution away from $a^* = 1$ to smaller values of a^*. As mentioned in Section 4.4.5.1, for $\sigma_{\rm H} = 0.1$, the peak average of the spin distribution from the second-order effect is located at $a^* = 0.64$. Note that either the first- or second-order effects could dominate in realistic PBH formation mechanisms.

The upper panels of Fig. 4.16 show $\Delta N_{\rm eff}$ due to spin distributions dominated by the "first-order effect". One sees that for $\sigma_{\rm H}$ small enough, the largest PBH masses are *already excluded* by CMB^2, and in some cases even CMB^1. In the upper right panel, one sees in detail that for $\sigma_{\rm H} \lesssim 0.01$, $M > 10^8\,{\rm g}$ are excluded by CMB^2 constraints. For EMDE spin distributions dominated by the "first order effect", the entire PBH mass range $10^{-1}\,{\rm g} < M < 10^9\,{\rm g}$ will be probed by CMB-S4.

It is clear from the lower panels of Fig. 4.16 that PBH spin distributions from an EMDE are not constrained by current CMB or BBN limits on $\Delta N_{\rm eff}$ if the spin distribution is dominated by the "second-order effect". However, these would be probed by CMB-S4 measurements. One can see in the lower left panel of Fig. 4.16 that for $\sigma_{\rm H}$ small enough ($\lesssim 0.1$), all PBH masses in the range $10^{-1} - 10^9\,{\rm g}$ will be probed by CMB-S4. For the value $\sigma_{\rm H} = 0.1$, only PBHs in the high mass end

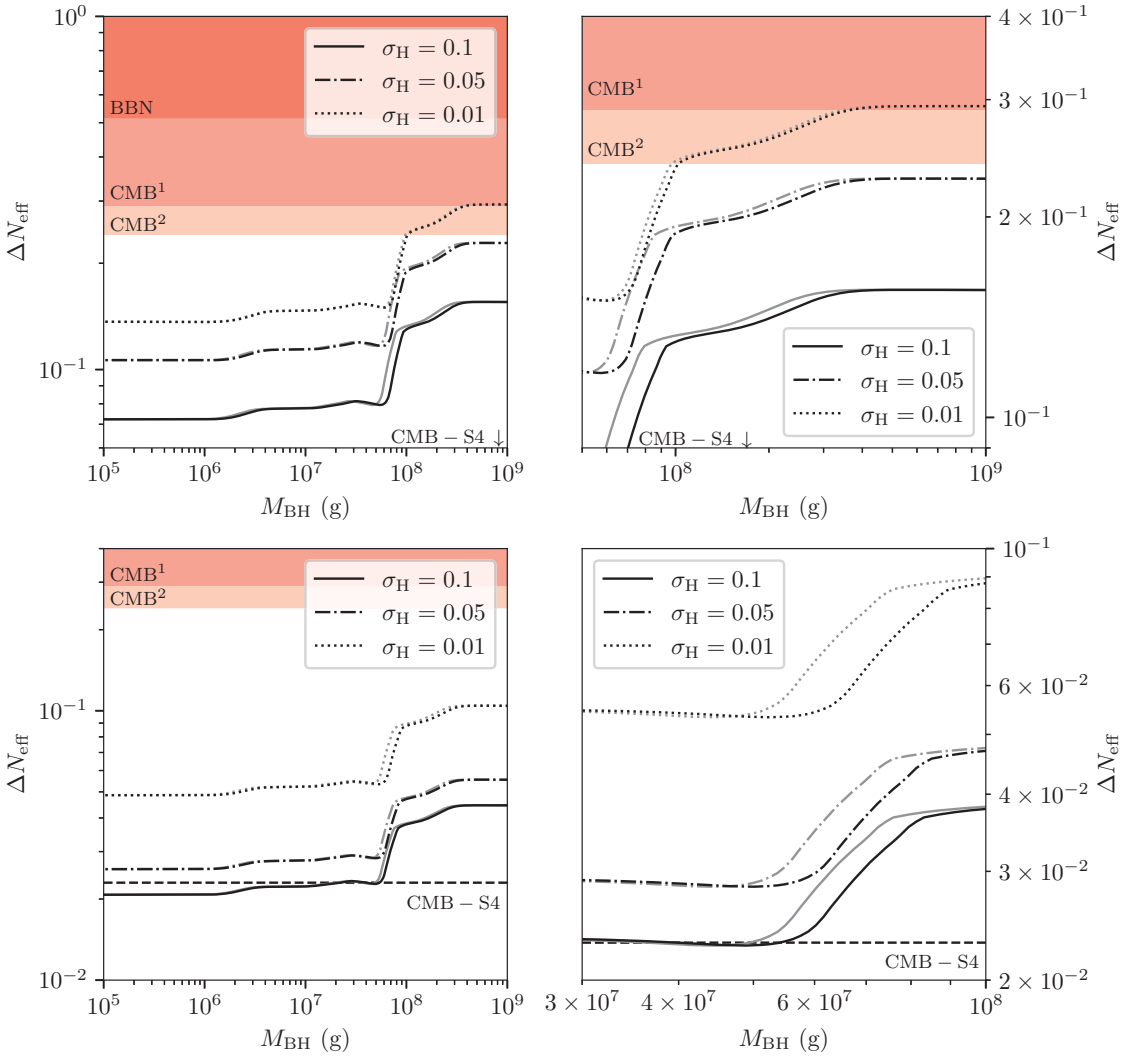

Figure 4.16: Upper left: $\Delta N_{\rm eff}$ results for PBH distributions formed during an EMDE due to the "first order effect" with $\sigma_{\rm H} = \{0.01, 0.05, 1\}$ (dotted, dot-dashed and solid respectively). **Upper right:** A zoom into the region where $\Delta N_{\rm eff}$ is constrained by current CMB limits. **Lower left:** $\Delta N_{\rm eff}$ results for PBH distributions formed during an early matter domination era due to second order effect [65] with $\sigma_{\rm H} = \{0.01, 0.05, 1\}$ (dotted, dot-dashed and solid respectively). **Lower right:** A zoom into the region where $\Delta N_{\rm eff}$ shows brutal change due to the step shape of $g_*(T_{\rm RH})$. The black (grey) curves correspond to instantaneous reheating at the weighted average value of the PBH lifetimes (last PBH evaporation). The CMB limits are the same as in Fig. 4.15; the 95% CL limit from BBN is computed in Section V of Ref. [584]. [taken from [584]]

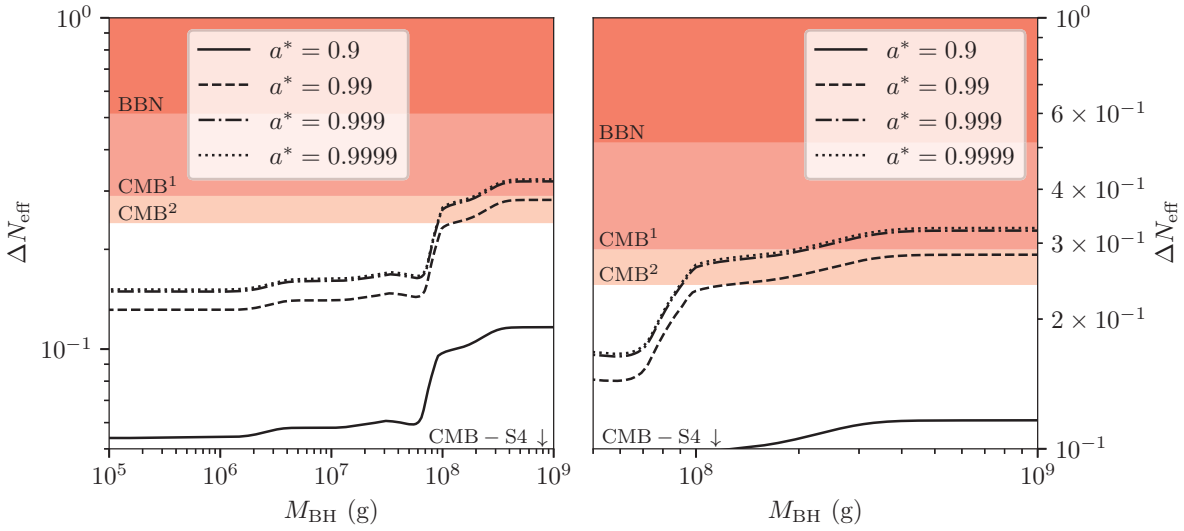

Figure 4.17: Left: Results for high spin PBHs with $a^* = \{0.9, 0.99, 0.999, 0.9999\}$ (solid, dashed, dot-dashed and dotted respectively). The last two curves are difficult to distinguish. **Right:** A zoom-in of the CMB exclusion region for highly spinning massive PBHs. The 95% CL limits are the same as in Fig. 4.16. [taken from [584]]

of this range $3 \times 10^7 - 10^9$ g will be accessible to CMB-S4.

Another noticeable feature in all panels of Fig. 4.16 is the shift of $\Delta N_{\rm eff}$ towards higher PBH masses if one takes reheating time as the average weighted lifetime $\langle \tau \rangle$ (black curves) compared to the time of evaporation of the last PBH (grey curves). This is consistent with what was observed in Fig. 4.14. This shift is most sizeable for extremal spin distribution for which the average spin is $\langle a^* \rangle \sim 1$, *i.e.* small $\sigma_{\rm H}$. This is especially clear in the lower right panel of Fig. 4.16, which zooms in to the region of strong variation of $\Delta N_{\rm eff}$ in the lower left panel. The difference in these results due to the different prescriptions for reheating time particularly affects $\Delta N_{\rm eff}$ in the mass range $M \sim 5 - 9 \times 10^7$ g. This is also the region where $\Delta N_{\rm eff}$ is most affected by the precise shape of $g_*(T)$ and $g_{*,S}(T)$. I next turn to an investigation of $\Delta N_{\rm eff}$ for near-extremal PBH spins. In Fig. 4.17, I present $\Delta N_{\rm eff}$ for monochromatic spin distributions with $a^* \gtrsim 0.9$, under the assumption that the PBHs dominate the energy density of the universe before BBN. As in Fig. 4.15, one sees that these highly spinning PBHs are *already excluded* by current CMB^2 constraints for large enough PBH masses. One also remarks that the excluded mass range grows as the spin increases, due to the shorter lifetime of spinning PBHs. Furthermore, for the largest PBH spins considered, the increase in $\Delta N_{\rm eff}$, which is due to the enhanced emission of high spin particles (spin 2 most of all), saturates. Indeed, the Hawking emissivity of near extremal PBHs seems not to grow to infinity as $a^* \to 1$ but instead saturates somehow.

To be specific, one observes in Fig. 4.15 that the future CMB-S4 measurements will be sensitive to extremal values of PBH spins $a^* \gtrsim 0.9$. From the right panel of Fig. 4.17 it is evident that PBHs

with spin $a^* \gtrsim 0.99$ and mass $M \gtrsim 10^8\,\mathrm{g}$ are excluded by the CMB[2] stringent constraints. PBHs with even higher spin $a^* \gtrsim 0.999$ are constrained by the CMB[1] conservative constraints, but only for masses $M \gtrsim 2\times10^8\,\mathrm{g}$. This is, to my knowledge, the first constraints put on light spinning PBHs from $\Delta N_{\rm eff}$ from *current* CMB limits, under the assumption that PBHs can radiate gravitons.

Finally, I explore the capability of the CMB-S4 experiment to probe PBHs with monochromatic spins, assuming that PBHs dominated the energy density of the universe prior to BBN. In Fig. 4.18, I present the smallest monochromatic spin for which CMB-S4 will be sensitive to the *entire* mass range considered here, $a^*_{\rm min,\,all}$, as well as the largest monochromatic spin for which CMB-S4 will not be sensitive to any part of the mass range, $a^*_{\rm max,\,no}$. I find that the smallest monochromatic spin for which CMB-S4 will be sensitive to the whole range of masses is $a^*_{\rm min,\,all} \simeq 0.81$. For a monochromatic spin distribution with $a^* > a^*_{\rm min,\,all}$, CMB-S4 will probe all PBH masses $10^{-1}\,\mathrm{g} < M < 10^9\,\mathrm{g}$. On the other hand, the smallest monochromatic spin value for which CMB-S4 cannot constrain any of the PBH masses is $a^*_{\rm max,\,no} \simeq 0.69$. For $a^* \lesssim a^*_{\rm max,\,no}$, the entire mass range would be inaccessible to CMB-S4, while for $a^* \gtrsim a^*_{\rm max,\,no}$ only the heaviest PBHs ($M \sim 10^9\,\mathrm{g}$) will be probed.

While the results in Fig. 4.18 apply to monochromatic spin distributions, the same question can in principle be answered for various types of extended spin distributions. As discussed in Section 4.4.5.1 and demonstrated in Fig. 4.14, one can expect a $\sim 25-60\%$ relative discrepancy between the $\Delta N_{\rm eff}$ prediction for monochromatic spin distributions relative to the extended distributions considered here. Indeed, for a scenario such as early matter domination, which induces a particular spin distribution for PBHs, one could even explore the range of cosmological parameters that yield $\Delta N_{\rm eff}$ to which next generation experiments will be sensitive.

4.4.6 Conclusion

The purpose of this study has been to conduct precision studies of DR emanating from spinning PBHs, focused on the case of gravitons. The precision calculations incorporated spin distributions of PBHs and a careful treatment of the reheating temperature and relativistic d.o.f. I studied the impacts of each of these three precision elements on the calculation of $\Delta N_{\rm eff}$ due to graviton emission from PBHs, and applied the calculation to a scenario with extended PBH spin distributions due to an EMDE.

There are two main effects related to incorporating extended PBH spin distributions relative to monochromatic spin distributions. First, since a BH lifetime is related to its spin, a spin distribution will result in a distribution of evaporation times. The second, dominant, effect is that PBHs with high spins emit more particles with higher spins, *i.e.* gravitons. Thus a spin distribution that extends to higher spins will result in more graviton emission relative to a corresponding monochromatic spin approximation, and thus a larger prediction for $\Delta N_{\rm eff}$.

In undertaking this precision study, I find that it is also important to consider a precise formulation for the number of relativistic d.o.f. as a function of temperature. It is shown that different characterizations for the d.o.f. lead to different conclusions regarding experimental sensitivity to various models. In fact, for PBHs with masses $M \gtrsim$ few $\times\, 10^7\,\mathrm{g}$ that dominated the universe before BBN, one finds very different predictions for $\Delta N_{\rm eff}$. Different prescriptions for the reheating temperature due to PBH evaporation also lead to variations of $\Delta N_{\rm eff}$. These are relatively small

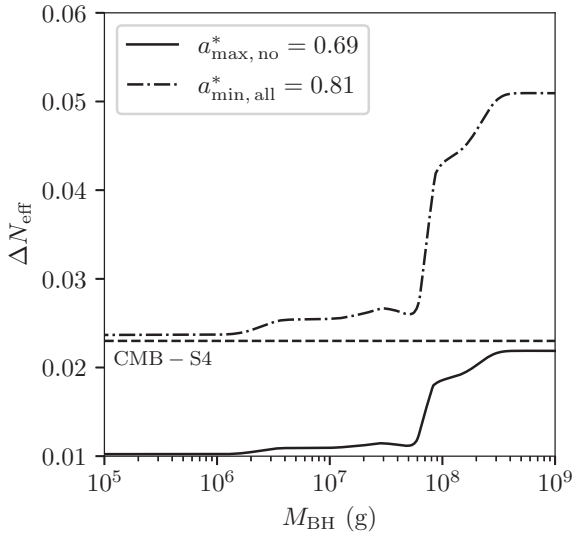

Figure 4.18: Low and high cut-off values for CMB-S4 exclusion (same limit as in Fig. 4.17), corresponding to $a^*_{\rm max,\,no} = 0.69$ and $a^*_{\rm min,\,all} = 0.81$ (solid and dot-dashed respectively). [taken from [584]]

in comparison to the other effects considered, but careful attention to the reheating temperature is relevant to make a precise statement regarding experimental sensitivity for some PBH masses.

The main application was to study gravitons coming from HR of PBHs created during an EMDE. If such PBHs come to dominate the universe prior to final evaporation, the resulting DR can be probed by current BBN and CMB constraints, as well as future CMB-S4 experiments. It is found that PBHs with a spin distribution due to the "first-order effect" are constrained by current CMB bounds on $\Delta N_{\rm eff}$ in the mass range $10^8 - 10^9\,$g, and would be completely constrained in the mass range $10^{-1} - 10^9\,$g by CMB-S4. PBHs formed during an EMDE with a spin distribution due to the "second-order effect", while not constrained by current BBN or CMB bounds on $\Delta N_{\rm eff}$, would be completely constrained in the mass range $10^{-1} - 10^9\,$g by CMB-S4 experiments for all scenarios except for the largest $\sigma_{\rm H}$ considered here.

I also explored $\Delta N_{\rm eff}$ for near-extremal PBH spins. One finds that if PBHs with monochromatic spin distributions with $a^* \gtrsim 0.99$ dominate the energy density of the universe before BBN, current CMB constraints exclude PBHs with masses $M \gtrsim 10^8\,$g. As the spin increases toward 1, $\Delta N_{\rm eff}$ increases until it saturates, since the Hawking emissivity of near extremal PBHs seems not to grow indefinitely as spin approaches 1 but instead saturates. I therefore find that for increasing a^* the minimal PBH mass excluded by current CMB measurements is shifted to lower PBH masses until saturation. I also find that for PBHs with monochromatic spins $a^* > 0.81$, all PBH masses in the range $10^{-1}\,{\rm g} < M < 10^9\,{\rm g}$ will be probed by CMB-S4 experiments.

4.5 Non-standard particles

[33]In this Section, I present results obtained with `BlackHawk` in the context of BSM theories. Since update `v2.0` [152], `BlackHawk` can compute the spectrum of BSM particles emitted via HR of PBHs. This is of utmost importance as many high-energy SM extensions predict new d.o.f. The emission of unknown d.o.f. by BHs is a phenomenon applied to PBH studies since the first constraints. To my knowledge, the first ideas were that PBHs were sources of ultra-heavy GUT bosons at the $10^{14}-10^{16}$ GeV scale in the early universe, themselves causing the baryon asymmetry of the universe (*i.e.* the "Weinberg model" in Section 4.1.2.1). Later on, as particle theories of DM were constructed, it became evident that the emission of a great number of new d.o.f. would alter the evaporation rate of PBHs drastically, as discussed in [133]. The most radical examples are:

- supersymmetric theories, in which every SM particle has a BSM superpartner, causing the total number of d.o.f. to double (or more) [359, 603];
- "mirror matter" models, where the mirror partners retablish the parity symmetry [604];
- string axiverse theories, in which a great number of axion scalar d.o.f. naturally appear [228, 605–607].

In the simplest particle DM model, there exists a single stable particle, hereafter denoted as PDM (for "particle DM"). This can be the "lightest supersymmetric particle" (LSP, for supersymmetric theories), the "least interacting particle" (LIP, for mirror matter models) or any other WIMP or heavy neutrino candidate [608–610]. A famous candidate for DM is the gravitino, heavy spin $3/2$ superpartner of the graviton. The GFs for the gravitino have been added to `BlackHawk v2.0` [152], which should allow to refine early studies like [611]. The link between PBHs and PDM HR remained a quite marginal subject until the 2010's, while the subject is exploding now [612] (it denoted as the "melanopogenesis" scenario in [613]).[34] The consequences of DM emission by HR from PBHs are detailed below, with a particular focus on the warm DM (WDM) constraints.

4.5.1 General paradigm

In Ref. [25], light DM candidates are considered, originated from the pre-BBN evaporation of SBHs with masses in the range $10^{-5}-10^{9}$ g. PDM candidates must be BSM particles, neutral and stable. Having so far escaped detection, they must have tiny interactions with SM particles. It would be even possible that they interact only gravitationally.[35] These DM candidates belong to the category of WDM, because their important kinetic energy at the time of matter-radiation equality

[33]This Section is based on the paper "Bounds on warm dark matter from Schwarzschild primordial black holes" [25] I wrote with I. Masina and G. Orlando.

[34]The constraints on PBH+PDM scenarios that do not rely on HR are reviewed in Section 4.1.3.

[35]Ref. [614] postulated laconically that:

> *[...] even if experiments rule out the existence of the LIPs, the fact that Nature has chosen not to realize particles that interact only gravitationally must be indicating some very deep fact.* [614]

could spoil structure formation. I demonstrate below that the impact is softer for increasing values of the candidate spin s. Requiring such candidates to fully account for the observed DM, it is found that a scenario of BH domination (BHD) before evaporation is ruled out for all spin values up to $s = 2$. For a scenario of RD, upper limits are derived on the parameter β (the PBH energy density at formation over the radiation one), which are less stringent the higher the candidate spin is.

A possible production mechanism for DM particles, taking place in the early universe, is via evaporation of PBHs. It has been proposed that the particles produced via HR might be responsible for the observed DM abundance [595, 596, 613, 615–619] and, if sufficiently light, also for DR [71, 228, 408, 584, 594, 595, 616]. It was even argued by [615, 620] that a common origin of DM and baryon asymmetry from PBH evaporation could be a natural explanation of their similar cosmological densities. Apart from the case of gravitino production [611] (see the review [621]), the PBH density at formation for the range $10^{-5} - 10^{9}$ g is at present unconstrained (see however Section 4.4).

Depending on the fraction of PBHs at formation with respect to radiation β, there is a possibility that the universe was BH dominated before the evanescence of the BHs [323, 615, 622]: this situation is referred to as BHD. The case in which the PBHs evaporate before they dominate the energy content of the universe has already been denoted as RD. I now review the results of some of the recent studies on the subject.

Fujita *et al.* [615] calculated the contribution to DM by PBH evaporation into new particles beyond the SM: they found that a significant contribution to DM could come from stable particles that are either superheavy or light—that is with masses in the MeV range. In the light case, DM candidates would be warm, while in the superheavy case they would be cold. Exploiting the WDM velocity constraints available at that time [623], Ref. [615] first discussed also the lower limits on the mass of the light DM candidates, using an order-of-magnitude argument essentially based on the GO high-energy approximation for HR (see Section 2.3.3.2). This approximation accounts quite well for the case in which the WDM candidate has $s = 0$, but misses to reproduce the case of different spins. For an up-to-date presentation of this argument see [596, 618].

A more sophisticated analysis was done by Lennon *et al.* [616]. They also adopted the GO approximation, but included the redshift effect in the calculation of the momentum distribution of the emitted particles. Their result is an estimate of the number of particles that are still relativistic, with a spin dependence reintroduced *a posteriori* and based on GFs derived from the older literature [107, 121]. As a rough-and-ready criterion for successful structure formation, they impose that when the temperature of the universe drops below 1 keV (at which stage the horizon mass is about $10^{9} M_{\odot}$), less than 10% of the DM is relativistic. The result of this ingenious, but quite arbitrary, argument is that, for BHD, WDM candidates with $s \leq 1$ are excluded, those with $s = 3/2$ are marginally allowed, while those with $s = 2$ naively survive. Summarizing, for the lower spin values (say $s = 0, 1/2, 1$), the order of magnitude results of Ref. [615] were confirmed by Ref. [616], but the latter analysis was however not fully conclusive for the higher spins ($s = 3/2, 2$).

The more recent analysis of Baldes *et al.* [618] goes some step further. As suggested in [616], they include the redshift effect in the momentum distribution of the emitted particles at evaporation, and derive the related phase-space distribution (PSD) as an input for the Boltzmann code `CLASS` [379–382]. The latter allows to extract the matter power spectrum for WDM from PBHs, and to compare it to the standard CDM case thanks to the transfer function. This enables to constrain WDM from

PBHs using the structure formation bounds from Lyman-α data already derived for the case of DM thermal relics. The analysis of Ref. [618] however relies on the GO approximation and, in particular, provides quantitative results only for the $s = 1/2$ case, which agree with previous order-of-magnitude estimates [596, 615], also based on the GO approximation. The case for the higher spins could thus not be quantitatively clarified (apart from a qualitative mention of the GF effects in Appendix A of Ref. [618]) with respect to the results of Ref. [616].

Given the present lack of robust results about the fate of WDM candidates with high spin values, the dedicated study Ref. [25] was published. The aim of this work was precisely to provide a complete and updated study on the viability of WDM candidates from the evaporation of PBHs. Below, I compare the numerical results from `BlackHawk` with the analytical ones derived in the GO approximation. Taking into account the redshift effects as suggested in Ref. [616], the impact on structure formation is studied by calculating the transfer function with `CLASS`, as suggested in Ref. [618].[36] I display the transfer function for all spins values, finding that, assuming BHD, the scenario of WDM from PBHs is excluded for all spins and for all BH masses in the range $10^{-5} - 10^{9}\,\mathrm{g}$. The results for the $s = 0$ case agree with previous order-of-magnitude estimates [596, 615]. For the RD scenario, the upper limits on β (or, equivalently, on the WDM mass) are derived for the various WDM spins. For the case $s = 1/2$ (the only for which the comparison is possible), conceptual differences with respect to the results of Ref. [618] are found, but substantial numerical agreement. Discussion of other DM production mechanisms is postponed to the concluding Section 4.5.8.

4.5.2 Cosmological context

Friedmann equation. During RD, $\rho \propto a^{-4}$, $a(t) \propto t^{1/2}$, and the Hubble parameter of the Friedmann equations (1.8) is $H(t) = 1/2t$. If PBHs come to dominate the energy density, $\rho \propto a^{-3}$, $a(t) \propto t^{2/3}$, and $H(t) = 2/3t$. The radiation energy density (at high temperatures) can be approximated by including only those particles which are in thermal equilibrium and have masses below the temperature of the radiation bath, as given in Eq. (4.28) with $T_{\rm RH}$ replaced by the general radiation temperature $T_{\rm R}$ (temperatures given without subscript are hereafter PBH quantities).

PBHs. The mass of PBHs should be larger than the Planck mass, namely $M \gtrsim 10^{-5}\,\mathrm{g}$. There is also an upper bound on the abundance of PBHs of mass $M \gtrsim 10^{9}\,\mathrm{g}$, because of their effects on BBN yields (see Section 4.1.2.3). The range of PBH masses between these bounds is at present generically unconstrained [28]. The radiation temperature at PBH formation $T_{\rm R}(t_{\rm f})$ during RD is obtained from Eqs. (1.8), (4.28) and (1.17)

$$T_{\rm R}(t_{\rm f}) = \left(\frac{45\gamma^2}{16\pi^3 g_*(t_{\rm f})}\right)^{1/4} M^{-1/2}\,. \tag{4.41}$$

$T_{\rm R}(t_{\rm f}(M))$ and $t_{\rm f}(M)$ are plotted *e.g.* in Fig. 1 of Ref. [596].

A SBH of mass M emits particles of type i and spin s_i at a rate, per dof, given by Eq. (2.146), in which the total energy is given by $E^2 = p^2 + m^2$ where p is the momentum and m is the particle

[36] I gracefully thank G. Orlando for deriving all the results with `CLASS`.

rest mass. As $E \to +\infty$, each species i approaches the GO limit which cross-section is given by Eq. (2.123), but falls off more quickly as $E \to 0$, with the higher spins producing the stronger cutoffs (see Fig. 2.9). When a massless particle scatters off a non-rotating, uncharged hole, the low-energy analytic form of Γ_{s_i} is given in Eqs. (2.11). The non-0 rest mass $m_{\rm DM}$ of the DM particles acts as a cutoff in their emission at low energy, but the precise shape of the GFs around this cutoff is not relevant here since I consider light candidates with $T(t) \gg m_{\rm DM}$ at all times.

The rate of mass loss for an evaporating BH is proportional to the total power emitted and is given by the Page coefficients (2.150). The BH lifetime τ is given by Eq. (2.152); defining $t_{\rm ev}$ as the time of the BH evanescence, one practically has $t_{\rm ev} \equiv t_{\rm f} + \tau \approx \tau$. Considering the SM only, the function $f(M)$ is constant over the range of PBH masses of interest here, because all SM d.o.f. are already radiated by a 10^9 g PBH. Its value (not including gravitons) is calculated inside `BlackHawk` to be $f(M) = 3.53 \times 10^{-22}\,\mathrm{g^3{\cdot}s^{-1}}$. This is the value that is going to be used in the following. Assuming $f(M)$ constant over the PBH lifetime, the latter is easily found in Eq. (2.153), giving the simple time dependence of the BH mass of Eq. (2.154).

DM emission. In this study I consider the possibility that, on top of the SM, a DM candidate of mass $m_{\rm DM}$ is produced in the evaporation process. There are two possible cases, denoted as "light" and "heavy" DM, according to the fact that the particles are produced during all the PBH lifetime ($m_{\rm DM} < T$) or just in its final stages ($m_{\rm DM} > T$). Eq. (2.146) gives the instantaneous spectrum of the particles of type i emitted by a single PBH. The maximum of the energy distribution is at $E \sim T$. For sufficiently light DM, the ultra relativistic limit, $E \approx p \gg m_{\rm DM}$, is thus justified. As the BH evaporates, its temperature increases, and the relativistic limit is always satisfied. All the further equations will be given as functions of the momentum p instead of the usual total energy E, with simple conversion $E \to p$ from the formulas of the rest of that manuscript.[37] It should also be noted that in general in Eq. (2.146), $E \to p = p(t)$. Below, I drop the t dependency for the quantities taken at PBH formation but keep it otherwise. To obtain the number densities (per dof) of the emitted particles of spin s, one has to multiply Eq. (2.146) by the number density of PBHs $n_{\rm PBH}(t)$

$$\frac{\mathrm{d}^2 n_i}{\mathrm{d}t\mathrm{d}p} = n_{\rm PBH}(t) Q_s(p(t))\,. \tag{4.42}$$

In the left panel of Fig. 4.19, I show the instantaneous momentum distributions Q_s, as a function of $x(t_{\rm f}) \equiv p/T$, for bosons (B) and fermions (F) respectively, in the GO approximation. The full numerical results obtained from `BlackHawk` are shown in the right panel (see also Fig. 2.9).

One can see that the $s = 0$ case is quite similar with respect to the GO limit for the boson, while the $s = 1/2$ case is a bit suppressed with respect to the GO limit for the fermion. The higher the spin is, the more the distribution is suppressed at low energies, so that the mean momentum gets higher. A more precise comparison with the geometrical optics approximation can be established by studying the cross-sections normalized to the GO limit, as shown in Fig. 2.9 (left panel). The ratio for $s = 0$ and $s = 1/2$ at low energy is a constant, respectively equal to $16/27$ and $2/27$; while the higher spins ratios go to 0.

[37] I kindly thank I. Masina for all the analytical calculations performed below.

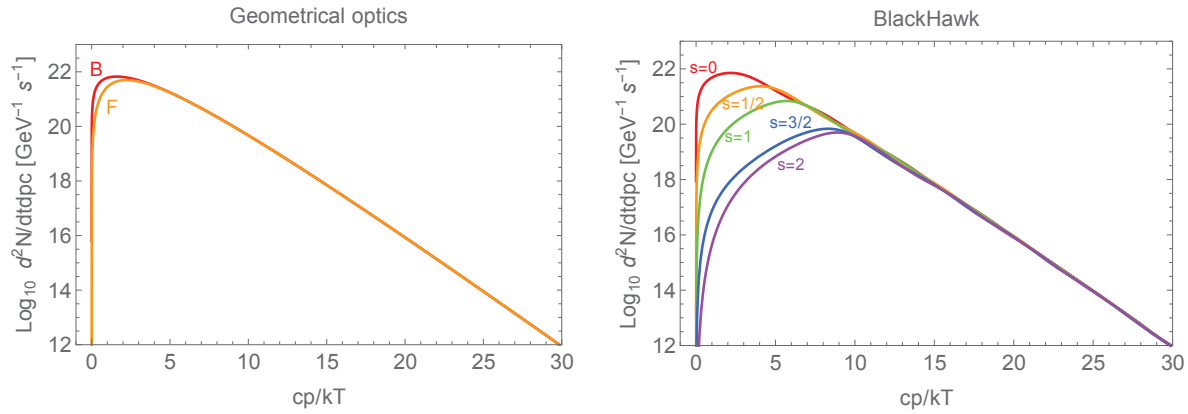

Figure 4.19: Left: Instantaneous distribution as a function of $x(t_{\rm f})$ in the GO approximation. **Right:** The same using the numerical results from `BlackHawk`. [taken from [25]]

4.5.3 From formation to evaporation

The ratio $\rho_{\rm PBH}(t)/\rho_{\rm R}(t)$ scales as $a(t)$. As time increases, it is then possible that PBHs come to dominate the energy content of the universe before they completely evaporate [323, 615, 622].

Radiation domination. One defines $\overline{\beta}$ the maximum value of β corresponding to RD, namely the value leading to $\rho_{\rm PBH}(t_{\rm ev})/\rho_{\rm R}(t_{\rm ev}) = 1$; this value can be obtained from the following relation

$$\overline{\beta} \simeq \frac{\beta}{\rho_{\rm PBH}(t_{\rm ev})/\rho_{\rm R}(t_{\rm ev})} = \frac{a(t_{\rm f})}{a(t_{\rm ev})} = \left(\frac{t_{\rm f}}{t_{\rm ev}}\right)^{1/2} = \left(\frac{3f(M)}{\gamma}\right)^{1/2} \frac{1}{M}\,, \tag{4.43}$$

I will focus on that particular scenario below. The value of $\overline{\beta}$ as a function of the PBH mass is drawn in Fig. 4.20, taking for definiteness $f(M)$ as in the SM and $\gamma = 0.2$. For all the values of $\beta \lesssim \overline{\beta}$ (red solid line), PBHs never dominate the energy content of the universe.

PBH domination. First, there is RD from the formation time, $t_{\rm f}$, to the time when PBHs start to dominate, $t_{\rm BH}$, such that $\rho_{\rm PBH}(t_{\rm BH})/\rho_{\rm R}(t_{\rm BH}) = 1$; and second, there is BHD from $t_{\rm BH}$ to $t_{\rm ev}$.[38] The first period is characterized by the following increase in the scale factor

$$\beta \simeq \frac{\beta}{\rho_{\rm PBH}(t_{\rm BH})/\rho_{\rm R}(t_{\rm BH})} = \frac{a(t_{\rm f})}{a(t_{\rm BH})} = \left(\frac{t_{\rm f}}{t_{\rm BH}}\right)^{1/2}. \tag{4.44}$$

The second period is characterized by

$$\frac{a(t_{\rm BH})}{a(t_{\rm ev})} = \left(\frac{t_{\rm BH}}{t_{\rm ev}}\right)^{2/3} = \left(\frac{1}{\beta^2}\frac{t_{\rm f}}{t_{\rm ev}}\right)^{2/3} = \frac{1}{\beta^{4/3}}\left(\frac{3f(M)}{\gamma}\right)^{2/3} M^{-4/3} = \left(\frac{\overline{\beta}}{\beta}\right)^{4/3}. \tag{4.45}$$

[38] Note that the calculation in this case is quite similar to the one that was used to obtain $\Delta N_{\rm eff}$ in the DR study of Section 4.4.

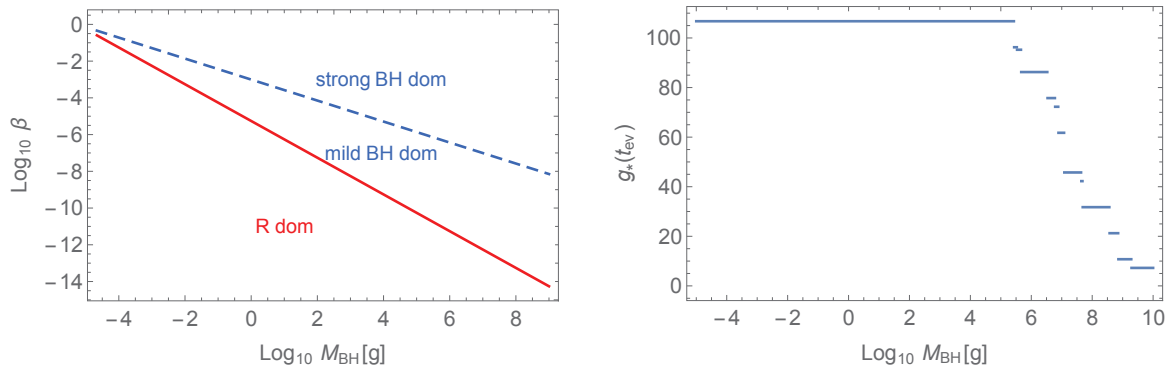

Figure 4.20: Left: The solid (red) line is $\overline{\beta}$, and the dashed (blue) line separates *mild* and *strong* BHD. **Right:** A step function approximation of $g_*(t_{\rm ev})$ for RD. [taken from [25]]

Putting together

$$\frac{a(t_{\rm f})}{a(t_{\rm ev})} = \frac{a(t_{\rm f})}{a(t_{\rm BH})}\frac{a(t_{\rm BH})}{a(t_{\rm ev})} = \frac{1}{\beta^{1/3}}\left(\frac{3f(M)}{\gamma}\right)^{2/3} M^{-4/3} = \frac{\overline{\beta}^{4/3}}{\beta^{1/3}}. \tag{4.46}$$

One can define as *mild* and *strong* BHD the regions where the increase in the scale factor in the first period is respectively larger and smaller than the second one, with equality given by the line $\beta = \overline{\beta}^{4/7}$, as shown in the left panel of Fig. 4.20. Notice that in the very strong BHD region (close to $\beta \sim 1$) one can neglect the first period and obtains $a(t_{\rm f})/a(t_{\rm ev}) \sim \overline{\beta}^{4/3}$, which I will denote as "full BHD"; I will focus on that simple case hereafter.

4.5.3.1 Radiation temperature at evaporation

The radiation bath temperature at PBH evaporation in the RD case is obtained as

$$T_{\rm R}(t_{\rm ev}) = (3f(M))^{1/2}\left(\frac{45}{16\pi^3 g_*(t_{\rm ev})}\right)^{1/4} M^{-3/2}. \tag{4.47}$$

The values of $g_*(t_{\rm ev})$ as a function of the BH mass are shown in the right panel of Fig. 4.20.[39]

For full BHD, one can grossly assume that all the energy stored in the PBH density goes, after their evaporation, into the radiation energy density of the (B)SM particles emitted by the PBHs. These particles rapidly thermalize as soon as they are emitted, so that $\rho_{\rm R}(t_{\rm ev}^+) \approx \rho_{\rm BH}(t_{\rm ev}^-)$.[40] Using Eqs. (1.8) and $\rho_{\rm PBH} \propto a^{-3}$, one has

$$\frac{8\pi}{3}\rho_{\rm R}(t_{\rm ev}^+) = \frac{8\pi}{3}\rho_{\rm PBH}(t_{\rm ev}^-) = \frac{4}{9\tau^2} \quad \Longrightarrow \quad \frac{T_{\rm R}^{\rm R}(t_{\rm ev})}{T_{\rm R}^{\rm BH}(t_{\rm ev}^+)} = \left(\frac{9}{16}\right)^{1/4}. \tag{4.48}$$

[39] Clearly, this is an approximation by a step function, while the real function $g_*(t_{\rm ev})$ is smooth and can be extracted *e.g.* from `SuperIso Relic` for precision studies (see Section 4.4).

[40] This is the instantaneous reheating of Section 4.4.

Hence, for BHD, the radiation temperature after evaporation gets slightly reheated with respect to RD, the difference is about 15%.

4.5.4 Distribution at evaporation

The distribution of DM momentum at evaporation $F(p(t_{\rm ev}), t_{\rm ev})$ is a superposition of all the instantaneous distributions, each redshifted appropriately from its time of emission $t_{\rm em}$

$$F(p, t_{\rm ev}) = \int_{t_{\rm f}}^{t_{\rm ev}} Q_{\rm DM}\big(p(t)a(t_{\rm ev})/a(t)\big)\frac{a(t_{\rm ev})}{a(t)}{\rm d}t\,. \tag{4.49}$$

For RD from formation to evaporation, the redshift is given by $a(t_{\rm ev})/a(t) = (t_{\rm ev}/t)^{1/2}$, while for full BHD $a(t_{\rm ev})/a(t) = (t_{\rm ev}/t)^{2/3}$. Using $x(t_{\rm ev}) \equiv p(t_{\rm ev})/T$, Eq. (4.49) can be put under the dimensionless form

$$\tilde{F}(x(t_{\rm ev})) \equiv T^3 F(p, t_{\rm ev}). \tag{4.50}$$

GO approximation. In the GO limit, Eq. (4.49) becomes

$$F(p, t_{\rm ev}) = p(t_{\rm ev})^2 \frac{9}{2\pi}\frac{M^5}{f(M)}\mathcal{I}(x(t_{\rm ev}))\,, \tag{4.51}$$

where

$$\mathcal{I}_{\rm R,BH}(x(t_{\rm ev})) \equiv \int_{t_{\rm f}/t_{\rm ev}}^{1} \frac{(1-y)^{2/3} y^{a_{\rm R,BH}}}{e^{x(t_{\rm ev})(1-y)^{1/3} y^{b_{\rm R,BH}}} - (-1)^{2s}}{\rm d}y\,, \tag{4.52}$$

with $a_{\rm R(BH)} = -3/2(-2)$ and $b_{\rm R,BH} = -1/2(-2/3)$. The dimensionless momentum distribution at evaporation, Eq. (4.50), becomes

$$\tilde{F}_{\rm R,BH}(x(t_{\rm ev})) = \frac{1}{(8\pi)^5}\frac{9}{2\pi}\frac{1}{f(M)}x(t_{\rm ev})^2 \mathcal{I}_{\rm R,BH}(x(t_{\rm ev}))\,. \tag{4.53}$$

This quantity is shown in the left panel of Fig. 4.21 for RD with $\beta = \overline{\beta}$, and for full BHD; with quite small difference. To reproduce the case of RD with a different value of β, one suppresses $\tilde{F}$ by the factor $\beta/\overline{\beta}$. These results agree with the ones of [616].

BlackHawk results. The quantity $\tilde{F}$ derived from `BlackHawk` is shown in the right panel of Fig. 4.21. The suppression due to the different values of the DM spin s is manifest. The case $s = 0$ is quite similar to the bosonic case of the GO limit. For higher spins, the GO approximation becomes worse. Again, one can see that the difference between RD and BHD is quite small.

4.5.5 The dark matter phase space distribution

I now turn to the calculation of the DM PSD, as it is the essential ingredient to derive both the DM abundance and, using the publicly available code `CLASS`, the transfer function for structure formation. This derivation is quite cumbersome, as `CLASS` accepts input files with a very precise

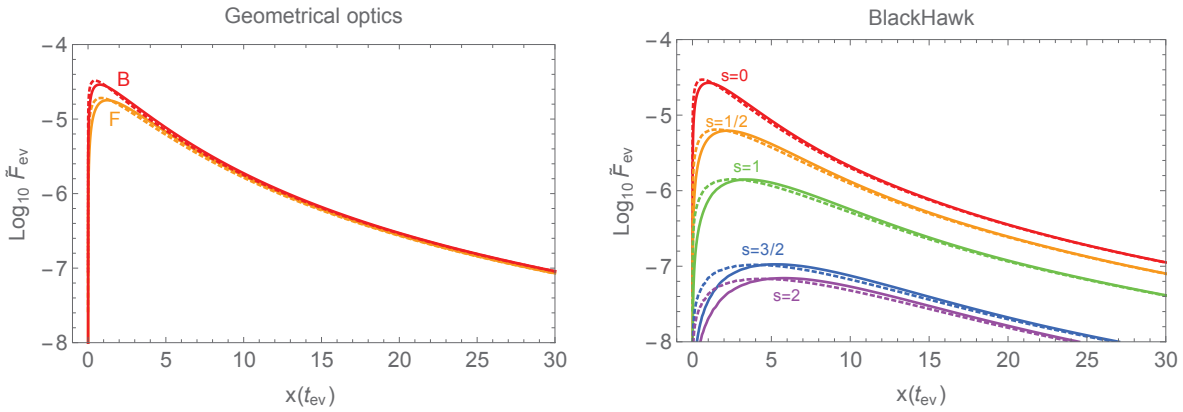

Figure 4.21: Left: Solid (dotted) lines are the momentum distribution at evaporation including redshift and assuming RD (BHD), in the GO approximation. **Right:** Same but calculated with `BlackHawk` for various spins. [taken from [25]]

format. Moreover, the careful choice of the dimensionless quantities can impact the results, as comparison with [618] has shown. The DM PSD per dof, $f_{\rm DM}$, at time t, is defined as

$$f_{\rm DM}(p,t) \equiv \frac{1}{g_{\rm DM}}\frac{{\rm d}n_{\rm DM}}{{\rm d}^3p} = \frac{1}{g_{\rm DM}}\frac{1}{p^2{\rm d}\Omega}\frac{{\rm d}n_{\rm DM}}{{\rm d}p}\,, \tag{4.54}$$

where $g_{\rm DM}$ is the number of DM d.o.f., $n_{\rm DM}$ the DM number density (scaling as a^{-3} from evaporation time), p is the DM momentum (scaling as a^{-1}) and ${\rm d}\Omega = 4\pi$ is the solid angle. For DM produced by evaporating PBHs, by using Eqs. (4.42) and (4.49), one obtains at $t_{\rm ev}$

$$f_{\rm DM}(p,t_{\rm ev}){\rm d}\Omega = \frac{1}{(p(t_{\rm ev}))^2}n_{\rm PBH}(t_{\rm ev})F(p,t_{\rm ev}) = n_{\rm PBH}(t_{\rm ev})T^{-5}\frac{\tilde{F}(x(t_{\rm ev}))}{x(t_{\rm ev})^2}\,. \tag{4.55}$$

Using the definition of β, one can prove that

$$f_{\rm DM}(p,t_{\rm ev}) = A_{\rm R,BH}\frac{\tilde{F}(x(t_{\rm ev}))}{x(t_{\rm ev})^2}\,, \tag{4.56}$$

with

$$A_{\rm R} \equiv \beta 3(8\pi)^2(4\pi)\gamma^{1/2}(3f(M))^{3/2}M^{-1}\,, \quad \text{and} \quad A_{\rm BH} \equiv 3(8\pi)^2(4\pi)(3f(M))^2M^{-2}\,. \tag{4.57}$$

4.5.5.1 Thermal dark matter

In order to proceed further toward the calculation of the DM abundance and transfer function, it is useful to establish a comparison with a thermal DM candidate. An hypothetical thermal PDM decoupling a $t = t_{\rm d}$ would have the following PSD (per dof)

$$f^{\rm th}_{\rm DM}(p,t_{\rm d}) = \frac{1}{(2\pi)^3}\frac{1}{e^{p(t_{\rm d})/T_{\rm DM}(t_{\rm d})} - (-1)^{2s}}\,, \tag{4.58}$$

where $T_{\rm DM}(t_{\rm d})$ is the temperature of the DM, identified with the temperature of the radiation bath from which it decouples, namely $T_{\rm DM}(t_{\rm d}) = T_{\rm R}(t_{\rm d})$.

At later times $t > t_{\rm d}$, both $p(t)$ and $T_{\rm DM}(t)$ scale as a^{-1}. It is then useful to define the dimensionless time independent parameter

$$q \equiv \frac{p(t)}{T_{\rm DM}(t)}\,, \tag{4.59}$$

and to re-express the PSD in terms of q

$$f_{\rm DM}^{\rm th}(q) = \frac{1}{(2\pi)^3}\frac{1}{e^q - (-1)^{2s}}\,. \tag{4.60}$$

It is also useful to express the DM temperature now, $T_{\rm DM}(t_0)$, in units of the photon temperature now, $T_\gamma(t_0) \simeq 2.7\,{\rm K}$. If decoupling happened just before recombination, $t_{\rm d} = t_{\rm r}^-$, clearly $T_{\rm DM}(t_{\rm r}^-) = T_\nu(t_{\rm r}^-) = T_\gamma(t_{\rm r}^-)$. Because of the successive reheating of the photons, at the present time t_0

$$T_{\rm DM}(t_0) = T_\nu(t_0) = \left(\frac{4}{11}\right)^{1/3} T_\gamma(t_0)\,. \tag{4.61}$$

`CLASS` precisely takes as an argument $T_{\rm DM}(t_0)/T_\gamma(t_0)$.

4.5.5.2 Dark matter from primordial black holes

DM particles from PBHs *were never in thermal equilibrium*, which is the fundamental difference with thermal DM that gives the PBH → DM scenario such a prolific zoology. Nevertheless one can imagine to deal with their distribution as if they were "decoupling" at $t_{\rm ev}$, so that they would have the decoupling temperature $T_{\rm DM}(t_{\rm ev}) = T_{\rm R}(t_{\rm ev}^+)$, which has already been derived in Eqs. (4.47) and (4.48).

The time independent quantity q, defined in Eq. (4.59), is thus

$$q = \frac{p(t_{\rm ev})}{T_{\rm DM}(t_{\rm ev})} = \frac{p(t_{\rm ev})}{T_{\rm R}(t_{\rm ev}^+)} = \frac{T}{T_{\rm R}(t_{\rm ev}^+)}\frac{p(t_{\rm ev})}{T} \equiv \alpha_{\rm R,BH} x(t_{\rm ev})\,, \tag{4.62}$$

where

$$\alpha_{\rm R} = \frac{1}{8\pi}\frac{1}{(3f(M))^{1/2}}\left(\frac{16\pi^3 g_*(t_{\rm ev})}{45}\right)^{1/4} M^{1/2}\,, \quad \text{and} \quad \alpha_{\rm BH} = (9/16)^{1/4}\alpha_{\rm R}\,. \tag{4.63}$$

In Ref. [25], it is argued that Ref. [618] incorrectly takes $q \equiv x(t_{\rm ev}) = p(t_{\rm ev})/T$ as a definition. In terms of q, the PSD of Eq. (4.56) then becomes simply

$$f_{\rm DM}^{\rm R,BH}(q) = A_{\rm R,BH}(\alpha_{\rm R,BH}/q)^2 \tilde{F}(q/\alpha_{\rm R,BH})\,. \tag{4.64}$$

In the right panel of Fig. 4.22, I display the PSD obtained from `BlackHawk`, taking $M = 1\,{\rm g}$ for definiteness, for RD with $\overline{\beta}$ and full BHD. For RD with other values of β, the PSD has to be suppressed by a factor $\beta/\overline{\beta}$. Comparison to the GO limit used in the left panel shows that

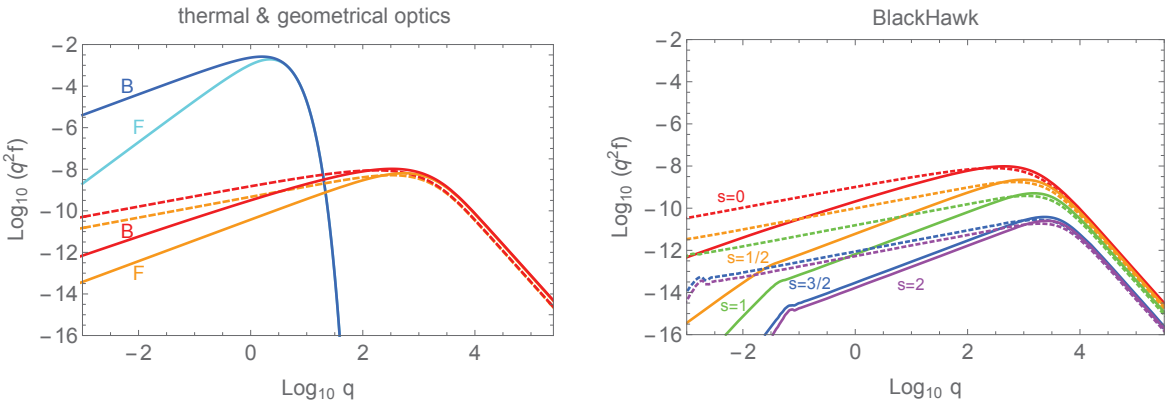

Figure 4.22: Left: PSD for RD with $\beta = \overline{\beta}$ (solid) and full BHD (dashed) with $M = 1\,\mathrm{g}$, in the GO approximation. Also shown is the thermal PSD with $g_i = 1$. **Right:** Same but calculated with `BlackHawk`.

the suppression in the PSD associated to higher spins is manifest. In the left panel the thermal distribution (4.60) is also shown, with one d.o.f. $g_i = 1$. It is clear that the spectrum of particles emitted by a 1 g PBH is much harder than the thermal one, which thus does not reproduce PBH results.

The PSD for other values of the PBH mass can be easily reconstructed in remarking that the peak should be at $\log_{10}(q) \sim 3 + \log_{10}(M/(1\,\mathrm{g}))/2$. In addition, the PSD gets suppressed by the factor $(1\,\mathrm{g}/M)^{1/2}$.

4.5.6 Dark matter abundance

The present abundance of the PDM produced by PBH evaporation is trivially obtained through

$$\Omega_{\rm DM} = \frac{m_{\rm DM}}{\rho_{\rm c}} n_{\rm DM}(t_{\rm ev}) \left(\frac{a(t_{\rm ev})}{a(t_0)}\right)^3 . \tag{4.65}$$

The DM number density at evaporation is calculated by integrating the DM spectrum over all momenta. Using the definition of the PSD given in Eq. (4.54), one has

$$n_{\rm DM}(t_{\rm ev}) = g_{\rm DM} \int f_{\rm DM}(p, t_{ev})\, \mathrm{d}^3 p = T_{\rm DM}(t_0)^3 \left(\frac{a(t_0)}{a(t_{\rm ev})}\right)^3 \int 4\pi q^2 g_{\rm DM} f_{\rm DM}(q)\, \mathrm{d}q\,, \tag{4.66}$$

where the integration variable was changed using Eq. (4.62) and in the scaling $T \propto a^{-1}$ was used. Inserting the last result in Eq. (4.65), the DM abundance is simply given by

$$\Omega_{\rm DM} = \frac{m_{\rm DM}}{\rho_{\rm c}} T_{\rm DM}(t_0)^3 \int 4\pi q^2 g_{\rm DM} f_{\rm DM}(q)\, \mathrm{d}q\,. \tag{4.67}$$

	B	F	$s=0$	$s=1/2$	$s=1$	$s=3/2$	$s=2$
$\overline{m}_{\rm BH}$	0.114	0.076	0.112	0.155	0.344	2.28	2.59
$\overline{m}_{\rm R}$	0.086	0.057	0.084	0.116	0.259	1.71	1.94

Table 4.3: Values of $\overline{m}_{\rm BH}$ and $\overline{m}_{\rm R}$ in MeV, calculated in the GO approximation for a boson and a fermion; and from `BlackHawk`, with increasing values of the spin. Numerical errors are of order of a few percent.

4.5.6.1 Dark matter from primordial black holes

Assuming that the DM is fully given by a stable PDM candidate from the PBH evaporation, I now calculate the required value for its mass. This analysis is, to my knowledge, the first that accounts for the differences due to the spin of the DM candidate. The analytical results for the PSD obtained in the GO limit and the numerical ones obtained using `BlackHawk` are compared. As for the d.o.f., the SM is considered with the addition of the DM candidate, under the minimal choice, considering just the d.o.f. associated to polarization $g_{\rm DM} = 2s_{\rm DM} + 1$.

For $M \lesssim 10^7$ g, I obtain the following results:

$$m_{\rm DM}^{\rm R,BH} = \left(\frac{\Omega_{\rm DM}}{0.25}\right)\left(\frac{0.1}{g_{*,S}(t_{\rm r})/g_{*,S}(t_{\rm ev})}\right)\left(\frac{M}{1\,{\rm g}}\right)^{1/2}\begin{cases}\overline{m}_{\rm BH}\,, & \text{full BHD}\\ \dfrac{\overline{\beta}}{\beta}\overline{m}_{\rm R}\,, & \text{RD}\end{cases} \tag{4.68}$$

where the values of the parameter $\overline{m}_{\rm BH,R}$ are collected in Table 4.3. The scaling with the BH mass of Eq. (4.68) slightly breaks at $M \gtrsim 10^7$ g, where one obtains smaller values for $\overline{m}_{\rm BH,R}$, as an effect of the decrease of $g_*(t_{\rm ev})$, see Fig. 4.20. For instance, for $M = 10^8\,(10^9)$ g, the suppression in $\overline{m}_{\rm BH,R}$ is by a factor of $0.74\,(0.56)$.

As expected, the result for $s = 0$ from `BlackHawk` is consistent with the GO limit for a boson. It then perfectly matches with previous literature results (see *e.g.* Fig. 7 of [596]). The masses $\overline{m}_{\rm BH}$ and $\overline{m}_{\rm R}$ are really close in the GO limit for the bosonic case and for the spin 0 numerical result, the last being slightly lower than the previous. This difference depends on the precise shape of the peak in the PSD. For other spins, the suppression of the PSD compared to GO causes a clear increase of the masses $\overline{m}_{\rm BH/R}$ compared to this limit.

Notice that for RD with $\beta = \overline{\beta}$, the values of $\overline{m}_{\rm BH/R}$ are systematically smaller by a factor of about 0.75 with respect to BHD. Such difference could not be appreciated in previous literature, as no difference between the two scenarios was made. This discrepancy is indeed due to the difference of the ratio of the scale factors in the integrands, not to the slight difference in $T_{\rm R}(t_{\rm ev})$ which was already included.

The strong increase in the masses for increasing values of the spin allows to hope to escape bounds from structure formation. In the following Section I will study in detail the impact on structure formation of these WDM candidates. Before doing this, and in view of the comparison to be done in the next Section, it is useful to recall the relevant formulas for the DM abundance for a thermal DM candidate.

4.5.6.2 Thermal dark matter

Let's consider a fermion X, with $g_X = 2$, as a thermal DM candidate. If decoupling happens just before reheating, so that $T_X(t_0) = T_\nu(t_0)$, the value of the DM mass for which $\Omega_X = 0.25$, would be $m_X \approx 11\,\mathrm{eV}$ [623]; for an early decoupling, when $g_{*,S}(t_\mathrm{d}) = 106.75$, the temperature of the DM candidate now is suppressed, $(T_X(t_0)/T_\nu(t_0))^3 = g_{*,S}(t_\mathrm{r})/g_{*,S}(t_\mathrm{d}) = 0.1$, so that its mass gets enhanced to $m_X = 110\,\mathrm{eV}$.

One can summarize as follows

$$\Omega_X = 0.25 \left(\frac{T_X(t_0)}{T_\nu(t_0)}\right)^3 \left(\frac{m_X}{11\,\mathrm{eV}}\right) = 0.25 \left(\frac{g_{*,S}(t_\mathrm{r})/g_{*,S}(t_\mathrm{d})}{0.1}\right) \left(\frac{m_X}{110\,\mathrm{eV}}\right) , \tag{4.69}$$

or, for a direct comparison with the case of DM from evaporating PBHs

$$m_X = 110\,\mathrm{eV} \left(\frac{\Omega_X}{0.25}\right) \left(\frac{0.1}{g_{*,S}(t_\mathrm{r})/g_{*,S}(t_\mathrm{d})}\right) . \tag{4.70}$$

4.5.7 Constraints from structure formation

Candidates PDM are classified according to their velocity dispersion, which defines a free-streaming length. On scales smaller than the free-streaming length, fluctuations in the DM density are erased and gravitational clustering is suppressed.

The velocity dispersion of CDM particles is by definition so small that the corresponding free-streaming length is irrelevant for cosmological structure formation. That of hot DM is only one or two orders of magnitude smaller than the speed of light, and smooths out fluctuations in the total matter density even on galaxy cluster scales, which leads to strong bounds on their mass and density. Between these two limits, there exists an intermediate range of DM candidates generically called WDM.

The matter power spectrum $P(k)$ is very sensitive to the presence of WDM particles with large free-streaming lengths. Due to their free-streaming velocity, WDM particles slow down the growth of structure and suppress $P(k)$ on scales smaller than their free-streaming scale. The effect of the free-streaming on the matter distribution can be described by a relative "transfer function" which is the square root of the ratio of the matter power spectrum in the presence of WDM to that in the presence of purely CDM, for fixed cosmological parameters

$$T(k) \equiv \left(\frac{P(k)_{\Lambda\mathrm{WDM}}}{P(k)_{\Lambda\mathrm{CDM}}}\right)^{1/2} . \tag{4.71}$$

For the majority of the cosmological models in which the universe contains only WDM (in addition to the usual baryon, radiation and cosmological constant components), the transfer function can be approximated by the analytical fitting function (see *e.g.* [624])

$$T(k) = (1 + (\alpha_\mathrm{B} k)^\nu)^\gamma , \tag{4.72}$$

where α_B (labelling the scale of the break), ν and γ are free parameters sensitive to the details of the WDM candidate. For pure WDM models, the combined data on the CMB and the Lyman-α

forest [623] provide a lower bound on the scale where the transfer function starts to fall. This lower limit was estimated in [623] to be $\alpha_{\rm B} \lesssim 0.11\,{\rm Mpc}/h$ at the 2σ CL.

A well known case is the one of thermal relics[41] as WDM. In such a case Eq. (4.72) simplifies into (see *e.g.* [625])

$$T_X(k) = \left(1 + (\alpha_{\rm B} k)^{2\nu}\right)^{-5/\nu} , \tag{4.73}$$

where $\alpha_{\rm B}$ is a function of the thermal relic mass and temperature, and the index $\nu = 1.12$ is fixed. The bound on $\alpha_{\rm B}$ derived in the pioneering analysis of [623], translated into a lower bound on the thermal relic mass, gives $m_X \gtrsim 0.5\,{\rm keV}$. A more recent analysis [626] showed that the lower limit is now $m_X \gtrsim 3\,{\rm keV}$. Standard thermal relics (those with mass $m_X \approx 11\,{\rm eV}$) are completely ruled out, as well as early decoupled ones (those with $g_*(t_{\rm d}) = 106.75$), with mass $m_X \approx 110\,{\rm eV}$. Only very early decoupled thermal relics could manage to be as heavy as 3 keV: this would require a huge amount of d.o.f. at decoupling. I display the transfer function for such early and very early decoupled thermal relics in Fig. 4.23.

Using the PSDs obtained with `BlackHawk` (taking the d.o.f. of the SM plus those of the PDM candidate), for various values of M and of the DM spin, the associated transfer function were calculated with `CLASS`, requiring that $\Omega_{\rm DM} = 0.25$. By fixing the PBH mass and the DM spin, the mass of the WDM candidate is univoquely determined, as shown by Eq. (4.68).

The transfer functions are shown in Fig. 4.23. The top panels apply to the case of full BHD (dashed lines) and the case of RD with $\beta = \overline{\beta}$ (solid lines): these scenarios give quite similar results. Notice that the transfer functions of Fig. 4.23 actually apply to all values[42] of the PBH masses in the range $10^{-5} - 10^{7}\,{\rm g}$, according to the DM spin. It turns out that, even for the higher spins, there is a conflict with the constraints from structure formation (at contrary with the expectations of Ref. [616]). For BHs with masses in the range $10^{7} - 10^{9}\,{\rm g}$, the situation is even worse, because the parameter $\overline{m}_{\rm R,BH}$ is smaller and the ratio $T_{\rm DM}(t_0)/T_\gamma(t_0)$ is larger than in the previous case, being proportional to $g_{*,S}(t_{\rm ev})^{-1/3}$.

The only possibility left is then RD with a sufficiently small value of β. In the bottom panel of Fig. 4.23, RD is considered with increasingly smaller values of β. In particular, focusing on the $s = 0$ case,the transfer function with $\beta = \overline{\beta}$ (solid) are compared with the ones obtained taking $\beta/\overline{\beta} = 1/10, 1/30, 1/100$ (dot dashed). One can see that the upper limit on $\beta/\overline{\beta}$ is about $1/100$: this confirms previous estimates [596, 615] based on a simplified method.

For the different values of the spin, $s = 0, 1/2, 1, 3/2, 2$, by fitting the right and bottom panels of Fig. 4.23 with Eq. (4.72), one can derive a general formula for $\alpha_{\rm B}$,

$$\alpha_{\rm B} \simeq \left(\beta/\overline{\beta}\right)^{0.8} (0.95,\, 0.85,\, 0.51,\, 0.14,\, 0.13)\,{\rm Mpc}/h\,. \tag{4.74}$$

Since for the transfer function associated to the 3 keV thermal relic one has $\alpha_{\rm B} \simeq 0.03\,{\rm Mpc}/h$, one can derive an upper limit on $\beta/\overline{\beta}$. From Eq. (4.74), for the different values of the spin $s = 0, 1/2, 1, 3/2, 2$, the maximum value of β that allows to satisfy the bounds from structure formation

[41] There exist however many other WDM candidates whose origin is rooted in particle physics, *e.g.* the gravitino.

[42] The Fig. 2 of [618] and their Eq. (5.8) then look at least misleading, as the PBH mass M, $\Omega_{\rm DM}$ and the DM mass $m_{\rm DM}$ are not independent.

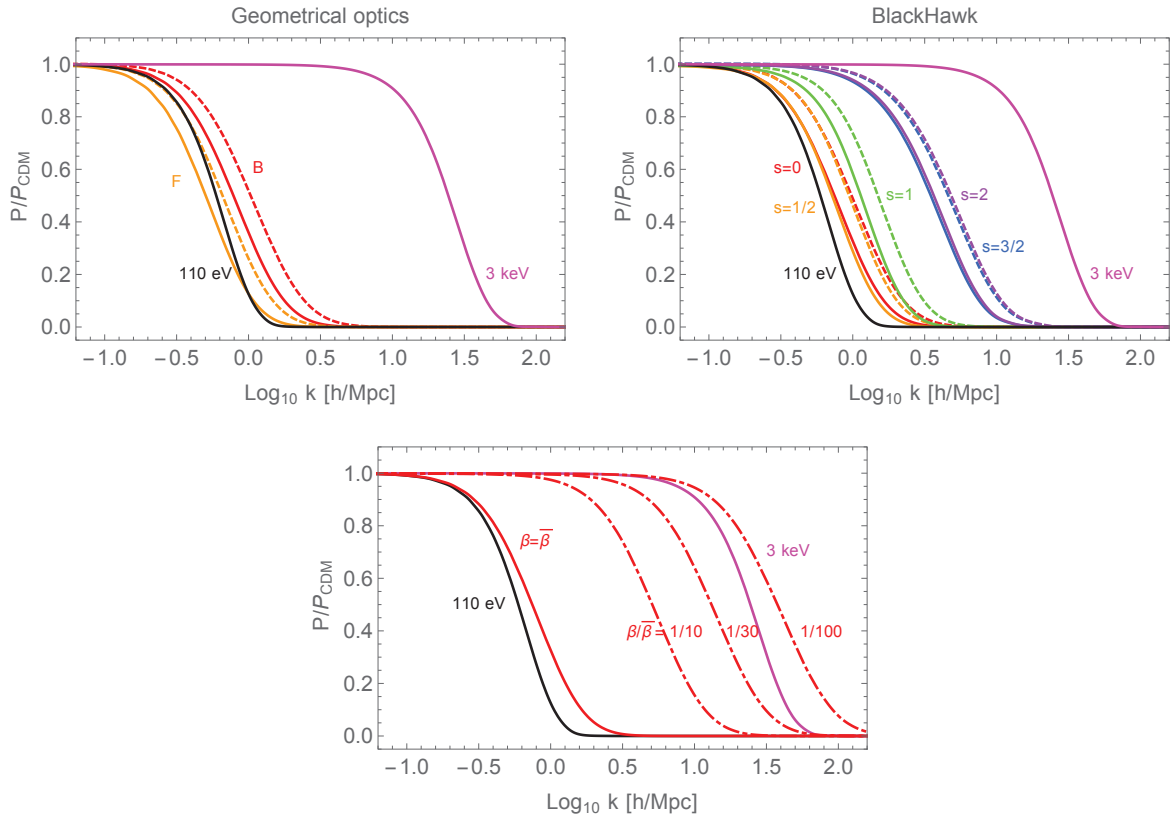

Figure 4.23: Squared transfer function for various WDM models providing full DM contribution, computed with `CLASS`. In all cases, the same (default) cosmological parameters have been used. The (very) early decoupled thermal fermion with mass $m_X = 110\,\text{eV}$ (3 keV) is shown as a black (pink) solid line. **Top-Left:** Massive boson $s = 0$ and fermion $s = 1/2$ from the evaporation of PBHs, for RD with $\beta = \overline{\beta}$ (solid lines), and for full BHD (dashed lines), using the PSD calculated within the GO approximation. **Top-Right:** Same for massive spin $s = 0, 1/2, 1, 3/2, 2$ particles using the PSD calculated with `BlackHawk`. **Bottom:** $s = 0$ WDM candidate from PBH evaporation with Rd, for various values of $\beta/\overline{\beta}$. [taken from [25]]

turns out to be

$$\beta/\overline{\beta} \lesssim (0.013,\, 0.015,\, 0.029,\, 0.15,\, 0.16)\,. \tag{4.75}$$

The result for the spin 1/2 case agrees with Eq. (6.1) of Ref. [618], where they obtained $\beta < 0.016\,\overline{\beta}$. This is the first time precise results are obtained for the higher spins $s > 1/2$, constituting the first WDM PBH constraints for $M \lesssim 10^9$ g.

One might also be interested in mixed scenarios with the simultaneous presence of both CDM and WDM, with the WDM candidate coming from the evaporation of PBHs accounting only partially for the full DM. For the case of thermal relics, it has been shown [623] that in mixed models

small-scale structures are not completely erased below α_B and the free-streaming effect leads to a step-like transfer function, with the standard ΛCDM matter power spectrum recovered in the limit $\Omega_{WDM} \to 0$. However, in such models the scale of the break α_B becomes larger than pure WDM models, increasing with the inverse of the mass of the DM candidate. It was verified that the same scenario arises with candidates coming from the evaporation of PBHs, see Fig. 4.24. In such a case the mass of the WDM candidate drops as its abundance is reduced, according to Eq. (4.67).

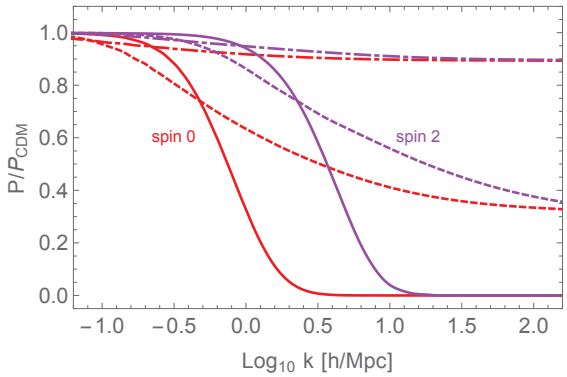

Figure 4.24: Squared transfer function for mixed WDM-CDM models computed with the same cosmological parameters and candidates as Fig. 4.23, top-right panel, for two different spin particles and RD with $\beta = \overline{\beta}$. Solid lines: $\Omega_{WDM} = \Omega_{DM,\,total}$, dashed lines: $\Omega_{WDM} = 1/10\,\Omega_{DM,\,total}$, dot-dashed lines: $\Omega_{WDM} = 1/100\,\Omega_{DM,\,total}$. [taken from [25]]

4.5.8 Conclusion

Ref. [25] improved previous analyses of the constraints on WDM from PBHs evaporation [596, 615, 616, 618], by taking into account the effect of the DM spin by means of the code `BlackHawk`. Assuming that this kind of WDM provides the full contribution to the observed DM, the associated transfer function was calculated thanks to the code `CLASS`.

Contrary to expectations based on [616], it turns out that, for BHD, such candidates are excluded for all spin values from 0 to 2, in the whole PBH mass range $10^{-5} - 10^{9}$ g under consideration. Only RD is allowed, if the values β are smaller than indicated in Eq. (4.75), according to the WDM spin.

A couple of possibilities to evade the previous conclusions should be mentioned, which rely on the introduction of additional particles or fields. As suggested in [615], some mechanism providing entropy non conservation and taking place after the evaporation of PBHs (like *e.g.* moduli decay) might succeed in saving the WDM candidates with BHD. Another possibility to evade the bound would be to have a huge increase in the d.o.f. at evaporation. This is not possible to be studied within the present version of the `BlackHawk` code, but since analytically it is known that $\Omega_X \propto 1/f(M)^{1/2}$ (see *e.g.* [596]), the required increase in the Page coefficient would have to be really huge: a factor of about 10^4 for $s = 0, 1/2$. The effect of early PBH accretion does not help [596]. It was shown

subsequently by Masina [595], using `BlackHawk`, that a non-zero PBH spin is also a deterrent for this scenario.

In this work, which is already tough, only non-interacting DM from PBH evaporation was considered. Interestingly enough, allowing for self-interacting DM (freeze-in and/or freeze-out models) offers the possibility to escape the structure formation bound in the light case for BHD [627]. Thermalization in the DM sector indeed decreases the mean DM kinetic energy, which together with number-changing processes, can have a strong impact, in particular to enhance the DM relic abundance by several orders of magnitude. The consequences of allowing for other production mechanisms were recently explored in Refs. [332, 627–629]. For a mixed model of DM production, Ref. [630] proved that a PBH dominated period of DM creation by evaporation cannot explain the abundance observed today. In particular, the authors of Refs. [138, 261] developed a public code complementary to `BlackHawk` to compute the abundance of DM evaporated by PBHs, taking self-interactions into account.

Note that apart from being directly evaporated by PBHs, PDM could also be constantly boosted by scattering with the HR products, both mechanisms increasing its detectability [631–634]. The frozen PDM density could have been diluted by PBH evaporation in the early universe [635] or PBHs could be responsible for a direct reheating of the sole dark sector [593].

4.6 Non-standard primordial black holes

[43]Most of the constraints on PBHs are derived in the Schwarzschild limit. Many BH studies have been pursued in alternative theories, but most of them are purely theoretical and aim at finding new exotic solutions to the Einstein equations of general relativity. As I have pointed out in Section 4.1, the only notable exception is the case of HDBHs, which was historically motivated.

Much less work have focused on polymerized BHs [163, 194, 203, 211, 212, 636] (see in particular [213]). Polymerized BHs have emerged as an effective template for BHs in LQG.[44] They are studied by applying the techniques of LQG and loop quantum cosmology [639] to mini-superspace BH spacetimes. Although many models have been proposed in the literature (see *e.g.* the non-exhaustive list [640–655]), depending on the details of the regularization of the Hamiltonian, here I focus for definiteness on the particular class of effective metrics derived in [194, 656]. These metrics are regular, *i.e.* do not admit a singularity at $r = 0$, and remain asymptotically flat. The resolution of the singularity arises from effects of quantum geometry which become relevant at the Planck scale. I consider these metrics as phenomenological ansatz for BHs taking into account LQG corrections at the semi-classical level.

Identifying possible signatures of quantum gravity has recently regained interest due to the increasing precision in the detection of GWs. Indeed, the last phase of BH merging, known as the ringdown phase, is extremely sensitive to the details of the metric structure of BHs. The deformed

[43]This Section is based on the paper "Hawking radiation by spherically-symmetric static black holes for all spins. II. Numerical emission rates, analytical limits and new constraints" [150] I wrote with A. Arbey, M. Geiller, E. R. Livine & F. Sartini.

[44]The term "polymerized" refers to the polymer-like quantization scheme inherited from LQG [637], for a recent review see [638].

BH resulting from the coalescence of two BHs settles down to a stable (axially) symmetric shape by emitting GWs of defined frequencies known as QNMs. The determination of these modes for a given metric and the comparison with the ringdown signal could discriminate between different models of (P)BHs [164].

4.6.1 Presentation of the model

I turn now to the description of the model. The polymerized BH spherically symmetric and static metric studied in [194, 656] has defining functions F, G and H given by Eqs. (2.93). These equations depend on 2 parameters, a_0 and ε, which encode the quantum gravity deformation from the Schwarzschild metric. The parameter a_0 is the minimal area in LQG, also referred to as the *area gap*. It is typically of the Planck scale. The deformation parameter $\varepsilon \geq 0$ is an *a priori* independent parameter indicating the typical scale of the geometry fluctuations in the Hamiltonian constraints of the theory as they get renormalized from the Planck scale to astrophysical scales. Although one can be tempted to keep it very small $\varepsilon \ll 1$, nothing *a priori* forbids it from growing large and it can be interesting to consider possible high values of this deformation parameter in order to understand the effects of LQG corrections. I remain totally agnostic concerning the formation rate of such LQGBHs in the early universe, as should be self-consistently described by loop quantum cosmology.

The two roots of the metric components are $r_+ = 2\mathfrak{m}$ and $r_- = 2\mathfrak{m}P(\varepsilon)^2$, as shown in Section 2.3.1.5. This identifies the first important effect of the polymerization: the BH, even without electric charge, acquires a Cauchy horizon at $r = r_-$ on top of the event horizon at $r = r_+$. If the deformation parameter ε is sent to 0, the radius r_- is also sent to 0 (even if the area gap remains non-vanishing) and one recovers a Schwarzschild-like metric. On the other hand, as ε grows large, r_- grows to r_+ (although always remaining smaller) and the polymerized BH geometrically behaves as if it carried a non-vanishing charged energy-momentum tensor although it of course does not create an EM field. Another fundamental difference between RNBHs (KBHs) and LQGBHs is that the charge (angular momentum) is radiated away during the BH evaporation. Thus, the behaviour of the BH is expected to follow a Schwarzschild trajectory once these parameters are back to small values. The polymerization factor ε, on the other hand, is a constant inherited from the quantum nature of gravity. Thus, the specific behaviour associated with a high value of ε (namely a decrease of the BH temperature compared to the Schwarzschild case, and smaller emission rates) should last during the whole PBH lifetime.

The temperature of a LQGBH is given in Eq. (2.141), and the associated GFs and primary spectra are displayed in Figs. 2.12 and 2.13. One can see that when $\varepsilon \ll 1$, the change in the temperature is quite negligible compared to the Schwarzschild case, and thus the rates of emission for polymerized BHs are very close to the classical SBH case. However, one sees that in the limit $\varepsilon \to +\infty$, the radii collapse $r_- \to r_+$ and the temperature goes to $T_{\rm LQG} \to 0$, cancelling HR, similarly to the RNBH with $Q \to M$.

The LQGBH HR was studied in [163, 194, 203, 211–213, 636] for spins 0 and 2. The results for spin 1 are new to this study. In Ref. [213] one can find some results for the massless field of spin $1/2$. Our results for this case however differ quantitatively from [213], as shown in Section 2.4. It is

noteworthy that no constraint has yet been derived for these polymerized BHs using HR. For the first time, Ref. [150] obtained such a constraint on the PBH abundance as a DM component, as shown in the next Section.

4.6.2 AMEGO constraints

I use the computed emission rates for LQGBHs to reassess the MeV-GeV photon constraint on PBHs from AMEGO, and show that a sufficiently high value of the polymerization parameter ε reopens the mass window $M \lesssim 10^{18}\,\mathrm{g}$ for all DM in the form of PBHs. This is the first constraint ever set on LQGBHs with HR.

There are two parameters at stake, a_0 and ε. First, a_0 is expected to be negligible for BHs with a radius $r_+^2 \gg a_0$ (see Section 2.4), and to play a role only at the end of the PBH evaporation, when its radius reaches values close to the Planck length, out of the HR constraint range. The parameter ε, on the other hand, has an effect which is proportional to its value, with small values of ε leading to very little changes in the HR emission, while larger values may have a dramatic impact. There are two major outcomes expected when considering the evaporation constraints on LQGBHs:

- a decrease of the Hawking temperature and emission rates at high ε, which results in a longer lifetime, shifting the (time-dependent) constraints towards smaller PBH masses;
- this decrease also leads to weaker (instantaneous) constraints.

Thus, the most striking result from this study is that one expects the window for light PBHs to represent all of DM to be reopened in the case of high values of ε, down to smaller PBH masses than in the Schwarzschild case.

In order to illustrate this proposal, I compute the prospective evaporation constraints from MeV to GeV photons as will be measured by AMEGO in the GC, whose expected sensitivity can be found in [551], motivated by the fact that this limit lies among the most stringent ones in the disputed mass range where PBHs may represent all DM (see Section 4.2). The effects which are described below apply to all the other evaporation constraints. I follow exactly the setup chosen by [255]: a NFW distribution of DM in the Milky Way, and observation in some small window of angular width $5°$, which gives $\Delta\Omega = 2.39 \times 10^{-2}\,\mathrm{sr}$ (therefore method M_2^2). The expected emission is thus given by Eq. (4.5), where the integral over the LOS has value [255, 567]

$$J = 1.597 \times 10^{26}\,\mathrm{MeV}\cdot\mathrm{cm}^{-2}\cdot\mathrm{sr}^{-1}\,. \tag{4.76}$$

The results are shown in Fig. 4.25 where I plot the constraints for $\varepsilon = \{1, 5, 10\}$ as well as the fiducial constraint for the classical case and the constraint from [255] for comparison. The constraints are obtained by maximizing f_{PBH} while keeping $E^2\mathrm{d}\Phi_{\mathrm{gal}}/\mathrm{d}E$ below the AMEGO sensitivity.

One observes that the constraints derived for the classical SBH case have differences with the results of [255] that were already discussed in Section 4.2.5.2. As expected, the constraints for the classical SBH and the LQGBH with $\varepsilon = 1$ (small polymerization factor) are similar, as their HR rates are very close.[45] Then, as ε increases to 5 and then 10, one sees that the constraints get

[45] The fact that the constraints are slightly more restrictive for $\varepsilon = 1$ than for $\varepsilon = 0$ is easily explained by the "bump" in the LQGBH temperature at medium values of ε, see Fig. 2.8.

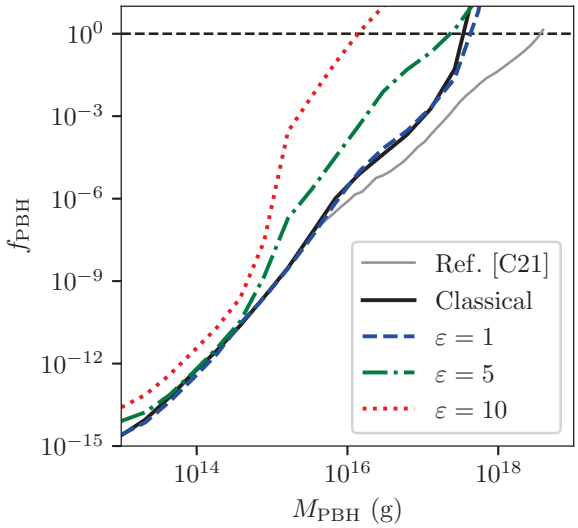

Figure 4.25: Constraints on the PBH fraction in DM from the measurement of MeV-GeV photons in the GC by AMEGO. This work (SBH, solid black) is to be compared to the same limit from [255] (solid grey, denoted as [C21]). The constraints computed for increasing values of $\varepsilon = \{1, 5, 10\}$ are displayed (dashed blue, dot dashed green and dotted red, from right to left). The horizontal dashed line denotes the overclosure limit $f_{\rm PBH} = 1$. [taken from [150]]

weaker in the high mass range $M \gtrsim 10^{15}\,$g, allowing the DM fraction $f_{\rm PBH}$ to be 1 for $M_{\rm PBH} \gtrsim 10^{17}\,$g (or $10^{16}\,$g for $\varepsilon = 10$). This is due to the fact that the main contribution to the photon spectra for these PBHs comes from the directly emitted primary photons, whose emission rate is strongly suppressed when ε increases (see Fig. 2.13). However, in the lower mass range $M_{\rm PBH} \lesssim 10^{15}\,$g, the constraints remain of the same order of magnitude. In this energy range, the constraints come from the secondary photons generated by neutral pion decay. As pions are spin 0 particles, their emission rate decreases slowly as ε increases (see Fig. 2.13); the effect of the polymerization factor becomes sizeable only for extreme values. In this constraint plot, I have extended the mass range to masses $M = 10^{13}\,$g, which is 2 orders of magnitude below the usual evaporation limit $M \lesssim 10^{15}\,$g set by the lifetime of the PBHs, because it is expected that the decreased emission rates will result in an increased PBH lifetime, thus allowing smaller PBHs to contribute to DM today. This effect should be quantitatively studied.

4.6.3 Conclusion

Focusing on the case of polymerized BHs, whose peculiar metric form is the heart of our analytical study, I conclude that the HR signals are not much different from the Schwarzschild case in the limit $\varepsilon \ll 1$ of small polymerization parameter. I have shown however that if the polymerization parameter takes high values $\varepsilon \gtrsim 1$, then all the evaporation constraints would need to be re-evaluated with

two major effects: shifting the constraints towards smaller PBH masses, and relaxing the constraints on the fraction of DM which light PBHs can represent. The modification of the constraints depends in a non-trivial way on the spin of the primary particles involved in the secondary observed spectrum; the effect of the quantum deformation ε is very spin-dependent. The main consequence of this result is that the mass range usually excluded by (future) evaporation limits $10^{16}\,\mathrm{g} < M < 10^{18}\,\mathrm{g}$ for all DM in the form of PBHs is reopened. This is a striking result in PBH DM studies, and the first constraint ever set on the fraction of polymerized PBHs as DM using HR signals. As a final remark, a new window has been opened on the study of HR from other regular BH metrics, which is an exciting prospect.

In this study, I have remained purely phenomenological about polymerized BHs. I precise that the LQG paradigm is under a lot of pressure from both theoretical and experimental advances. I must then point out several drawbacks:

- the LQG application to cosmology may not be as robustly settled as commonly thought [193];
- BH solutions in LQG may not be simply described by "effective metrics" [657];
- the phenomenological high ε limit that causes the most interesting PBH constraints may not be physically realistic.[46]

A recent discussion dedicated to HR of BHs in the LQG paradigm can be found in [658].

Nevertheless, I stress that the derivation of the potentials for HR of Sections 2.3.1.3 applies in general to the class of regular BHs, which are BH solutions showing no singularity at the coordinate origin. Polymerized BHs, inspired by LQG, are only an example of regular BHs [640–655], and the metric derivation of [194, 656] is just one among different polymerization schemes. Recent work on other regular BH solutions include *e.g.* [165, 166, 659–661], some of which also discuss HR. It would be most interesting to extend the HR constraints to these other metrics; an inverse idea would be to determine what are the necessary ingredients such that HR rates are dramatically modified, *e.g.* by studying the analytical properties of the potentials (2.83).

One last aspect, which I have not quantitatively explored, is the rate of final bursts of PBHs and their observation by (prospective) γ-ray instruments (see Section 4.1.2.8). Since in the high ε limit PBHs evaporating today would have a lower initial mass than in the Schwarzschild case, their number abundance should be larger if they represent some fixed fraction of DM. Thus, the rate of nearby final bursts would be higher, leading to more stringent constraints. However, the non-trivial modification of the final light curves (energies, duration) makes it difficult to predict the sensitivity of the γ-ray instruments to these polymerized PBH bursts.

[46] This was pointed out to me by C. Rovelli during my contribution to the International Loop Quantum Gravity Seminar. The in-person meetings of the LQG community were the occasion of vehement debate in which I was admittedly lost.

Conclusion

In this concluding Chapter, I first review the results obtained above and then closes this thesis manuscript with some general ideas about PBHs, HR and physics in general.

In Chapter 1, I have reviewed the paradigm of PBHs inside the standard model of cosmology. An historical overview has shown that the PBH idea dates back to the 1960's. The formation channels have been briefly discussed, with a focus on the more realistic mass and spin distributions. I have pointed out that efficient PBH formation may require "beyond stardard" cosmology, which disfavors them as a "classical physics" DM candidate. In Chapter 2, I have described the phenomenon of HR, in the SM of particle physics. The historical overview showed that all the relevant physical ingredients are well-known since the 1990's, but that precise numerical methods were lacking in the community to obtain the rate of emission of particles of all kinds. I have emphasized the link between HR and more fundamental BH properties, such as thermodynamics and the information paradox. I have derived all the fundamental equations one needs to compute HR, with the primary spectra of (B)SM particles and the secondary spectra after hadronization and decay. I have given the general method to obtain the HR rates for the general class of spherically symmetric BHs, with examples given of RNBH, HDBH and LQGBH. I have finally discussed the characteristics of the radiation and evolution of KBHs. In Chapter 3, I have presented the public code `BlackHawk`, whose development has been the major part of this thesis work. I have listed the main features, programs and options of the code, and I have stressed out some of its capabilities. I concluded by giving perspectives of future updates beyond the current `v2.1`. Finally, Chapter 4 represented the bulk of this thesis manuscript. In this Chapter, I have presented the up-to-date status of the constraints on PBHs, linked to their possible signatures on astronomical observations and with a particular focus on HR signals and the ability of PBHs to be a candidate to the missing DM. Then, I exposed in details the constraints on PBHs from their HR I obtained with `BlackHawk`. These were of 5 kinds:

1. precise constraints on SBHs with the `BlackHawk` tool `Isatis`: I showed that despite good resolution of the observations and a complete theory of HR, the constraints on PBHs in the asteroid mass range suffer from dramatic uncertainties;

2. γ-ray constraints on PBHs with an extended mass distribution and a non-zero spin: I showed how the PHL is modified in this case to close part of the remaining mass window for all DM into PBHs;

3. DR emitted by light PBHs evaporating before BBN: I showed that the future CMB-S4 experiment will be very sensitive to spinning PBHs with monochromatic or extended spin distributions;

4. DM produced by PBHs evaporating before BBN: I showed that recovering the correct abundance of DM in this case requires some fine-tuning and is constrained by the fact that PDM would be warm and alter structure formation, the scenario of BHD being totally excluded;

5. constraints on non-standard PBHs: I computed the GC constraints for polymerized PBHs from LQG and showed that these are reduced in the case of heuristically high quantum deformation parameter, opening a new window on HR studies.

Finally, I give in the Appendix B the results of one study on inhomogeneous BBN signatures possibly linked to PBH formation that relies on the public code `AlterBBN`, and of two studies on putative planetary-mass PBHs and their gravitational capture by stellar systems with the example of the Planet 9 search.

The release of `BlackHawk` has re-kindled interest for PBH constraints from their HR, as shown by the list of publications given in Appendix A.2. People are now using precise computation of the HR rates and other numerical codes are released (CosmoLED, ULYSSES). The launching of new instruments to observe the CMB, the MeV sky and the low and high GW frequency bands will provide even more data to explore the DM PBH scenario.

General ideas. The study described in the present manuscript is based on a tremendous number of assumptions. The most evident ones are the SM of particle physics and the standard cosmology history. Both are well tested against observations but still lack complete explanation of all the phenomena. This points towards a necessitated exceedance of these fundamental theories. The failure to unify the fundamental interactions with gravity in a quantum theory of general relativity calls for more theoretical work.

A far more trivial assumption is the very existence of *primordial* BHs, and of the HR process. There are indeed observational data that strongly suggest the existence of BHs of various masses (supermassive and stellar), and the "missing mass" problem seems not to reduce with accumulating evidence. However, *not a single observation requires the existence of PBHs in any mass range*; and *there is no direct detection of HR from a BH*. Hence, for now, the study of HR by PBHs is at the same level as PDM theories, that is, it is not based on empirical data. Probing the confirmed BHs for their faint HR phenomenon is a huge (but necessary) technical challenge.

While performing the bibliography for the review article [8] on PBH HR constraints, I have seen to what extent the search for PBHs or new particles as DM have fluctuated and followed *trends* as much as *empirical observations*. Nowadays, the PDM community is far more numerous than the PBH one, which is immediately proven by the fact that most of the recent PBH constraints on HR are just more or less refined adaptations of existing PDM studies. That fact leads me to follow the path drawn by Peebles, which tries to examine the history of ideas in cosmology with a totally empirical point of view. Let me cite a 1972 paper by Peebles about BHs [662]:

> *Are there in astrophysics phenomena that call for more than "classical" physics – Newtonian gravitation plus atomic and particle physics and special relativity? Are there in astrophysics collapsed objects [...] where gravitational potential is large, [...] so that on the usual understanding space curvature ought to play a central rôle? [...] Astronomers must try to deduce properties of complex systems from schematic and confused observations. The inability to experiment in astronomy may be offset to some extent by the chance to observe diverse systems, yet clearly in any particular case we are wide open to romantic, if not false, interpretation. [...] I hope this orderly presentation of ideas and references does not give the impression that there is some sort of consensus on where or how to find collapsed objects. There is none, and indeed it would be madness to have a consensus before we have an object.* [662]

The PBH theories are completely heuristic, and following Peebles' concluding sentence "there can be no conclusions until we find a black hole", that I can extend to the present discussion by stating that there can be no conclusions until we observe *directly* the Hawking evaporation of a single PBH. Other conclusions would depart from empiricism and reduce to ideology.

Let me finish with some general ideas about physics. The fact that I have participated in the development of a public code has sensitized me to the problematic of open science. Most papers' results are not reproducible if the authors do not give the numerical recipes used to compute them. It is distressing to observe that some numerical tools are still "private" in the sense that authors will not provide their source. I hope that the present generation of researchers will not follow that competitive pathway.

On a broader point of view, new astronomy and particle physics data are obtained thanks to instruments that are always bigger (and more expensive). Even theorists rely on computing programs that run on distant servers. First, these instruments and supercomputers require the extraction and the consumption of a great amount of resources. Most of these are absolutely not sustainable, and will probably run dry by the end of the century. Furthermore, the research community travels a lot, taking the plane very often to go to conferences and visit foreign laboratories (I did so myself twice during my thesis). While this may enhance the scientific production, which I doubt regarding the publication rate during the ongoing Covid crisis, there should be restrictions on the mobility of researchers based on the most polluting transport means. Second, and this is a direct cause of the first point, there is no democratic control of the way of production of scientific knowledge, by which I mean that *people*, and not public institutions or private companies, never have to discuss if the construction of this or that billion-euro instrument should be done. This is deeply linked to the fact that in order to protect academic liberty, which is under attack even in France due to reactionary ideology and private interests, the research community is an *inter se*. It seems to me that if people were to decide from scratch what research should be done, worth of extracting non-sustainable mineral resources and burning ever more fossil fuel, they would chose 1) medical research, 2) ecology/climate studies and 3) well-being/human sciences. Even if fundamental research discoveries could be associated with the progress of human knowledge, access to it is reserved to an elite. On the other hand, the glorification of research with industrial outcome confines to propaganda; while astronomy and particle physics with heavy instrumental facilities are sciences of a privileged industrial society in an infinite resource world, which we are definitely not.

Appendix A

BlackHawk supplementary material

A.1 Using BlackHawk

BlackHawk can be downloaded freely on the website:

https://blackhawk.hepforge.org

The compilation of BlackHawk has been tested on Linux, Mac and Windows (using Cygwin64) distributions. The code is written in C99 standard. To compile the code, simply cd into the main directory and type:[1]

```
>>> make BlackHawk_*
```

where * denotes tot or inst. This will create a library file libblackhawk.a and an executable file BlackHawk_*.x. The compiler and compilation flags can be modified in Makefile if needed. To run the code, cd to the main directory and type:[2]

```
>>> ./BlackHawk_*.x parameter_file
```

where parameter_file is the name of a parameter file (*e.g.* parameters.txt for the pre-built one). To compile only the library, just cd into the main directory and type:

```
>>> make
```

The BlackHawk authors can be reached by e-mail and will gladly answer any code-related question.

[1] In case of problems of memory size at compilation, editing src/include.h and commenting #define HARDTABLES can solve the problem at the price of a longer execution time.

[2] In case of memory problem at execution, increasing the stack size with the command ulimit -s unlimited can help solving the problem.

A.2 Publications that use BlackHawk

Pub.	date	topic	version	extended	spin	nstd-part	nstd-BH	tables
[236]*	10/06/19	KBH	1.0		✓			✓
[514]*	11/06/19	EGXB	1.0	✓	✓			
[437]	24/06/19	GC/$e^{\pm}$	1.0	✓				
[503]	24/06/19	EGXB	1.0					
[411]	02/12/19	511 keV/ν	1.0	✓	✓			
[513]	01/04/20	GC	1.1					
[170]	15/05/20	EGXB/HDBH	1.2				✓	
[663]*	04/06/20	P9	1.2		✓			
[664]	11/07/20	GC/$e^{\pm}$	1.2	✓				
[443]	15/07/20	LeoT/$e^{\pm}$	1.2					
[444]	24/09/20	LeoT/$e^{\pm}$	1.2		✓			
[255]	09/10/20	GC/Hazma	1.2					
[413]	29/10/20	ν	1.2					
[360]	22/11/20	BBN	1.2	✓				
[665]	16/12/20	Earth/Sun	1.2					
[25]*	17/12/20	WDM	1.2/2.0			✓		
[505]	25/01/21	EGXB/GC	1.2					
[507]	12/02/21	EGXB/GC	1.2	✓	✓			
[445]	23/03/21	ISM/$e^{\pm}$	1.2	✓				
[595]	24/03/21	WDM	1.2/2.0		✓	✓		
[504]	07/04/21	EGXB/$e^{\pm}$	1.2	✓	✓			
[584]*	08/04/21	$\Delta N_{\rm eff}$	1.2/2.0	✓	✓			
[471]	21/05/21	FB/DM	1.2			✓		✓
[515]	24/05/21	PS	1.2					
[414]	04/06/21	ν	1.2					
[412]	09/06/21	ν	1.2	✓	✓			
[138]	30/06/21	DM	1.2			✓		✓
[390]	05/07/21	21 cm	1.2					
[150]*	07/07/21	nstd-BH/GC	1.2/2.0				✓	
[398]	26/07/21	21 cm	1.2		✓			
[634]	27/07/21	DM	1.2			✓		
[566]	31/07/21	GC	2.0					
[631]	12/08/21	ν/DM	2.0					
[397]	30/08/21	21 cm	2.0	✓	✓			
[666]	08/09/21	RetII/$e^{\pm}$	2.0					
[216]	20/09/21	FB/RNBH	2.0				✓	

Table A.1: List of the publications using `BlackHawk`. See Table A.2.

Pub.	date	topic	version	extended	spin	nstd-part	nstd-BH	tables
[506]	07/10/21	EGXB	2.0		✓			
[257]	11/10/21	FB/ν	2.0		✓			
[509]	22/10/21	EGXB	2.0		✓			
[251]	20/12/21	LT	2.1	✓				✓
[391]	20/12/21	21 cm	2.1		✓			
[667]	29/12/21	EGXB	2.1					
[510]	31/12/21	EGXB/GC/$e^{\pm}$	2.1					
[262]*	04/01/22	Isatis	2.1					
[171]	27/01/22	HDBH	2.1				✓	✓
[668]	09/02/22	GC	2.1					✓
[508]	15/02/22	GC/$e^{\pm}$	2.1					
[252]	11/03/22	LT	2.1	✓				✓
[632]	28/03/22	DM	2.1			✓		
[415]	28/03/22	ν	2.1	✓				
[633]	31/03/22	DM	2.1			✓		
[8]	06/06/22	review	2.1	✓	✓	✓	✓	

Table A.2: List of the publications using BlackHawk. Publications with an asterisk [X]* are those in which I was involved; it is difficult to associate them with a precise version of BlackHawk as I am constantly modifying the source. **Header:** Pub. = Publication, date = DD/MM/YY, version = BlackHawk, extended = PBH distributions, spin = KBHs, nstd-part = non-standard particles, nstd-BH = non-standard BHs, tables = use of the numerical tables of BlackHawk. **Bulk:** PS = point source, FB = final burst, LT = lifetime.

Appendix B

Other work

B.1 Inhomogeneous Big Bang Nucleosynthesis

[1]The BBN success described in Section 4.1.2.3 is based on the fundamental assumption that the production of light elements is homogeneous in the early universe, such that their abundance can be deduced from observation of some remote (ancient) or chemically stable locations. However, the same models that predict fluctuations on small scales that give rise to PBHs also predict that BBN could be inhomogeneous. Here, I evaluate abundance anomalies generated in patches of the universe where the baryon-to-photon ratio was locally enhanced by possibly many orders of magnitude in the range $\eta = 10^{-10} - 10^{-1}$. This study is motivated by the possible survival of rare dense regions in the early universe, the most extreme of which, above a critical threshold, collapsed to form PBHs. If this occurred, one may expect there to also be a significant population of early-forming stars that formed in similar but sub-threshold patches. A range of element abundance signatures is derived by performing BBN simulations at high values of η that may be detectable in any surviving first generation stars of around a solar mass. These predictions apply to metal-poor galactic halo stars, to old globular star clusters and to dwarf galaxies, and are compared with observations in each of these cases.

B.1.1 General paradigm

BBN is a fundamental probe of the first few minutes of the universe. Strong constraints are set on the physics of the early universe [81]. Both the baryon density and possible deviations in the number of relativistic species from the standard value are severely constrained, especially in the light of the Planck data on the (CMB) fluctuations [346]. There are however persistent anomalies, including the primordial ^{7}Li abundance [670] and possible indications of ^{4}He and other light element discrepancies that are presumably due to as yet unresolved issues in stellar evolution modelling [671].

One needs to carefully test the homogeneity of BBN, which is one of the fundamental assumptions of standard BBN. Here I evaluate abundance anomalies generated in patches of the universe where η was locally enhanced by possibly many orders of magnitude. Such regions are commonly thought to derive from primordial isocurvature perturbations, where the initial baryon-to-photon ratio is considerably enhanced relative to the standard model. These overdense regions might have later formed stars that retained a memory of inhomogeneous BBN.

Here I explore further the inhomogeneous BBN signatures for extreme values of $\eta = 10^{-10} - 10^{-1}$ motivated by PBH formation, on the grounds that fluctuations below the density threshold on the horizon scale to form a PBH [672] could still form rare stars, or even anti-stars, at very early epochs; but I retain only baryon density fluctuations with positive η over a very broad range. Previous studies, following the pioneering work by Wagoner *et al.* [352–354], were limited to probing only a restricted range in $\eta \lesssim 10^{-3}$ [673–675]. It will be demonstrated that exotic abundance signatures, most notably produced by rapid neutron capture in rare core-collapse supernovae (SNe) or binary neutron star mergers [676–679], may also contain a possible tracer of inhomogeneous BBN as predicted in [680]. These r-process abundances are observed to be enhanced in metal-poor halo

[1]This Section is based on the paper "Stellar signatures of inhomogeneous big bang nucleosynthesis" [669] I wrote with A. Arbey and J. Silk. It benefited from the `AlterBBN` update in which I was involved [246].

stellar populations [681] and in metal-poor dwarf galaxies [682], where Ref. [669] argues that exotic BBN signatures may also be hidden.

Rare patches of the universe may have initially had extremely high baryon-to-photon ratios. This is motivated by the possibility that rare large amplitude primordial isocurvature perturbations with an extremely blue spectrum and with residual power on stellar mass-scales were present in the very early universe. These fluctuations may have been responsible for PBH formation over a variety of horizon masses, the natural scale for PBH formation. Extreme isocurvature fluctuations, admittedly on somewhat smaller scales, provide, for example, the primordial intermediate mass BHs needed to seed the observed SMBHs [683]. Indeed some (or even all) SMBHs themselves could plausibly be primordial and would have naturally formed at the BBN epoch, when the horizon enclosed $\sim 10^9\,M_\odot$. The DM window for PBHs remains open at much lower PBH masses. The inhomogeneous regions that are invoked here could equally be the tail of the mass distribution that generated much smaller PBHs at a correspondingly earlier epoch.

The PBH hypothesis has an important consequence. For any plausible initial conditions, one is likely to have many un-collapsed isocurvature fluctuations ("failed" PBHs). These will have late epoch signatures. One is GW production, possibly observable as a stochastic background [684]. A second consequence is that there are implications for the epoch of BBN, when the universe may be inhomogeneous on scales comparable to those of the hypothesized PBH masses, albeit admittedly in rare patches. Such patches are rare for two reasons: firstly standard BBN is a great success and limits on inhomogeneity on horizon patches are $\lesssim 17\%$, expressed in terms of $\Delta\eta$ [685]; secondly, the universe at BBN epoch is highly radiation-dominated, and the associated PBHs must be subdominant by a factor of at least $(1+z_{\rm BBN})/(1+z_{\rm eq}) \sim 10^4$ [33].

Now BBN of neutron-capture elements in high η patches occurred at an epoch $t \sim 10^3\,$s when the baryon content of the horizon is around $10^4\,{\rm M}_\odot$. This gives the natural (minimum) scale of the patches of high η that is hypothesised as inhomogeneous sites of BBN. It is not a large step to imagine that such inhomogeneities may occur on the scales of the smallest dwarf galaxies or star clusters at the epoch of first star formation, once $\rm H_{II}$ cooling develops at $z \sim 10-20$. These are the scales on which one may search for signatures of inhomogeneous BBN.

Let's define the degree of inhomogeneity that is considered. At BBN, the required baryon overdensity of an isocurvature fluctuation is at least $(1+z_{\rm BBN})/(1+z_{\rm eq}) \sim 10^5\,\eta_0$ where the standard value of the baryon-to-photon ratio is $\eta_0 = (6.104 \pm 0.058) \times 10^{-10}$ [346]. In this study, the range $\eta = 1 - 10^9\,\eta_0$ is explored. It will be shown that the most interesting region for possible abundance signatures is at relatively high η, a range that has not previously been explored in any detail.

Should evidence for stellar mass PBHs be confirmed, it will be argued that there is a strong case for searching for stellar relics that are in effect failed PBHs. These can be distinguished from Pop III stellar survivors by the unique abundance signatures that are found below. Note that recent simulations of the mass function of Pop III, long considered to be massive stars of $\sim 100-1000\,M_\odot$, demonstrate that ongoing fragmentation to below a solar mass can indeed occur [686].

Any such imprints will also result in inhomogeneous BBN, surviving on similar mass scales that have not collapsed—being sub-threshold—but would be greatly diluted by the present epoch because of mass mixing on galactic scales, stellar evolution, stellar mass loss and baryonic circulation in the

ISM. However initial signals could still survive as anomalous primordial abundances and be visible in a small fraction of the oldest stars, in the galactic halo and in the oldest, most metal-poor dwarf galaxies.

The baryon-to-photon ratio $\eta \equiv n_{\rm b}/n_\gamma$, while tightly constrained by the CMB data in homogeneous BBN to be $\eta = (6.104 \pm 0.058) \times 10^{-10}$ [346], can take on a wide range of values. Signatures of a high-η value include elevated ^{4}He abundances and trace amounts of exotic elements normally produced in stars but possibly overproduced in nonstandard BBN. Rare patches of inhomogeneity in η at the epoch of BBN can have late-time stellar signatures once mixing occurs on galactic scales. Recall that the baryon content within the particle horizon at the onset of BBN is only $\sim 100\,M_\odot$. If sufficiently anomalous in terms of rare elements produced by extremely high η BBN is localized to rare patches, late formation of stars may reflect contamination by unusual abundance patterns.

A prime motivation for such extremely inhomogeneous BBN comes from the fact that the existence of PBHs is most plausibly explained by extreme but rare isocurvature fluctuations generated in an Affleck–Dine-like early phase transition associated with baryogenesis [687]. Such an early phase transition even allows the sign of the baryon-to-photon ratio to be inverted. Indeed PBHs have formed in patches with positive or negative baryon number. An extreme signature of such an effect would be provided by inhomogeneous BBN in patches where η changes sign. If they survived to the present epoch, such patches of antimatter could later form anti-stars, distinguishable by their abundance patterns as contaminated by the unusual local BBN history. The present BBN predictions are independent of the sign of η, and apply equally to any relic anti-stars. Anti-stars have long been advocated by Dolgov and collaborators [52, 688, 689] in the context of baryon number fluctuations generated by an early universe first order phase transition. Arguments based on measurement of cosmic ray antihelium nuclei by AMS-02 have recently been put forward [690] to motivate such a scenario.

B.1.2 Numerical methods

When the baryon-to-photon ratio reaches high values, one expects heavy elements to form in appreciable quantities compared to standard BBN where only the light elements have a detectable final abundance. As one does not know *a priori* at which atomic number A the nuclear grid should be stopped, the full REACLIB grid [691] is considered for the nuclear chains. BBN calculations rely one the public code `AlterBBN` [245, 246] which allows the user to compute the abundances of the elements in standard and alternative cosmological scenarios and which was recently updated [246]—*e.g.* to include the REACLIB database for nuclear reactions and to reach $\eta \sim \mathcal{O}(1)$ with an acceptable precision. As explained in Section 4.1.2.3, numerous public (and private) codes have been used in the last decades to increase the predictive power of BBN on alternative, *e.g.* PBH, cosmologies.[2]

A first `AlterBBN` computation was performed for $\eta = 10^{-15} - 10^{1}$ using the full nuclear grid. The nuclei that do not play a significant role in the BBN evolution at large η were identified, and removed from the grid; *i.e.* nuclei whose abundance relative to hydrogen did not exceed a lower cutoff of 10^{-12} at any time during BBN computation and for all η values in the considered range.

[2] I refer the reader to the conference of C. Pitrou for a recent review in the framework of the TOOLS 2020 conference.

In this way the number of nuclei was reduced from several thousands to ~ 800. It was also checked that the abundances of these ~ 800 nuclei where unchanged when performing a BBN computation with this subset of nuclei only. Then, in the remaining nuclei, those for which the abundance is at least $[X]/[H] \gtrsim 10^{-10}$ for some value of η were identified. This led to a final set of 132 nuclei (corresponding to 54 chemical elements) for which the abundances are presented here.[3] The numerical methods needed to compute the abundances of such a great number of nuclei—from H to ^{250}Cf—converge slowly (see [246] for details about these methods). In addition the results for $\eta \gtrsim 0.1$ are difficult to interpret because of the unclear numerical errors, and in the following the discussion is restricted to $\eta < 0.1$.

B.1.3 Results and comparisons with observations

B.1.3.1 Comparison with solar abundances

First, I compare the data obtained with `AlterBBN` at high-η with the solar abundances of Asplund *et al.* [692]. When η is larger than the standard BBN value $\eta_0 \sim 6 \times 10^{-10}$, I find that groups of elements in addition to He are overproduced compared to the solar abundances. Throughout this paper, abundances are given in the standard stellar physics form: if I consider element X then

$$[\mathrm{X}] \equiv \log_{10}\left(\frac{n(\mathrm{X})}{n(\mathrm{H})}\right) + 12\,, \tag{B.1}$$

where $n(\mathrm{X})$ (respectively $n(\mathrm{H})$) is the number density of X nuclei (respectively hydrogen ^{1}H). Fig. B.1 shows that when $\eta = 10^{-4}$, the overproduced elements have $Z \sim 60$, while when $\eta = 10^{-1}$ the overproduction concerns $Z \sim 25$, with a continuous evolution between these extreme values. When η is smaller than 10^{-5} no heavy elements ($Z \gtrsim 10$) are produced. These results are comparable to those of Refs. [673–675], even if in the latter references the computations were limited to $\eta \lesssim 10^{-3}$ and used a less complete set of nuclei. The shift between high-Z r-process elements for $\eta \lesssim 10^{-3}$ and lower Z p-process elements for $\eta \gtrsim 10^{-3}$ is described in [673] and results from an efficient active proton capture that prevents synthesis of heavier elements due to Coulomb barrier effects. The competition between the expansion rate that is modified in high-η regions due to local MD and the nuclear rate can also contribute to this shift.

The purpose is now to compare the predicted high η signatures of inhomogeneous BBN with the abundance signatures in the oldest stellar systems, where the first generations of stars may have retained anomalies even if greatly diluted by mixing at dwarf galaxy scales. As discussed below, mixing was incomplete in r-process enhanced ultra metal-poor dSphs such as Reticulum II and Tucana III, and signatures of inhomogeneous BBN might conceivably have survived.

B.1.3.2 High helium abundance and globular clusters

I focus here on the ^{4}He abundance in globular star clusters. There is a long history of helium abundance determinations in these systems. The original motivation was that the oldest stars in

[3] The full sets of data—both reduced and not reduced—in the form of numerical tables and a file containing plots of the reduced data were provided as supplemental material to this article.

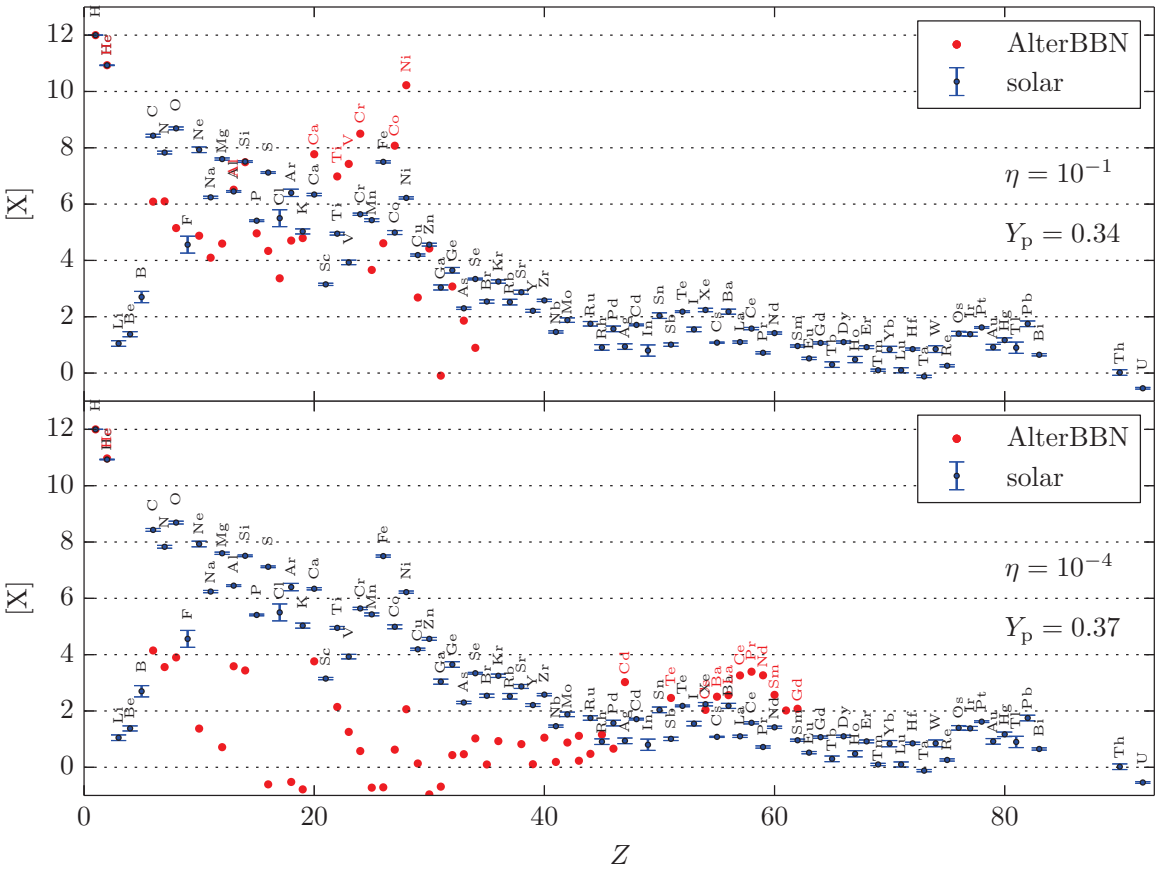

Figure B.1: Abundances of the elements for fixed values of $\eta = \{10^{-1}, 10^{-4}\}$ corresponding to $Y_p = \{0.34, 0.37\}$ computed by `AlterBBN` (red dots) and compared to solar abundances of [692] (blue dots, when available). The names of overproduced elements compared to solar abundances are written in red. See text for the definition of the [X] notation. [taken from [669]]

the galaxies could provide clues for the primordial abundance. It was soon realized that the initial helium abundance affects several aspects of the evolution of globular cluster stars, including the red giant and horizontal branch populations [693]. White dwarf properties are also affected [694].

Helium over-abundances by as much as $\Delta Y_p = 0.1$ have been reported in massive globular clusters such as ωCentauri [695] (see also [696] and references therein) and have more recently been shown to be correlated with abundance indicators of multiple stellar populations in globular clusters [697]. Second generation recycling provides a means of enhancing the primordial helium abundance [698].

To summarise, there are observational indications of enhanced helium in certain old stars. This

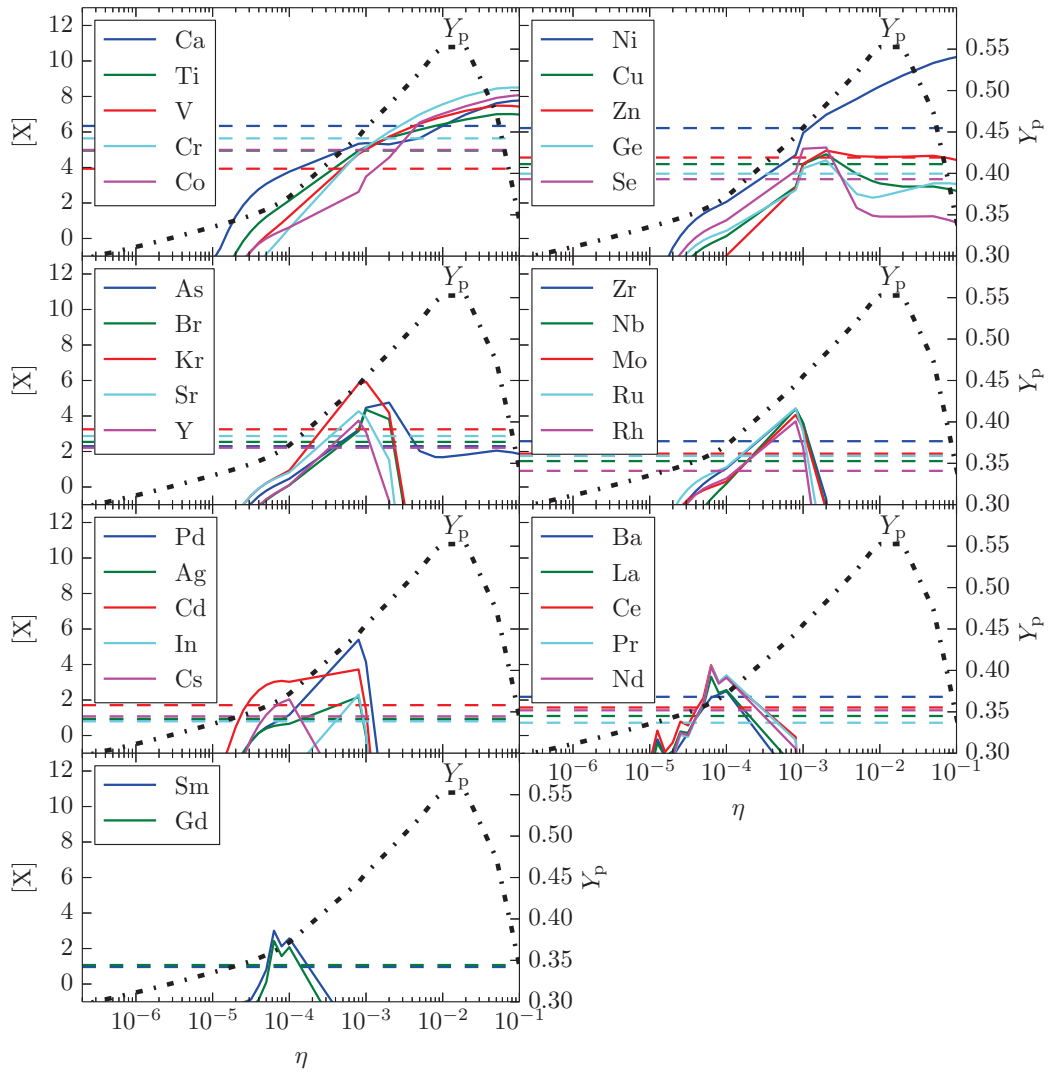

Figure B.2: Abundance of nuclei computed by `AlterBBN` (plain curves) and compared to solar abundances of [692] (dashed curves, the error bars fit within their width). The Y_p abundance is shown as a dashed-dotted black line. In this figure I have retained only the elements (sorted by their atomic number Z) whose abundance exceeds the solar abundance somewhere in the η range where $Y_p \gtrsim 0.3$. [taken from [669]]

is most likely due to mixing and evolutionary issues, and is expected to mask any possible primordial component. However should there be any surviving primordial abundance anomalies, they should be correlated in the same way that multiple population chromosome mapping has been performed in globular clusters [699].

The hope is that the primordial inhomogeneous η values indicative of a possible helium enhancement may reveal other abundance anomalies that are now discussed. With this program for evaluating high η signatures I have indeed confirmed that there is a range of η for which the ^{4}He abundance is enhanced, namely $0.3 \lesssim Y_{\rm p} \lesssim 0.5$, corresponding to $10^{-7} \lesssim \eta \lesssim 10^{-1}$, as can be seen on Fig. B.2. While a little overproduction of ^{4}He occurs at $\eta \lesssim 10^{-7}$, it is not accompanied by the production of heavy elements.

This η range of enhanced ^{4}He corresponds to an overproduction (compared to solar values) of a variety of heavier elements, continuously dispersed in the range $A = 40 - 141$ ($Z = 20 - 59$). I plot in Fig. B.2 the predictions of the abundances of the elements (when summed upon their various isotopes) in the range of η where the ^{4}He abundance is $Y_{\rm p} \gtrsim 0.3$. I restricted the plots to elements for which the abundance is larger than the solar abundance for some values of η.

Very high values of $\eta \gtrsim 10^{-3}$ are associated with an overproduction of elements in the iron group $Z \sim 25$ (see also the upper panel of Fig. B.1) while somewhat lower values of the baryon-to-photon ratio $\eta \sim 10^{-4}$ are associated with an overproduction of neutron-capture elements in the $Z \sim 60$ region (see also the lower panel of Fig. B.1), some of which usually associated with r-process enhancement like barium and strontium (*e.g.* [700]).

B.1.4 Comparison with metal-poor stars in the Galactic halo

The Galactic halo has proven to provide a remarkable environment for studying the oldest stars in the universe and for deciphering their evolution by chemical tagging [704]. It is possible that such stars may contain signatures, hitherto overlooked, of high η patches in the early universe that survived on the scales of the smallest dwarf galaxies, the oldest galaxies in the universe. Many of these systems later hierarchically merged into the halos of galaxies such as the Milky Way where they account for the enhanced r-process features observed for $2-4\%$ of metal-poor halo stars [705].

The distinguishing characteristic of these metal-poor halo stars is that α/Fe and other chemical signatures monitor the role of short time-scale core-collapse SNe enrichment [706]. Hence they are a natural laboratory for our proposed signature of inhomogeneous BBN.

In this Section, I compare the abundances obtained with `AlterBBN` at high η to some observed abundances in distant metal-poor stars [701] (see Fig. B.3, blue dashed areas). One finds that elements like Ni, Cr, Ca and Si, which are rare products in metal-poor (population II) stars, are produced in great quantities in the high-η BBN scenario. This could give hints of observable signatures in distant metal-poor stars. Normal stellar thermonuclear fusion and non-standard high-η BBN do not give the same chemical products. In principle, these differences could also be used as a distinguishing characteristic of inhomogeneous BBN.

B.1.5 Comparison with metal-poor stars in dwarf spheroidal and ultrafaint galaxies

DSphs galaxies are most likely the oldest stellar systems in the universe, and the ultrafaint dSphs have metal-poor components that formed at least 10 Gyr ago and are enriched in r-process elements by some currently uncertain combination of core-collapse supernovae and neutron star mergers, with the latter contribution ranging from essentially all [676] to some [677] or only a minor fraction [679].

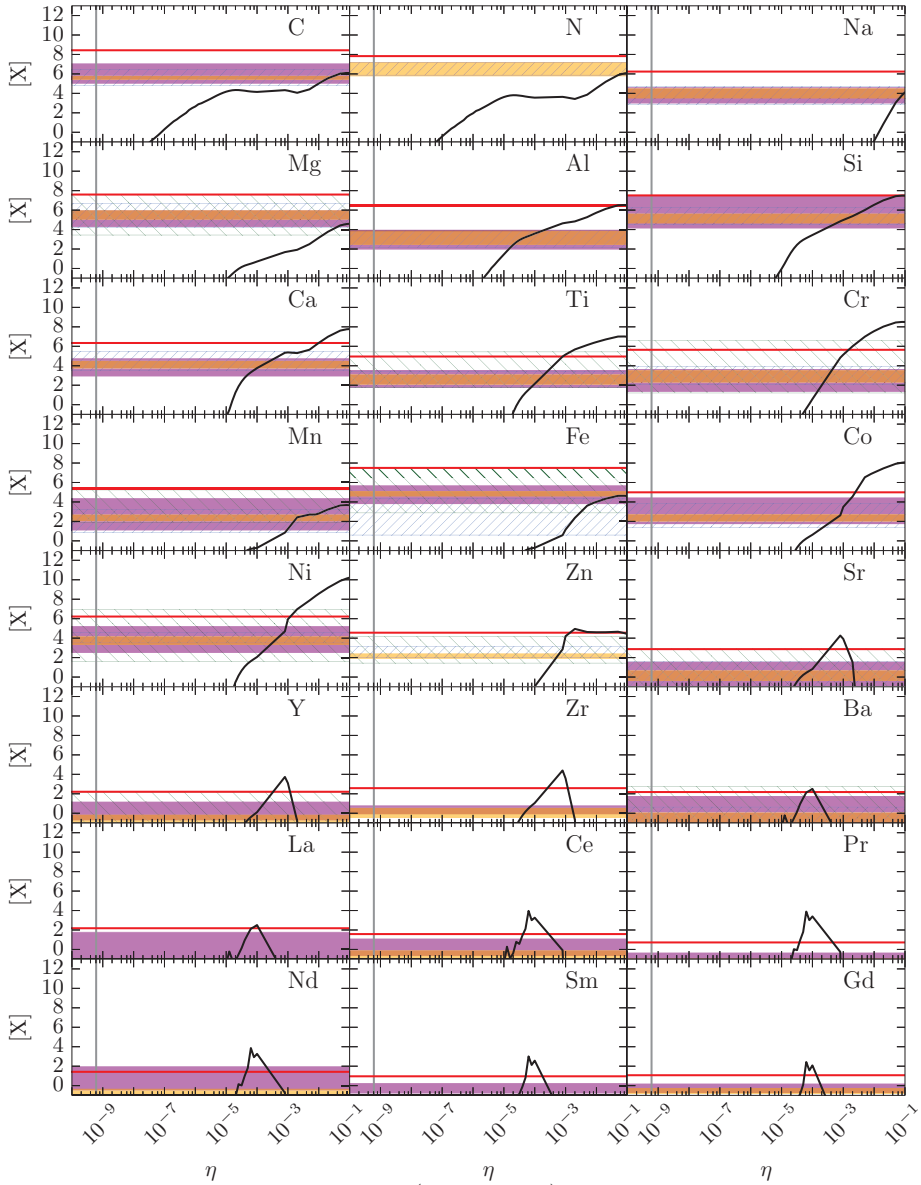

Figure B.3: Comparison of `AlterBBN` data (black lines) as functions of η with 1σ data from metal-poor halo stars [701] (blue dashed areas), dSph faint galaxies [702] (green dashed areas), and two r-process enhanced dwarf galaxies: Reticulum II [700] (purple areas) and Tucana III [703] (orange areas) while the red lines are the solar abundances [692]. The grey vertical line is the standard BBN 1σ value for $\eta = (6.140 \pm 0.058) \times 10^{-10}$ [346]. *Error bars are smaller than the lines.* [taken from [669]]

The core-collapse supernovae contribute on a time-scale of $\sim 10^8$ yr while neutron star mergers on a much longer time-scale comparable to that of SNIa Fe enrichment of $\sim 4 \times 10^9$ yr [707]. Such a delayed bimodal enrichment history allows the possibility that some stars, the prompt-forming, extremely metal-poor component, avoided late enrichment, and any exotic primordial BBN signatures would be, at least relatively, chemically undiluted.

In this Section, I compare the predicted inhomogeneous BBN data with the abundances recently measured in 12 dSphs or faint galaxies [702] (see Fig. B.3, green dashed areas). The Reticulum II galaxy was extracted from their data because it is treated separately, see below. One remarks that several elements could be detectable at $\eta \gtrsim 10^{-5}$, including Co, Ni, Sr, Y, Zr, Ce, Pr, Nd, Sm, Gd. The present model predicts relative abundance excesses for these at fixed values of η, which may well of course be diluted by mixing of r-process chemical enrichment.

In particular, the nearby ultra-faint dwarf galaxies Reticulum II and Tucana III are fascinating laboratories for studying the evolution of and enrichment by the first stars in the universe. Unlike typical dwarfs, their r-process history demonstrates a lack of complete mixing of supernovae ejecta with the ambient gas in their early gas-rich phase as compared to most other dwarfs [708]. In Fig. B.3 I highlight the comparison of abundances obtained with `AlterBBN` at high η to metal-poor stars observed in the dwarf galaxy Reticulum II [700] (purple areas) and in Tucana III [703] (orange areas). In these galaxies, which are highly DM-dominated, there are hints of an enrichment in r-process elements which in the absence of the most established astrophysical explanation, namely neutron star binaries [709], could possibly correspond to a primordial component. A test of this would be to look for neutron-capture signatures that anti-correlate with the most common r-process product, europium, and that is relatively un-enhanced in the inhomogeneous BBN models,[4] as highlighted in Fig. B.4. Europium suffers from an observable bias due to its very low abundance in metal-poor stars, unless it is enhanced as in Reticulum II or Tucana III, thus the comparison between different metal-poor stars populations may be flawed.

B.1.6 Conclusion

While the horizon size is of order $10^5\, M_\odot$ at the onset of BBN, when the neutron abundance is frozen in at an epoch of $T \sim 1$ MeV, Ref. [33] notes that extreme curvature fluctuations on horizon scales could form rare PBHs in this mass range provided the initial conditions are highly non-Gaussian, so that extreme perturbations that affect BBN only occur in rare inhomogeneous patches of the universe. Such scales are important as they provide PBHs of masses that are capable of seeding SMBHs observed at $z \lesssim 10$, when such seeding may be needed [683], and even could simultaneously accelerate galaxy formation. It is argued that a corollary is the possible but rare neutron-capture signatures in the oldest stars.

If sufficiently anomalous in terms of rare elements, the much later formation of stars in these regions may reflect primordial contamination by unusual abundance patterns. Of course this depends on the possible effects of radiation damping, not significant for isocurvature fluctuations, and of gas mixing throughout galactic evolution. Hence Ref. [669] suggests looking at either extremely

[4] I had to specifically extract the europium data from the complete set of `AlterBBN` data since its abundance does not exceed the lower cut-offs that had been set.

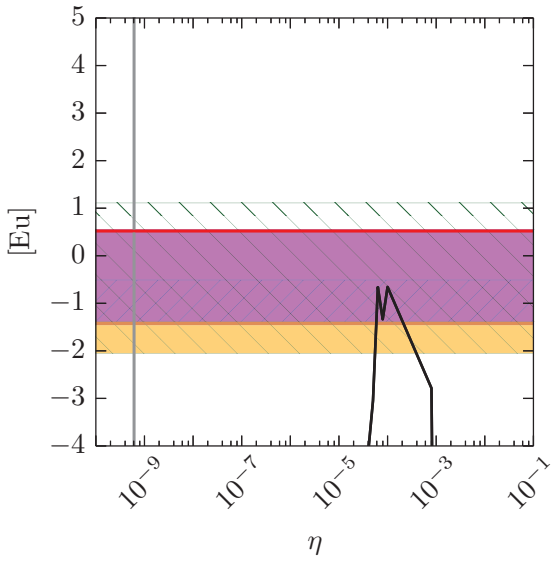

Figure B.4: Comparison of `AlterBBN` Europium abundance (black line, summed over the isotopes) as a function of η with metal-poor halo stars data [701] (blue dashed areas), dwarf spheroidal faint galaxies data [702] (green dashed areas), and two r-process enhanced dwarf galaxies data: Reticulum II [700] (purple areas) and Tucana III [703] (orange areas). I also represent the 1σ spread of the data. The solar abundance [692] is indicated as a red line. The standard BBN 1σ value for $\eta = (6.140 \pm 0.058) \times 10^{-10}$ [346] is represented as a grey vertical line. The error bars are smaller than the width of the lines. [taken from [669]]

metal-poor components of dwarf galaxies, which have mostly not undergone mergers, or the halo stars that most likely formed in now-merged dwarf building blocks.

Any r-process enhancement is a signature of inefficient mixing at the epoch of the events, whether core-collapse SNe or neutron star mergers, that sourced the r-process elements. Hence we suggest targeting the metal-poor dwarf spheroidals Reticulum II and Tucana III as ideal candidates for our proposed signatures. These DM-dominated galaxies are also compelling targets for PBH direct detection [443, 444, 666], which could further advocate this model.

Another test of the present hypothesis would be to look for neutron-capture signatures that anti-correlate with the most common r-process product, europium, which is relatively un-enhanced in this inhomogeneous BBN model, compared to other neutron-capture elements.

I finally mention that Ref. [710], which appeared after the present study, discusses quantitatively the mixing of elements produced in inhomogeneous BBN and concludes that if inhomogeneity remained limited on sub-horizon scales, element diffusion should have diluted any local inhomogeneity. It proves however that be the inhomogeneity super-horizon scaled, then the inhomogeneity could have survived on stellar formation scales.

B.2 Planet-mass primordial black holes

B.2.1 What if Planet 9 is a PBH?

[5]Concordant evidence points towards the existence of a ninth planet in the Solar System at more than 400 AU from the Sun. In particular, trans-Neptunian object (TNO) orbits are perturbed by the presence of a putative gravitational source. Since this planet has not yet been observationally found with conventional telescope research, it has been argued that it could be a dark compact object, namely a BH of probably primordial origin.

Within this assumption, I discuss here the possibility of detecting Planet 9 via a sub-relativistic spacecraft fly-by and the measure of its HR in the radio band and conclude that it is too faint compared to the CMB. I thus present other perspectives with rather a satellite mission and conclude that smaller BHs would give much more interesting signals. I emphasize the importance of the study of such HR laboratories in the Solar System.

Perturbations of orbits of known objects in the Solar System have led astronomers to search for gravitational sources from which they originate, under the form of unknown planets. After the discovery of Neptune in 1846, no more planets were found beyond dwarf planets such as Pluto or Eris. However concordant evidence have recently appeared in direction of what has been a proofless obsession for many astronomers: the existence of Planet 9, which may become an object under even more intense scrutiny. The apparent clustering of TNO orbits in the Kuiper belt suggests the presence of a massive body of a mass $M \sim 5 - 10\,M_\oplus$ orbiting between 300 and 1000 AU [711–714]. Even though the statistics of clustered TNOs is not sufficient to robustly exclude coincidental observations [715], the probability of accidental correlations is $\lesssim 1\%$ [716]. The parameters of this hypothetical Planet 9 are further constrained by ephemeride measurements such as those of Cassini [717, 718].

In spite of telescope searches, no new object has been found in the sky to be Planet 9 [719–721]. Ref. [722] thus suggests that Planet 9 may be a compact dark object, invisible to telescopes—namely, a BH. A BH with such a light mass certainly points towards a non-stellar origin because of the TOV limit (see however [300]); this BH could be one of the putative PBHs. The fraction of DM under the form of PBHs is expected to be $f_{\rm PBH} \sim 0.1{-}0.01$ in the Planet 9 mass region [28]. No confirmed PBH has been observed yet, but OGLE has recently found PBH candidates in microlensing events [273] whose masses would correspond to the mass of Planet 9, and their mergers may be detectable in future GW experiments [723, 724]. Thus, it is plausible to consider that if a population of terrestrial mass PBHs exists, one of them could have been captured by the Sun gravity and could be orbiting beyond Neptune, providing an explanation for the "invisible" body responsible for the gravitational anomalies of TNOs.

Successively, two experiments have been proposed to detect Planet 9 if it were a BH (hereafter called P9). Both are based on ideas similar to the Breakthrough Starshot proposal,[6] in which it is proposed to send a fleet of very small spacecrafts ($m \sim$ g$-$kg) at sub-relativistic speeds ($v \sim 0.001\,c$) in different directions of the sky to reach nearby stars in order to study their planetary systems

[5]This Section is based on the paper "Detecting Planet 9 via Hawking radiation" [663] I wrote with A. Arbey.
[6]https://breakthroughinitiatives.org/Initiative/3

and achieve the most distant explorations ever [725]. The advantage is that such light and fast spacecrafts would reach the orbit of an eventual P9 in a few years. By sending many of those across the sky towards the hypothetical location of P9 orbit, one gets a chance that one of them experiences a fly-by of P9. The first proposal is to measure the time delay in the line of sight trajectory of a given spacecraft (hereafter called SC0 for spacecraft 0, the discoverer), induced by the presence of a nearby massive body [726]. This would necessitate an on-board precision clock to measure a $\sim 10^{-5}$ s time delay over a one year trajectory. The second proposal is to measure the transverse inclination of the trajectory of SC0 induced by the presence of P9 [727]. This alleviates the on-board clock problem but necessitates a $\sim 10^{-9}$ rad angular displacement measurement, which could be achievable with VLBI for example. However, in Ref. [728] the authors examined the environment in which SC0 would travel to reach the orbit of P9 and concluded that the interstellar medium turbulence—drag and magnetic fields—would make the precise gravitation-perturbed trajectory measurements cited above impossible to achieve due to noise signals from unknown medium local properties.

There also exists a completely different approach to P9 detection proposed in [729], based on the fact that icy objects of the Oort cloud would get disrupted by the P9 gravitational field and the accretion of such material could cause flares detectable by the LSST survey [730]. A few of such events could occur per year, making them detectable. In addition, it would prove the BH nature of P9, and solve the trajectory difficulties of the sub-relativistic spacecrafts described in [728]. The continuous search for TNOs also continues, and the DES collaboration claims that they would be able to detect many more of them, among which more clustered TNOs pleading in favor of P9, if not P9 itself [731, 732].

Here I suggest a new proposal, based on the fact that P9, if it is indeed a BH, will emit HR. Thus even if P9 is not visible from the Earth (not being a reflective planet but a BH), it would still emit a small amount of radiation. This was already considered in the original paper about the BH nature of P9 [722] but the authors concluded that the amount of HR was too small to be detectable *from Earth*, which is true. What is considered here is the detection of this very HR by the flying-by SC0, *in the vicinity* of P9, as described below. This would be of particular importance since, even if rather well theoretically motivated, HR has not yet been observed. HR by smaller BHs results in constraints on their abundance but not yet in detection signals, despite the intense search for their final burst (see Section 4.1.2.8). As a further motivation, the precise spectrum of HR may contain information on the quantum structure of BH horizons (see *e.g.* Section 4.6). Therefore directly observing a BH HR would be of great importance, and a PBH in our Solar System would represent the best laboratory to study it.

B.2.1.1 Setup

The setup of the experiment would be the following. SC0 passes by P9 at speed v and with impact parameter b. Let's define $t = 0$ to be the time of minimal approach. When SC0 approaches P9, the radiation flux will increase, reach maximum at $t = 0$ and then decrease. Since sub-relativistic velocities are considered, the Doppler effect is negligible. The spatial displacements considered in [726–728] have however to be taken into account as an uncertainty on the precise trajectory of the ship. I neglect them for the moment and consider an ideal straight line trajectory for SC0.

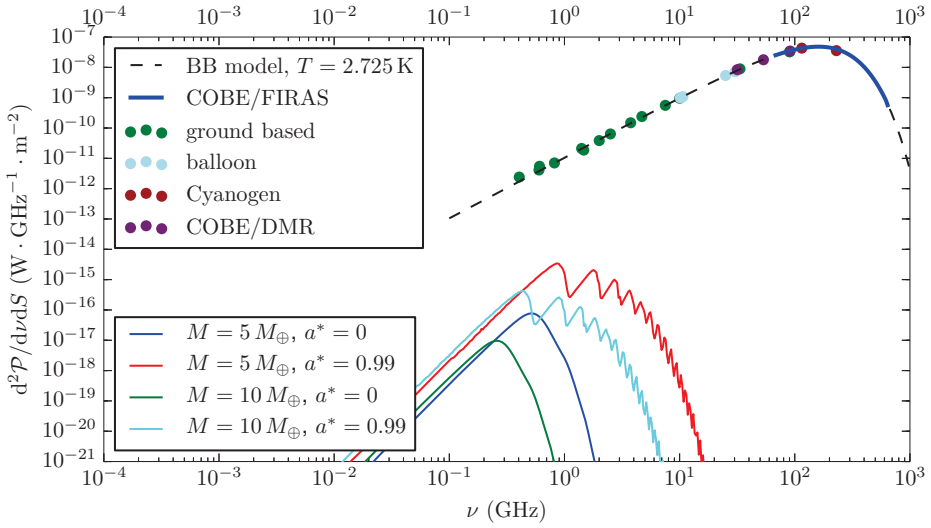

Figure B.5: Total power emission of photons by P9 as a function of frequency for different values of the P9 parameters $M = \{5, 10\}M_\oplus$ and $a^* = \{0, 0.99\}$ (bottom solid lines). The CMB spectrum is also shown for comparison, as measured by different instruments [733] (dots and thick blue line) and with a blackbody model fit with temperature $T = 2.725\,\mathrm{K}$ (dashed black line). [taken from [663]]

P9 has a super-terrestrial mass $M_{\mathrm{P9}} \sim 5 - 10\,M_\oplus$, thus its peak EM emission frequency lies around the GHz radio band. One does not have any indication of P9 dimensionless spin a^*; as a PBH it is expected to have a negligible spin but it has been shown that transient matter-domination era at the end of inflation can produce high-spin PBHs that can conserve their spin until today despite Hawking evaporation (see Section 2.7). In Fig. B.5 the power emission per horizon area unit

$$\frac{\mathrm{d}^2\mathcal{P}}{\mathrm{d}\nu\mathrm{d}S} = \frac{1}{4\pi r_{\mathrm{S}}^2} E \frac{\mathrm{d}^2 N}{\mathrm{d}t\mathrm{d}\nu}\,, \tag{B.2}$$

is shown as a function of frequency for different P9 masses and spins, where $\mathrm{d}^2N/\mathrm{d}t\mathrm{d}\nu$ is the number of photons emitted by HR per units of time and *frequency*. One clearly sees that the low-mass high-spin setup is favored by detection because it implies more energetic and abundant emission. In this figure I also show the CMB spectrum which is very well approximated by a blackbody radiation

$$\frac{\mathrm{d}^2\mathcal{P}_{\mathrm{CMB}}}{\mathrm{d}\nu\mathrm{d}S} = \frac{8\pi\nu^3}{e^{E/T_{\mathrm{CMB}}} - 1}\,, \tag{B.3}$$

with temperature $T_{\mathrm{CMB}} = 2.725\,\mathrm{K}$ [253]. The comparison with the CMB intensity in the HR energy range shows that even in the most favorable case, P9 radiation represents $\sim 0.1 - 1\%$ of the CMB intensity, a difficulty that will be discussed below. Indeed, a PBH with mass $M \sim 5\,M_\oplus$ has a temperature of $T \sim 2 \times 10^{-3}\,T_{\mathrm{CMB}}$, therefore its HR is subdominant compared to the CMB, and

it is generally believed that the PBH would then *accrete* ambient radiation rather than emit it, as dictated by the 2nd law of thermodynamics.

Let's consider that the Solar sail of the Breakthrough Starshot-like spacecrafts is used as a radio antenna in the GHz band, with a surface area of $\mathcal{S} \sim \mathrm{m}^2$ [725]. As Breakthrough Starshot already considers very large sails, it is natural to imagine a way to use these sails as on-board detectors to perform EM measurements. This would require to adapt the sail technology to implement GHz photon collecting, a possible challenge as the sails have to be extremely thin and light for solar propulsion into such small spacecrafts. The power received by the ship, if its sail is considered perpendicular to its trajectory, is then of the form

$$\mathcal{P}(t) = \eta \frac{S(t)}{4\pi r(t)^2} \int_0^{+\infty} E Q_\gamma \, \mathrm{d}E \,, \tag{B.4}$$

where the energy integral covers the radio GHz band, $r(t)$ is the distance between SC0 and P9 and $S(t)$ is the area of the sail projected in the direction of P9. Here Q_γ is the number of photons emitted per units of time and energy given in Eq. (2.147). The emission rates of particles by evaporating BHs are computed with `BlackHawk`. The efficiency coefficient η corresponding to the absorption of the sail is considered in Eq. (B.4) for completeness, but since I do not make any assumption on the material or technology, I do not have an estimation of it; in any case it has to be maximized. Finally I assume the sail to be perpendicular to the direction of motion for simplicity, but I note that there probably exists more optimized geometries to maximize the power received during a fly-by while keeping a sufficient acceleration via laser propulsion technology [725].

Ideal straight line trajectory. I geometrically compute $S(t)$ and $r(t)$ by defining α as the angle between SC0 velocity $\mathbf{v}$ and position $\mathbf{r}$ relative to the origin at P9, and consider that the (one dimensional) sides of an area A have lengths of the order $\sqrt{A}$. I obtain

$$\cos\alpha = \frac{\sqrt{S(t)}}{\sqrt{\mathcal{S}}} \iff S(t) = \cos^2\alpha \mathcal{S} \,, \tag{B.5}$$

and

$$\tan\alpha = \frac{b - \sqrt{\mathcal{S}}}{|r^*(t)|} \,, \tag{B.6}$$

where the $-\sqrt{\mathcal{S}}$ term comes from the definition of b which is the distance between P9 and the *center* of the solar sail. This factor can be safely neglected. Thus the projected area is

$$S(t) = \cos\left[\arctan\left(\frac{b - \sqrt{\mathcal{S}}}{|r^*(t)|}\right)\right]^2 \mathcal{S} \,, \tag{B.7}$$

where $r^*(t) = vt$ is the distance to minimal approach in the straight trajectory approximation and $r(t) = \sqrt{r^*(t)^2 + b^2}$. One sees that even if the distance is minimal at $(t = 0,\, r^*(t) = 0,\, r(t) = b)$, the projection of the flux on the sail is zero at this point. Thus one expects a peak feature in the time-dependent radio signal with a discontinuity at $t = 0$.

Perturbed trajectory. If the kinetic energy carried by SC0 becomes comparable to the gravitational potential energy of P9, then a gravitational perturbation of the trajectory is expected, *i.e.* for

$$E_{\rm kin} \sim E_{\rm pot} \iff \frac{1}{2}mv^2 \sim \frac{GMm}{r} \iff r \sim \frac{2GM}{v^2}\,. \tag{B.8}$$

Considering the speed and mass at stake here, it occurs when $b \lesssim 100\,{\rm km}$. The trajectory will be deviated as given in [727, 728] because of the time build-up of small shifts, but this will occur at timescales much larger than this fly-by detection time. However, if the impact parameter becomes very small, the full trajectory needs to be taken into account to predict the form of the signal. This can be done by taking again the geometrical definitions given in the previous section and redefining an effective instantaneous (at time t) impact parameter $\overline{b}(t)$ and effective instantaneous distance to the minimal approach point $\overline{r}^*(t)$, which could be seen as the geometric quantities obtained in case SC0 were to continue in a straight line from time t. Thus, the $\overline{\alpha}(t)$ angle is the angle between the instantaneous velocity and position vectors

$$\cos\overline{\alpha} = \frac{\mathbf{v}\cdot\mathbf{r}}{vr}\,, \tag{B.9}$$

and the perturbed quantities to be considered in the area projection formula in Eq. (B.7) are

$$\overline{b} = r\sin\overline{\alpha}\,, \quad \text{and} \quad \overline{r}^* = r\cos\overline{\alpha}\,. \tag{B.10}$$

Results. The expressions (B.4) and (B.7) (with ideal or perturbed geometrical quantities) allow to compute the light curve received by SC0 as it passes by P9. A test result is shown in Fig. B.6. The main aspect of this test signal is that it is symmetrical, making the detection easier with respect to the background. Doppler effect would make it asymmetrical but due to the sub-relativistic speed it has negligible effects in the present analysis. One can extract the parameters from the signal by using the following approximation, which is valid far from the minimal approach position $vt \gg b$

$$\mathcal{P}(t) = \frac{S(t)}{4\pi r(t)^2}\int_0^{+\infty} E\frac{{\rm d}^2N}{{\rm d}t{\rm d}E} \equiv \frac{S(t)}{4\pi r(t)^2}\mathcal{P}_0 \approx \frac{\mathcal{P}_0\mathcal{S}}{4\pi}\frac{1}{(vt)^2}\left(1-2\left(\frac{b}{vt}\right)^2\right), \tag{B.11}$$

as can be seen in Fig. B.6. This approximation is valid in the straight line trajectory approximation, which is a good approximation as shown below. In Fig. B.7 I show the light curves for different setups as summarized in Table B.1. According to Eq. (B.11) one has to draw the detection signal with a rescaled time

$$t_0 = \left(\frac{3\times10^4\,{\rm m}}{b}\right){\rm s}\,, \tag{B.12}$$

in order to display all signals of Fig. B.7 in the same plot. Only in the favourable setup 1, one gets an order of magnitude for the radio signal that is comparable with the currently most precise (Earth-based) detection tools. For example, the project Breakthrough Listen[7] aims at detecting

[7] https://breakthroughinitiatives.org/initiative/1

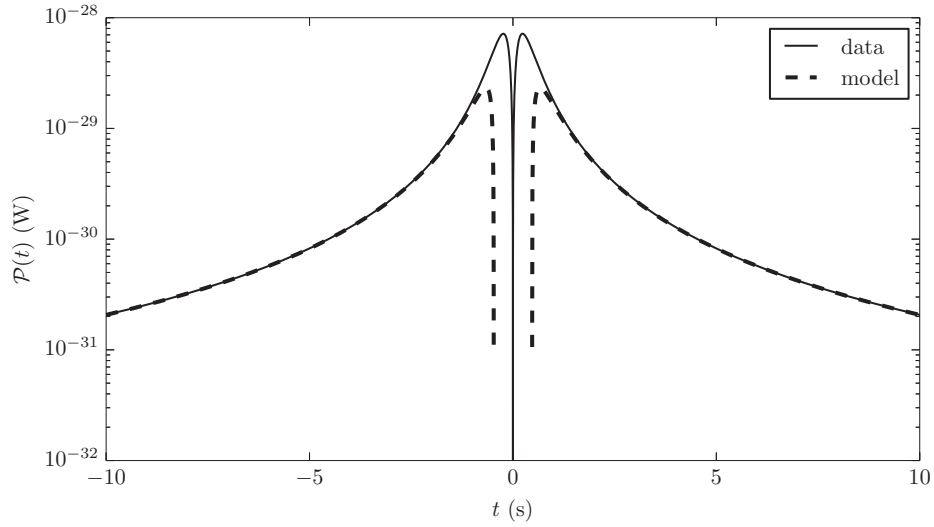

Figure B.6: Example of a light curve for a speed $v = 0.001\,c$, impact parameter $b = 10^3\,\mathrm{m}$, sail area $\mathcal{S} = 1\,\mathrm{m}^2$, and P9 parameters $M = 5\,M_\oplus$ and $a^* = 0$ (solid line). The approximation of Eq. (B.11) leads to the dashed line. [taken from [663]]

setup	M	a^*	b	$\mathcal{S}$
setup 1	$5\,M_\oplus$	0.99	$10^5\,\mathrm{m}$	$100\,\mathrm{m}^2$
setup 2	$5\,M_\oplus$	0	$10^6\,\mathrm{m}$	$10\,\mathrm{m}^2$
setup 3	$10\,M_\oplus$	0	1 AU	$1\,\mathrm{m}^2$

Table B.1: Parameters of the P9 and SC0 setups used in Fig. B.7.

GHz signals from nearby stars to search for artificial signals as hints of advanced civilizations. Ref. [734] claims a minimal flux detection of $7.14 \times 10^{-26}\,\mathrm{W{\cdot}m^{-2}}$ using the Green Bank Telescope—a 100 m diameter collecting antenna [735]. I do not expect the signal extraction from ambient noise to be any more difficult in P9 neighbourhood than on Earth. In Fig. B.7 I show also the results with the exact trajectory calculations taking into account the gravitational well of P9. One sees that for the considered setups the effect is very small.

P9 mass M affects the energy of emission and thus its power. The resulting signal is proportional to the inverse of the mass squared (temperature squared). The degeneracy in mass is small for P9, hence one expects a $\mathcal{O}(10)$ factor at best when going from higher masses to lower masses as permitted by current constraints. P9 spin a^* affects the emission rate and the power received, and Fig. 2.14 shows that the signal can be enhanced by a factor of $\mathcal{O}(100)$ for photons when the spin is near extremal. The signal reception is proportional to the sail area $\mathcal{S}$, so multiplying the area by $\mathcal{O}(10)$ gives an amplification factor of $\mathcal{O}(100)$. The impact parameter b fixes the minimum distance $r(t)$

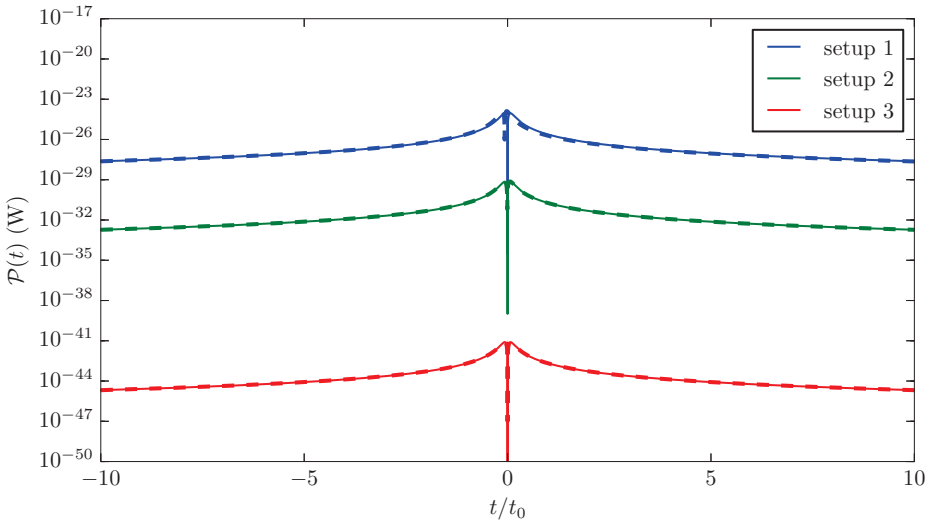

Figure B.7: Radio signals received by SC0 for different setups with parameters given in Table B.1. Both the ideal straight trajectories (plain lines) and the fully perturbed trajectories (dashed lines) are displayed. [taken from [663]]

that can be achieved, so the peak result is inversely proportional to b^2. The impact parameter on the other hand is a highly random parameter, which depends on the density of spacecrafts launched in the direction of the orbit of P9.

This fly-by scenario would be a totally independent and EM based mean of detection of P9 if it were a BH. However, as has been shown in this Section, the CMB intensity is much larger than the HR intensity in the considered energy range. In setup 1, the most favorable scenario considered here, this represents a signal-to-CMB ratio of $\sim 10^{-10}$, which is even smaller than the CMB fluctuations. Thus it seems unrealistic to detect P9 during a fly-by with this method. However, I show in the next Section that the same method can be used to search for lighter PBHs.

B.2.1.2 Other perspectives

Observation by a satellite. Optimizations of proposals presented in [726, 727], while taking into account the trajectory shifts estimated in [728], or proposal [729], may lead to a drastic reduction in the possible sky localization of P9 along its already constrained orbit. Therefore, it will be of utmost importance to send a mission orbiting P9, or at least to try to achieve the closest possible fly-by for a radio mission as described in this work. HR would be the only direct measurement of the presence of P9, gravitational perturbations being only indirect evidence. The *in situ* measure of radio emission will give access to the form and properties of the BH horizon, thus giving exciting prospects for BH and fundamental physics. In case of satellization of a spacecraft around P9,

Fig. B.8 shows the radio flux F as a function of the orbit radius r

$$F = \frac{1}{4\pi r^2} \int_0^{+\infty} EQ_\gamma \, \mathrm{d}E \,. \tag{B.13}$$

A satellized mission would offer the possibility to extensively study the EM emission of P9 if it were a BH. For example, one could imagine a directional parabolic antenna focused on the BH localization to reduce the impact of the CMB background, which will in addition be reduced by the screening due to the BH "shadow". This requires to reach high-precision focus of the order of the wavelength ($\sim$ cm) at more than a hundred kilometers. It would then be achievable to distinguish the shadow of the BH on the CMB background, making it an indirect observation of P9. The long-exposure measure of this shadow as the spacecraft orbits P9 should be compared with the numerically predictable shadow on a constant CMB background, and then a radio signal coming out of the center of the shadow could be searched for. One can also imagine a mission constituted of two spacecrafts, one of which acting as a CMB shield screening the background and aligned with P9 and the antenna on the opposite location on the orbit. Then a signal received from P9 would constitute a direct measurement of its genuine emission. Very recently, Ref. [736] thoroughly examined for the first time what would be the "picture" of a BH taken by a detector sensitive to its HR. They calculate the two-point correlation function $\langle X_1, X_2 \rangle$ of the signal received by two independent receptors and reconstruct the BH "image" by interferometry—Fourier transform of $\langle X_1, X_2 \rangle$. It is shown in this paper that highly spinning KBHs would exhibit rather different pictures compared to SBHs.

Another direct probe of the presence of such a heavy BH via HR is the emission of GWs: if the graviton is indeed a fundamental particle, it can be expected to be emitted by HR. It has already been conjectured that graviton emission by PBH evaporation in the primordial universe could constitute a stochastic background carrying information on the first seconds after the Big Bang. The detection of this high-frequency background remains a technical challenge. The amount of GWs emitted by present day BHs is again usually considered too low to be detectable *from Earth*. If one were to put spacecrafts in orbit around P9, search for such gravitational waves would be of utmost importance to probe the existence and properties of the graviton, constituting a portal to quantum gravity. In Fig. B.9 I show the density of GHz GWs that such a satellite would receive as a function of its orbit radius

$$\Omega_{\mathrm{GW}} = \frac{1}{c\rho_{\mathrm{c}}} \left(\frac{H_0}{100\,\mathrm{km}\cdot\mathrm{s}^{-1}\cdot\mathrm{Mpc}^{-1}} \right)^2 \frac{1}{4\pi r^2} \int_0^{+\infty} EQ_{\mathrm{G}} \, \mathrm{d}E \,, \tag{B.14}$$

where c is the speed of light, $\rho_{\mathrm{c}} \approx 8.523 \times 10^{-30}\,\mathrm{g{\cdot}cm^{-3}}$ is the critical density and $H_0 \equiv h \times (100\,\mathrm{km}\cdot \mathrm{s}^{-1}\cdot\mathrm{Mpc}^{-1})$ with $h \approx 0.67$ the reduced Hubble parameter [253]. Since it would constitute a constant signal, extraction from the noise may be easy. One sees from Fig. B.9 that a high P9 spin increases the amplitude of GWs by 4 orders of magnitude (see Fig. 2.14). The SNR is however complicated to forecast since no GW detector has for now explored the GHz domain.

Lighter PBHs. One can extrapolate the present discussion to lighter BHs that could have been captured by the gravitational field of the Sun (see Section B.2.2 below).[8] A $\sim 0.01\,M_\oplus$ body of

[8] Ref. [737] recently conducted a study of the possibility of PBH-Earth collision in this framework.

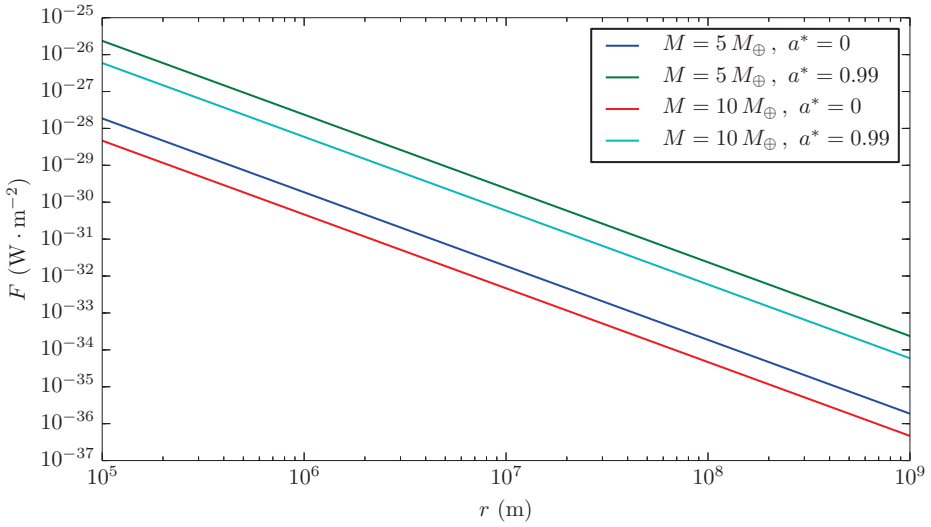

Figure B.8: Radio flux as a function of orbit radius for different P9 masses $M = \{5, 10\}M_\oplus$ and spins $a^* = \{0, 0.99\}$. [taken from [663]]

the mass of Mercury would emit in the same band of energy and with an intensity close to the CMB, because its temperature is $T \sim T_{\rm CMB}$, making its putative detectability much easier. In Fig. B.10 I show the same emissivity as in Fig. B.5 but for lighter PBHs. The energy range of the emission lies in the CMB peak at $\sim 2.7\,$K, but the emissivity is higher than the CMB one for PBHs with mass $M \lesssim 10^{-2}\,M_\oplus$. There is no evidence of such light hidden bodies in the outer Solar System, contrarily to the P9 gravitational perturbations, but the expected perturbations would be too small to be detected by TNOs orbits clustering. During the last years, several light bodies have been discovered in the outer Kuiper belt: Eris, Haumea, MakeMake... showing that a large population of such objects can exist beyond Neptune's orbit. However, the fraction of DM that these objects can represent is more tightly constrained by microlensing than terrestrial mass objects, with a fraction $f \lesssim 1\%$ [28]. A satellized mission around one of those objects as described above may lead to the first direct measurement of HR, thus allowing comparisons with models alternative to the seminal Hawking prediction.

B.2.1.3 Conclusion

In this exploratory work I have proposed a new way to probe the presence of a hypothetical Planet 9 in the outer Solar System if it were actually a black hole, by using a Breakthrough Starshot-like fleet of nano-spacecrafts. Considering the difficulties of measuring tiny longitudinal or transverse displacements that P9 would induce on a spacecraft during a fly-by, mostly related to the fact that trajectory perturbations arising from the interstellar medium would be of the same order, Ref. [663] proposes to measure *in situ* the HR emitted by P9 in the form of GHz radio photons. This method

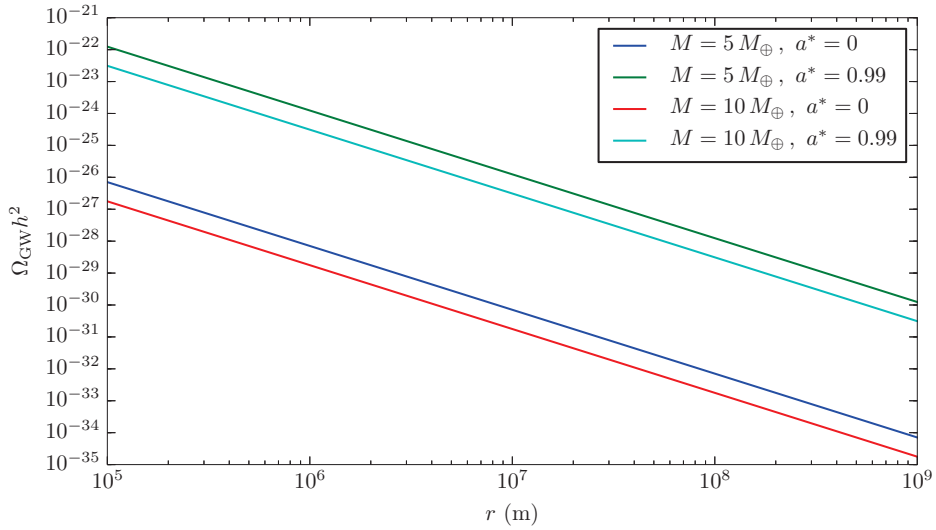

Figure B.9: GWs density as a function of orbit radius for different P9 masses $M = \{5, 10\}M_\oplus$ and spins $a^* = \{0, 0.99\}$. [taken from [663]]

has two main advantages, first it is not affected by the trajectory noise because it only relies on classical on-board EM detection, second it would be a unique occasion to measure and thus prove the existence of HR, a long-standing prediction of BH thermodynamics. The principal difficulty is to measure a very faint signal in the radio GHz band, with an amplitude inversely proportional to the square of the impact parameter b, therefore requiring either great luck or a multitude of spacecrafts in order to reach a fly-by of P9 at $\sim 100\,\text{km}$ distance, or the use of an extremely precise radio detection technology. Furthermore, it seems unrealistic to extract this faint signal from the dominant CMB contribution during a fly-by mission. Nevertheless, if P9 were indirectly localized using *e.g.* spacecraft trajectory measurements or LSST flares, an orbital mission would be of great importance to study the properties of BHs and HR, and would allow for more advanced measurement techniques, *e.g.* by screening the CMB and focusing an antenna on P9. Finally, I extrapolated the present discussion to lighter PBHs that could have been captured by the gravitational field of the Sun and concluded on the advantages of these configurations for the detection of HR, since their emissivity would be dominant as compared to the CMB.

I must add that I am very worried about the general direction taken by the small satellites technology. Their small size and simplicity has turned them into a common industrial product that can be launched in space by loads of more than a hundred. Some well-known societies, not to name them, have started programs to crowd the lower Earth orbits with small satellites, under the disguise of providing Internet to everyone. The link to a recent movie where this was used as a mean to control the entire population is spurious, but the impact on astronomical observations and

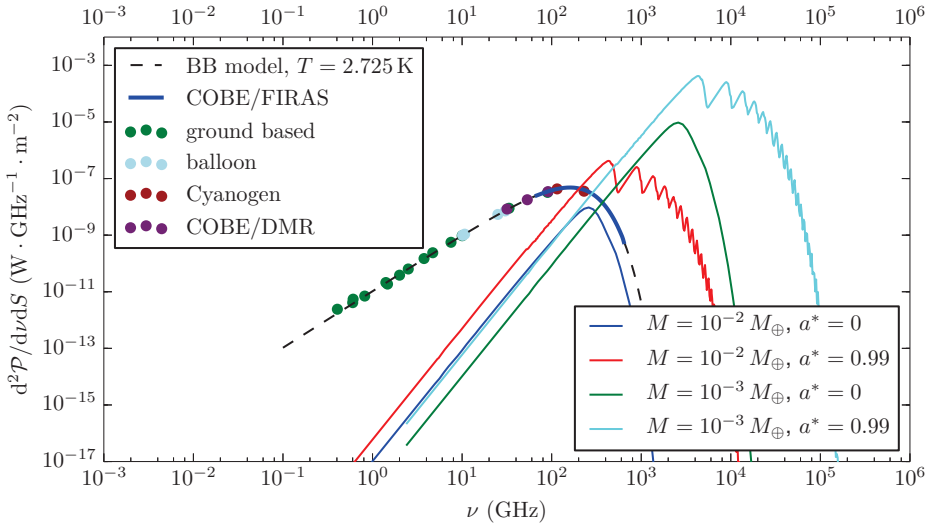

Figure B.10: Total power emission of photons by light PBHs as a function of frequency for different masses $M = \{10^{-3}, 10^{-2}\}M_\oplus$ and $a^* = \{0, 0.99\}$ (bottom solid lines). The CMB spectrum is the same as in Fig. B.5. [taken from [663]]

the risks of collision with more useful scientific satellite missions are dramatic [738–745].[9] These companies go deeper in megalomania as they receive investments from multinationals to deploy fleets of satellites that would display luminous advertisements on sky-scale. Some time ago, I was night-walking with companions, we had a look at the clear sky, and the first thing we saw was the Starlink trails. People around me were so dismayed, claiming that the night sky was stolen from them. Democratic control on these technologies is urgent. In that sense, I found with great interest the proposal of a "space environmentalism" [748] which states that as long as the human kind "uses" outer space for of its development, the latter should be protected by environmental laws.

B.2.2 Constraining the non planetary substellar objects abundance

[10]This small Section deals with direct observation of PBHs in planetary exosystems, through the possible existence of non planetary compact sub-stellar objects (CSSOs), such as BHs, but also non-standard objects such as boson stars (X-stars) in these systems. The challenge is to detect and

[9]The Nature paper [746] states that a "a mutually acceptable pathway for the development of this potentially rewarding family of technologies" is possible; while the other Nature publication [747] claims that "there are clearly real societal [...] benefits from enhanced communication systems and space-based data services"; to which I completely disagree.

[10]This Section is based on the research note "Constraining the non planetary substellar objects abundance" [749] I have published with A. Arbey and J. Schneider.

distinguish them from ordinary planets.[11] Here I present the new approach to this problem taken by Ref. [749], which consists in detecting directly these CSSOs using exoplanet searches by transits, RV measurements and astrometry and comparing the results to standard planet models.

On the one hand, Xstars [750–752] can have masses of the order of the Jupiter mass $M_{\rm Jup}$ with radii as low as a few meters [753]. On the other hand, sub-stellar mass BHs can only be primordial since the stellar collapse can only lead to $M \gtrsim M_\odot$ BHs (see however [300]). Even if they can evaporate via HR, the lifetime of a $1\,M_{\rm Jup}$ mass PBH is much larger than the age of the universe. PBHs would have at least two impacts: as a possible source of DM and as constraints on Big Bang models (see the reviews [28, 266]). Below, possible techniques for their direct detection are explored.

B.2.2.1 Methods to detect CSSOs

One can foresee four methods for the detection of CSSOs: transits, microlensing, radial velocity (RV) and astrometry. Direct optical detection is not realistic since these objects are not expected to emit visible light. For sub-stellar BHs a possibility would be to search for their HR. The latter would be so weak that it could be detected only for PBHs present in the Solar System (see above). I therefore explore the other claimed methods.

Microlensing. Microlensing gives only the mass of CSSOs and there is no way to make the distinction with an ordinary planet, unless it is transiting.

Transits. Transits give the radius of objects. When in addition the mass is given by RV and/or astrometry, one can compare the observed mass-radius with standard planet models. An odd mass-radius ($M-R$) relation would lead to a CSSO candidate.

In addition, a CSSO with a mass M would cause during transits around a star with radius R a gravitational amplification $A = (M/M_\odot)(R_\odot/R)^2 = 100$ for a $M = 10\,M_{\rm Jup}$ CSSO transiting a white dwarf of radius 7000 km [754].

One could argue that a CSSO can be surrounded by a large atmosphere leading to a standard $M-R$ relation. But it would then be surprising that for all objects their atmosphere is sufficiently large to mimic a standard planet. In the Solar System several objects have no atmosphere. Such atmosphere-less objects would have an odd $M-R$ relation compared to standard planet models and would make these objects CSSO candidates. Moreover, if the CSSO is indeed a PBH, it should not have formed at the same moment as the stellar system but rather have been dynamically captured by it. Thus, there is small chance that it can accrete an atmosphere sufficient to mimic a planet radius.

Direct imaging. Astrometry and RV can easily detect $0.003 - 100\,M_{\rm Jup}$ objects. But then, here again, the problem is to disentangle them from ordinary substellar objects. Ref. [749] therefore explores another strategy to constrain the number of CSSOs. It is proposed to constrain their abundance by the direct optical and near-IR search of substellar objects confirmed by RV and/or

[11] The same challenge exists in distinguishing low-mass BH binaries from neutron star mergers, in the absence of an EM counterpart [299].

astrometry. Presently, about 2000 of them are known and many more will be detected by Gaia [755]. Exoplanets known from RV and/or astrometry will be searched for in direct images with future ground based and space based projects. $0.003-100\,M_{\rm Jup}$ objects known from RV and/or astrometry will have, depending essentially on their distance, a flux predicted by planetary surface models. If the flux is not detected it will be a reasonable candidate for a CSSO. Again one could argue that a CSSO can be surrounded by a large atmosphere leading to a standard mass-spectrum relation; but it would then be surprising that for all objects the mass-spectrum relation exactly fits standard planet models.

B.2.2.2 Primordial black hole companion population

The estimation of the PBH companion population rests on two steps: the number of PBHs, and the fraction of them captured by stars.

Amount of PBHs and X-stars. The number of PBHs and/or X-stars of planetary mass in the present universe is constrained by microlensing surveys. In the Jupiter mass range, the tightest constraints are obtained by the microlensing events of OGLE [272, 273]. Some events could be interpreted as microlensing by free-floating planets, or conceivably PBHs, within the observational limit that these objects represent at most $\sim 1\%$ of the total DM density.

Fraction of PBHs and X-stars captured by stars. The rate of PBHs and/or X-stars capture by stars is estimated by [722] to be $\Gamma = \langle \sigma n v \rangle$ where the density is the local DM density $\rho_{\rm DM} \approx 0.4\,{\rm GeV\cdot cm^{-3}}$ (which depend on the Galactic halo model, see Section 4.2), such that $n = f_{\rm PBH}\rho_{\rm DM}/M$ for a monochromatic distribution. The velocity is the DM local radial velocity $v \approx 220\,{\rm km\cdot s^{-1}}$ and the cross section σ can be estimated by comparing the gravitational potential of the Sun with the kinetic energy of the compact object such as $GM/\sigma^{1/2} \sim v^2/2$, which gives [722]

$$\Gamma_{\rm PBH} = \langle \sigma n_{\rm PBH} v \rangle \sim \frac{4G^2 M_\odot^2 f_{\rm PBH}\rho_{\rm DM}}{v^3 M} \sim 10^{-17}\,{\rm s^{-1}} \times \left(\frac{f_{\rm PBH}}{0.01}\right) \times \left(\frac{220\,{\rm km\cdot s^{-1}}}{v}\right)^3 \times \left(\frac{M_\oplus}{M}\right). \tag{B.15}$$

Thus, following this very rough estimate, through the galactic history of $\sim 10\,{\rm Gyr}$, nearby stars would have captured ~ 2.5 PBHs of Earth mass $M_\oplus$, and a fraction $f \sim 1\%$ of stars would have captured a $M_{\rm Jup}$ mass PBH. However, for example, most of the simulations for Planet 9 capture are unsuccessful if it were a PBH are unsuccessful, or predict that it should be ejected away by dynamical effects from inside the system due to other planets or from outside the system due to fly-bys. Thus, depending on the structure and history of the exoplanet systems, stable CSSO capture could be very much improbable [756–758]. Finally, if the clustering of PBHs at formation were important (see *e.g.* [523]), PBHs could look like planetary mass objects when observed in microlensing events, while being in reality smaller objects individually. The capture rate inferred in the previous discussion is to be refined on many aspects with dynamical simulations.

B.2.2.3 Expectations from future direct imaging programmes

There are several future direct imaging programmes, with the goal to detect Earth-like planets and to expand the prolific catalog of exoplanets.[12] From the ground, there are three Extremely Large Telescope projects: GMT, TMT and E-ELT, but being not dedicated to exoplanet imaging, their yield will be modest. More promising are the HabEx and LUVOIR space projects. HabEx will detect at least 150 planets within 10 pc (see Fig. 3.3.5 of [759]) and LUVOIR about 700 planets (LUVOIR Team (2019) Fig. 1.6) within 30 pc (see Fig. 1.6 of [760]). If a known companion is not detected as expected, it will be a hint for either a PBH or an X-star.

A last speculation came to me following my earlier work with G. Laibe [761], that is the possible observation of distortions of the disk of dust and gas around nearby stars in which planetary systems are forming. Visible distortion by an off-plane CSSO orbit at a stage where no planet is formed yet would point towards exotic origin.

[12] http://exoplanet.eu

Bibliography

[1] P. J. E. Peebles, *Cosmology's Century: An Inside History of our Modern Understanding of the Universe* (2020).
[2] P. Peter and J. P. Uzan, *Cosmologie primordiale* (2012).
[3] M. L. Humason, N. U. Mayall, and A. R. Sandage, Redshifts and magnitudes of extragalactic nebulae., Astron. J. **61**, 97–162 (1956).
[4] P. W. Hodge, Humason, Mayall, & Sandage's Determination of the Hubble Expansion, Astrophys. J. **525C**, 713 (1999).
[5] S. Smith, The Mass of the Virgo Cluster, Astrophys. J. **83**, 23 (1936).
[6] H. Andernach and F. Zwicky, English and Spanish Translation of Zwicky's (1933) The Redshift of Extragalactic Nebulae, arXiv e-prints (2017), [Helv. Phys. Acta **6**, 110 (1933)], arXiv:1711.01693 [astro-ph.IM].
[7] G. Bertone and D. Hooper, History of dark matter, Rev. Mod. Phys. **90**, 045002 (2018), arXiv:1605.04909 [astro-ph.CO].
[8] J. Auffinger, Primordial black hole constraints with Hawking radiation, Prog. Part. Nucl. Phys. (2022), [to be published], arXiv:2206.02672 [astro-ph.CO].
[9] K. Schwarzschild, Über das Gravitationsfeld eines Massenpunktes nach der Einsteinschen Theorie, Sitzungsberichte der Königlich Preußischen Akademie der Wissenschaften (Berlin) , 189–196 (1916), [arxiv:physics/9905030 (1999)].
[10] K. Landsman, Singularities, Black Holes, and Cosmic Censorship: A Tribute to Roger Penrose, Found. Phys. **51**, 42 (2021), arXiv:2101.02687 [gr-qc].
[11] S. Van den Bergh, Collapsed Objects in Clusters of Galaxies, Nature **224**, 891 (1969).
[12] A. M. Wolfe and G. R. Burbidge, Black Holes in Elliptical Galaxies, Astrophys. J. **161**, 419 (1970).
[13] H. Reissner, Über die Eigengravitation des elektrischen Feldes nach der Einsteinschen Theorie, Annalen der Physik **355**, 106–120 (1916).
[14] G. Nordström, On the Energy of the Gravitation field in Einstein's Theory, Koninklijke Nederlandse Akademie van Wetenschappen Proceedings Series B Physical Sciences **20**, 1238–1245 (1918).
[15] R. P. Kerr, Gravitational Field of a Spinning Mass as an Example of Algebraically Special Metrics, Phys. Rev. Lett. **11**, 237–238 (1963).
[16] E. T. Newman and A. I. Janis, Note on the Kerr Spinning-Particle Metric, J. Math. Phys. **6**, 915–917 (1965).
[17] E. T. Newman, E. Couch, K. Chinnapared, A. Exton, A. Prakash, and R. Torrence, Metric of a Rotating, Charged Mass, J. Math. Phys. **6**, 918–919 (1965).
[18] R. C. Tolman, Static Solutions of Einstein's Field Equations for Spheres of Fluid, Phys. Rev. **55**, 364–373 (1939).
[19] J. R. Oppenheimer and G. M. Volkoff, On Massive Neutron Cores, Phys. Rev. **55**, 374–381 (1939).
[20] I. Bombaci, The maximum mass of a neutron star, Astron. Astrophys. **305**, 871 (1996).
[21] Y. B. Zel'dovich and I. D. Novikov, The Hypothesis of Cores Retarded during Expansion and the Hot Cosmological Model, Soviet Ast. **10**, 602 (1967), [Astron. Zh. **43**, 758 (1966)].
[22] I. D. Novikov, Delayed Explosion of a Part of the Fridman Universe and Quasars, Soviet Ast. **8**, 857

(1965), [Astron. Zh. **41**, 1075 (1964)].
[23] S. Hawking, Gravitationally collapsed objects of very low mass, Mon. Not. Roy. Astron. Soc. **152**, 75 (1971).
[24] B. J. Carr and S. W. Hawking, Black holes in the early Universe, Mon. Not. Roy. Astron. Soc. **168**, 399–416 (1974).
[25] J. Auffinger, I. Masina, and G. Orlando, Bounds on warm dark matter from Schwarzschild primordial black holes, Eur. Phys. J. Plus **136**, 261 (2021), arXiv:2012.09867 [hep-ph].
[26] D. K. Nadezhin, I. D. Novikov, and A. G. Polnarev, The hydrodynamics of primordial black hole formation, Soviet Ast. **22**, 129–138 (1978), [Astron. Zh. **55**, 216 (1978)].
[27] A. Escrivà, PBH Formation from Spherically Symmetric Hydrodynamical Perturbations: A Review, Universe **8**, 66 (2022), arXiv:2111.12693 [gr-qc].
[28] B. Carr, K. Kohri, Y. Sendouda, and J. Yokoyama, Constraints on primordial black holes, Rep. Prog. Phys. **84**, 116902 (2021), arXiv:2002.12778 [astro-ph.CO].
[29] Y. Akrami *et al.* (Planck), Planck 2018 results. X. Constraints on inflation, Astron. Astrophys. **641**, A10 (2020), arXiv:1807.06211 [astro-ph.CO].
[30] D. Baumann, Inflation, in *Physics of the Large and the Small: TASI 2009*, edited by C. Csaki and S. Dodelson (2011) pp. 523–686, arXiv:0907.5424 [hep-th] .
[31] K. Aoki, M. A. Gorji, S. Mizuno, and S. Mukohyama, Inflationary gravitational waves in consistent D $\to$ 4 Einstein-Gauss-Bonnet gravity, J. Cosmology Astropart. Phys. **2021**, 054 (2021), arXiv:2010.03973 [gr-qc].
[32] A. Bedroya and C. Vafa, Trans-Planckian Censorship and the Swampland, J. High Energy Phys. **2020**, 123 (2020), arXiv:1909.11063 [hep-th].
[33] B. Carr and J. Silk, Primordial black holes as generators of cosmic structures, Mon. Not. Roy. Astron. Soc. **478**, 3756–3775 (2018), arXiv:1801.00672 [astro-ph.CO].
[34] B. Carr, F. Kühnel, and L. Visinelli, Constraints on stupendously large black holes, Mon. Not. Roy. Astron. Soc. **501**, 2029–2043 (2021), arXiv:2008.08077 [astro-ph.CO].
[35] A. M. Green and B. J. Kavanagh, Primordial black holes as a dark matter candidate, J. Phys. G **48**, 043001 (2021), arXiv:2007.10722 [astro-ph.CO].
[36] S. W. Hawking, I. G. Moss, and J. M. Stewart, Bubble collisions in the very early universe, Phys. Rev. D **26**, 2681–2693 (1982).
[37] A. R. Liddle and A. M. Green, Cosmological constraints from primordial black holes., Phys. Rep. **307**, 125–131 (1998), arXiv:gr-qc/9804034 [gr-qc].
[38] A. G. Polnarev and M. Y. Khlopov, Cosmology, primordial black holes, and supermassive particles, Soviet Phys. Usp. **28**, 213–232 (1985), [Usp. Fiz. Nauk **145**, 369 (1985)].
[39] A. M. Green, A. R. Liddle, and A. Riotto, Primordial black hole constraints in cosmologies with early matter domination, Phys. Rev. D **56**, 7559–7565 (1997), arXiv:astro-ph/9705166 [astro-ph].
[40] G. Kane, K. Sinha, and S. Watson, Cosmological moduli and the post-inflationary universe: A critical review, Int. J. Mod. Phys. D **24**, 1530022-324 (2015), arXiv:1502.07746 [hep-th].
[41] T. Harada, C.-m. Yoo, K. Kohri, K.-i. Nakao, and S. Jhingan, Primordial Black Hole Formation in the Matter-dominated Phase of the Universe, Astrophys. J. **833**, 61 (2016), arXiv:1609.01588 [astro-ph.CO].
[42] J. Georg, G. Şengör, and S. Watson, Nonthermal WIMPs and primordial black holes, Phys. Rev. D **93**, 123523 (2016), arXiv:1603.00023 [hep-ph].
[43] J. Georg and S. Watson, A preferred mass range for primordial black hole formation and black holes as dark matter revisited, J. High Energy Phys. **2017**, 138 (2017), arXiv:1703.04825 [astro-ph.CO].
[44] T. Kokubu, K. Kyutoku, K. Kohri, and T. Harada, Effect of inhomogeneity on primordial black hole formation in the matter dominated era, Phys. Rev. D **98**, 123024 (2018), arXiv:1810.03490 [astro-

ph.CO].
[45] J. Georg, B. Melcher, and S. Watson, Primordial black holes and Co-Decaying dark matter, J. Cosmology Astropart. Phys. **2019**, 014 (2019), arXiv:1902.04082 [astro-ph.CO].
[46] T. Matsubara, T. Terada, K. Kohri, and S. Yokoyama, Clustering of primordial black holes formed in a matter-dominated epoch, Phys. Rev. D **100**, 123544 (2019), arXiv:1909.04053 [astro-ph.CO].
[47] B. J. Carr, The primordial black hole mass spectrum., Astrophys. J. **201**, 1–19 (1975).
[48] W. H. Press and P. Schechter, Formation of Galaxies and Clusters of Galaxies by Self-Similar Gravitational Condensation, Astrophys. J. **187**, 425–438 (1974).
[49] J. Yokoyama, Cosmological constraints on primordial black holes produced in the near-critical gravitational collapse, Phys. Rev. D **58**, 107502 (1998), arXiv:gr-qc/9804041 [gr-qc].
[50] J. C. Niemeyer and K. Jedamzik, Near-Critical Gravitational Collapse and the Initial Mass Function of Primordial Black Holes, Phys. Rev. Lett. **80**, 5481–5484 (1998), arXiv:astro-ph/9709072 [astro-ph].
[51] J. C. Niemeyer and K. Jedamzik, Dynamics of primordial black hole formation, Phys. Rev. D **59**, 124013 (1999), arXiv:astro-ph/9901292 [astro-ph].
[52] A. Dolgov and J. Silk, Baryon isocurvature fluctuations at small scales and baryonic dark matter, Phys. Rev. D **47**, 4244–4255 (1993).
[53] H. Tashiro and N. Sugiyama, Constraints on primordial black holes by distortions of the cosmic microwave background, Phys. Rev. D **78**, 023004 (2008), arXiv:0801.3172 [astro-ph].
[54] C. Germani and I. Musco, Abundance of Primordial Black Holes Depends on the Shape of the Inflationary Power Spectrum, Phys. Rev. Lett. **122**, 141302 (2019), arXiv:1805.04087 [astro-ph.CO].
[55] A. M. Green, Microlensing and dynamical constraints on primordial black hole dark matter with an extended mass function, Phys. Rev. D **94**, 063530 (2016), arXiv:1609.01143 [astro-ph.CO].
[56] B. Carr, M. Raidal, T. Tenkanen, V. Vaskonen, and H. Veermäe, Primordial black hole constraints for extended mass functions, Phys. Rev. D **96**, 023514 (2017), arXiv:1705.05567 [astro-ph.CO].
[57] B. J. Carr, K. Kohri, Y. Sendouda, and J. Yokoyama, Constraints on primordial black holes from the Galactic gamma-ray background, Phys. Rev. D **94**, 044029 (2016), arXiv:1604.05349 [astro-ph.CO].
[58] F. Kühnel and K. Freese, Constraints on primordial black holes with extended mass functions, Phys. Rev. D **95**, 083508 (2017), arXiv:1701.07223 [astro-ph.CO].
[59] N. Bellomo, J. L. Bernal, A. Raccanelli, and L. Verde, Primordial black holes as dark matter: converting constraints from monochromatic to extended mass distributions, J. Cosmology Astropart. Phys. **2018**, 004 (2018), arXiv:1709.07467 [astro-ph.CO].
[60] B. V. Lehmann, S. Profumo, and J. Yant, The maximal-density mass function for primordial black hole dark matter, J. Cosmology Astropart. Phys. **2018**, 007 (2018), arXiv:1801.00808 [astro-ph.CO].
[61] S. Clesse and J. García-Bellido, Massive primordial black holes from hybrid inflation as dark matter and the seeds of galaxies, Phys. Rev. D **92**, 023524 (2015), arXiv:1501.07565 [astro-ph.CO].
[62] K. Inomata, M. Kawasaki, K. Mukaida, Y. Tada, and T. T. Yanagida, Inflationary primordial black holes as all dark matter, Phys. Rev. D **96**, 043504 (2017), arXiv:1701.02544 [astro-ph.CO].
[63] V. De Luca, V. Desjacques, G. Franciolini, A. Malhotra, and A. Riotto, The initial spin probability distribution of primordial black holes, J. Cosmology Astropart. Phys. **2019**, 018 (2019), arXiv:1903.01179 [astro-ph.CO].
[64] T. Chiba and S. Yokoyama, Spin distribution of primordial black holes, Prog. Theor. Exp. Phys. **2017**, 083E01 (2017), arXiv:1704.06573 [gr-qc].
[65] T. Harada, C.-M. Yoo, K. Kohri, and K.-I. Nakao, Spins of primordial black holes formed in the matter-dominated phase of the Universe, Phys. Rev. D **96**, 083517 (2017), arXiv:1707.03595 [gr-qc].
[66] E. Cotner and A. Kusenko, Primordial black holes from scalar field evolution in the early universe, Phys. Rev. D **96**, 103002 (2017), arXiv:1706.09003 [astro-ph.CO].
[67] R. Allahverdi *et al.*, The First Three Seconds: a Review of Possible Expansion Histories of the Early

Universe, Open J. Astrophys. **4**, 1 (2021), arXiv:2006.16182 [astro-ph.CO].
[68] S. Chongchitnan and J. Silk, Extreme-value statistics of the spin of primordial black holes, Phys. Rev. D **104**, 083018 (2021), arXiv:2109.12268 [astro-ph.CO].
[69] V. De Luca, G. Franciolini, P. Pani, and A. Riotto, The evolution of primordial black holes and their final observable spins, J. Cosmology Astropart. Phys. **2020**, 052 (2020), arXiv:2003.02778 [astro-ph.CO].
[70] M. Fishbach, D. E. Holz, and B. Farr, Are LIGO's Black Holes Made from Smaller Black Holes?, Astrophys. J. Lett. **840**, L24 (2017), arXiv:1703.06869 [astro-ph.HE].
[71] D. Hooper, G. Krnjaic, J. March-Russell, S. D. McDermott, and R. Petrossian-Byrne, Hot Gravitons and Gravitational Waves From Kerr Black Holes in the Early Universe, arXiv e-prints (2020), arXiv:2004.00618 [astro-ph.CO].
[72] J. J. Samueli, *Le modèle standard de la physique des particules : de l'électron au boson de Higgs* (2013).
[73] R. Hagedorn, Statistical thermodynamics of strong interactions at high energies, Nuovo Cimento, Suppl. **3**, 147–186 (1965).
[74] R. Hagedorn, Thermodynamics of Strong Interactions at High Energy and its Consequences for Astrophysics, Astron. Astrophys. **5**, 184 (1970).
[75] R. Hagedorn and I. Montvay, A model study in hadron statistical bootstrap, Nucl. Phys. B **59**, 45–86 (1973).
[76] M. Gell-Mann, A schematic model of baryons and mesons, Phys. Lett. **8**, 214–215 (1964).
[77] G. Zweig, An SU_3 model for strong interaction symmetry and its breaking; Version 2, CERN documents (1964), [Version 1 is CERN preprint 8182/TH.401, Jan. 17, 1964].
[78] F. Englert and R. Brout, Broken Symmetry and the Mass of Gauge Vector Mesons, Phys. Rev. Lett. **13**, 321–323 (1964).
[79] P. W. Higgs, Broken Symmetries and the Masses of Gauge Bosons, Phys. Rev. Lett. **13**, 508–509 (1964).
[80] G. S. Guralnik, C. R. Hagen, and T. W. Kibble, Global Conservation Laws and Massless Particles, Phys. Rev. Lett. **13**, 585–587 (1964).
[81] M. Tanabashi *et al.* (Particle Data Group), Review of Particle Physics, Phys. Rev. D **98**, 030001 (2018).
[82] A. Arbey and F. Mahmoudi, Dark matter and the early Universe: A review, Prog. Part. Nucl. Phys. **119**, 103865 (2021), arXiv:2104.11488 [hep-ph].
[83] D. N. Page, Hawking radiation and black hole thermodynamics, New J. Phys. **7**, 203 (2005), arXiv:hep-th/0409024 [hep-th].
[84] W. Israel, Event Horizons in Static Vacuum Space-Times, Phys. Rev. **164**, 1776–1779 (1967).
[85] W. Israel, Event horizons in static electrovac space-times, Commun. Math. Phys. **8**, 245–260 (1968).
[86] B. Carter, Axisymmetric Black Hole Has Only Two Degrees of Freedom, Phys. Rev. Lett. **26**, 331–333 (1971).
[87] D. N. Page, Information in black hole radiation, Phys. Rev. Lett. **71**, 3743–3746 (1993), arXiv:hep-th/9306083 [hep-th].
[88] J. D. Bekenstein, Black Holes and Entropy, Phys. Rev. D **7**, 2333–2346 (1973).
[89] J. M. Bardeen, B. Carter, and S. W. Hawking, The four laws of black hole mechanics, Commun. Math. Phys. **31**, 161–170 (1973).
[90] D. Wallace, The case for black hole thermodynamics part I: Phenomenological thermodynamics, Stud. Hist. Philos. Sci. B **64**, 52–67 (2018), arXiv:1710.02724 [gr-qc].
[91] D. Wallace, The case for black hole thermodynamics, Part II: statistical mechanics, arXiv e-prints (2017), arXiv:1710.02725 [gr-qc].
[92] C. W. Misner, Interpretation of Gravitational-Wave Observations, Phys. Rev. Lett. **28**, 994–997 (1972).
[93] W. H. Press and S. A. Teukolsky, Floating Orbits, Superradiant Scattering and the Black-hole Bomb,

Nature **238**, 211–212 (1972).
[94] R. Brito, V. Cardoso, and P. Pani, Superradiance, in *New Frontiers in Black Hole Physics*, Vol. 971 (2020) pp. 1–293, arXiv:1501.06570 [gr-qc] .
[95] S. A. Teukolsky, Perturbations of a Rotating Black Hole. I. Fundamental Equations for Gravitational, Electromagnetic, and Neutrino-Field Perturbations, Astrophys. J. **185**, 635–648 (1973).
[96] W. H. Press and S. A. Teukolsky, Perturbations of a Rotating Black Hole. II. Dynamical Stability of the Kerr Metric, Astrophys. J. **185**, 649–674 (1973).
[97] S. A. Teukolsky and W. H. Press, Perturbations of a rotating black hole. III. Interaction of the hole with gravitational and electromagnetic radiation., Astrophys. J. **193**, 443–461 (1974).
[98] B. Carter, Hamilton-Jacobi and Schrodinger Separable Solutions of Einstein's Equations, Commun. Math. Phys. **10**, 280–310 (1968).
[99] A. A. Starobinskiĭ, Amplification of waves during reflection from a rotating "black hole", J. Exp. Theor. Phys. **37**, 28 (1973), [Pis'ma Zh. Eksp. Teor. Fiz. **64**, 48 (1973)].
[100] A. A. Starobinskiĭ and S. M. Churilov, Amplification of electromagnetic and gravitational waves scattered by a rotating "black hole", J. Exp. Theor. Phys. **38**, 1 (1974), [Pis'ma Zh. Eksp. Teor. Fiz. **65**, 3 (1973)].
[101] W. Unruh, Separability of the Neutrino Equations in a Kerr Background, Phys. Rev. Lett. **31**, 1265–1267 (1973).
[102] S. W. Hawking, Black hole explosions?, Nature **248**, 30–31 (1974).
[103] J. D. Bekenstein, Statistical black-hole thermodynamics, Phys. Rev. D **12**, 3077–3085 (1975).
[104] S. W. Hawking, Black holes and thermodynamics, Phys. Rev. D **13**, 191–197 (1976).
[105] S. W. Hawking, Particle creation by black holes, Commun. Math. Phys. **43**, 199–220 (1975).
[106] J. Traschen, An Introduction to Black Hole Evaporation, in *Mathematical Methods in Physics*, edited by A. A. Bytsenko and F. L. Williams (2000) p. 180, arXiv:gr-qc/0010055 [gr-qc] .
[107] D. N. Page, Particle emission rates from a black hole: Massless particles from an uncharged, nonrotating hole, Phys. Rev. D **13**, 198–206 (1976).
[108] J. B. Hartle and S. W. Hawking, Path-integral derivation of black-hole radiance, Phys. Rev. D **13**, 2188–2203 (1976).
[109] V. P. Frolov, Black holes and quantum processes in them, Soviet Phys. Usp. **19**, 244–262 (1976), [Usp. Fiz. Nauk **118**, 473 (1976)].
[110] G. W. Gibbons, Vacuum polarization and the spontaneous loss of charge by black holes, Commun. Math. Phys. **44**, 245–264 (1975).
[111] B. Carter, Charge and Particle Conservation in Black-Hole Decay, Phys. Rev. Lett. **33**, 558–561 (1974).
[112] J. Schwinger, On Gauge Invariance and Vacuum Polarization, Phys. Rev. **82**, 664–679 (1951).
[113] W. T. Zaumen, Upper bound on the electric charge of a black hole, Nature **247**, 530–531 (1974).
[114] N. G. Sanchez, Scattering of scalar waves from a Schwarzschild black hole., J. Math. Phys. **17**, 688–692 (1976).
[115] N. Sanchez, Absorption and emission spectra of a Schwarzschild black hole, Phys. Rev. D **18**, 1030–1036 (1978).
[116] T. Elster, Vacuum polarization near a black hole creating particles, Phys. Lett. A **94**, 205–209 (1983).
[117] T. Elster, Polarisation of the vacuum near a black hole inside a spherical cavity, J. Phys. A **16**, 989–996 (1983).
[118] R. D. Simkins, *Massive Scalar Particle Emission from Schwarzschild Black Holes*, Ph.D. thesis, Pennsylvania State University (1986).
[119] D. N. Page, Particle emission rates from a black hole. II. Massless particles from a rotating hole, Phys. Rev. D **14**, 3260–3273 (1976).
[120] D. N. Page, Particle emission rates from a black hole. III. Charged leptons from a nonrotating hole,

Phys. Rev. D **16**, 2402–2411 (1977).
[121] J. H. MacGibbon and B. R. Webber, Quark- and gluon-jet emission from primordial black holes: The instantaneous spectra, Phys. Rev. D **41**, 3052–3079 (1990).
[122] T. Regge and J. A. Wheeler, Stability of a Schwarzschild Singularity, Phys. Rev. **108**, 1063–1069 (1957).
[123] R. A. Matzner, Scattering of Massless Scalar Waves by a Schwarzschild "Singularity", J. Math. Phys. **9**, 163–170 (1968).
[124] D. R. Brill, P. L. Chrzanowski, C. M. Pereira, E. D. Fackerell, and J. R. Ipser, Solution of the Scalar Wave Equation in a Kerr Background by Separation of Variables, Phys. Rev. D **5**, 1913–1915 (1972).
[125] S. Chandrasekhar and S. Detweiler, On the Equations Governing the Axisymmetric Perturbations of the Kerr Black Hole, Proc. R. Soc. Lond. A **345**, 145–167 (1975).
[126] S. Detweiler, On the Equations Governing the Electromagnetic Perturbations of the Kerr Black Hole, Proc. R. Soc. Lond. A **349**, 217–230 (1976).
[127] S. Chandrasekhar and S. Detweiler, On the Equations Governing the Gravitational Perturbations of the Kerr Black Hole, Proc. R. Soc. Lond. A **350**, 165–174 (1976).
[128] S. Chandrasekhar and S. Detweiler, On the Reflexion and Transmission of Neutrino Waves by a Kerr Black Hole, Proc. R. Soc. Lond. A **352**, 325–338 (1977).
[129] H. Kodama and A. Ishibashi, A Master Equation for Gravitational Perturbations of Maximally Symmetric Black Holes in Higher Dimensions, Prog. Theor. Phys. **110**, 701–722 (2003), arXiv:hep-th/0305147 [hep-th].
[130] B. Carter, G. W. Gibbons, D. N. C. Lin, and M. J. Perry, Black hole emission process in the high energy limit., Astron. Astrophys. **52**, 427–438 (1976).
[131] B. J. Carr, Some cosmological consequences of primordial black-hole evaporations., Astrophys. J. **206**, 8–25 (1976).
[132] J. Oliensis and C. T. Hill, Ultra high energy radiation from a black hole, Phys. Lett. B **143**, 92–96 (1984).
[133] J. H. MacGibbon, Quark- and gluon-jet emission from primordial black holes. II. The emission over the black-hole lifetime, Phys. Rev. D **44**, 376–392 (1991).
[134] M. J. Perry, Black holes are coloured, Phys. Lett. B **71**, 234–236 (1977).
[135] G. Marchesini and B. R. Webber, Simulation of QCD jets including soft gluon interference, Nucl. Phys. B **238**, 1–29 (1984).
[136] B. R. Webber, A QCD model for jet fragmentation including soft gluon interference, Nucl. Phys. B **238**, 492–528 (1984).
[137] G. Marchesini and B. R. Webber, Monte Carlo simulation of general hard processes with coherent QCD radiation, Nucl. Phys. B **310**, 461–526 (1988).
[138] A. Cheek, L. Heurtier, Y. F. Perez-Gonzalez, and J. Turner, Primordial black hole evaporation and dark matter production. I. Solely Hawking radiation, Phys. Rev. D **105**, 015022 (2022), arXiv:2107.00013 [hep-ph].
[139] D. B. Cline and W. Hong, Possibility of Unique Detection of Primordial Black Hole Gamma-Ray Bursts, Astrophys. J. Lett. **401**, L57 (1992).
[140] A. F. Heckler, Formation of a Hawking-radiation photosphere around microscopic black holes, Phys. Rev. D **55**, 480–488 (1997), arXiv:astro-ph/9601029 [astro-ph].
[141] A. F. Heckler, Calculation of the Emergent Spectrum and Observation of Primordial Black Holes, Phys. Rev. Lett. **78**, 3430–3433 (1997), arXiv:astro-ph/9702027 [astro-ph].
[142] J. Kapusta, The Last Eight Minutes of a Primordial Black Hole, arXiv e-prints (1999), arXiv:astro-ph/9911309 [astro-ph].
[143] R. G. Daghigh and J. I. Kapusta, High temperature matter and neutrino spectra from microscopic

black holes, Phys. Rev. D **67**, 044006 (2003), arXiv:astro-ph/0211579 [astro-ph].
[144] A. A. Belyanin, V. V. Kocharovsky, and V. V. Kocharovsky, Gamma-ray bursts from the final stage of primordial black hole evaporation, Mon. Not. Roy. Astron. Soc. **283**, 626 (1996).
[145] M. J. Rees, A better way of searching for black-hole explosions?, Nature **266**, 333–334 (1977).
[146] R. D. Blandford, Spectrum of a radio pulse from an exploding black hole., Mon. Not. Roy. Astron. Soc. **181**, 489–498 (1977).
[147] J. M. Cline, M. Mostoslavsky, and G. Servant, Numerical study of Hawking radiation photosphere formation around microscopic black holes, Phys. Rev. D **59**, 063009 (1999), arXiv:hep-ph/9810439 [hep-ph].
[148] J. H. MacGibbon, B. J. Carr, and D. N. Page, Do evaporating black holes form photospheres?, Phys. Rev. D **78**, 064043 (2008), arXiv:0709.2380 [astro-ph].
[149] A. Arbey, J. Auffinger, M. Geiller, E. R. Livine, and F. Sartini, Hawking radiation by spherically-symmetric static black holes for all spins. I. Teukolsky equations and potentials, Phys. Rev. D **103**, 104010 (2021), arXiv:2101.02951 [gr-qc].
[150] A. Arbey, J. Auffinger, M. Geiller, E. R. Livine, and F. Sartini, Hawking radiation by spherically-symmetric static black holes for all spins. II. Numerical emission rates, analytical limits, and new constraints, Phys. Rev. D **104**, 084016 (2021), arXiv:2107.03293 [gr-qc].
[151] A. Arbey and J. Auffinger, BlackHawk: a public code for calculating the Hawking evaporation spectra of any black hole distribution, Eur. Phys. J. C **79**, 693 (2019), arXiv:1905.04268 [gr-qc].
[152] A. Arbey and J. Auffinger, Physics beyond the standard model with BlackHawk v2.0, Eur. Phys. J. C **81**, 910 (2021), arXiv:2108.02737 [gr-qc].
[153] S. Chandrasekhar, *The mathematical theory of black holes* (1983).
[154] A. Z. Petrov, The Classification of Spaces Defining Gravitational Fields, Gen. Relativ. Gravit. **32**, 1665–1685 (2000), [UZKGU **114**, 55 (1954)].
[155] D. KofroÅ, Separability of test fields equations on the C -metric background, Phys. Rev. D **92**, 124064 (2015), arXiv:1603.01451 [gr-qc].
[156] D. KofroÅ, Separability of test fields equations on the C -metric background. II. Rotating case and the Meissner effect, Phys. Rev. D **93**, 104012 (2016), arXiv:1604.05638 [gr-qc].
[157] M. Jiang, X. Wang, and Z. Li, Spin field equations and Heun's equations, Astrophys. Space Sci. **357**, 139 (2015).
[158] E. Newman and R. Penrose, An Approach to Gravitational Radiation by a Method of Spin Coefficients, J. Math. Phys. **3**, 566–578 (1962).
[159] C. M. Harris and P. Kanti, Hawking radiation from a (4+n)-dimensional black hole: exact results for the Schwarzschild phase, J. High Energy Phys. **2003**, 014 (2003), arXiv:hep-ph/0309054 [hep-ph].
[160] G. F. Torres del Castillo, Rarita-Schwinger fields in algebraically special vacuum space-times, J. Math. Phys. **30**, 446–451 (1989).
[161] G. Li and J. Mo, The generalized uncertainty principle and the thermodynamic quantities near a black hole, Astrophys. Space Sci. **336**, 441–445 (2011).
[162] E. C. Vagenas, A. F. Ali, M. Hemeda, and H. Alshal, Massless charged particles tunneling radiation from a RN-dS horizon and the linear and quadratic GUP, Ann. Phys. **432**, 168574 (2021), arXiv:2008.09853 [hep-th].
[163] S. Hossenfelder, L. Modesto, and I. Prémont-Schwarz, Emission spectra of self-dual black holes, arXiv e-prints (2012), arXiv:1202.0412 [gr-qc].
[164] F. Moulin, A. Barrau, and K. Martineau, An Overview of Quasinormal Modes in Modified and Extended Gravity, Universe **5**, 202 (2019), arXiv:1908.06311 [gr-qc].
[165] T. Berry, A. Simpson, and M. Visser, General class of "quantum deformed" regular black holes, arXiv e-prints (2021), arXiv:2102.02471 [gr-qc].

[166] Á. Rincón and V. Santos, Greybody factor and quasinormal modes of Regular Black Holes, Eur. Phys. J. C **80**, 910 (2020), arXiv:2009.04386 [gr-qc].
[167] O. P. Fernandez Piedra, Gravitino Perturbations in Schwarzschild Black Holes, Int. J. Mod. Phys. D **20**, 93–109 (2011), arXiv:1006.3327 [gr-qc].
[168] F.-W. Shu and Y.-G. Shen, Quasinormal modes of Rarita Schwinger field in Reissner Nordström black hole spacetimes, Phys. Lett. B **614**, 195–200 (2005), arXiv:gr-qc/0505161 [gr-qc].
[169] R. C. Myers and M. J. Perry, Black holes in higher dimensional space-times, Ann. Phys. **172**, 304–347 (1986).
[170] G. Johnson, Primordial black hole constraints with large extra dimensions, J. Cosmology Astropart. Phys. **2020**, 046 (2020), arXiv:2005.07467 [astro-ph.CO].
[171] A. Friedlander, K. J. Mack, S. Schon, N. Song, and A. C. Vincent, Primordial Black Hole Dark Matter in the Context of Extra Dimensions, arXiv e-prints (2022), arXiv:2201.11761 [hep-ph].
[172] L. Randall and R. Sundrum, Large Mass Hierarchy from a Small Extra Dimension, Phys. Rev. Lett. **83**, 3370–3373 (1999), arXiv:hep-ph/9905221 [hep-ph].
[173] L. Randall and R. Sundrum, An Alternative to Compactification, Phys. Rev. Lett. **83**, 4690–4693 (1999), arXiv:hep-th/9906064 [hep-th].
[174] N. Arkani-Hamed, S. Dimopoulos, and G. Dvali, The hierarchy problem and new dimensions at a millimeter, Phys. Lett. B **429**, 263–272 (1998), arXiv:hep-ph/9803315 [hep-ph].
[175] I. Antoniadis, N. Arkani-Hamed, S. Dimopoulos, and G. Dvali, New dimensions at a millimeter to a fermi and superstrings at a TeV, Phys. Lett. B **436**, 257–263 (1998), arXiv:hep-ph/9804398 [hep-ph].
[176] N. Arkani-Hamed, S. Dimopoulos, and G. Dvali, Phenomenology, astrophysics, and cosmology of theories with submillimeter dimensions and TeV scale quantum gravity, Phys. Rev. D **59**, 086004 (1999), arXiv:hep-ph/9807344 [hep-ph].
[177] E. G. Adelberger, J. H. Gundlach, B. R. Heckel, S. Hoedl, and S. Schlamminger, Torsion balance experiments: A low-energy frontier of particle physics, Prog. Part. Nucl. Phys. **62**, 102–134 (2009).
[178] P. Kanti and E. Winstanley, Hawking Radiation from Higher-Dimensional Black Holes, in *Quantum Aspects of Black Holes* (2015) pp. 229–265, arXiv:1402.3952 [hep-th] .
[179] P. Kanti, Black Holes in Theories with Large Extra Dimensions: A Review, Int. J. Mod. Phys. A **19**, 4899–4951 (2004), arXiv:hep-ph/0402168 [hep-ph].
[180] S. Dimopoulos and G. Landsberg, Black Holes at the Large Hadron Collider, Phys. Rev. Lett. **87**, 161602 (2001), arXiv:hep-ph/0106295 [hep-ph].
[181] J. L. Feng and A. D. Shapere, Black Hole Production by Cosmic Rays, Phys. Rev. Lett. **88**, 021303 (2001), arXiv:hep-ph/0109106 [hep-ph].
[182] L. A. Anchordoqui, J. L. Feng, H. Goldberg, and A. D. Shapere, Black holes from cosmic rays: Probes of extra dimensions and new limits on TeV-scale gravity, Phys. Rev. D **65**, 124027 (2002), arXiv:hep-ph/0112247 [hep-ph].
[183] V. Cardoso, E. Berti, and M. Cavaglià, What we (don't) know about black-hole formation in high-energy collisions, Class. Quantum Gravity **22**, L61–L69 (2005), arXiv:hep-ph/0505125 [hep-ph].
[184] P. Kanti, Black Holes at the Large Hadron Collider, in *Physics of Black Holes*, Vol. 769 (2009) p. 387, arXiv:0802.2218 [hep-th] .
[185] S. B. Giddings and S. Thomas, High energy colliders as black hole factories: The end of short distance physics, Phys. Rev. D **65**, 056010 (2002), arXiv:hep-ph/0106219 [hep-ph].
[186] C. M. Harris, P. Richardson, and B. R. Webber, CHARYBDIS: a black hole event generator, J. High Energy Phys. **2003**, 033 (2003), arXiv:hep-ph/0307305 [hep-ph].
[187] J. A. Frost, J. R. Gaunt, M. O. P. Sampaio, M. Casals, S. R. Dolan, M. A. Parker, and B. R. Webber, Phenomenology of production and decay of spinning extra-dimensional black holes at hadron colliders, J. High Energy Phys. **2009**, 014 (2009), arXiv:0904.0979 [hep-ph].

[188] M. Cavaglià, R. Godang, L. Cremaldi, and D. Summers, Catfish: A Monte Carlo simulator for black holes at the LHC, Comput. Phys. Commun. **177**, 506–517 (2007), arXiv:hep-ph/0609001 [hep-ph].
[189] D.-C. Dai, G. Starkman, D. Stojkovic, C. Issever, E. Rizvi, and J. Tseng, BlackMax: A black-hole event generator with rotation, recoil, split branes, and brane tension, Phys. Rev. D **77**, 076007 (2008), arXiv:0711.3012 [hep-ph].
[190] D.-C. Dai, C. Issever, E. Rizvi, G. Starkman, D. Stojkovic, and J. Tseng, Manual of BlackMax, a black-hole event generator with rotation, recoil, split branes, and brane tension, arXiv e-prints (2009), arXiv:0902.3577 [hep-ph].
[191] D.-C. Dai, C. Issever, E. Rizvi, G. Starkman, D. Stojkovic, and J. Tseng, Manual of BlackMax. A black-hole event generator with rotation, recoil, split branes, and brane tension. Version 2.02, Comput. Phys. Commun. **236**, 285–301 (2019).
[192] D. M. Gingrich, Monte Carlo event generator for black hole production and decay in proton-proton collisions - QBH version 1.02, Comput. Phys. Commun. **181**, 1917–1924 (2010), arXiv:0911.5370 [hep-ph].
[193] M. Bojowald, Critical Evaluation of Common Claims in Loop Quantum Cosmology, Universe **6**, 36 (2020), arXiv:2002.05703 [gr-qc].
[194] L. Modesto, Semiclassical Loop Quantum Black Hole, Int. J. Theor. Phys. **49**, 1649–1683 (2010), arXiv:0811.2196 [gr-qc].
[195] R. Arnowitt, S. Deser, and C. W. Misner, Republication of: The dynamics of general relativity, Gen. Relativ. Gravit. **40**, 1997–2027 (2008), arXiv:gr-qc/0405109 [gr-qc].
[196] G. F. Del Torres del Castillo and G. Silva-Ortigoza, Rarita-Schwinger fields in the Kerr geometry, Phys. Rev. D **42**, 4082–4086 (1990).
[197] G. F. Torres del Castillo and G. Silva-Ortigoza, Spin-3/2 perturbations of the Kerr-Newman solution, Phys. Rev. D **46**, 5395–5398 (1992).
[198] F. Gray and M. Visser, Greybody factors for Schwarzschild black holes: Path-ordered exponentials and product integrals, arXiv e-prints (2015), arXiv:1512.05018 [gr-qc].
[199] R. Dong, W. H. Kinney, and D. Stojkovic, Gravitational wave production by Hawking radiation from rotating primordial black holes, J. Cosmology Astropart. Phys. **2016**, 034 (2016), arXiv:1511.05642 [astro-ph.CO].
[200] F.-W. Shu and Y.-G. Shen, Quasinormal modes in Schwarzschild black holes due to arbitrary spin fields, Phys. Lett. B **619**, 340–346 (2005), arXiv:gr-qc/0501098 [gr-qc].
[201] Y. Décanini, A. Folacci, and B. Raffaelli, Unstable circular null geodesics of static spherically symmetric black holes, Regge poles, and quasinormal frequencies, Phys. Rev. D **81**, 104039 (2010), arXiv:1002.0121 [gr-qc].
[202] Y. Décanini, G. Esposito-Farèse, and A. Folacci, Universality of high-energy absorption cross sections for black holes, Phys. Rev. D **83**, 044032 (2011), arXiv:1101.0781 [gr-qc].
[203] M. A. Anacleto, F. A. Brito, J. A. V. Campos, and E. Passos, Absorption and scattering of a self-dual black hole, arXiv e-prints (2020), arXiv:2002.12090 [hep-th].
[204] P. P. Fiziev, Teukolsky-Starobinsky identities: A novel derivation and generalizations, Phys. Rev. D **80**, 124001 (2009), arXiv:0906.5108 [gr-qc].
[205] M. Cvetič and F. Larsen, Greybody factors for black holes in four dimensions: Particles with spin, Phys. Rev. D **57**, 6297–6310 (1998), arXiv:hep-th/9712118 [hep-th].
[206] P. Kanti and J. March-Russell, Calculable corrections to brane black hole decay. I. The scalar case, Phys. Rev. D **66**, 024023 (2002), arXiv:hep-ph/0203223 [hep-ph].
[207] P. Kanti and J. March-Russell, Calculable corrections to brane black hole decay. II. Greybody factors for spin 1/2 and 1, Phys. Rev. D **67**, 104019 (2003), arXiv:hep-ph/0212199 [hep-ph].
[208] H. Motohashi and S. Noda, Exact solution for wave scattering from black holes: Formulation,

Prog. Theor. Exp. Phys. **2021**, 083E03 (2021), arXiv:2103.10802 [gr-qc].
[209] L. C. B. Crispino, S. R. Dolan, and E. S. Oliveira, Scattering of massless scalar waves by Reissner-Nordström black holes, Phys. Rev. D **79**, 064022 (2009), arXiv:0904.0999 [gr-qc].
[210] S. Creek, O. Efthimiou, P. Kanti, and K. Tamvakis, Graviton emission in the bulk from a higher-dimensional Schwarzschild black hole, Phys. Lett. B **635**, 39–49 (2006), arXiv:hep-th/0601126 [hep-th].
[211] E. Alesci and L. Modesto, Particle Creation by Loop Black Holes, arXiv e-prints (2011), arXiv:1101.5792 [gr-qc].
[212] E. Alesci and L. Modesto, Hawking radiation from Loop Black Holes, in *Loops 11: International Conference on Quantum Gravity*, J. Phys. Conf. Ser., Vol. 360 (2012) p. 012036.
[213] F. Moulin, K. Martineau, J. Grain, and A. Barrau, Quantum fields in the background spacetime of a polymeric loop black hole, Class. Quantum Gravity **36**, 125003 (2019), arXiv:1808.00207 [gr-qc].
[214] M. Bouhmadi-López, S. Brahma, C.-Y. Chen, P. Chen, and D.-h. Yeom, A consistent model of non-singular Schwarzschild black hole in loop quantum gravity and its quasinormal modes, J. Cosmology Astropart. Phys. **2020**, 066 (2020), arXiv:2004.13061 [gr-qc].
[215] Y. Bai and N. Orlofsky, Primordial extremal black holes as dark matter, Phys. Rev. D **101**, 055006 (2020), arXiv:1906.04858 [hep-ph].
[216] K. Kritos and J. Silk, Mergers of maximally charged primordial black holes, Phys. Rev. D **105**, 063011 (2022), arXiv:2109.09769 [gr-qc].
[217] D. Clancy, R. Guedens, and A. R. Liddle, Primordial black holes in braneworld cosmologies: Astrophysical constraints, Phys. Rev. D **68**, 023507 (2003), arXiv:astro-ph/0301568 [astro-ph].
[218] Y. Sendouda, S. Nagataki, and K. Sato, Constraints on the mass spectrum of primordial black holes and braneworld parameters from the high-energy diffuse photon background, Phys. Rev. D **68**, 103510 (2003), arXiv:astro-ph/0309170 [astro-ph].
[219] A. S. Majumdar and N. Mukherjee, Braneworld Black Holes in Cosmology and Astrophysics, Int. J. Mod. Phys. D **14**, 1095–1129 (2005), arXiv:astro-ph/0503473 [astro-ph].
[220] P. C. Argyres, S. Dimopoulos, and J. March-Russell, Black holes and sub-millimeter dimensions, Phys. Lett. B **441**, 96–104 (1998), arXiv:hep-th/9808138 [hep-th].
[221] R. Emparan, G. T. Horowitz, and R. C. Myers, Black Holes Radiate Mainly on the Brane, Phys. Rev. Lett. **85**, 499–502 (2000), arXiv:hep-th/0003118 [gr-qc].
[222] R. Casadio and B. Harms, Black hole evaporation and large extra dimensions, Phys. Lett. B **487**, 209–214 (2000), arXiv:hep-th/0004004 [hep-th].
[223] R. Casadio and B. Harms, Black hole evaporation and compact extra dimensions, Phys. Rev. D **64**, 024016 (2001), arXiv:hep-th/0101154 [hep-th].
[224] D.-C. Dai and D. Stojkovic, Analytic explanation of the strong spin-dependent amplification in Hawking radiation from rotating black holes, J. High Energy Phys. **2010**, 16 (2010), arXiv:1008.4586 [gr-qc].
[225] K. Kohri and J. Yokoyama, Primordial black holes and primordial nucleosynthesis: Effects of hadron injection from low mass holes, Phys. Rev. D **61**, 023501 (1999), arXiv:astro-ph/9908160 [astro-ph].
[226] C. M. Chambers, W. A. Hiscock, and B. Taylor, Spinning Down a Black Hole with Scalar Fields, Phys. Rev. Lett. **78**, 3249–3251 (1997), arXiv:gr-qc/9703018 [gr-qc].
[227] B. E. Taylor, C. M. Chambers, and W. A. Hiscock, Evaporation of a Kerr black hole by emission of scalar and higher spin particles, Phys. Rev. D **58**, 044012 (1998), arXiv:gr-qc/9801044 [gr-qc].
[228] M. Calzà, J. March-Russell, and J. G. Rosa, Evaporating primordial black holes, the string axiverse, and hot dark radiation, arXiv e-prints (2021), arXiv:2110.13602 [astro-ph.CO].
[229] R. Bean and J. Magueijo, Could supermassive black holes be quintessential primordial black holes?, Phys. Rev. D **66**, 063505 (2002), arXiv:astro-ph/0204486 [astro-ph].
[230] N. Düchting, Supermassive black holes from primordial black hole seeds, Phys. Rev. D **70**, 064015 (2004), arXiv:astro-ph/0406260 [astro-ph].

[231] K. J. Mack, J. P. Ostriker, and M. Ricotti, Growth of Structure Seeded by Primordial Black Holes, Astrophys. J. **665**, 1277–1287 (2007), arXiv:astro-ph/0608642 [astro-ph].
[232] M. Kawasaki, A. Kusenko, and T. T. Yanagida, Primordial seeds of supermassive black holes, Phys. Lett. B **711**, 1–5 (2012), arXiv:1202.3848 [astro-ph.CO].
[233] Y. Ali-Haïmoud, E. D. Kovetz, and M. Kamionkowski, Merger rate of primordial black-hole binaries, Phys. Rev. D **96**, 123523 (2017), arXiv:1709.06576 [astro-ph.CO].
[234] M. Sasaki, T. Suyama, T. Tanaka, and S. Yokoyama, Primordial black holes—perspectives in gravitational wave astronomy, Class. Quantum Gravity **35**, 063001 (2018), arXiv:1801.05235 [astro-ph.CO].
[235] A. Arbey and J.-F. Coupechoux, Black hole mergers, gravitational waves and scaling relations, arXiv e-prints (2019), arXiv:1911.10219 [gr-qc].
[236] A. Arbey, J. Auffinger, and J. Silk, Evolution of primordial black hole spin due to Hawking radiation, Mon. Not. Roy. Astron. Soc. **494**, 1257–1262 (2020), arXiv:1906.04196 [astro-ph.CO].
[237] D. N. Page and K. S. Thorne, Disk-Accretion onto a Black Hole. Time-Averaged Structure of Accretion Disk, Astrophys. J. **191**, 499–506 (1974).
[238] K. S. Thorne, Disk-Accretion onto a Black Hole. II. Evolution of the Hole, Astrophys. J. **191**, 507–520 (1974).
[239] S. W. Hawking and J. B. Hartle, Energy and angular momentum flow into a black hole, Commun. Math. Phys. **27**, 283–290 (1972).
[240] M. Kesden, G. Lockhart, and E. S. Phinney, Maximum black-hole spin from quasicircular binary mergers, Phys. Rev. D **82**, 124045 (2010), arXiv:1005.0627 [gr-qc].
[241] A. Sadowski, M. Bursa, M. Abramowicz, W. Kluźniak, J. P. Lasota, R. Moderski, and M. Safarzadeh, Spinning up black holes with super-critical accretion flows, Astron. Astrophys. **532**, A41 (2011), arXiv:1102.2456 [astro-ph.HE].
[242] M. A. Abramowicz and J. P. Lasota, Spin-up of black holes by thick accretion disks, Acta Astron. **30**, 35–39 (1980).
[243] S. Nampalliwar and C. Bambi, Accreting Black Holes, arXiv e-prints (2018), arXiv:1810.07041 [astro-ph.HE].
[244] P. B. Ferraz, T. W. Kephart, and J. G. Rosa, Superradiant pion clouds around primordial black holes, arXiv e-prints (2020), arXiv:2004.11303 [gr-qc].
[245] A. Arbey, AlterBBN: A program for calculating the BBN abundances of the elements in alternative cosmologies, Comput. Phys. Commun. **183**, 1822–1831 (2012), arXiv:1106.1363 [astro-ph.CO].
[246] A. Arbey, J. Auffinger, K. P. Hickerson, and E. S. Jenssen, AlterBBN v2: A public code for calculating Big-Bang nucleosynthesis constraints in alternative cosmologies, Comput. Phys. Commun. **248**, 106982 (2020).
[247] B. J. Carr, K. Kohri, Y. Sendouda, and J. Yokoyama, New cosmological constraints on primordial black holes, Phys. Rev. D **81**, 104019 (2010), arXiv:0912.5297 [astro-ph.CO].
[248] T. Sjöstrand, S. Ask, J. R. Christiansen, R. Corke, N. Desai, P. Ilten, S. Mrenna, S. Prestel, C. O. Rasmussen, and P. Z. Skands, An introduction to PYTHIA 8.2, Comput. Phys. Commun. **191**, 159–177 (2015), arXiv:1410.3012 [hep-ph].
[249] M. Cirelli, G. Corcella, A. Hektor, G. Hütsi, M. Kadastik, P. Panci, M. Raidal, F. Sala, and A. Strumia, PPPC 4 DM ID: a poor particle physicist cookbook for dark matter indirect detection, J. Cosmology Astropart. Phys. **2011**, 051 (2011), arXiv:1012.4515 [hep-ph].
[250] P. Ciafaloni, D. Comelli, A. Riotto, F. Sala, A. Strumia, and A. Urbano, Weak corrections are relevant for dark matter indirect detection, J. Cosmology Astropart. Phys. **2011**, 019 (2011), arXiv:1009.0224 [hep-ph].
[251] Y.-F. Cai, C. Chen, Q. Ding, and Y. Wang, Cosmological Standard Timers from Unstable Primordial Relics, arXiv e-prints (2021), arXiv:2112.10422 [astro-ph.CO].

[252] M. R. Mosbech and Z. S. C. Picker, Effects of Hawking evaporation on PBH distributions, arXiv e-prints (2022), arXiv:2203.05743 [astro-ph.HE].
[253] N. Aghanim *et al.* (Planck), Planck 2018 results. VI. Cosmological parameters, Astron. Astrophys. **641**, A6 (2020), arXiv:1807.06209 [astro-ph.CO].
[254] J. Bellm *et al.*, Herwig 7.0/Herwig++ 3.0 release note, Eur. Phys. J. C **76**, 196 (2016), arXiv:1512.01178 [hep-ph].
[255] A. Coogan, L. Morrison, and S. Profumo, Direct Detection of Hawking Radiation from Asteroid-Mass Primordial Black Holes, Phys. Rev. Lett. **126**, 171101 (2021), arXiv:2010.04797 [astro-ph.CO].
[256] A. Coogan, L. Morrison, and S. Profumo, Hazma: a python toolkit for studying indirect detection of sub-GeV dark matter, J. Cosmology Astropart. Phys. **2020**, 056 (2020), arXiv:1907.11846 [hep-ph].
[257] A. Capanema, A. Esmaeili, and A. Esmaili, Evaporating primordial black holes in gamma ray and neutrino telescopes, J. Cosmology Astropart. Phys. **2021**, 051 (2021), arXiv:2110.05637 [hep-ph].
[258] C. W. Bauer, N. L. Rodd, and B. R. Webber, Dark matter spectra from the electroweak to the Planck scale, J. High Energy Phys. **2021**, 121 (2021), arXiv:2007.15001 [hep-ph].
[259] C. Bierlich *et al.*, A comprehensive guide to the physics and usage of PYTHIA 8.3, arXiv e-prints (2022), arXiv:2203.11601 [hep-ph].
[260] J. Bellm *et al.*, Herwig 7.2 release note, Eur. Phys. J. C **80**, 452 (2020), arXiv:1912.06509 [hep-ph].
[261] A. Cheek, L. Heurtier, Y. F. Perez-Gonzalez, and J. Turner, Primordial black hole evaporation and dark matter production. II. Interplay with the freeze-in or freeze-out mechanism, Phys. Rev. D **105**, 015023 (2022), arXiv:2107.00016 [hep-ph].
[262] J. Auffinger, Limits on primordial black holes detectability with Isatis: A BlackHawk tool, arXiv e-prints (2022), arXiv:2201.01265 [astro-ph.HE].
[263] D. N. Page, B. J. Carr, and J. H. MacGibbon, Bremsstrahlung effects around evaporating black holes, Phys. Rev. D **78**, 064044 (2008), arXiv:0709.2381 [astro-ph].
[264] I. D. Novikov, A. G. Polnarev, A. A. Starobinskiĭ, and I. B. Zel'dovich, Primordial black holes, Astron. Astrophys. **80**, 104–109 (1979).
[265] B. J. Carr, J. H. Gilbert, and J. E. Lidsey, Black hole relics and inflation: Limits on blue perturbation spectra, Phys. Rev. D **50**, 4853–4867 (1994), arXiv:astro-ph/9405027 [astro-ph].
[266] B. Carr and F. Kühnel, Primordial Black Holes as Dark Matter: Recent Developments, Annu. Rev. Nucl. Part. Sci. **70**, 355–394 (2020), arXiv:2006.02838 [astro-ph.CO].
[267] B. J. Kavanagh, bradkav/PBHbounds: Release version, Zenodo (2019).
[268] S. Bird *et al.*, Snowmass2021 Cosmic Frontier White Paper:Primordial Black Hole Dark Matter, arXiv e-prints (2022), arXiv:2203.08967 [hep-ph].
[269] M. Bartelmann, Gravitational lensing, Class. Quantum Gravity **27**, 233001 (2010), arXiv:1010.3829 [astro-ph.CO].
[270] C. Alcock *et al.* (MACHO), The MACHO Project: Microlensing Results from 5.7 Years of Large Magellanic Cloud Observations, Astrophys. J. **542**, 281–307 (2000), arXiv:astro-ph/0001272 [astro-ph].
[271] P. Tisserand *et al.* (EROS-2), Limits on the Macho content of the Galactic Halo from the EROS-2 Survey of the Magellanic Clouds, Astron. Astrophys. **469**, 387–404 (2007), arXiv:astro-ph/0607207 [astro-ph].
[272] H. Niikura, M. Takada, S. Yokoyama, T. Sumi, and S. Masaki, Constraints on Earth-mass primordial black holes from OGLE 5-year microlensing events, Phys. Rev. D **99**, 083503 (2019), arXiv:1901.07120 [astro-ph.CO].
[273] P. Mróz *et al.*, No large population of unbound or wide-orbit Jupiter-mass planets, Nature **548**, 183–186 (2017), arXiv:1707.07634 [astro-ph.EP].
[274] N. Smyth, S. Profumo, S. English, T. Jeltema, K. McKinnon, and P. Guhathakurta, Updated con-

straints on asteroid-mass primordial black holes as dark matter, Phys. Rev. D **101**, 063005 (2020), arXiv:1910.01285 [astro-ph.CO].
[275] H. Niikura *et al.*, Microlensing constraints on primordial black holes with Subaru/HSC Andromeda observations, Nat. Astron. **3**, 524–534 (2019), arXiv:1701.02151 [astro-ph.CO].
[276] A. Barnacka, J. F. Glicenstein, and R. Moderski, New constraints on primordial black holes abundance from femtolensing of gamma-ray bursts, Phys. Rev. D **86**, 043001 (2012), arXiv:1204.2056 [astro-ph.CO].
[277] A. Katz, J. Kopp, S. Sibiryakov, and W. Xue, Femtolensing by dark matter revisited, J. Cosmology Astropart. Phys. **2018**, 005 (2018), arXiv:1807.11495 [astro-ph.CO].
[278] A. Katz, J. Kopp, S. Sibiryakov, and W. Xue, Looking for MACHOs in the spectra of fast radio bursts, Mon. Not. Roy. Astron. Soc. **496**, 564–580 (2020), arXiv:1912.07620 [astro-ph.CO].
[279] B. J. Carr and M. Sakellariadou, Dynamical Constraints on Dark Matter in Compact Objects, Astrophys. J. **516**, 195–220 (1999).
[280] M. A. Monroy-Rodríguez and C. Allen, The End of the MACHO Era, Revisited: New Limits on MACHO Masses from Halo Wide Binaries, Astrophys. J. **790**, 159 (2014), arXiv:1406.5169 [astro-ph.GA].
[281] F. Capela, M. Pshirkov, and P. Tinyakov, Constraints on primordial black holes as dark matter candidates from star formation, Phys. Rev. D **87**, 023507 (2013), arXiv:1209.6021 [astro-ph.CO].
[282] F. Capela, M. Pshirkov, and P. Tinyakov, Constraints on primordial black holes as dark matter candidates from capture by neutron stars, Phys. Rev. D **87**, 123524 (2013), arXiv:1301.4984 [astro-ph.CO].
[283] F. Capela, M. Pshirkov, and P. Tinyakov, A comment on "Exclusion of the remaining mass window for primordial black holes ...", arXiv:1401.3025, arXiv e-prints (2014), arXiv:1402.4671 [astro-ph.CO].
[284] G. Defillon, E. Granet, P. Tinyakov, and M. H. G. Tytgat, Tidal capture of primordial black holes by neutron stars, Phys. Rev. D **90**, 103522 (2014), arXiv:1409.0469 [gr-qc].
[285] P. Montero-Camacho, X. Fang, G. Vasquez, M. Silva, and C. M. Hirata, Revisiting constraints on asteroid-mass primordial black holes as dark matter candidates, J. Cosmology Astropart. Phys. **2019**, 031 (2019), arXiv:1906.05950 [astro-ph.CO].
[286] Y. Inoue and A. Kusenko, New X-ray bound on density of primordial black holes, J. Cosmology Astropart. Phys. **2017**, 034 (2017), arXiv:1705.00791 [astro-ph.CO].
[287] P. D. Serpico, V. Poulin, D. Inman, and K. Kohri, Cosmic microwave background bounds on primordial black holes including dark matter halo accretion, Phys. Rev. Res. **2**, 023204 (2020), arXiv:2002.10771 [astro-ph.CO].
[288] T. Nakama, B. Carr, and J. Silk, Limits on primordial black holes from μ distortions in cosmic microwave background, Phys. Rev. D **97**, 043525 (2018), arXiv:1710.06945 [astro-ph.CO].
[289] B. P. Abbott *et al.* (LIGO, VIRGO), Observation of Gravitational Waves from a Binary Black Hole Merger, Phys. Rev. Lett. **116**, 061102 (2016), arXiv:1602.03837 [gr-qc].
[290] B. P. Abbott *et al.* (LIGO, VIRGO), The Rate of Binary Black Hole Mergers Inferred from Advanced LIGO Observations Surrounding GW150914, Astrophys. J. Lett. **833**, L1 (2016), arXiv:1602.03842 [astro-ph.HE].
[291] S. Bird, I. Cholis, J. B. Muñoz, Y. Ali-Haïmoud, M. Kamionkowski, E. D. Kovetz, A. Raccanelli, and A. G. Riess, Did LIGO Detect Dark Matter?, Phys. Rev. Lett. **116**, 201301 (2016), arXiv:1603.00464 [astro-ph.CO].
[292] M. Sasaki, T. Suyama, T. Tanaka, and S. Yokoyama, Primordial Black Hole Scenario for the Gravitational-Wave Event GW150914, Phys. Rev. Lett. **117**, 061101 (2016), [Phys. Rev. Lett. **121**, 059901 (2018)], arXiv:1603.08338 [astro-ph.CO].
[293] M. Raidal, V. Vaskonen, and H. Veermäe, Gravitational waves from primordial black hole mergers, J. Cosmology Astropart. Phys. **2017**, 037 (2017), arXiv:1707.01480 [astro-ph.CO].

[294] B. P. Abbott *et al.* (LIGO, VIRGO), All-sky search for short gravitational-wave bursts in the second Advanced LIGO and Advanced Virgo run, Phys. Rev. D **100**, 024017 (2019), arXiv:1904.08976 [astro-ph.CO].
[295] Z.-C. Chen, C. Yuan, and Q.-G. Huang, Pulsar Timing Array Constraints on Primordial Black Holes with NANOGrav 11-Year Dataset, Phys. Rev. Lett. **124**, 251101 (2020), arXiv:1910.12239 [astro-ph.CO].
[296] R. Caldwell *et al.*, Detection of Early-Universe Gravitational Wave Signatures and Fundamental Physics, arXiv e-prints (2022), arXiv:2203.07972 [gr-qc].
[297] G. Franciolini *et al.*, Quantifying the evidence for primordial black holes in LIGO/Virgo gravitational-wave data, arXiv e-prints (2021), arXiv:2105.03349 [gr-qc].
[298] Z.-C. Chen and Q.-G. Huang, Distinguishing primordial black holes from astrophysical black holes by Einstein Telescope and Cosmic Explorer, J. Cosmology Astropart. Phys. **2020**, 039 (2020), arXiv:1904.02396 [astro-ph.CO].
[299] J. F. Coupechoux, A. Arbey, R. Chierici, H. Hansen, J. Margueron, and V. Sordini, Discriminating same-mass neutron stars and black holes gravitational waveforms, Phys. Rev. D **105**, 064063 (2022), arXiv:2106.05805 [gr-qc].
[300] B. Dasgupta, R. Laha, and A. Ray, Low Mass Black Holes from Dark Core Collapse, Phys. Rev. Lett. **126**, 141105 (2021), arXiv:2009.01825 [astro-ph.HE].
[301] K. Inomata, M. Kawasaki, K. Mukaida, T. Terada, and T. T. Yanagida, Gravitational wave production right after a primordial black hole evaporation, Phys. Rev. D **101**, 123533 (2020), arXiv:2003.10455 [astro-ph.CO].
[302] G. Domènech, V. Takhistov, and M. Sasaki, Exploring evaporating primordial black holes with gravitational waves, Phys. Lett. B **823**, 136722 (2021), arXiv:2105.06816 [astro-ph.CO].
[303] V. Vaskonen and H. Veermäe, Did NANOGrav See a Signal from Primordial Black Hole Formation?, Phys. Rev. Lett. **126**, 051303 (2021), arXiv:2009.07832 [astro-ph.CO].
[304] F. Kühnel, Enhanced detectability of spinning primordial black holes, Eur. Phys. J. C **80**, 243 (2020), arXiv:1909.04742 [astro-ph.CO].
[305] P. Auclair *et al.* (LISA), Cosmology with the Laser Interferometer Space Antenna, arXiv e-prints (2022), arXiv:2204.05434 [astro-ph.CO].
[306] N. Upadhyay, P. Das Gupta, and R. P. Saxena, Baryogenesis from primordial black holes after the electroweak phase transition, Phys. Rev. D **60**, 063513 (1999), arXiv:astro-ph/9903253 [astro-ph].
[307] A. D. Sakharov, Violation of CP Invariance, C Asymmetry, and Baryon Asymmetry of the Universe, J. Exp. Theor. Phys. Lett. **5**, 24 (1967), [Pis'ma Zh. Eksp. Teor. Fiz. **5**, 32 (1967)].
[308] M. S. Turner and D. N. Schramm, The origin of baryons in the Universe, Nature **279**, 303–305 (1979).
[309] M. S. Turner, Baryon production by primordial black holes, Phys. Lett. B **89**, 155–159 (1979).
[310] D. Toussaint, S. B. Treiman, F. Wilczek, and A. Zee, Matter-antimatter accounting, thermodynamics, and black-hole radiation, Phys. Rev. D **19**, 1036–1045 (1979).
[311] S. Weinberg, Cosmological production of baryons, Phys. Rev. Lett. **42**, 850–853 (1979).
[312] D. V. Nanopoulos and S. Weinberg, Mechanisms for cosmological baryon production, Phys. Rev. D **20**, 2484–2493 (1979).
[313] A. D. Dolgov, Quantum evaporation of black holes and the baryon asymmetry of the Universe, J. Exp. Theor. Phys. **52**, 169 (1980), [Pis'ma Zh. Eksp. Teor. Fiz. **79**, 337 (1980)].
[314] A. D. Dolgov, Hiding of the conserved (anti)baryonic charge into black holes, Phys. Rev. D **24**, 1042–1044 (1981).
[315] Y. Nagatani, Electroweak baryogenesis by black holes, Phys. Rev. D **59**, 041301 (1999), arXiv:hep-ph/9811485 [hep-ph].
[316] V. A. Kuzmin, V. A. Rubakov, and M. E. Shaposhnikov, On anomalous electroweak baryon-number

non-conservation in the early universe, Phys. Lett. B **155**, 36–42 (1985).
[317] J. H. Christenson, J. W. Cronin, V. L. Fitch, and R. Turlay, Evidence for the 2π Decay of the K20 Meson, Phys. Rev. Lett. **13**, 138–140 (1964).
[318] B. V. Lehmann, C. Johnson, S. Profumo, and T. Schwemberger, Direct detection of primordial black hole relics as dark matter, J. Cosmology Astropart. Phys. **2019**, 046 (2019), arXiv:1906.06348 [hep-ph].
[319] J. D. Barrow, Primordial baryon generation by black holes, Mon. Not. Roy. Astron. Soc. **192**, 427–438 (1980).
[320] J. D. Barrow, Cosmological baryon annihilation, Mon. Not. Roy. Astron. Soc. **192**, 19P–23P (1980).
[321] J. D. Barrow and G. G. Ross, Cosmological constraints on the scale of grand unification, Nucl. Phys. B **181**, 461–486 (1981).
[322] J. D. Barrow, E. J. Copeland, E. W. Kolb, and A. R. Liddle, Baryogenesis in extended inflation. I. Baryogenesis via production and decay of supermassive bosons, Phys. Rev. D **43**, 977–983 (1991).
[323] J. D. Barrow, E. J. Copeland, E. W. Kolb, and A. R. Liddle, Baryogenesis in extended inflation. II. Baryogenesis via primordial black holes, Phys. Rev. D **43**, 984–994 (1991).
[324] J. D. Barrow, The baryon asymmetry of the Universe., Surv. High Energy Phys. **1**, 183–212 (1980).
[325] A. D. Dolgov, Non-GUT baryogenesis, Phys. Rep. **222**, 309–386 (1992).
[326] D. Lindley, Primordial black holes and the cosmic baryon number, Mon. Not. Roy. Astron. Soc. **196**, 317–338 (1981).
[327] D. Lindely, Primordial black holes and the cosmic baryon number. II, Mon. Not. Roy. Astron. Soc. **199**, 775–784 (1982).
[328] A. Boudon, B. Bose, H. Huang, and L. Lombriser, Baryogenesis through asymmetric Hawking radiation from primordial black holes as dark matter, Phys. Rev. D **103**, 083504 (2021), arXiv:2010.14426 [astro-ph.CO].
[329] N. Smyth, L. Santos-Olmsted, and S. Profumo, Gravitational baryogenesis and dark matter from light black holes, J. Cosmology Astropart. Phys. **2022**, 013 (2022), arXiv:2110.14660 [hep-ph].
[330] D. Hooper and G. Krnjaic, GUT baryogenesis with primordial black holes, Phys. Rev. D **103**, 043504 (2021), arXiv:2010.01134 [hep-ph].
[331] Y. F. Perez-Gonzalez and J. Turner, Assessing the tension between a black hole dominated early universe and leptogenesis, Phys. Rev. D **104**, 103021 (2021), arXiv:2010.03565 [hep-ph].
[332] B. Barman, D. Borah, S. J. Das, and R. Roshan, Non-thermal origin of asymmetric dark matter from inflaton and primordial black holes, J. Cosmology Astropart. Phys. **2022**, 031 (2022), arXiv:2111.08034 [hep-ph].
[333] N. Bernal, C. S. Fong, Y. F. Perez-Gonzalez, and J. Turner, Rescuing High-Scale Leptogenesis using Primordial Black Holes, arXiv e-prints (2022), arXiv:2203.08823 [hep-ph].
[334] Y. B. Zel'dovich and A. A. Starobinskiĭ, Possibility of a cold cosmological singularity in the spectrum of primordial black holes, J. Exp. Theor. Phys. Lett. **24**, 571–573 (1976), [Pis'ma Zh. Eksp. Teor. Fiz. **24**, 616 (1976)].
[335] J. García-Bellido, A. Linde, and D. Wands, Density perturbations and black hole formation in hybrid inflation, Phys. Rev. D **54**, 6040–6058 (1996), arXiv:astro-ph/9605094 [astro-ph].
[336] B. V. Vainer and P. D. Nasel'skii, Observable consequences of the evaporation of low-mass primordial black holes, Soviet Ast. Lett. **3**, 76–78 (1977), [Pis'ma Astron. Zh. **3**, 147 (1977)].
[337] I. B. Zel'dovich, A. A. Starobinskiĭ, M. I. Khlopov, and V. M. Chechetkin, Primordial black holes and the deuterium problem, Soviet Ast. Lett. **3**, 110–112 (1977), [Pis'ma Astron. Zh. **3**, 208 (1977)].
[338] S. Miyama and K. Sato, An Upper Bound on the Number Density of Primordial Black Holes from the Big Bang Nucleosynthesis, Prog. Theor. Phys. **59**, 1012–1013 (1978).
[339] B. V. Vainer, O. V. Dryzhakova, and P. D. Nasel'skii, Primordial black holes and cosmological nucleosynthesis, Soviet Ast. Lett. **4**, 185–187 (1978), [Pis'ma Astron. Zh. **4**, 344 (1978)].

[340] B. V. Vainer and P. D. Nasel'skii, Cosmological implications of the process of primordial black hole evaporation, Soviet Ast. **22**, 138–140 (1978), [Astron. Zh. **55**, 231 (1978)].
[341] T. Rothman and R. Matzner, Upper Limits on Micro-Mini Black Holes, Astrophys. Space Sci. **75**, 229–236 (1981).
[342] V. M. Chechetkin, M. Y. Khlopov, M. G. Sapozhnikov, and Y. B. Zel'dovich, Astrophysical aspects of antiproton interaction with ^{4}He (antimatter in the universe), Phys. Lett. B **118**, 329–332 (1982).
[343] D. Lindley, Radiative decay of massive neutrinos and cosmic element abundances., Mon. Not. Roy. Astron. Soc. **188**, 15P–19P (1979).
[344] D. Lindley, Primordial black holes and the deuterium abundance, Mon. Not. Roy. Astron. Soc. **193**, 593–601 (1980).
[345] M. Kawasaki, K. Kohri, and T. Moroi, Big-bang nucleosynthesis and hadronic decay of long-lived massive particles, Phys. Rev. D **71**, 083502 (2005), arXiv:astro-ph/0408426 [astro-ph].
[346] B. D. Fields, K. A. Olive, T.-H. Yeh, and C. Young, Big-Bang Nucleosynthesis after Planck, J. Cosmology Astropart. Phys. **2020**, 010 (2020), arXiv:1912.01132 [astro-ph.CO].
[347] X. Fu, A. Bressan, P. Molaro, and P. Marigo, Lithium evolution in metal-poor stars: from pre-main sequence to the Spite plateau, Mon. Not. Roy. Astron. Soc. **452**, 3256–3265 (2015), arXiv:1506.05993 [astro-ph.SR].
[348] A. J. Korn, F. Grundahl, O. Richard, P. S. Barklem, L. Mashonkina, R. Collet, N. Piskunov, and B. Gustafsson, A probable stellar solution to the cosmological lithium discrepancy, Nature **442**, 657–659 (2006), arXiv:astro-ph/0608201 [astro-ph].
[349] M. Pospelov and J. Pradler, Metastable GeV-scale particles as a solution to the cosmological lithium problem, Phys. Rev. D **82**, 103514 (2010), arXiv:1006.4172 [hep-ph].
[350] A. Goudelis, M. Pospelov, and J. Pradler, Light Particle Solution to the Cosmic Lithium Problem, Phys. Rev. Lett. **116**, 211303 (2016), arXiv:1510.08858 [hep-ph].
[351] K. Jedamzik, Did something decay, evaporate, or annihilate during big bang nucleosynthesis?, Phys. Rev. D **70**, 063524 (2004), arXiv:astro-ph/0402344 [astro-ph].
[352] R. V. Wagoner, W. A. Fowler, and F. Hoyle, On the Synthesis of Elements at Very High Temperatures, Astrophys. J. **148**, 3 (1967).
[353] R. V. Wagoner, Synthesis of the Elements Within Objects Exploding from Very High Temperatures, Astrophys. J. Suppl. **18**, 247 (1969).
[354] R. V. Wagoner, Big-Bang Nucleosynthesis Revisited, Astrophys. J. **179**, 343–360 (1973).
[355] L. Kawano, Let's go: Early universe 2. Primordial nucleosynthesis the computer way (1992).
[356] M. S. Smith, L. H. Kawano, and R. A. Malaney, Experimental, Computational, and Observational Analysis of Primordial Nucleosynthesis, Astrophys. J. Suppl. **85**, 219 (1993).
[357] E. V. Sedel'nikov, Primordial black holes and nonequilibrium cosmological nucleosynthesis, Astron. Lett. **22**, 797–802 (1996), [Pis'ma Astron. Zh. **22**, 889 (1996)].
[358] S. K. Acharya and R. Khatri, CMB and BBN constraints on evaporating primordial black holes revisited, J. Cosmology Astropart. Phys. **2020**, 018 (2020), arXiv:2002.00898 [astro-ph.CO].
[359] C. Keith, D. Hooper, N. Blinov, and S. D. McDermott, Constraints on primordial black holes from big bang nucleosynthesis revisited, Phys. Rev. D **102**, 103512 (2020), arXiv:2006.03608 [astro-ph.CO].
[360] Y. Luo, C. Chen, M. Kusakabe, and T. Kajino, Impacts of Hawking radiation from primordial black holes in critical collapse model on the light element abundances, J. Cosmology Astropart. Phys. **2021**, 042 (2021), arXiv:2011.10937 [astro-ph.CO].
[361] J. V. Narlikar and N. C. Rana, Hawking process and the cosmic microwave background in a steady state universe, Phys. Lett. A **72**, 75–77 (1979).
[362] A. A. Penzias and R. W. Wilson, A Measurement of Excess Antenna Temperature at 4080 Mc/s., Astrophys. J. **142**, 419–421 (1965).

[363] J. C. Mather *et al.*, A Preliminary Measurement of the Cosmic Microwave Background Spectrum by the Cosmic Background Explorer (COBE) Satellite, Astrophys. J. Lett. **354**, L37 (1990).
[364] M. Gibilisco, Reionization of the Universe Induced by Primordial Black Holes, Int. J. Mod. Phys. A **11**, 5541–5567 (1996), arXiv:astro-ph/9611227 [astro-ph].
[365] M. Gibilisco, The Gunn-Peterson Effect:. A Test for a Black-Hole-Induced Photoionization of the Intergalactic Medium, Int. J. Mod. Phys. A **12**, 2855–2887 (1997), arXiv:astro-ph/9609053 [astro-ph].
[366] M. Gibilisco, The Influence of Quarks and Gluons Jets Coming from Primordial Black Holes on the Reionization of the Universe, Int. J. Mod. Phys. A **12**, 4167–4198 (1997), arXiv:astro-ph/9604116 [astro-ph].
[367] C. L. Bennett *et al.*, First-Year Wilkinson Microwave Anisotropy Probe (WMAP) Observations: Preliminary Maps and Basic Results, Astrophys. J. Suppl. **148**, 1–27 (2003), arXiv:astro-ph/0302207 [astro-ph].
[368] G. Hinshaw *et al.*, First-Year Wilkinson Microwave Anisotropy Probe (WMAP) Observations: The Angular Power Spectrum, Astrophys. J. Suppl. **148**, 135–159 (2003), arXiv:astro-ph/0302217 [astro-ph].
[369] S. J. Clark, B. Dutta, Y. Gao, L. E. Strigari, and S. Watson, Planck constraint on relic primordial black holes, Phys. Rev. D **95**, 083006 (2017), arXiv:1612.07738 [astro-ph.CO].
[370] V. Poulin, J. Lesgourgues, and P. D. Serpico, Cosmological constraints on exotic injection of electromagnetic energy, J. Cosmology Astropart. Phys. **2017**, 043 (2017), arXiv:1610.10051 [astro-ph.CO].
[371] Y. Yang, Constraints on the small-scale curvature perturbation using Planck-2015 data, Mon. Not. Roy. Astron. Soc. **486**, 4569–4573 (2019), arXiv:1904.09104 [astro-ph.CO].
[372] P. D. Nasel'Skii and Y. G. Shevelev, Primordial black holes and spectrum of the background electromagnetic radiation, Astrophysics **14**, 386–390 (1978), [Astrofizika **14**, 679 (1978)].
[373] E. I. Dorosheva and P. D. Nasel'Skii, "Relics" of the early universe and secondary ionization of pregalactic matter, Astrophysics **24**, 321–330 (1986), [Astrofizika **24**, 561 (1986)].
[374] E. I. Dorosheva and P. D. Nasel'skii, Secondary Ionization of Primordial Hydrogen and the Microwave-Background Anisotropy, Soviet Ast. **31**, 1 (1987), [Astron. Zh. **64**, 1 (1987)].
[375] P. D. Nasel'skii and A. G. Polnarev, Nonequilibrium Ionization of the Pregalactic Plasma and the Suppression of Microwave Background Anisotropies, Soviet Ast. Lett. **13**, 67 (1987), [Pis'ma Astron. Zh. **13**, 167 (1987)].
[376] M. Lucca, N. Schöneberg, D. C. Hooper, J. Lesgourgues, and J. Chluba, The synergy between CMB spectral distortions and anisotropies, J. Cosmology Astropart. Phys. **2020**, 026 (2020), arXiv:1910.04619 [astro-ph.CO].
[377] P. D. Nasel'Skii, Kinetics of hydrogen recombination in the presence of low-mass primordial black holes, Astrophysics **14**, 82–91 (1978), [Astrofizika **14**, 145 (1978)].
[378] P. D. Nasel'skii, Hydrogen recombination kinetics in the presence of low-mass primordial black holes, Soviet Ast. Lett. **4**, 209–211 (1978), [Pis'ma Astron. Zh. **4**, 387 (1978)].
[379] J. Lesgourgues, The Cosmic Linear Anisotropy Solving System (CLASS) I: Overview, arXiv e-prints (2011), arXiv:1104.2932 [astro-ph.IM].
[380] D. Blas, J. Lesgourgues, and T. Tram, The Cosmic Linear Anisotropy Solving System (CLASS). Part II: Approximation schemes, J. Cosmology Astropart. Phys. **2011**, 034 (2011), arXiv:1104.2933 [astro-ph.CO].
[381] J. Lesgourgues, The Cosmic Linear Anisotropy Solving System (CLASS) III: Comparision with CAMB for LambdaCDM, arXiv e-prints (2011), arXiv:1104.2934 [astro-ph.CO].
[382] J. Lesgourgues and T. Tram, The Cosmic Linear Anisotropy Solving System (CLASS) IV: efficient implementation of non-cold relics, J. Cosmology Astropart. Phys. **2011**, 032 (2011), arXiv:1104.2935 [astro-ph.CO].

[383] A. Lewis, A. Challinor, and A. Lasenby, Efficient Computation of Cosmic Microwave Background Anisotropies in Closed Friedmann-Robertson-Walker Models, Astrophys. J. **538**, 473–476 (2000), arXiv:astro-ph/9911177 [astro-ph].
[384] N. Lee and Y. Ali-Haïmoud, HYREC-2: A highly accurate sub-millisecond recombination code, Phys. Rev. D **102**, 083517 (2020), arXiv:2007.14114 [astro-ph.CO].
[385] P. Stöcker, M. Krämer, J. Lesgourgues, and V. Poulin, Exotic energy injection with ExoCLASS: application to the Higgs portal model and evaporating black holes, J. Cosmology Astropart. Phys. **2018**, 018 (2018), arXiv:1801.01871 [astro-ph.CO].
[386] H. Poulter, Y. Ali-Haïmoud, J. Hamann, M. White, and A. G. Williams, CMB constraints on ultra-light primordial black holes with extended mass distributions, arXiv e-prints (2019), arXiv:1907.06485 [astro-ph.CO].
[387] S. K. Acharya and R. Khatri, CMB spectral distortions constraints on primordial black holes, cosmic strings and long lived unstable particles revisited, J. Cosmology Astropart. Phys. **2020**, 010 (2020), arXiv:1912.10995 [astro-ph.CO].
[388] J. Cang, Y. Gao, and Y.-Z. Ma, Prospects of future CMB anisotropy probes for primordial black holes, J. Cosmology Astropart. Phys. **2021**, 051 (2021), arXiv:2011.12244 [astro-ph.CO].
[389] A. Halder and M. Pandey, Probing the effects of primordial black holes on 21-cm EDGES signal along with interacting dark energy and dark matter-baryon scattering, Mon. Not. Roy. Astron. Soc. **508**, 3446–3454 (2021), arXiv:2101.05228 [astro-ph.CO].
[390] S. Mittal, A. Ray, G. Kulkarni, and B. Dasgupta, Constraining primordial black holes as dark matter using the global 21-cm signal with X-ray heating and excess radio background, J. Cosmology Astropart. Phys. **2022**, 030 (2022), arXiv:2107.02190 [astro-ph.CO].
[391] A. K. Saha and R. Laha, Sensitivities on non-spinning and spinning primordial black hole dark matter with global 21 cm troughs, arXiv e-prints (2021), arXiv:2112.10794 [astro-ph.CO].
[392] K. J. Mack and D. H. Wesley, Primordial black holes in the Dark Ages: Observational prospects for future 21cm surveys, arXiv e-prints (2008), arXiv:0805.1531 [astro-ph].
[393] S. J. Clark, B. Dutta, Y. Gao, Y.-Z. Ma, and L. E. Strigari, 21 cm limits on decaying dark matter and primordial black holes, Phys. Rev. D **98**, 043006 (2018), arXiv:1803.09390 [astro-ph.HE].
[394] Y. Yang, Constraints on primordial black holes and curvature perturbations from the global 21-cm signal, Phys. Rev. D **102**, 083538 (2020), arXiv:2009.11547 [astro-ph.CO].
[395] A. Halder, M. Pandey, D. Majumdar, and R. Basu, Exploring multimessenger signals from heavy dark matter decay with EDGES 21-cm result and IceCube, J. Cosmology Astropart. Phys. **2021**, 033 (2021), arXiv:2105.14356 [astro-ph.CO].
[396] A. Halder and S. Banerjee, Bounds on abundance of primordial black hole and dark matter from EDGES 21-cm signal, Phys. Rev. D **103**, 063044 (2021), arXiv:2102.00959 [astro-ph.CO].
[397] J. Cang, Y. Gao, and Y.-Z. Ma, 21-cm constraints on spinning primordial black holes, J. Cosmology Astropart. Phys. **2022**, 012 (2022), arXiv:2108.13256 [astro-ph.CO].
[398] P. K. Natwariya, A. C. Nayak, and T. Srivastava, Constraining spinning primordial black holes with global 21-cm signal, Mon. Not. Roy. Astron. Soc. **510**, 4236–4241 (2022), arXiv:2107.12358 [astro-ph.CO].
[399] U. Mukhopadhyay, D. Majumdar, and A. Halder, Constraining and constructing mass distributions of Primordial Black Holes from 21cm signal, arXiv e-prints (2022), arXiv:2203.13008 [astro-ph.CO].
[400] R. Davis, D. S. Harmer, and K. C. Hoffman, Search for Neutrinos from the Sun, Phys. Rev. Lett. **20**, 1205–1209 (1968).
[401] T. K. Gaisser, T. Stanev, and G. Barr, Cosmic-ray neutrinos in the atmosphere, Phys. Rev. D **38**, 85–95 (1988).
[402] J. H. MacGibbon and B. J. Carr, Cosmic Rays from Primordial Black Holes, Astrophys. J. **371**, 447

(1991).
[403] B. V. Vainer, Kinetics of neutrino radiation in the hot model of the universe with primordial black holes, Astrophysics **14**, 185–193 (1978), [Astrofizika **14**, 325 (1978)].
[404] F. Halzen, B. Keszthelyi, and E. Zas, Neutrinos from primordial black holes, Phys. Rev. D **52**, 3239–3247 (1995), arXiv:hep-ph/9502268 [hep-ph].
[405] B. Pontecorvo, Mesonium and Antimesonium, J. Exp. Theor. Phys. **6**, 429 (1958), [Pis'ma Zh. Eksp. Teor. Fiz. **33**, 549 (1957)].
[406] B. Pontecorvo, Neutrino Experiments and the Problem of Conservation of Leptonic Charge, J. Exp. Theor. Phys. **26**, 984 (1968), [Pis'ma Zh. Eksp. Teor. Fiz. **53**, 1717 (1967)].
[407] D. Bambeck and W. A. Hiscock, Effects of nonzero neutrino masses on black hole evaporation, Class. Quantum Gravity **22**, 4247–4251 (2005), arXiv:gr-qc/0506050 [gr-qc].
[408] C. Lunardini and Y. F. Perez-Gonzalez, Dirac and Majorana neutrino signatures of primordial black holes, J. Cosmology Astropart. Phys. **2020**, 014 (2020), arXiv:1910.07864 [hep-ph].
[409] E. V. Bugaev and K. V. Konishchev, Constraints on diffuse neutrino background from primordial black holes, Phys. Rev. D **65**, 123005 (2002), arXiv:astro-ph/0005295 [astro-ph].
[410] E. V. Bugaev and K. V. Konishchev, Cosmological constraints from evaporation of primordial black holes, Phys. Rev. D **66**, 084004 (2002), arXiv:astro-ph/0206082 [astro-ph].
[411] B. Dasgupta, R. Laha, and A. Ray, Neutrino and Positron Constraints on Spinning Primordial Black Hole Dark Matter, Phys. Rev. Lett. **125**, 101101 (2020), arXiv:1912.01014 [hep-ph].
[412] V. De Romeri, P. Martínez-Miravé, and M. Tórtola, Signatures of primordial black hole dark matter at DUNE and THEIA, J. Cosmology Astropart. Phys. **2021**, 051 (2021), arXiv:2106.05013 [hep-ph].
[413] S. Wang, D.-M. Xia, X. Zhang, S. Zhou, and Z. Chang, Constraining primordial black holes as dark matter at JUNO, Phys. Rev. D **103**, 043010 (2021), arXiv:2010.16053 [hep-ph].
[414] R. Calabrese, D. F. G. Fiorillo, G. Miele, S. Morisi, and A. Palazzo, Primordial black hole dark matter evaporating on the neutrino floor, Phys. Lett. B **829**, 137050 (2022), arXiv:2106.02492 [hep-ph].
[415] N. Bernal, V. Muñoz-Albornoz, S. Palomares-Ruiz, and P. Villanueva-Domingo, Current and future neutrino limits on the abundance of primordial black holes, arXiv e-prints (2022), arXiv:2203.14979 [hep-ph].
[416] A. D. Dolgov, P. D. Naselsky, and I. D. Novikov, Gravitational waves, baryogenesis, and dark matter from primordial black holes, arXiv e-prints (2000), arXiv:astro-ph/0009407 [astro-ph].
[417] G. S. Bisnovatyi-Kogan and V. N. Rudenko, Very high frequency gravitational wave background in the universe, Class. Quantum Gravity **21**, 3347–3359 (2004), arXiv:gr-qc/0406089 [gr-qc].
[418] A. D. Dolgov and D. Ejlli, Relic gravitational waves from light primordial black holes, Phys. Rev. D **84**, 024028 (2011), arXiv:1105.2303 [astro-ph.CO].
[419] A. D. Dolgov and D. Ejlli, Resonant high energy graviton to photon conversion at the post-recombination epoch, Phys. Rev. D **87**, 104007 (2013), arXiv:1303.1556 [gr-qc].
[420] A. Ejlli, D. Ejlli, A. M. Cruise, G. Pisano, and H. Grote, Upper limits on the amplitude of ultra-high-frequency gravitational waves from graviton to photon conversion, Eur. Phys. J. C **79**, 1032 (2019), arXiv:1908.00232 [gr-qc].
[421] A. Arbey, J. Auffinger, and J. Silk, Primordial Kerr Black Holes, in *40th International Conference on High Energy Physics (ICHEP2020)*, Proc. Sci. (2021) p. 585, arXiv:2012.14767 [astro-ph.CO] .
[422] P. D. Nasel'skii and N. V. Pelikhov, Primordial Black Holes and the Galactic Radio Spectrum, Soviet Ast. **23**, 402 (1979), [Astron. Zh. **56**, 714 (1979)].
[423] D. N. Page and S. W. Hawking, Gamma rays from primordial black holes., Astrophys. J. **206**, 1–7 (1976).
[424] J. L. Fanselow, R. C. Hartman, R. H. Hildebrad, and P. Meyer, Charge Composition and Energy Spectrum of Primary Cosmic-Ray Electrons, Astrophys. J. **158**, 771 (1969).

[425] A. C. Cummings, *A study of cosmic-ray positron and electron spectra in interplanetary and interstellar space and the solar modulation of cosmic rays*, Ph.D. thesis, Caltech, USA (1973).
[426] V. L. Ginzburg and V. S. Ptuskin, On the origin of cosmic rays: Some problems in high-energy astrophysics, Soviet Phys. Usp. **18**, 931–959 (1975), [Usp. Fiz. Nauk **117**, 585 (1975)].
[427] Y. Génolini *et al.*, New minimal, median, and maximal propagation models for dark matter searches with Galactic cosmic rays, Phys. Rev. D **104**, 083005 (2021), arXiv:2103.04108 [astro-ph.HE].
[428] I. Johnson, W. N., J. Harnden, F. R., and R. C. Haymes, The Spectrum of Low-Energy Gamma Radiation from the Galactic-Center Region., Astrophys. J. Lett. **172**, L1 (1972).
[429] I. Johnson, W. N. and R. C. Haymes, Detection of a Gamma-Ray Spectral Line from the Galactic-Center Region, Astrophys. J. **184**, 103–126 (1973).
[430] R. C. Haymes, G. D. Walraven, C. A. Meegan, R. D. Hall, F. T. Djuth, and D. H. Shelton, Detection of nuclear gamma rays from the galactic center region., Astrophys. J. **201**, 593–602 (1975).
[431] M. Leventhal, C. J. MacCallum, and P. D. Stang, Detection of 511 keV positron annihilation radiation from the galactic center direction., Astrophys. J. Lett. **225**, L11–L14 (1978).
[432] P. N. Okeke and M. J. Rees, Observational consequences of positron production by evaporating black holes, Astron. Astrophys. **81**, 263 (1980).
[433] P. N. Okeke, The Primary Source and the Fates of Galactic Positrons, Astrophys. Space Sci. **71**, 371–375 (1980).
[434] C. Bambi, A. D. Dolgov, and A. A. Petrov, Primordial black holes and the observed Galactic 511 keV line, Phys. Lett. B **670**, 174–178 (2008), arXiv:0801.2786 [astro-ph].
[435] S. W. Barwick *et al.*, Cosmic Ray Positrons at High Energies: A New Measurement, Phys. Rev. Lett. **75**, 390–393 (1995).
[436] B. J. Carr and J. H. MacGibbon, Cosmic rays from primordial black holes and constraints on the early universe., Phys. Rep. **307**, 141–154 (1998).
[437] R. Laha, Primordial Black Holes as a Dark Matter Candidate Are Severely Constrained by the Galactic Center 511 keV γ -Ray Line, Phys. Rev. Lett. **123**, 251101 (2019), arXiv:1906.09994 [astro-ph.HE].
[438] W. DeRocco and P. W. Graham, Constraining Primordial Black Hole Abundance with the Galactic 511 keV Line, Phys. Rev. Lett. **123**, 251102 (2019), arXiv:1906.07740 [astro-ph.CO].
[439] C. Keith and D. Hooper, 511 keV excess and primordial black holes, Phys. Rev. D **104**, 063033 (2021), arXiv:2103.08611 [astro-ph.CO].
[440] J. D. Wells, A. Moiseev, and J. F. Ormes, Illuminating Dark Matter and Primordial Black Holes with Interstellar Antiprotons, Astrophys. J. **518**, 570–575 (1999), arXiv:hep-ph/9811325 [hep-ph].
[441] E. C. Stone, A. C. Cummings, F. B. McDonald, B. C. Heikkila, N. Lal, and W. R. Webber, Voyager 1 Observes Low-Energy Galactic Cosmic Rays in a Region Depleted of Heliospheric Ions, Science **341**, 150–153 (2013).
[442] M. Boudaud and M. Cirelli, Voyager 1 $e^{\pm}$ Further Constrain Primordial Black Holes as Dark Matter, Phys. Rev. Lett. **122**, 041104 (2019), arXiv:1807.03075 [astro-ph.HE].
[443] H. Kim, A constraint on light primordial black holes from the interstellar medium temperature, Mon. Not. Roy. Astron. Soc. **504**, 5475–5484 (2021), arXiv:2007.07739 [hep-ph].
[444] R. Laha, P. Lu, and V. Takhistov, Gas heating from spinning and non-spinning evaporating primordial black holes, Phys. Lett. B **820**, 136459 (2021), arXiv:2009.11837 [astro-ph.CO].
[445] C. Lee and M. Ho Chan, The Evaporating Primordial Black Hole Fraction in Cool-core Galaxy Clusters, Astrophys. J. **912**, 24 (2021), arXiv:2103.12354 [astro-ph.HE].
[446] P. Kiraly, J. Szabelski, J. Wdowczyk, and A. W. Wolfendale, Antiprotons in the cosmic radiation, Nature **293**, 120–122 (1981).
[447] R. L. Golden, S. Horan, B. G. Mauger, G. D. Badhwar, J. L. Lacy, S. A. Stephens, R. R. Daniel, and J. E. Zipse, Evidence for the Existence of Cosmic-Ray Antiprotons, Phys. Rev. Lett. **43**, 1196–1199

(1979).
[448] A. Buffington, S. M. Schindler, and C. R. Pennypacker, A measurement of the cosmic-ray antiproton flux and a search for antihelium, Astrophys. J. **248**, 1179–1193 (1981).
[449] M. S. Turner, Could primordial black holes be the source of the cosmic ray antiprotons?, Nature **297**, 379–381 (1982).
[450] K. Yoshimura *et al.*, Observation of cosmic-ray antiprotons at energies below 500 MeV, Phys. Rev. Lett. **75**, 3792–3795 (1995).
[451] K. Maki, T. Mitsui, and S. Orito, Local Flux of Low-Energy Antiprotons from Evaporating Primordial Black Holes, Phys. Rev. Lett. **76**, 3474–3477 (1996), arXiv:astro-ph/9601025 [astro-ph].
[452] T. Mitsui, K. Maki, and S. Orito, Expected enhancement of the primary antiproton flux at the solar minimum, Phys. Lett. B **389**, 169–175 (1996), arXiv:astro-ph/9608123 [astro-ph].
[453] T. Sjöstrand, High-energy-physics event generation with PYTHIA 5.7 and JETSET 7.4, Comput. Phys. Commun. **82**, 74–89 (1994).
[454] E. V. Bugaev *et al.*, Experimental search of bursts of gamma rays from primordial black holes using different evaporation models, arXiv e-prints (2009), arXiv:0906.3182 [astro-ph.CO].
[455] N. A. Porter, Searches for gamma-ray bursts from exploding primordial black holes., Irish Astron. J. **13**, 173–175 (1978).
[456] N. A. Porter and T. C. Weekes, A search for high energy gamma-ray bursts from primordial black holes or other astronomical objects., Mon. Not. Roy. Astron. Soc. **183**, 205–210 (1978).
[457] A. Albert *et al.* (HAWC), Constraining the local burst rate density of primordial black holes with HAWC, J. Cosmology Astropart. Phys. **2020**, 026 (2020), arXiv:1911.04356 [astro-ph.HE].
[458] T. Tavernier, J. F. Glicenstein, and F. Brun, Search for Primordial Black Hole evaporations with H.E.S.S., in *36th International Cosmic Ray Conference (ICRC2019)*, Proc. Sci., Vol. 36 (2019) p. 804, arXiv:1909.01620 [astro-ph.HE] .
[459] T. Tavernier, F. Brun, J. F. Glicenstein, and V. Marandon (HESS), Limits on primordial black hole evaporation from H.E.S.S. observations, in *37th International Cosmic Ray Conference (ICRC2021)*, Proc. Sci. (2021) p. 518.
[460] M. Ackermann *et al.*, Search for Gamma-Ray Emission from Local Primordial Black Holes with the Fermi Large Area Telescope, Astrophys. J. **857**, 49 (2018).
[461] R. López-Coto, M. Doro, A. de Angelis, M. Mariotti, and J. P. Harding, Prospects for the observation of Primordial Black Hole evaporation with the Southern Wide field of view Gamma-ray Observatory, J. Cosmology Astropart. Phys. **2021**, 040 (2021), arXiv:2103.16895 [astro-ph.HE].
[462] F. Halzen, E. Zas, J. H. MacGibbon, and T. C. Weekes, Gamma rays and energetic particles from primordial black holes, Nature **353**, 807–815 (1991).
[463] D. E. Alexandreas *et al.*, New limit on the rate-density of evaporating black holes, Phys. Rev. Lett. **71**, 2524–2527 (1993).
[464] D. V. Semikoz, On the Detection of Individual Primordial Black Hole Explosions, Astrophys. J. **436**, 254 (1994).
[465] T. N. Ukwatta, D. R. Stump, J. T. Linnemann, J. H. MacGibbon, S. S. Marinelli, T. Yapici, and K. Tollefson, Primordial Black Holes: Observational characteristics of the final evaporation, Astropart. Phys. **80**, 90–114 (2016), arXiv:1510.04372 [astro-ph.HE].
[466] N. A. Porter, The atmospheric Čerenkov technique in the search for PBH, Space Sci. Rev. **75**, 67–69 (1996).
[467] A. Barrau, Primordial black holes as a source of extremely high energy cosmic rays, Astropart. Phys. **12**, 269–275 (2000), arXiv:astro-ph/9907347 [astro-ph].
[468] K. Greisen, End to the Cosmic-Ray Spectrum?, Phys. Rev. Lett. **16**, 748–750 (1966).
[469] G. T. Zatsepin and V. A. Kuz'min, Upper Limit of the Spectrum of Cosmic Rays,

J. Exp. Theor. Phys. Lett. **4**, 78 (1966), [Pis'ma Zh. Eksp. Teor. Fiz. **4**, 114 (1966)].
[470] M. Takeda *et al.* (AGASA), Extension of the Cosmic-Ray Energy Spectrum beyond the Predicted Greisen-Zatsepin-Kuz'min Cutoff, Phys. Rev. Lett. **81**, 1163–1166 (1998), arXiv:astro-ph/9807193 [astro-ph].
[471] M. J. Baker and A. Thamm, Probing the Particle Spectrum of Nature with Evaporating Black Holes, arXiv e-prints (2021), arXiv:2105.10506 [hep-ph].
[472] A. A. Belyanin, V. V. Kocharovsky, and V. Kocharovsky v., Gamma-ray bursts from evaporating primordial black holes, Radiophys. Quantum Electron. **41**, 22–27 (1998).
[473] M. W. E. Smith *et al.*, The Astrophysical Multimessenger Observatory Network (AMON), Astropart. Phys. **45**, 56–70 (2013), arXiv:1211.5602 [astro-ph.HE].
[474] G. Tešić, Searching for primordial black hole evaporation signal with AMON, in *34th International Cosmic Ray Conference (ICRC2015)*, Proc. Sci., Vol. 34 (2015) p. 328.
[475] P. I. Dyadina, B. N. Latosh, and S. O. Alexeyev, On evaporation of Randall-Sundrum black holes, in *Almost 100 years after Einstein Revolution (ERE2014)*, J. Phys. Conf. Ser., Vol. 600 (2015) p. 012034.
[476] S. E. Cutchin, J. H. Simonetti, S. W. Ellingson, A. S. Larracuente, and M. J. Kavic, Constraining the Rate of Primordial Black Hole Explosions and Extra-Dimension Scale Using a Low-Frequency Radio Antenna Array, Publ. Astron. Soc. Pac. **127**, 1269 (2015), arXiv:1608.01945 [astro-ph.HE].
[477] J. H. MacGibbon, Can Planck-mass relics of evaporating black holes close the Universe?, Nature **329**, 308–309 (1987).
[478] M. Davis, G. Efstathiou, C. S. Frenk, and S. D. M. White, The evolution of large scale structure in a universe dominated by cold dark matter, Astrophys. J. **292**, 371–394 (1985).
[479] J. D. Barrow, E. J. Copeland, and A. R. Liddle, The cosmology of black hole relics, Phys. Rev. D **46**, 645–657 (1992).
[480] A. G. Doroshkevich and P. D. Naselsky, Ultra - High Energy Cosmic Rays from decay of the Super Heavy Dark Matter Relics, arXiv e-prints (2000), arXiv:astro-ph/0011320 [astro-ph].
[481] M. P. Hertzberg, E. D. Schiappacasse, and T. T. Yanagida, Implications for dark matter direct detection in the presence of LIGO-motivated primordial black holes, Phys. Lett. B **807**, 135566 (2020), arXiv:1910.10575 [astro-ph.CO].
[482] Y. N. Eroshenko, Dark matter around primordial black hole at the radiation-dominated stage, Int. J. Mod. Phys. A **35**, 2040046 (2020), arXiv:1910.01564 [astro-ph.CO].
[483] M. Boudaud, T. Lacroix, M. Stref, J. Lavalle, and P. Salati, In-depth analysis of the clustering of dark matter particles around primordial black holes. Part I. Density profiles, J. Cosmology Astropart. Phys. **2021**, 053 (2021), arXiv:2106.07480 [astro-ph.CO].
[484] Y. N. Eroshenko, Dark matter density spikes around primordial black holes, Astron. Lett. **42**, 347–356 (2016), arXiv:1607.00612 [astro-ph.HE].
[485] S. M. Boucenna, F. Kühnel, T. Ohlsson, and L. Visinelli, Novel constraints on mixed dark-matter scenarios of primordial black holes and WIMPs, J. Cosmology Astropart. Phys. **2018**, 003 (2018), arXiv:1712.06383 [hep-ph].
[486] R.-G. Cai, Y.-C. Ding, X.-Y. Yang, and Y.-F. Zhou, Constraints on a mixed model of dark matter particles and primordial black holes from the galactic 511 keV line, J. Cosmology Astropart. Phys. **2021**, 057 (2021), arXiv:2007.11804 [astro-ph.CO].
[487] K. Kadota and H. Tashiro, Primordial black hole dark matter in the presence of p-wave WIMP annihilation, J. Cosmology Astropart. Phys. **2022**, 045 (2022), arXiv:2112.04179 [astro-ph.CO].
[488] G. Bertone, A. M. Coogan, D. Gaggero, B. J. Kavanagh, and C. Weniger, Primordial black holes as silver bullets for new physics at the weak scale, Phys. Rev. D **100**, 123013 (2019), arXiv:1905.01238 [hep-ph].
[489] J. Adamek, C. T. Byrnes, M. Gosenca, and S. Hotchkiss, WIMPs and stellar-mass primordial black

holes are incompatible, Phys. Rev. D **100**, 023506 (2019), arXiv:1901.08528 [astro-ph.CO].
[490] B. C. Lacki and J. F. Beacom, Primordial Black Holes as Dark Matter: Almost All or Almost Nothing, Astrophys. J. Lett. **720**, L67–L71 (2010), arXiv:1003.3466 [astro-ph.CO].
[491] B. Carr, F. Kühnel, and L. Visinelli, Black holes and WIMPs: all or nothing or something else, Mon. Not. Roy. Astron. Soc. **506**, 3648–3661 (2021), arXiv:2011.01930 [astro-ph.CO].
[492] G. F. Chapline, Cosmological effects of primordial black holes, Nature **253**, 251–252 (1975).
[493] C. E. Fichtel *et al.*, High-energy gamma-ray results from the second Small Astronomy Satellite., Astrophys. J. **198**, 163–182 (1975).
[494] V. Schönfelder, U. Graser, and J. Daugherty, Diffuse cosmic and atmospheric MeV gamma radiation from balloon observations., Astrophys. J. **217**, 306–319 (1977).
[495] J. M. Overduin and P. S. Wesson, Constraints on Dark Matter from Intergalactic Radiation, Vistas Astron. **35**, 439 (1992).
[496] M. T. Ressell and M. S. Turner, The Grand Unified Photon Spectrum: A Coherent View of the Diffuse Extragalactic Background Radiation, Comments Astrophys. **14**, 323 (1990).
[497] J. M. Overduin and P. S. Wesson, Dark matter and background light, Phys. Rep. **402**, 267–406 (2004), arXiv:astro-ph/0407207 [astro-ph].
[498] S. C. Kappadath *et al.*, The preliminary cosmic diffuse γ-ray spectrum from 800keV to 30MeV measured with COMPTEL., Astron. Astrophys. Suppl. **120**, 619–622 (1996).
[499] P. Sreekumar *et al.*, EGRET Observations of the Extragalactic Gamma-Ray Emission, Astrophys. J. **494**, 523–534 (1998), arXiv:astro-ph/9709257 [astro-ph].
[500] H. I. Kim, C. H. Lee, and J. H. MacGibbon, Diffuse γ-ray background and primordial black hole constraints on the spectral index of density fluctuations, Phys. Rev. D **59**, 063004 (1999), arXiv:astro-ph/9901030 [astro-ph].
[501] G. D. Kribs, A. K. Leibovich, and I. Z. Rothstein, Bounds from primordial black holes with a near critical collapse initial mass function, Phys. Rev. D **60**, 103510 (1999), arXiv:astro-ph/9904021 [astro-ph].
[502] A. Barrau, G. Boudoul, and L. Derome, An improved gamma-ray limit on the density of PBHs, arXiv e-prints (2003), arXiv:astro-ph/0304528 [astro-ph].
[503] G. Ballesteros, J. Coronado-Blázquez, and D. Gaggero, X-ray and gamma-ray limits on the primordial black hole abundance from Hawking radiation, Phys. Lett. B **808**, 135624 (2020), arXiv:1906.10113 [astro-ph.CO].
[504] J. Iguaz, P. D. Serpico, and T. Siegert, Isotropic x-ray bound on primordial black hole dark matter, Phys. Rev. D **103**, 103025 (2021), arXiv:2104.03145 [astro-ph.CO].
[505] A. Coogan, A. Moiseev, L. Morrison, and S. Profumo, Hunting for Dark Matter and New Physics with (a) GECCO, arXiv e-prints (2021), arXiv:2101.10370 [astro-ph.HE].
[506] D. Ghosh, D. Sachdeva, and P. Singh, Future Constraints on Primordial Black Holes from XGIS-THESEUS, arXiv e-prints (2021), arXiv:2110.03333 [astro-ph.CO].
[507] A. Ray, R. Laha, J. B. Muñoz, and R. Caputo, Near future MeV telescopes can discover asteroid-mass primordial black hole dark matter, Phys. Rev. D **104**, 023516 (2021), arXiv:2102.06714 [astro-ph.CO].
[508] J. Berteaud, F. Calore, J. Iguaz, P. D. Serpico, and T. Siegert, Strong constraints on primordial black hole dark matter from 16 years of INTEGRAL/SPI observations, arXiv e-prints (2022), arXiv:2202.07483 [astro-ph.HE].
[509] S. Mittal and G. Kulkarni, Background of radio photons from primordial black holes, Mon. Not. Roy. Astron. Soc. **510**, 4992–4997 (2022), arXiv:2110.11975 [astro-ph.CO].
[510] S. Chen, H.-H. Zhang, and G. Long, Revisiting the constraints on primordial black hole abundance with the isotropic gamma-ray background, Phys. Rev. D **105**, 063008 (2022), arXiv:2112.15463 [astro-ph.CO].

[511] Y. Sendouda, S. Nagataki, and K. Sato, Mass spectrum of primordial black holes from inflationary perturbation in the Randall Sundrum braneworld: a limit on blue spectra, J. Cosmology Astropart. Phys. **2006**, 003 (2006), arXiv:astro-ph/0603509 [astro-ph].
[512] S. Sajad Tabasi and J. T. Firouzjaee, New constraint on the Hawking evaporation of primordial black holes in the radiation-dominated era, arXiv e-prints (2021), arXiv:2112.02818 [astro-ph.CO].
[513] R. Laha, J. B. Muñoz, and T. R. Slatyer, INTEGRAL constraints on primordial black holes and particle dark matter, Phys. Rev. D **101**, 123514 (2020), arXiv:2004.00627 [astro-ph.CO].
[514] A. Arbey, J. Auffinger, and J. Silk, Constraining primordial black hole masses with the isotropic gamma ray background, Phys. Rev. D **101**, 023010 (2020), arXiv:1906.04750 [astro-ph.CO].
[515] Y.-F. Cai, C. Chen, Q. Ding, and Y. Wang, Ultrahigh-energy Gamma Rays and Gravitational Waves from Primordial Exotic Stellar Bubbles, arXiv e-prints (2021), arXiv:2105.11481 [astro-ph.CO].
[516] G. Dvali, A Microscopic Model of Holography: Survival by the Burden of Memory, arXiv e-prints (2018), arXiv:1810.02336 [hep-th].
[517] G. Dvali, L. Eisemann, M. Michel, and S. Zell, Black hole metamorphosis and stabilization by memory burden, Phys. Rev. D **102**, 103523 (2020), arXiv:2006.00011 [hep-th].
[518] R. Torres, Mechanism of quasistabilization of primordial black holes, Phys. Rev. D **87**, 123514 (2013).
[519] A. Raccanelli, F. Vidotto, and L. Verde, Effects of primordial black holes quantum gravity decay on galaxy clustering, J. Cosmology Astropart. Phys. **2018**, 003 (2018), arXiv:1708.02588 [astro-ph.CO].
[520] E. L. Wright, On the Density of Primordial Black Holes in the Galactic Halo, Astrophys. J. **459**, 487 (1996), arXiv:astro-ph/9509074 [astro-ph].
[521] P. Meszaros, The behaviour of point masses in an expanding cosmological substratum., Astron. Astrophys. **37**, 225–228 (1974).
[522] B. J. Carr, The statistical clustering of primordial black holes., Astron. Astrophys. **56**, 377–383 (1977).
[523] J. R. Chisholm, Clustering of primordial black holes: Basic results, Phys. Rev. D **73**, 083504 (2006), arXiv:astro-ph/0509141 [astro-ph].
[524] K. M. Belotsky, A. E. Dmitriev, E. A. Esipova, V. A. Gani, A. V. Grobov, M. Y. Khlopov, A. A. Kirillov, S. G. Rubin, and I. V. Svadkovsky, Signatures of primordial black hole dark matter, Mod. Phys. Lett. A **29**, 1440005 (2014), arXiv:1410.0203 [astro-ph.CO].
[525] K. M. Belotsky *et al.*, Clusters of Primordial Black Holes, Eur. Phys. J. C **79**, 246 (2019), arXiv:1807.06590 [astro-ph.CO].
[526] L. Bouchet, A. W. Strong, T. A. Porter, I. V. Moskalenko, E. Jourdain, and J.-P. Roques, Diffuse Emission Measurement with the SPectrometer on INTEGRAL as an Indirect Probe of Cosmic-Ray Electrons and Positrons, Astrophys. J. **739**, 29 (2011), arXiv:1107.0200 [astro-ph.HE].
[527] A. W. Strong *et al.*, Diffuse continuum gamma rays from the Galaxy observed by COMPTEL., Astron. Astrophys. **292**, 82–91 (1994).
[528] A. W. Strong and J. R. Mattox, Gradient model analysis of EGRET diffuse Galactic γ-ray emission., Astron. Astrophys. **308**, L21–L24 (1996).
[529] A. W. Strong, H. Bloemen, R. Diehl, W. Hermsen, and V. Schönfelder, COMPTEL Skymapping: a New Approach Using Parallel Computing, Astrophys. Lett. Commun. **39**, 209 (1999), arXiv:astro-ph/9811211 [astro-ph].
[530] A. W. Strong, Interstellar Gamma Rays and Cosmic Rays: New Insights from Fermi-LAT and INTEGRAL, in *Cosmic Rays for Particle and Astroparticle Physics (ICATPP2010)*, edited by S. Giani, C. Leroy, and P. G. Rancoita (2011) pp. 473–481, arXiv:1101.1381 [astro-ph.HE] .
[531] J. F. Beacom and H. Yüksel, Stringent Constraint on Galactic Positron Production, Phys. Rev. Lett. **97**, 071102 (2006), arXiv:astro-ph/0512411 [astro-ph].
[532] R. Bartels, D. Gaggero, and C. Weniger, Prospects for indirect dark matter searches with MeV photons, J. Cosmology Astropart. Phys. **2017**, 001 (2017), arXiv:1703.02546 [astro-ph.HE].

[533] D. E. Gruber, J. L. Matteson, L. E. Peterson, and G. V. Jung, The Spectrum of Diffuse Cosmic Hard X-Rays Measured with HEAO 1, Astrophys. J. **520**, 124–129 (1999), arXiv:astro-ph/9903492 [astro-ph].
[534] P. Ruiz-Lapuente, L.-S. The, D. H. Hartmann, M. Ajello, R. Canal, F. K. Röpke, S. T. Ohlmann, and W. Hillebrandt, The Origin of the Cosmic Gamma-ray Background in the MeV Range, Astrophys. J. **820**, 142 (2016), arXiv:1502.06116 [astro-ph.HE].
[535] A. W. Strong, I. V. Moskalenko, and O. Reimer, A New Determination of the Extragalactic Diffuse Gamma-Ray Background from EGRET Data, Astrophys. J. **613**, 956–961 (2004), arXiv:astro-ph/0405441 [astro-ph].
[536] M. Ackermann *et al.*, The Spectrum of Isotropic Diffuse Gamma-Ray Emission between 100 MeV and 820 GeV, Astrophys. J. **799**, 86 (2015), arXiv:1410.3696 [astro-ph.HE].
[537] A. Moretti, A New Measurement of the Cosmic X-ray Background, in *SIMBOL-X: Focusing on the Hard X-ray Universe*, Am. Inst. Phys. Conf. Proc., Vol. 1126, edited by J. Rodriguez and P. Ferrando (2009) pp. 223–226, arXiv:0811.1444 [astro-ph] .
[538] K. K. Boddy and J. Kumar, Indirect detection of dark matter using MeV-range gamma-ray telescopes, Phys. Rev. D **92**, 023533 (2015), arXiv:1504.04024 [astro-ph.CO].
[539] S. S. Kimura, K. Murase, and P. Mészáros, Soft gamma rays from low accreting supermassive black holes and connection to energetic neutrinos, Nat. Commun. **12**, 5615 (2021), arXiv:2005.01934 [astro-ph.HE].
[540] M. A. Roth, M. R. Krumholz, R. M. Crocker, and S. Celli, The diffuse γ-ray background is dominated by star-forming galaxies, Nature **597**, 341–344 (2021), arXiv:2109.07598 [astro-ph.HE].
[541] Y. Inoue, D. Khangulyan, S. Inoue, and A. Doi, On High-energy Particles in Accretion Disk Coronae of Supermassive Black Holes: Implications for MeV Gamma-rays and High-energy Neutrinos from AGN Cores, Astrophys. J. **880**, 40 (2019), arXiv:1904.00554 [astro-ph.HE].
[542] M. Ajello, J. Greiner, G. Sato, D. R. Willis, G. Kanbach, A. W. Strong, R. Diehl, G. Hasinger, N. Gehrels, C. B. Markwardt, and J. Tueller, Cosmic X-Ray Background and Earth Albedo Spectra with Swift BAT, Astrophys. J. **689**, 666–677 (2008), arXiv:0808.3377 [astro-ph].
[543] K. Watanabe, D. H. Hartmann, M. D. Leising, and L. S. The, The Diffuse Gamma-Ray Background from Supernovae, Astrophys. J. **516**, 285–296 (1999), arXiv:astro-ph/9809197 [astro-ph].
[544] P. Gandhi and A. C. Fabian, X-ray background synthesis: the infrared connection, Mon. Not. Roy. Astron. Soc. **339**, 1095–1102 (2003), arXiv:astro-ph/0211129 [astro-ph].
[545] W. N. Brandt and G. Yang, Surveys of the Cosmic X-ray Background, arXiv e-prints (2021), arXiv:2111.01156 [astro-ph.HE].
[546] J. F. Navarro, C. S. Frenk, and S. D. M. White, A Universal Density Profile from Hierarchical Clustering, Astrophys. J. **490**, 493–508 (1997), arXiv:astro-ph/9611107 [astro-ph].
[547] P. J. McMillan, Mass models of the Milky Way, Mon. Not. Roy. Astron. Soc. **414**, 2446–2457 (2011), arXiv:1102.4340 [astro-ph.GA].
[548] A. Coogan, L. Morrison, and S. Profumo, Precision gamma-ray constraints for sub-GeV dark matter models, J. Cosmology Astropart. Phys. **2021**, 044 (2021), arXiv:2104.06168 [hep-ph].
[549] T. Dzhatdoev and E. Podlesnyi, Massive Argon Space Telescope (MAST): A concept of heavy time projection chamber for γ-ray astronomy in the 100 MeV-1 TeV energy range, Astropart. Phys. **112**, 1–7 (2019), arXiv:1902.01491 [astro-ph.HE].
[550] S. D. Hunter *et al.*, A pair production telescope for medium-energy gamma-ray polarimetry, Astropart. Phys. **59**, 18–28 (2014), arXiv:1311.2059 [astro-ph.IM].
[551] J. McEnery *et al.* (AMEGO), All-sky Medium Energy Gamma-ray Observatory: Exploring the Extreme Multimessenger Universe, in *Decadal Survey on Astronomy and Astrophysics (Astro2020)*, Bull. Am. Astron. Soc., Vol. 51 (2019) p. 245, arXiv:1907.07558 [astro-ph.IM] .

[552] C. A. Kierans (AMEGO), AMEGO: exploring the extreme multimessenger universe, in *Astronomical Telescopes + Instrumentation 2020*, Soc. Photo-Optical Instrumentation Eng. Conf. S., Vol. 11444 (2020) p. 1144431, arXiv:2101.03105 [astro-ph.IM] .
[553] A. De Angelis *et al.* (e-ASTROGAM), The e-ASTROGAM mission. Exploring the extreme Universe with gamma rays in the MeV - GeV range, Exp. Astron. **44**, 25–82 (2017), arXiv:1611.02232 [astro-ph.HE].
[554] A. de Angelis *et al.* (e-ASTROGRAM), Science with e-ASTROGAM. A space mission for MeV-GeV gamma-ray astrophysics, J. High Energy Astrophys. **19**, 1–106 (2018), arXiv:1711.01265 [astro-ph.HE].
[555] M. Mallamaci *et al.* (AS-ASTROGRAM), All-Sky-ASTROGAM: a MeV Companion for Multimessenger Astrophysics, in *36th International Cosmic Ray Conference (ICRC 2019)*, Proc. Sci., Vol. 358 (2019) p. 579.
[556] E. Orlando *et al.*, Exploring the MeV Sky with a Combined Coded Mask and Compton Telescope: The Galactic Explorer with a Coded Aperture Mask Compton Telescope (GECCO), arXiv e-prints (2021), arXiv:2112.07190 [astro-ph.HE].
[557] T. Aramaki, P. O. H. Adrian, G. Karagiorgi, and H. Odaka, Dual MeV gamma-ray and dark matter observatory - GRAMS Project, Astropart. Phys. **114**, 107–114 (2020), arXiv:1901.03430 [astro-ph.HE].
[558] T. Aramaki *et al.*, Snowmass 2021 Letter of Interest: The GRAMS Project: MeV Gamma-Ray Observations and Antimatter-Based Dark Matter Searches, arXiv e-prints (2020), arXiv:2009.03754 [astro-ph.HE].
[559] T. Aramaki *et al.* (GRAMS), Overview of the GRAMS (Gamma-Ray AntiMatter Survey) Project, in *37th International Cosmic Ray Conference (ICRC 2021)*, Proc. Sci., Vol. 395 (2021) p. 653.
[560] X. Wu, M. Su, A. Bravar, J. Chang, Y. Fan, M. Pohl, and R. Walter, PANGU: A high resolution gamma-ray space telescope, in *Space Telescopes and Instrumentation 2014: Ultraviolet to Gamma Ray*, Soc. Photo-Optical Instrumentation Eng. Conf. S., Vol. 9144, edited by T. Takahashi, J.-W. A. den Herder, and M. Bautz (2014) p. 91440F, arXiv:1407.0710 [astro-ph.IM] .
[561] X. Wu *et al.* (PANGU), PANGU: A High Resolution Gamma-Ray Space Telescope, in *34th International Cosmic Ray Conference (ICRC 2015)*, Proc. Sci., Vol. 236 (2015) p. 653.
[562] C. Labanti *et al.*, The X/Gamma-ray Imaging Spectrometer (XGIS) on-board THESEUS: design, main characteristics, and concept of operation, in *Astronomical Telescopes + Instrumentation 2020*, Soc. Photo-Optical Instrumentation Eng. Conf. S. (2020) arXiv:2102.08701 [astro-ph.IM] .
[563] R. Campana *et al.*, The XGIS instrument on-board THESEUS: Monte Carlo simulations for response, background, and sensitivity, in *Astronomical Telescopes + Instrumentation 2020*, Soc. Photo-Optical Instrumentation Eng. Conf. S. (2020) arXiv:2102.08699 [astro-ph.IM] .
[564] K. Engel *et al.*, The Future of Gamma-Ray Experiments in the MeV-EeV Range, arXiv e-prints (2022), arXiv:2203.07360 [astro-ph.HE].
[565] T. Bringmann, M. Doro, and M. Fornasa, Dark matter signals from Draco and Willman 1: prospects for MAGIC II and CTA, J. Cosmology Astropart. Phys. **2009**, 016 (2009), arXiv:0809.2269 [astro-ph].
[566] J. LeyVa *et al.* (GRAMS), Exploring MeV gamma rays from dark matter annihilation and evaporating primordial black holes in the GRAMS experiment) Project, in *37th International Cosmic Ray Conference (ICRC 2021)*, Proc. Sci., Vol. 395 (2021) p. 552.
[567] P. F. de Salas, K. Malhan, K. Freese, K. Hattori, and M. Valluri, On the estimation of the local dark matter density using the rotation curve of the Milky Way, J. Cosmology Astropart. Phys. **2019**, 037 (2019), arXiv:1906.06133 [astro-ph.GA].
[568] J. Einasto, On the Construction of a Composite Model for the Galaxy and on the Determination of the System of Galactic Parameters., Trudy Inst. Astrofiz. Alma-Ata **5**, 87–100 (1965).
[569] D. Merritt, A. W. Graham, B. Moore, J. Diemand, and B. Terzić, Empirical Models for Dark Matter Halos. I. Nonparametric Construction of Density Profiles and Comparison with Parametric Models,

Astron. J. **132**, 2685–2700 (2006), arXiv:astro-ph/0509417 [astro-ph].
[570] R. Abuter *et al.* (Gravity), Detection of the gravitational redshift in the orbit of the star S2 near the Galactic centre massive black hole, Astron. Astrophys. **615**, L15 (2018), arXiv:1807.09409 [astro-ph.GA].
[571] S. Amoroso, S. Caron, A. Jueid, R. Ruiz de Austri, and P. Skands, Estimating QCD uncertainties in Monte Carlo event generators for gamma-ray dark matter searches, J. Cosmology Astropart. Phys. **2019**, 007 (2019), arXiv:1812.07424 [hep-ph].
[572] A. Jueid, Studying QCD modeling of uncertainties in particle spectra from dark-matter annihilation into jets, in *17th International Conference on Topics in Astroparticle and Underground Physics (TAUP2021)*, J. Phys. Conf. Ser., Vol. 2156 (2021) p. 012057, arXiv:2110.09747 [hep-ph] .
[573] A. Jueid, J. Kip, R. Ruiz de Austri, and P. Skands, Impact of QCD uncertainties on antiproton spectra from dark-matter annihilation, arXiv e-prints (2022), arXiv:2202.11546 [hep-ph].
[574] R. C. Henry, J. Murthy, J. Overduin, and J. Tyler, The Mystery of the Cosmic Diffuse Ultraviolet Background Radiation, Astrophys. J. **798**, 14 (2015), arXiv:1404.5714 [astro-ph.GA].
[575] S. R. Kulkarni *et al.*, Science with the Ultraviolet Explorer (UVEX), arXiv e-prints (2021), arXiv:2111.15608 [astro-ph.GA].
[576] A. Yalinewich and M. E. Caplan, Crater morphology of primordial black hole impacts, Mon. Not. Roy. Astron. Soc. **505**, L115–L119 (2021), arXiv:2104.00033 [astro-ph.HE].
[577] S. Jung and T. Kim, Gamma-ray burst lensing parallax: Closing the primordial black hole dark matter mass window, Phys. Rev. Res. **2**, 013113 (2020), arXiv:1908.00078 [astro-ph.CO].
[578] K. K. Y. Ng, S. Vitale, O. A. Hannuksela, and T. G. F. Li, Constraints on Ultralight Scalar Bosons within Black Hole Spin Measurements from the LIGO-Virgo GWTC-2, Phys. Rev. Lett. **126**, 151102 (2021), arXiv:2011.06010 [gr-qc].
[579] H. Tagawa, Z. Haiman, I. Bartos, B. Kocsis, and K. Omukai, Signatures of hierarchical mergers in black hole spin and mass distribution, Mon. Not. Roy. Astron. Soc. **507**, 3362–3380 (2021), arXiv:2104.09510 [astro-ph.HE].
[580] L. Gou, J. E. McClintock, M. J. Reid, J. A. Orosz, J. F. Steiner, R. Narayan, J. Xiang, R. A. Remillard, K. A. Arnaud, and S. W. Davis, The Extreme Spin of the Black Hole in Cygnus X-1, Astrophys. J. **742**, 85 (2011), arXiv:1106.3690 [astro-ph.HE].
[581] G. Risaliti *et al.*, A rapidly spinning supermassive black hole at the centre of NGC 1365, Nature **494**, 449–451 (2013), arXiv:1302.7002 [astro-ph.HE].
[582] O. Burke, J. R. Gair, J. Simón, and M. C. Edwards, Constraining the spin parameter of near-extremal black holes using LISA, Phys. Rev. D **102**, 124054 (2020), arXiv:2010.05932 [gr-qc].
[583] B. Carr, F. Kühnel, and M. Sandstad, Primordial black holes as dark matter, Phys. Rev. D **94**, 083504 (2016), arXiv:1607.06077 [astro-ph.CO].
[584] A. Arbey, J. Auffinger, P. Sandick, B. Shams Es Haghi, and K. Sinha, Precision calculation of dark radiation from spinning primordial black holes and early matter-dominated eras, Phys. Rev. D **103**, 123549 (2021), arXiv:2104.04051 [astro-ph.CO].
[585] B. Dutta, L. Leblond, and K. Sinha, Mirage in the sky: Nonthermal dark matter, gravitino problem, and cosmic ray anomalies, Phys. Rev. D **80**, 035014 (2009), arXiv:0904.3773 [hep-ph].
[586] R. Allahverdi, B. Dutta, and K. Sinha, Successful supersymmetric dark matter with thermal over/under-abundance from late decay of a visible sector scalar, Phys. Rev. D **87**, 075024 (2013), arXiv:1212.6948 [hep-ph].
[587] B. S. Acharya, G. Kane, S. Watson, and P. Kumar, Nonthermal "WIMP miracle", Phys. Rev. D **80**, 083529 (2009), arXiv:0908.2430 [astro-ph.CO].
[588] B. S. Acharya, K. Bobkov, G. Kane, J. Shao, S. Watson, and P. Kumar, Non-thermal dark matter and the moduli problem in string frameworks, J. High Energy Phys. **2008**, 064 (2008), arXiv:0804.0863

[hep-ph].
[589] A. L. Erickcek, K. Sinha, and S. Watson, Bringing isolated dark matter out of isolation: Late-time reheating and indirect detection, Phys. Rev. D **94**, 063502 (2016), arXiv:1510.04291 [hep-ph].
[590] M. S. Delos, T. Linden, and A. L. Erickcek, Breaking a dark degeneracy: The gamma-ray signature of early matter domination, Phys. Rev. D **100**, 123546 (2019), arXiv:1910.08553 [astro-ph.CO].
[591] R. Allahverdi, B. Dutta, and K. Sinha, Baryogenesis and late-decaying moduli, Phys. Rev. D **82**, 035004 (2010), arXiv:1005.2804 [hep-ph].
[592] T. Papanikolaou, V. Vennin, and D. Langlois, Gravitational waves from a universe filled with primordial black holes, J. Cosmology Astropart. Phys. **2021**, 053 (2021), arXiv:2010.11573 [astro-ph.CO].
[593] P. Sandick, B. Shams Es Haghi, and K. Sinha, Asymmetric reheating by primordial black holes, Phys. Rev. D **104**, 083523 (2021), arXiv:2108.08329 [astro-ph.CO].
[594] D. Hooper, G. Krnjaic, and S. D. McDermott, Dark radiation and superheavy dark matter from black hole domination, J. High Energy Phys. **2019**, 1 (2019), arXiv:1905.01301 [hep-ph].
[595] I. Masina, Dark Matter and Dark Radiation from Evaporating Kerr Primordial Black Holes, Gravit. Cosmology **27**, 315–330 (2021), arXiv:2103.13825 [gr-qc].
[596] I. Masina, Dark matter and dark radiation from evaporating primordial black holes, Eur. Phys. J. Plus **135**, 552 (2020), arXiv:2004.04740 [hep-ph].
[597] A. Arbey and F. Mahmoudi, SuperIso Relic: A program for calculating relic density and flavor physics observables in Supersymmetry, Comput. Phys. Commun. **181**, 1277–1292 (2010), arXiv:0906.0369 [hep-ph].
[598] A. Arbey and F. Mahmoudi, SuperIso Relic v3.0: A program for calculating relic density and flavour physics observables: Extension to NMSSM, Comput. Phys. Commun. **182**, 1582–1583 (2011).
[599] A. Arbey, F. Mahmoudi, and G. Robbins, SuperIso Relic v4: A program for calculating dark matter and flavour physics observables in supersymmetry, Comput. Phys. Commun. **239**, 238–264 (2019), arXiv:1806.11489 [hep-ph].
[600] K. N. Abazajian *et al.* (CMB-S4), CMB-S4 Science Book, First Edition, arXiv e-prints (2016), arXiv:1610.02743 [astro-ph.CO].
[601] D. Baumann, D. Green, and B. Wallisch, Searching for light relics with large-scale structure, J. Cosmology Astropart. Phys. **2018**, 029 (2018), arXiv:1712.08067 [astro-ph.CO].
[602] S. Hanany *et al.* (NASA-PICO), PICO: Probe of Inflation and Cosmic Origins, arXiv e-prints (2019), arXiv:1902.10541 [astro-ph.IM].
[603] A. M. Green, Supersymmetry and primordial black hole abundance constraints, Phys. Rev. D **60**, 063516 (1999), arXiv:astro-ph/9903484 [astro-ph].
[604] N. F. Bell and R. R. Volkas, Mirror matter and primordial black holes, Phys. Rev. D **59**, 107301 (1999), arXiv:astro-ph/9812301 [astro-ph].
[605] F. Schiavone, D. Montanino, A. Mirizzi, and F. Capozzi, Axion-like particles from primordial black holes shining through the Universe, J. Cosmology Astropart. Phys. **2021**, 063 (2021), arXiv:2107.03420 [hep-ph].
[606] N. Bernal, F. Hajkarim, and Y. Xu, Axion dark matter in the time of primordial black holes, Phys. Rev. D **104**, 075007 (2021), arXiv:2107.13575 [hep-ph].
[607] N. Bernal, Y. F. Perez-Gonzalez, Y. Xu, and Ó. Zapata, ALP dark matter in a primordial black hole dominated universe, Phys. Rev. D **104**, 123536 (2021), arXiv:2110.04312 [hep-ph].
[608] T. Kitabayashi, Primordial black holes and scotogenic dark matter, Int. J. Mod. Phys. A **36**, 2150139 (2021), arXiv:2101.01921 [hep-ph].
[609] S. J. Das, D. Mahanta, and D. Borah, Low scale leptogenesis and dark matter in the presence of primordial black holes, J. Cosmology Astropart. Phys. **2021**, 019 (2021).
[610] T. Kitabayashi, Primordial black holes and lepton flavor violation with scotogenic dark matter,

Prog. Theor. Exp. Phys. **2022**, 033B02 (2022), arXiv:2107.11692 [hep-ph].
[611] M. Y. Khlopov, A. Barrau, and J. Grain, Gravitino production by primordial black hole evaporation and constraints on the inhomogeneity of the early universe, Class. Quantum Gravity **23**, 1875–1882 (2006), arXiv:astro-ph/0406621 [astro-ph].
[612] B. Barman, D. Borah, S. Jyoti Das, and R. Roshan, Cogenesis of Baryon Asymmetry and Gravitational Dark Matter from PBH, arXiv e-prints (2022), arXiv:2204.10339 [hep-ph].
[613] L. Morrison, S. Profumo, and Y. Yu, Melanopogenesis: dark matter of (almost) any mass and baryonic matter from the evaporation of primordial black holes weighing a ton (or less), J. Cosmology Astropart. Phys. **2019**, 005 (2019), arXiv:1812.10606 [astro-ph.CO].
[614] G. E. A. Matsas, J. C. Montero, V. Pleitez, and D. A. T. Vanzella, Dark matter: The Top of the iceberg?, in *Topics in Theoretical Physics II: Festschrift for A. H. Zimerman* (1998) arXiv:hep-ph/9810456 .
[615] T. Fujita, K. Harigaya, M. Kawasaki, and R. Matsuda, Baryon asymmetry, dark matter, and density perturbation from primordial black holes, Phys. Rev. D **89**, 103501 (2014), arXiv:1401.1909 [astro-ph.CO].
[616] O. Lennon, J. March-Russell, R. Petrossian-Byrne, and H. Tillim, Black hole genesis of dark matter, J. Cosmology Astropart. Phys. **2018**, 009 (2018), arXiv:1712.07664 [hep-ph].
[617] R. Allahverdi, J. Dent, and J. Osinski, Nonthermal production of dark matter from primordial black holes, Phys. Rev. D **97**, 055013 (2018), arXiv:1711.10511 [astro-ph.CO].
[618] I. Baldes, Q. Decant, D. C. Hooper, and L. Lopez-Honorez, Non-cold dark matter from primordial black hole evaporation, J. Cosmology Astropart. Phys. **2020**, 045 (2020), arXiv:2004.14773 [astro-ph.CO].
[619] R. Samanta and F. R. Urban, Testing Super Heavy Dark Matter from Primordial Black Holes with Gravitational Waves, arXiv e-prints (2021), arXiv:2112.04836 [hep-ph].
[620] A. Hook, Baryogenesis from Hawking radiation, Phys. Rev. D **90**, 083535 (2014), arXiv:1404.0113 [hep-ph].
[621] M. Y. Khlopov, Primordial black holes, Res. Astron. Astrophys. **10**, 495–528 (2010), arXiv:0801.0116 [astro-ph].
[622] D. Baumann, P. J. Steinhardt, and N. Turok, Primordial Black Hole Baryogenesis, arXiv e-prints (2007), arXiv:hep-th/0703250 [hep-th].
[623] M. Viel, J. Lesgourgues, M. G. Haehnelt, S. Matarrese, and A. Riotto, Constraining warm dark matter candidates including sterile neutrinos and light gravitinos with WMAP and the Lyman-α forest, Phys. Rev. D **71**, 063534 (2005), arXiv:astro-ph/0501562 [astro-ph].
[624] R. Murgia, A. Merle, M. Viel, M. Totzauer, and A. Schneider, "Non-cold" dark matter at small scales: a general approach, J. Cosmology Astropart. Phys. **2017**, 046 (2017), arXiv:1704.07838 [astro-ph.CO].
[625] P. Bode, J. P. Ostriker, and N. Turok, Halo Formation in Warm Dark Matter Models, Astrophys. J. **556**, 93–107 (2001), arXiv:astro-ph/0010389 [astro-ph].
[626] V. Iršič *et al.*, New constraints on the free-streaming of warm dark matter from intermediate and small scale Lyman-α forest data, Phys. Rev. D **96**, 023522 (2017), arXiv:1702.01764 [astro-ph.CO].
[627] N. Bernal and Ó. Zapata, Self-interacting dark matter from primordial black holes, J. Cosmology Astropart. Phys. **2021**, 007 (2021), arXiv:2010.09725 [hep-ph].
[628] N. Bernal and Ó. Zapata, Dark matter in the time of primordial black holes, J. Cosmology Astropart. Phys. **2021**, 015 (2021), arXiv:2011.12306 [astro-ph.CO].
[629] N. Bernal and Ó. Zapata, Gravitational dark matter production: Primordial black holes and UV freeze-in, Phys. Lett. B **815**, 136129 (2021), arXiv:2011.02510 [hep-ph].
[630] P. Gondolo, P. Sandick, and B. Shams Es Haghi, Effects of primordial black holes on dark matter models, Phys. Rev. D **102**, 095018 (2020), arXiv:2009.02424 [hep-ph].
[631] W. Chao, T. Li, and J. Liao, Connecting Primordial Black Hole to boosted sub-GeV Dark Matter

through neutrino, arXiv e-prints (2021), arXiv:2108.05608 [hep-ph].
[632] T. Li and J. Liao, Constraints on light Dark Matter evaporated from Primordial Black Hole through electron targets, arXiv e-prints (2022), arXiv:2203.14443 [hep-ph].
[633] R. Calabrese, M. Chianese, D. F. G. Fiorillo, and N. Saviano, Electron scattering of light new particles from evaporating primordial black holes, arXiv e-prints (2022), arXiv:2203.17093 [hep-ph].
[634] R. Calabrese, M. Chianese, D. F. G. Fiorillo, and N. Saviano, Direct detection of light dark matter from evaporating primordial black holes, Phys. Rev. D **105**, L021302 (2022), arXiv:2107.13001 [hep-ph].
[635] A. Chaudhuri and A. Dolgov, PBH Evaporation, Baryon Asymmetry, and Dark Matter, J. Exp. Theor. Phys. **133**, 552–566 (2021), arXiv:2001.11219 [astro-ph.CO].
[636] M. Bojowald, S. Brahma, and D.-h. Yeom, Effective line elements and black-hole models in canonical loop quantum gravity, Phys. Rev. D **98**, 046015 (2018), arXiv:1803.01119 [gr-qc].
[637] A. Ashtekar and J. Lewandowski, Background independent quantum gravity: a status report, Class. Quantum Gravity **21**, R53–R152 (2004), arXiv:gr-qc/0404018 [gr-qc].
[638] A. Ashtekar and E. Bianchi, A short review of loop quantum gravity, Rep. Prog. Phys. **84**, 042001 (2021), arXiv:2104.04394 [gr-qc].
[639] A. Ashtekar and P. Singh, Loop quantum cosmology: a status report, Class. Quantum Gravity **28**, 213001 (2011), arXiv:1108.0893 [gr-qc].
[640] A. Ashtekar and M. Bojowald, Quantum geometry and the Schwarzschild singularity, Class. Quantum Gravity **23**, 391–411 (2006), arXiv:gr-qc/0509075 [gr-qc].
[641] L. Modesto, Loop quantum black hole, Class. Quantum Gravity **23**, 5587–5601 (2006), arXiv:gr-qc/0509078 [gr-qc].
[642] C. G. Böhmer and K. Vandersloot, Loop quantum dynamics of the Schwarzschild interior, Phys. Rev. D **76**, 104030 (2007), arXiv:0709.2129 [gr-qc].
[643] J. Olmedo, S. Saini, and P. Singh, From black holes to white holes: a quantum gravitational, symmetric bounce, Class. Quantum Gravity **34**, 225011 (2017), arXiv:1707.07333 [gr-qc].
[644] A. Ashtekar, J. Olmedo, and P. Singh, Quantum extension of the Kruskal spacetime, Phys. Rev. D **98**, 126003 (2018), arXiv:1806.02406 [gr-qc].
[645] J. Ben Achour, F. Lamy, H. Liu, and K. Noui, Non-singular black holes and the limiting curvature mechanism: a Hamiltonian perspective, J. Cosmology Astropart. Phys. **2018**, 072 (2018), arXiv:1712.03876 [gr-qc].
[646] J. Ben Achour, F. Lamy, H. Liu, and K. Noui, Polymer Schwarzschild black hole: An effective metric, EPL **123**, 20006 (2018), arXiv:1803.01152 [gr-qc].
[647] N. Bodendorfer, F. M. Mele, and J. Münch, Effective quantum extended spacetime of polymer Schwarzschild black hole, Class. Quantum Gravity **36**, 195015 (2019), arXiv:1902.04542 [gr-qc].
[648] N. Bodendorfer, F. M. Mele, and J. Münch, A note on the Hamiltonian as a polymerisation parameter, Class. Quantum Gravity **36**, 187001 (2019), arXiv:1902.04032 [gr-qc].
[649] N. Bodendorfer, F. M. Mele, and J. Münch, (b,v)-type variables for black to white hole transitions in effective loop quantum gravity, Phys. Lett. B **819**, 136390 (2021), arXiv:1911.12646 [gr-qc].
[650] N. Bodendorfer, F. M. Mele, and J. Münch, Mass and Horizon Dirac Observables in Effective Models of Quantum Black-to-White Hole Transition, arXiv e-prints (2019), arXiv:1912.00774 [gr-qc].
[651] E. Alesci, S. Bahrami, and D. Pranzetti, Quantum gravity predictions for black hole interior geometry, Phys. Lett. B **797**, 134908 (2019), arXiv:1904.12412 [gr-qc].
[652] E. Alesci, S. Bahrami, and D. Pranzetti, Asymptotically de Sitter universe inside a Schwarzschild black hole, Phys. Rev. D **102**, 066010 (2020), arXiv:2007.06664 [gr-qc].
[653] F. Sartini and M. Geiller, Quantum dynamics of the black hole interior in loop quantum cosmology, Phys. Rev. D **103**, 066014 (2021), arXiv:2010.07056 [gr-qc].
[654] S. Brahma, C.-Y. Chen, and D.-h. Yeom, Testing Loop Quantum Gravity from Observational Conse-

quences of Nonsingular Rotating Black Holes, Phys. Rev. Lett. **126**, 181301 (2021), arXiv:2012.08785 [gr-qc].
[655] R. Gambini, J. Olmedo, and J. Pullin, Loop quantum black hole extensions within the improved dynamics, Front. Astron. Space Sci. **8**, 74 (2021), arXiv:2012.14212 [gr-qc].
[656] L. Modesto and I. Prémont-Schwarz, Self-dual black holes in loop quantum gravity: Theory and phenomenology, Phys. Rev. D **80**, 064041 (2009), arXiv:0905.3170 [hep-th].
[657] M. Bojowald, Black-Hole Models in Loop Quantum Gravity, Universe **6**, 125 (2020), arXiv:2009.13565 [gr-qc].
[658] A. Ashtekar, Black Hole Evaporation: A Perspective from Loop Quantum Gravity, Universe **6**, 21 (2020), arXiv:2001.08833 [gr-qc].
[659] X.-C. Cai and Y.-G. Miao, Quasinormal modes and shadows of a new family of Ayón-Beato-García black holes, arXiv e-prints (2021), arXiv:2104.09725 [gr-qc].
[660] O. Baake, C. Charmousis, M. Hassaine, and M. San Juan, Regular black holes and gravitational particle-like solutions in generic DHOST theories, J. Cosmology Astropart. Phys. **2021**, 021 (2021), arXiv:2104.08221 [hep-th].
[661] M. Molina and J. R. Villanueva, On the thermodynamics of the Hayward black hole, Class. Quantum Gravity **38**, 105002 (2021), arXiv:2101.07917 [gr-qc].
[662] P. J. E. Peebles, Gravitational collapse and related phenomena from an empirical point of view, or, black holes are where you find them., Gen. Relativ. Gravit. **3**, 63–82 (1972).
[663] A. Arbey and J. Auffinger, Detecting Planet 9 via Hawking radiation, arXiv e-prints (2020), arXiv:2006.02944 [gr-qc].
[664] M. H. Chan and C. M. Lee, Constraining primordial black hole fraction at the galactic centre using radio observational data, Mon. Not. Roy. Astron. Soc. **497**, 1212–1216 (2020), arXiv:2007.05677 [astro-ph.HE].
[665] J. F. Acevedo, J. Bramante, A. Goodman, J. Kopp, and T. Opferkuch, Dark matter, destroyer of worlds: neutrino, thermal, and existential signatures from black holes in the Sun and Earth, J. Cosmology Astropart. Phys. **2021**, 026 (2021), arXiv:2012.09176 [hep-ph].
[666] T. Siegert, C. Boehm, F. Calore, R. Diehl, M. G. H. Krause, P. D. Serpico, and A. C. Vincent, An INTEGRAL/SPI view of reticulum II: particle dark matter and primordial black holes limits in the MeV range, Mon. Not. Roy. Astron. Soc. **511**, 914–924 (2022), arXiv:2109.03791 [astro-ph.HE].
[667] D. Marfatia and P.-Y. Tseng, Correlated signals of first-order phase transitions and primordial black hole evaporation, arXiv e-prints (2021), arXiv:2112.14588 [hep-ph].
[668] K. Agashe, J. Hyeok Chang, S. J. Clark, B. Dutta, Y. Tsai, and T. Xu, Correlating Gravitational Wave and Gamma-ray Signals from Primordial Black Holes, arXiv e-prints (2022), arXiv:2202.04653 [astro-ph.CO].
[669] A. Arbey, J. Auffinger, and J. Silk, Stellar signatures of inhomogeneous big bang nucleosynthesis, Phys. Rev. D **102**, 023503 (2020), arXiv:2006.02446 [astro-ph.CO].
[670] F. Iocco, The lithium problem. A phenomenologist's perspective, Mem. Soc. Astron. Ital. Suppl. **22**, 19 (2012), arXiv:1206.2396 [astro-ph.GA].
[671] L. S. Lyubimkov, Light Chemical Elements in Stars: Mysteries and Unsolved Problems, Astrophysics **61**, 262–285 (2018), arXiv:1809.06129 [astro-ph.SR].
[672] I. Musco, Threshold for primordial black holes: Dependence on the shape of the cosmological perturbations, Phys. Rev. D **100**, 123524 (2019), arXiv:1809.02127 [gr-qc].
[673] S. Matsuura, A. D. Dolgov, and S. Nagataki, Affleck-Dine Baryogenesis and Heavy Element Production from Inhomogeneous Big Bang Nucleosynthesis, Prog. Theor. Phys. **112**, 971–981 (2004), arXiv:astro-ph/0405459 [astro-ph].
[674] R. Nakamura, M.-a. Hashimoto, S.-i. Fujimoto, N. Nishimura, and K. Sato, Observational Constraint

on Heavy Element Production in Inhomogeneous Big Bang Nucleosynthesis, arXiv e-prints (2010), arXiv:1007.0466 [astro-ph.CO].
[675] R. Nakamura, M.-a. Mashimoto, S.-i. Fujimoto, and K. Sato, Constraint on Heavy Element Production in Inhomogeneous Big-Bang Nucleosynthesis from The Light-Element Observations, arXiv e-prints (2013), arXiv:1307.7564 [astro-ph.CO].
[676] Y. Komiya and T. Shigeyama, Contribution of Neutron Star Mergers to the r-Process Chemical Evolution in the Hierarchical Galaxy Formation, Astrophys. J. **830**, 76 (2016), arXiv:1608.01772 [astro-ph.GA].
[677] G. E. Duggan, E. N. Kirby, S. M. Andrievsky, and S. A. Korotin, Neutron Star Mergers are the Dominant Source of the r-process in the Early Evolution of Dwarf Galaxies, Astrophys. J. **869**, 50 (2018), arXiv:1809.04597 [astro-ph.GA].
[678] J. J. Cowan *et al.*, Origin of the heaviest elements: The rapid neutron-capture process, Rev. Mod. Phys. **93**, 015002 (2021), arXiv:1901.01410 [astro-ph.HE].
[679] B. Côté *et al.*, Neutron Star Mergers Might Not Be the Only Source of r-process Elements in the Milky Way, Astrophys. J. **875**, 106 (2019), arXiv:1809.03525 [astro-ph.HE].
[680] J. H. Applegate, C. J. Hogan, and R. J. Scherrer, Cosmological Quantum Chromodynamics, Neutron Diffusion, and the Production of Primordial Heavy Elements, Astrophys. J. **329**, 572 (1988).
[681] T. T. Hansen *et al.*, The R-process Alliance: First Release from the Southern Search for R-process-enhanced Stars in the Galactic Halo, Astrophys. J. **858**, 92 (2018), arXiv:1804.03114 [astro-ph.SR].
[682] J. D. Simon, The Faintest Dwarf Galaxies, Annu. Rev. Astron. Astrophys. **57**, 375–415 (2019), arXiv:1901.05465 [astro-ph.GA].
[683] K. Inayoshi, E. Visbal, and Z. Haiman, The Assembly of the First Massive Black Holes, Annu. Rev. Astron. Astrophys. **58**, 27–97 (2020), arXiv:1911.05791 [astro-ph.GA].
[684] T. Nakama, J. Silk, and M. Kamionkowski, Stochastic gravitational waves associated with the formation of primordial black holes, Phys. Rev. D **95**, 043511 (2017), arXiv:1612.06264 [astro-ph.CO].
[685] J. D. Barrow and R. J. Scherrer, Constraining density fluctuations with big bang nucleosynthesis in the era of precision cosmology, Phys. Rev. D **98**, 043534 (2018), arXiv:1803.02383 [astro-ph.CO].
[686] A. Stacy, V. Bromm, and A. T. Lee, Building up the Population III initial mass function from cosmological initial conditions, Mon. Not. Roy. Astron. Soc. **462**, 1307–1328 (2016), arXiv:1603.09475 [astro-ph.GA].
[687] I. Affleck and M. Dine, A new mechanism for baryogenesis., Nuclear Physics B **2**, 361–380 (1985).
[688] A. D. Dolgov, M. Kawasaki, and N. Kevlishvili, Inhomogeneous baryogenesis, cosmic antimatter, and dark matter, Nucl. Phys. B **807**, 229–250 (2009), arXiv:0806.2986 [hep-ph].
[689] S. I. Blinnikov, A. D. Dolgov, and K. A. Postnov, Antimatter and antistars in the Universe and in the Galaxy, Phys. Rev. D **92**, 023516 (2015), arXiv:1409.5736 [astro-ph.HE].
[690] V. Poulin, P. Salati, I. Cholis, M. Kamionkowski, and J. Silk, Where do the AMS-02 antihelium events come from?, Phys. Rev. D **99**, 023016 (2019), arXiv:1808.08961 [astro-ph.HE].
[691] R. H. Cyburt, A. M. Amthor, R. Ferguson, Z. Meisel, K. Smith, S. Warren, A. Heger, R. D. Hoffman, T. Rauscher, A. Sakharuk, H. Schatz, F. K. Thielemann, and M. Wiescher, The JINA REACLIB Database: Its Recent Updates and Impact on Type-I X-ray Bursts, Astrophys. J. Suppl. **189**, 240–252 (2010).
[692] M. Asplund, N. Grevesse, A. J. Sauval, and P. Scott, The Chemical Composition of the Sun, Annu. Rev. Astron. Astrophys. **47**, 481–522 (2009), arXiv:0909.0948 [astro-ph.SR].
[693] R. Gratton, C. Sneden, and E. Carretta, Abundance Variations Within Globular Clusters, Annu. Rev. Astron. Astrophys. **42**, 385–440 (2004).
[694] W. Chantereau, C. Charbonnel, and G. Meynet, Evolution of long-lived globular cluster stars. IV. Initial helium content and white-dwarf properties, Astron. Astrophys. **602**, A13 (2017), arXiv:1704.07822

[astro-ph.SR].
[695] J. E. Norris, The Helium Abundances of ω Centauri, Astrophys. J. Lett. **612**, L25–L28 (2004).
[696] A. K. Dupree and E. H. Avrett, Direct Evaluation of the Helium Abundances in Omega Centauri, Astrophys. J. Lett. **773**, L28 (2013), arXiv:1307.5860 [astro-ph.SR].
[697] A. P. Milone *et al.*, The Hubble Space Telescope UV legacy survey of galactic globular clusters - XVI. The helium abundance of multiple populations, Mon. Not. Roy. Astron. Soc. **481**, 5098–5122 (2018), arXiv:1809.05006 [astro-ph.SR].
[698] N. Bastian and C. Lardo, Multiple Stellar Populations in Globular Clusters, Annu. Rev. Astron. Astrophys. **56**, 83–136 (2018), arXiv:1712.01286 [astro-ph.SR].
[699] S. Saracino *et al.*, Chromosome maps of young LMC clusters: an additional case of coeval multiple populations, Mon. Not. Roy. Astron. Soc. **493**, 6060–6070 (2020), arXiv:2003.01780 [astro-ph.SR].
[700] A. P. Ji, A. Frebel, J. D. Simon, and A. Chiti, Complete Element Abundances of Nine Stars in the r-process Galaxy Reticulum II, Astrophys. J. **830**, 93 (2016), arXiv:1607.07447 [astro-ph.GA].
[701] A. F. Marino *et al.*, Keck HIRES spectroscopy of SkyMapper commissioning survey candidate extremely metal-poor stars, Mon. Not. Roy. Astron. Soc. **485**, 5153–5167 (2019), arXiv:1902.10611 [astro-ph.SR].
[702] M. Reichert, C. J. Hansen, M. Hanke, Á. Skúladóttir, A. Arcones, and E. K. Grebel, Neutron-capture elements in dwarf galaxies. III. A homogenized analysis of 13 dwarf spheroidal and ultra-faint galaxies, Astron. Astrophys. **641**, A127 (2020), arXiv:2004.01195 [astro-ph.GA].
[703] J. L. Marshall *et al.* (DES), Chemical Abundance Analysis of Tucana III, the Second r-process Enhanced Ultra-faint Dwarf Galaxy, Astrophys. J. **882**, 177 (2019), arXiv:1812.01022 [astro-ph.GA].
[704] K. Freeman and J. Bland-Hawthorn, The New Galaxy: Signatures of Its Formation, Annu. Rev. Astron. Astrophys. **40**, 487–537 (2002), arXiv:astro-ph/0208106 [astro-ph].
[705] K. Brauer, A. P. Ji, A. Frebel, G. A. Dooley, F. A. Gómez, and B. W. O'Shea, The Origin of r-process Enhanced Metal-poor Halo Stars In Now-destroyed Ultra-faint Dwarf Galaxies, Astrophys. J. **871**, 247 (2019), arXiv:1809.05539 [astro-ph.GA].
[706] M. N. Ishigaki, Chemical abundances of field halo stars - Implications for the building blocks of the Milky Way, in *Star Clusters: From the Milky Way to the Early Universe*, J. Phys. Conf. Ser., Vol. 351, edited by A. Bragaglia, M. Davies, A. Sills, and E. Vesperini (2020) pp. 24–33, arXiv:1908.09623 [astro-ph.GA] .
[707] Á. Skúladóttir and S. Salvadori, Evidence for $\gtrsim$4 Gyr timescales of neutron star mergers from Galactic archaeology, Astron. Astrophys. **634**, L2 (2020), arXiv:2001.03628 [astro-ph.GA].
[708] A. Frebel, From Nuclei to the Cosmos: Tracing Heavy-Element Production with the Oldest Stars, Annu. Rev. Nucl. Part. Sci. **68**, 237–269 (2018), arXiv:1806.08955 [astro-ph.SR].
[709] M. Bonetti, A. Perego, M. Dotti, and G. Cescutti, Neutron star binary orbits in their host potential: effect on early r-process enrichment, Mon. Not. Roy. Astron. Soc. **490**, 296–311 (2019), arXiv:1905.12016 [astro-ph.HE].
[710] R. J. Scherrer, Does inhomogeneous big bang nucleosynthesis produce an inhomogeneous element distribution today?, Phys. Rev. D **103**, 123548 (2021), arXiv:2103.01832 [astro-ph.CO].
[711] K. Batygin and M. E. Brown, Evidence for a Distant Giant Planet in the Solar System, Astron. J. **151**, 22 (2016), arXiv:1601.05438 [astro-ph.EP].
[712] K. Batygin, F. C. Adams, M. E. Brown, and J. C. Becker, The planet nine hypothesis, Phys. Rep. **805**, 1–53 (2019), arXiv:1902.10103 [astro-ph.EP].
[713] M. E. Brown and K. Batygin, The Orbit of Planet Nine, Astron. J. **162**, 219 (2021), arXiv:2108.09868 [astro-ph.EP].
[714] K. E. Anderson and N. A. Kaib, Signatures of a Distant Planet on the Inclination Distribution of the Detached Kuiper Belt, Astrophys. J. Lett. **920**, L9 (2021), arXiv:2109.13307 [astro-ph.EP].

[715] K. J. Napier *et al.* (DES), No Evidence for Orbital Clustering in the Extreme Trans-Neptunian Objects, Planet. Sci. J. **2**, 59 (2021), arXiv:2102.05601 [astro-ph.EP].
[716] M. S. Clement and N. A. Kaib, Orbital Precession in the Distant Solar System: Further Constraining the Planet Nine Hypothesis with Numerical Simulations, Astron. J. **159**, 285 (2020), arXiv:2005.05326 [astro-ph.EP].
[717] A. Fienga, J. Laskar, H. Manche, and M. Gastineau, Constraints on the location of a possible 9th planet derived from the Cassini data, Astron. Astrophys. **587**, L8 (2016), arXiv:1602.06116 [astro-ph.EP].
[718] M. J. Holman and M. J. Payne, Observational Constraints on Planet Nine: Cassini Range Observations, Astron. J. **152**, 94 (2016), arXiv:1604.03180 [astro-ph.EP].
[719] S. Naess *et al.*, The Atacama Cosmology Telescope: A Search for Planet 9, Astrophys. J. **923**, 224 (2021), arXiv:2104.10264 [astro-ph.EP].
[720] M. E. Brown and K. Batygin, A Search for Planet Nine using the Zwicky Transient Facility Public Archive, Astron. J. **163**, 102 (2022), arXiv:2110.13117 [astro-ph.EP].
[721] M. Rowan-Robinson, A search for Planet 9 in the IRAS data, Mon. Not. Roy. Astron. Soc. **510**, 3716–3726 (2022), arXiv:2111.03831 [astro-ph.EP].
[722] J. Scholtz and J. Unwin, What if Planet 9 is a Primordial Black Hole?, Phys. Rev. Lett. **125**, 051103 (2020), arXiv:1909.11090 [hep-ph].
[723] A. L. Miller, S. Clesse, F. De Lillo, G. Bruno, A. Depasse, and A. Tanasijczuk, Probing planetary-mass primordial black holes with continuous gravitational waves, Phys. Dark Univ. **32**, 100836 (2021), arXiv:2012.12983 [astro-ph.HE].
[724] N. Herman, A. Fżzfa, L. Lehoucq, and S. Clesse, Detecting planetary-mass primordial black holes with resonant electromagnetic gravitational-wave detectors, Phys. Rev. D **104**, 023524 (2021), arXiv:2012.12189 [gr-qc].
[725] S. G. Turyshev, P. Klupar, A. Loeb, Z. Manchester, K. Parkin, E. Witten, and S. P. Worden, Exploration of the outer solar system with fast and small sailcraft, arXiv e-prints (2020), arXiv:2005.12336 [astro-ph.IM].
[726] E. Witten, Searching for a Black Hole in the Outer Solar System, arXiv e-prints (2020), arXiv:2004.14192 [astro-ph.EP].
[727] S. Lawrence and Z. Rogoszinski, The Brute-Force Search for Planet Nine, arXiv e-prints (2020), arXiv:2004.14980 [astro-ph.EP].
[728] T. Hoang and A. Loeb, Can Planet Nine Be Detected Gravitationally by a Subrelativistic Spacecraft?, Astrophys. J. Lett. **895**, L35 (2020), arXiv:2005.01120 [astro-ph.EP].
[729] A. Siraj and A. Loeb, Searching for Black Holes in the Outer Solar System with LSST, Astrophys. J. Lett. **898**, L4 (2020), arXiv:2005.12280 [astro-ph.HE].
[730] Ž. Ivezić *et al.* (LSST), LSST: From Science Drivers to Reference Design and Anticipated Data Products, Astrophys. J. **873**, 111 (2019), arXiv:0805.2366 [astro-ph].
[731] P. H. Bernardinelli *et al.* (DES), Testing the Isotropy of the Dark Energy Survey's Extreme Trans-Neptunian Objects, Planet. Sci. J. **1**, 28 (2020), arXiv:2003.08901 [astro-ph.EP].
[732] B. Henghes *et al.* (DES), Machine Learning for Searching the Dark Energy Survey for Trans-Neptunian Objects, Publ. Astron. Soc. Pac. **133**, 014501 (2021), arXiv:2009.12856 [astro-ph.EP].
[733] D. J. Fixsen, E. S. Cheng, J. M. Gales, J. C. Mather, R. A. Shafer, and E. L. Wright, The Cosmic Microwave Background Spectrum from the Full COBE FIRAS Data Set, Astrophys. J. **473**, 576 (1996), arXiv:astro-ph/9605054 [astro-ph].
[734] S. Z. Sheikh *et al.*, The Breakthrough Listen Search for Intelligent Life: A 3.95-8.00 GHz Search for Radio Technosignatures in the Restricted Earth Transit Zone, Astron. J. **160**, 29 (2020), arXiv:2002.06162 [astro-ph.EP].
[735] D. H. E. MacMahon *et al.*, The Breakthrough Listen Search for Intelligent Life: A Wideband Data

Recorder System for the Robert C. Byrd Green Bank Telescope, Publ. Astron. Soc. Pac. **130**, 044502 (2018), arXiv:1707.06024 [astro-ph.IM].
[736] Y. Nambu and S. Noda, Interferometry of black holes with Hawking radiation, Phys. Rev. D **105**, 045022 (2022), arXiv:2109.07044 [gr-qc].
[737] S. Rahvar, Possibility of primordial black holes collision with Earth and the consequences of this collision, Mon. Not. Roy. Astron. Soc. **507**, 914–918 (2021), arXiv:2107.11139 [gr-qc].
[738] S. Gallozzi, M. Scardia, and M. Maris, Concerns about ground based astronomical observations: a step to safeguard the astronomical sky, arXiv e-prints (2020), arXiv:2001.10952 [astro-ph.IM].
[739] S. Gallozzi, D. Paris, M. Scardia, and D. Dubois, Concerns about ground based astronomical observations: quantifying satellites' constellations damages, arXiv e-prints (2020), arXiv:2003.05472 [astro-ph.IM].
[740] J. C. McDowell, The Low Earth Orbit Satellite Population and Impacts of the SpaceX Starlink Constellation, Astrophys. J. Lett. **892**, L36 (2020), arXiv:2003.07446 [astro-ph.IM].
[741] A. Williams, O. Hainaut, A. Otarola, G. H. Tan, A. Biggs, N. Phillips, and G. Rotola, A Report to ESO Council on the Impact of Satellite Constellations, arXiv e-prints (2021), arXiv:2108.03999 [astro-ph.IM].
[742] A. Williams, O. Hainaut, A. Otarola, G. H. Tan, and G. Rotola, Analysing the Impact of Satellite Constellations and ESO's Role in Supporting the Astronomy Community, The Messenger **184**, 3–7 (2021), arXiv:2108.04005 [astro-ph.IM].
[743] M. L. Rawls, H. B. Thiemann, V. Chemin, L. Walkowicz, M. W. Peel, and Y. G. Grange, Satellite Constellation Internet Affordability and Need, Res. Notes Am. Astron. Soc. **4**, 189 (2020), arXiv:2011.05168 [physics.pop-ph].
[744] S. M. Lawler, A. C. Boley, and H. Rein, Visibility Predictions for Near-future Satellite Megaconstellations: Latitudes near 50° Will Experience the Worst Light Pollution, Astron. J. **163**, 21 (2022), arXiv:2109.04328 [astro-ph.EP].
[745] R. F. Green, C. B. Luginbuhl, R. J. Wainscoat, and D. Duriscoe, The growing threat of light pollution to ground-based observatories, Astron. Astrophys. Rev. **30**, 1 (2022).
[746] I. Levchenko, S. Xu, Y.-L. Wu, and K. Bazaka, Hopes and concerns for astronomy of satellite constellations, Nat. Astron. **4**, 1012–1014 (2020).
[747] R. Massey, S. Lucatello, and P. Benvenuti, The challenge of satellite megaconstellations, Nat. Astron. **4**, 1022–1023 (2020).
[748] A. Lawrence *et al.*, The case for space environmentalism, Nature Astronomy **6**, 428–435 (2022), arXiv:2204.10025 [astro-ph.IM].
[749] J. Schneider, A. Arbey, and J. Auffinger, Techniques for Constraining the Abundance of Nonplanetary Substellar Objects, Res. Notes Am. Astron. Soc. **4**, 129 (2020).
[750] E. W. Kolb and I. I. Tkachev, Axion miniclusters and Bose stars, Phys. Rev. Lett. **71**, 3051–3054 (1993), arXiv:hep-ph/9303313 [hep-ph].
[751] F. E. Schunck and E. W. Mielke, General relativistic boson stars, Class. Quantum Gravity **20**, R301–R356 (2003), arXiv:0801.0307 [astro-ph].
[752] P. Grandclément, C. Somé, and E. Gourgoulhon, Models of rotating boson stars and geodesics around them: New type of orbits, Phys. Rev. D **90**, 024068 (2014), arXiv:1405.4837 [gr-qc].
[753] E. W. Mielke and F. E. Schunck, Boson Stars: Early History and Recent Prospects, in *8th Marcel Grossmann Meeting on Recent Developments in Theoretical and Experimental General Relativity, Gravitation and Relativistic Field Theories (MG8)*, edited by T. Piran and R. Ruffini (1999) p. 1607, arXiv:gr-qc/9801063 [gr-qc] .
[754] J. Schneider, Possible gravitational amplification in the binary pulsar 1957+20., Astron. Astrophys. **214**, 1–3 (1989).

[755] M. Perryman, J. Hartman, G. Á. Bakos, and L. Lindegren, Astrometric Exoplanet Detection with Gaia, Astrophys. J. **797**, 14 (2014), arXiv:1411.1173 [astro-ph.EP].
[756] G. Li and F. C. Adams, Interaction Cross Sections and Survival Rates for Proposed Solar System Member Planet Nine, Astrophys. J. Lett. **823**, L3 (2016), arXiv:1602.08496 [astro-ph.EP].
[757] A. J. Mustill, S. N. Raymond, and M. B. Davies, Is there an exoplanet in the Solar system?, Mon. Not. Roy. Astron. Soc. **460**, L109–L113 (2016), arXiv:1603.07247 [astro-ph.EP].
[758] R. J. Parker, T. Lichtenberg, and S. P. Quanz, Was Planet 9 captured in the Sun's natal star-forming region?, Mon. Not. Roy. Astron. Soc. **472**, L75–L79 (2017), arXiv:1709.00418 [astro-ph.EP].
[759] B. S. Gaudi *et al.*, The Habitable Exoplanet Observatory (HabEx) Mission Concept Study Final Report, arXiv e-prints (2020), arXiv:2001.06683 [astro-ph.IM].
[760] The LUVOIR Team, The LUVOIR Mission Concept Study Final Report, arXiv e-prints (2019), arXiv:1912.06219 [astro-ph.IM].
[761] J. Auffinger and G. Laibe, Linear growth of streaming instability in pressure bumps, Mon. Not. Roy. Astron. Soc. **473**, 796–805 (2018), arXiv:1709.08660 [astro-ph.EP].